Universidade do Minho
Escola de Engenharia

Rodrigo Pimenta de Oliveira Monteiro

Relationships between mobile genetic elements, antimicrobial resistance, and virulence in clinically relevant Acinetobacter baumannii isolates

abril de 2024

Relationships between mobile genetic elements, antimicrobial resistance, and virulence in clinically relevant Acinetobacter baumannii isolates

Rodrigo Pimenta de Oliveira Monteiro

UMinho | 2024

This study was supported by the Portuguese Foundation for Science and Technology (FCT) under the scope of the strategic funding of UIDB/04469/2020 unit with DOI 10.54499/UIDB/04469/2020 and BioTecNorte operation (NORTE-01-0145-FEDER-000004) funded by the European Regional Development Fund under the scope of Norte2020 - Programa Operacional Regional do Norte. The author also acknowledges FCT for the PhD grant SFRH/BD/143639/2019 with DOI 10.54499/SFRH/BD/143639/2019. This study was supported by "la Caixa" Foundation and FCT under the grant agreement HR21-FCT-00533.

Universidade do Minho
Escola de Engenharia

Rodrigo Pimenta de Oliveira Monteiro

Relationships between mobile genetic elements, antimicrobial resistance, and virulence in clinically relevant *Acinetobacter baumannii* isolates

Doctoral thesis

Ph.D. in Chemical and Biological Engineering

Work performed under supervision of

Professor Joana Azeredo

and

Professor Jan Maarten van Dijl

April 2024

DIREITOS DE AUTOR E CONDIÇÕES DE UTILIZAÇÃO DO TRABALHO POR TERCEIROS

Este é um trabalho académico que pode ser utilizado por terceiros desde que respeitadas as regras e boas práticas internacionalmente aceites, no que concerne aos direitos de autor e direitos conexos.

Assim, o presente trabalho pode ser utilizado nos termos previstos na licença abaixo indicada.

Caso o utilizador necessite de permissão para poder fazer um uso do trabalho em condições não previstas no licenciamento indicado, deverá contactar o autor, através do RepositóriUM da Universidade do Minho.

Licença concedida aos utilizadores deste trabalho:



Atribuição-NãoComercial-CompartilhaIgual
CC BY-NC-SA

https://creativecommons.org/licenses/by-nc-sa/4.0/

ACKNOWLEDGMENTS / AGRADECIMENTOS

Quero começar por agradecer à minha orientadora Professora Joana Azeredo por ter sempre acreditado em mim, por todo o otimismo e alegria que sempre procurou transmitir, por me ouvir e ajudar a superar fases mais complicadas, por todas as discussões de trabalho, o meu muito muito obrigado! I would like to thank my co-supervisor Jan Maarten for taking me on this journey, for all the good mood on every occasion, for all the inputs and fruitful scientific discussions, and for helping me to look always to the bright side of things. Thank you for all your help, it was greatly appreciated and valuable! A word of gratitude also to Erik for the input on this work, for always being available to help, and, of course, for taking me to a typical Dutch lunch on my first days in Groningen!

Logicamente que tenho, e muito, a agradecer a quem me acompanhou nesta jornada desde o primeiro dia, a família LPHAGE, com quem partilhei frustrações e vitórias, mas que acima de tudo partilhei bons momentos e boa disposição! Um obrigado muito especial aos da "velha guarda" Ribeiro, Daniela, Graça, Ergun, Rute, Luciana, Brandão, por todos os bons momentos, incluindo os musicais, no lab e fora dele. E claro um agradecimento especial aos "velhos" da velha guarda (sem ordem especifica de idades) Luís, Priscila, Sílvio, Ana, e Hugo pelas discussões e inputs para me ajudar em vários momentos. Obrigado Luís por me aturares e aconselhares, mesmo estando a milhares de km de distância, dia e noite com um filho para criar (desculpa Graça). Obrigado 'Priscilha' por me azucrinares a cabeça noite e dia e me ajudares a crescer durante este percurso. Não posso deixar de agradecer a uma pessoa especial que apesar de já não estar presente no LPHAGE foi a responsável por me motivar a seguir com o PhD durante o meu mestrado, Ana Rita Costa, muito obrigado. Tenho que agradecer tambem aos quase da nova velha guarda do LPHAGE, Multibanco (MB), Rita, Alex Limes, Renates, Bea, Marta Gomes, David, MJ, e Gabs, por me terem acolhido tão bem neste regresso pós-Holanda, por toda a boa disposição e chocolates. Um especial obrigado à Bea pela partilha das nossas gordices e pelas nossas discussões quase existenciais de fim de turno. Muito obrigado à malta do CEB, em especial à Carla, Débora, Diana, Salomé, João, Sérgio, Mr Santos, e outros que tão bons momentos me fizeram passar lá, desde o volei até às discussões científicas do clube da marmita.

Many thanks to the Molbac group, in special to Tobi, Gerbren, Sjouke, Jolanda, Elias, Francis, Xiaofang, Rosário Ayşegül, Lisanne, Lei, and Pablo for being so nice and having me so well! A special thanks to my friend Tobi who showed me around, with whom I shared those delicious arepas and other amazing dishes, for introducing me to bouldering, and for our discussions on politics, society, science, and of course food. Thank you for sharing nice moments outside on the 'roof' while having good coffee and warm sun.

Porque a família é a base de tudo na nossa vida, queria começar por agradecer aos meus pais, Raquel e Dó por todo o suporte e paciência ao longo da minha vida, por sofrerem e exaltarem de alegria nos diversos momentos deste meu percurso, por estarem sempre lá. Obrigado aos meus irmãos Filipe, Catarina e Ana Belisa* pelo suporte ao longo destes anos; aos meus avós, que apesar de não perceberem nada do que andei aqui a fazer, sempre fizeram o esforço para tentar perceber e dar-me todo o apoio necessário. Obrigado à minha tia Tecas que apesar de me dar cabo da cabeça, sempre esteve lá quando precisei. Não podia deixar de agradecer ao meu Riscas, companheiro de viagem com quem fiz o curso e o PhD que agora termino, mesmo com os problemas todos que lhe surgiram nesta fase final, sempre me deu conforto e alegria em todos os momentos.

Finalmente, um grande, mas muito grande obrigado à minha noiva Sara, com quem à data da defesa deste trabalho estarei orgulhosamente casado, por todo o apoio incondicional durante esta jornada, por todas as lágrimas de frustração e de alegria que limpou, por ter sido o meu pilar principalmente nas fases mais difíceis, por superar tudo comigo e me acompanhar em todos os momentos. Obrigado meu amor.

STATEMENT OF INTEGRITY

I hereby declare having conducted this academic work with integrity. I confirm that I have not used plagiarism or any form of undue use of information or falsification of results along the process leading to its elaboration.

I further declare that I have fully acknowledged the Code of Ethical Conduct of the University of Minho.

ABSTRACT

Acinetobacter baumannii is considered one of the most dangerous pathogens causing nosocomial infections. This Gram-negative bacterium colonizes and infects immunocompromised patients and it is very difficult to eradicate. Its remarkable adaptability is facilitated by virulence factors, such as capsule, lipopolysaccharides, secreted proteins, iron acquisition factors, pili, outer membrane vesicles (OMVs), and the SOS response. In addition, its emergence as a multidrug-resistant (MDR) microorganism led the World Health Organization to include this species, Carbapenem-Resistant *A. baumannii* (CRAb) in particular, in the top priority list of pathogens for the development of new drugs. CRAb emerged through the acquisition of antibiotic-resistance determinants mediated by plasmids, prophages and OMVs. In this study, the main goal was to investigate the role of mobile genetic elements (MGEs) in the evolution of *A. baumannii* clinical isolates regarding antibiotic resistance and virulence.

Initially, a new Prophage Analysis Tool (ProphAnTool) was developed for the comprehensive analysis of prophages among all complete *A. baumannii* genomes deposited in the National Center for Biotechnology Information (NCBI) database. Using this tool, it was possible to show that intact prophages are present in *A. baumannii* with a very high prevalence. Next, the SOS response was studied with focus on the *ddrR* gene, which was deleted from an *A. baumannii* strain for genome-wide transcriptome analysis to assess its role in virulence and fitness, as well as prophage induction. DdrR was shown to influence several virulence and fitness-related genes, and a model for its involvement in the regulation of phage induction was proposed. Three new *A. baumannii* isolates from a hospital outbreak, including two CRAb, were sequenced and analyzed, showing the presence of a new plasmid in the CRAb isolates that encodes multiple antibiotic resistance genes, including carbapenemases. OMVs were isolated and characterized by mass spectrometry. This revealed several virulence factors, in particular active carbapenemases in OMVs from the CRAb isolates. Accordingly, these OMVs were shown to protect other susceptible bacteria against carbapenems. MGEs were analyzed revealing the presence of inducible prophages and various other plasmids in the CRAb isolates.

This study showed that mobile elements, such as plasmids, prophages, and OMVs, are all together involved in the genetic evolution of *A. baumannii*, which has ultimately led to the emergence of highly antibiotic-resistant and virulent variants, like CRAb. Besides, as *A. baumannii* has a unique SOS response, a potential role of DdrR in the regulation of prophage induction was unveiled, opening the field for further studies on these two important elements.

Keywords: A. baumannii; Antibiotic-resistance; Mobile genetic elements; Prophages; Virulence

SUMÁRIO

Acinetobacter baumannii é considerada uma das bactérias patogénicas mais perigosas, associadas a infeções hospitalares, devido às suas características intrínsecas (cápsula, LPS, secreção de proteínas, aquisição de ferro, fibras, vesículas da membrana externa, resposta SOS, entre outras). Além disto, dado o aumento da sua resistência a vários antibióticos, foi posicionada pela Organização Mundial de Saúde, na lista de organismos prioritários para desenvolvimento de novos antibióticos, especificamente a *Acinetobacter baumannii* resistente aos carbapenems (CRAb). O aparecimento de CRAB está associado à aquisição de resistência a antibióticos (RA) e fatores de virulência mediada por elementos como profagos, plasmídeos e vesículas da membrana externa. O objetivo deste trabalho é investigar o papel destes elementos na evolução das estirpes clínicas de *A. baumannii*, focando a virulência e RA.

Inicialmente foi elaborada uma nova ferramenta de análise e caracterização de profagos (ProphAnTool) que foi aplicada para analisar todos os genomas completos de *A. baumannii* depositados no NCBI. Esta análise confirmou a elevada prevalência dos profagos em estirpes de *A. baumannii*. A relação entre a presença de profagos em genomas de *A. baumanni* e o seu potencial para a transmissão de virulência, bem como o papel do gene *ddrR* neste fenómeno, foi estudada através da análise do transcriptomona de *A. baumannii* (estirpe selvagem e mutada no gene *ddrR*) submetidas a stresse. A DdrR mostrou influenciar vários genes de virulência e de fitness, além de mostrar potencial na regulação da indução de profagos. O trabalho incidiu também na caracterização de três novas estirpes de *A. baumannii* isoladas de um surto hospitalar, entre as quais, duas eram multirresistentes e CRAb. Os seus genomas foram sequenciados e analisados, revelando a presença de um novo plasmídeo que codifica diferentes genes de RA, tais como carbapenemases, nas duas CRAbs. As vesiculas segregadas por estas estirpes foram isoladas e caracterizadas por espetrofotometria de massa. Os resultados mostraram a presença de diversos fatores de virulência, especificamente carbapenemases nas vesiculas isoladas das duas estirpes CRAbs. As vesículas demonstraram capacidade de degradar carbapenems, e providenciar proteção a outras espécies sensíveis a esta classe de antibióticos. Foram ainda identificados e caracterizados vários elementos móveis genéticos, tais como profagos e outros plasmídeos.

Este estudo mostrou que elementos móveis como os plasmídeos, profagos e vesículas são fatores determinantes na adaptação e evolução desta espécie como agente patogénico altamente resistente a antibióticos. Foi possível ainda demonstrar que esta espécie apresenta um mecanismo de resposta a stresse único e potenciador de transmissão de virulência, com a proteína DdrR envolvida na regulação da indução de profagos.

Palavras-chave: *A. baumannii*; Elementos genéticos móveis; Resistência a antibióticos; Virulência

TABLE OF CONTENTS

Direitos de autor e condições de utilização do trabalho por terceiros ..... **ii**
Acknowledgements ..... **iii**
Statement of integrity ..... **iv**
Abstract ..... **v**
Sumário ..... **vi**
Table of contents ..... **vii**
List of abbreviations ..... **xii**
List of figures ..... **xv**
List of tables ..... **xx**
Scientific outputs ..... **xxi**
Objectives and structure of the thesis ..... **xxii**
Chapter 1. General Introduction **1**
1.1. *Acinetobacter baumannii* 2
1.1.1. *Acinetobacter baumannii* virulence factors 3
1.1.1.1. Outer membrane proteins 4
1.1.1.2. Pili 5
1.1.1.3. Capsule and LPS 6
1.1.1.4. Metal ion acquisition 6
1.1.1.5. Protein secretion 7
1.1.1.6. SOS response 9
1.1.1.7. Other virulence factors and antibiotic resistance mechanisms 10
1.1.2. Horizontal gene transfer and virulence spear among *A. baumannii* 10
1.1.2.1. Plasmids 13
1.1.2.2. Outer membrane vesicles 15
1.1.2.3. Prophages 17
1.2. Concluding remarks 21
1.3. References 22
Chapter 2. *Acinetobacter baumannii* prophages, a bioinformatic update **34**
Abstract 35
2.1. Introduction 36
2.2. Materials and Methods 37

2.2.1. General overview of the pipeline 37
2.2.2. PHASTEST results extraction workflow 38
2.2.3. Domain-based annotation workflow 39
2.2.4. Virulence genes detection workflow 40
2.2.5. Taxonomic classification workflow 40
2.2.6. Defense mechanism workflow 41
2.2.7. Phylogeny workflow 41
2.2.8. Data availability 41
2.3. Results 41
2.3.1. Prophage prevalence analyses in *A. baumannii* genomes 41
2.3.2. Prophage distribution within *A. baumannii* strains 42
2.3.3. Prophage taxonomy reveals a highly predominant family 44
2.3.4. Prophage-associated virulence 47
2.3.5. Prophages strongly influence *A. baumannii* lifestyle 50
2.3.6. Prophage regions specifying defense mechanisms 53
2.4. Discussion 55
2.5. Concluding Remarks 57
2.6. References 59
2.7. Supplemental Material 63
Chapter 3. Prophage induction control by DdrR in *A. baumannii* during early stages of the SOS response 65
Abstract 66
3.1. Introduction 67
3.2. Materials and Methods 68
3.2.1. Bacterial strains and growth conditions 68
3.2.2. Whole-genome sequencing of *A. baumannii* ATCC 17978 68
3.2.3. Prophage detection, phage induction and phage quantification 69
3.2.4. Construction of the different mutants 69
3.2.5. RNAseq experiments and analyses 70
3.2.6. Statistical analyses 71
3.3. Results and Discussion 71
3.3.1. DdrR and its role in bacterial processes including virulence and fitness 71
3.3.2. Early SOS response under DNA damage 73
3.3.3. DdrR influences a wide range of genes no-DNA-damage-inducible genes 75

3.3.4. DdrR has a critical regulatory role in prophage gene expression 76
3.3.5. *A. baumannii* 17978 inducible prophages 81
3.4. Concluding Remarks 84
3.5. References 86
3.6. Supplementary material 89
Chapter 4. Nosocomial transmission of *tet(x3)*, *bla*$_{NDM-1}$, and *bla*$_{OXA-97}$-carrying *Acinetobacter baumannii* conferring resistance to eravacycline and omadacycline, the Netherlands, March-August 2021 92
Abstract 93
4.1. Introduction 94
4.1.1. Outbreak detection 94
4.2. Materials and Methods 96
4.2.1. Settings and definitions 96
4.2.2. Rectal and environmental culture screening protocol 96
4.2.3. Additional testing of outbreak strains 96
4.2.4. Antibiotic susceptibility testing (AST) 96
4.2.5. Whole genome sequencing (WGS) 97
4.2.6. Sequence data analysis for antimicrobial resistance determinants and plasmids 98
4.2.7. Ethical statement and informed content 99
4.2.8. Data availability statement 99
4.3. Results 99
4.3.1. Antimicrobial susceptibility testing of the *A. baumannii* outbreak isolates 99
4.3.2. Genomic analysis of the outbreak *A. baumannii* isolates 101
4.3.3. Analysis of multidrug resistance plasmids 101
4.3.4. Outbreak control measures 103
4.4. Discussion 104
4.5. Concluding Remarks 106
4.6. References 107
4.7. Supplemental Material 110
Chapter 5. Outer membrane vesicles of clinical tet(x3), bla$_{NDM-1}$, and bla$_{OXA-97}$-carrying Acinetobacter baumannii isolates contribute to carbapenem resistance 121
Abstract 122
5.1. Introduction 123
5.2. Materials and Methods 125
5.2.1. Bacterial strains 125

5.2.2. OMV purification 125
5.2.3. Dynamic light scattering 125
5.2.4. Transmission electron microscopy (TEM) 126
5.2.5. LDS-PAGE 126
5.2.6. LC-MS/MS sample preparation 126
5.2.7. Proteome data analysis 127
5.2.8. Carbapenemase activity assays 127
5.2.9. OMV-mediated protection against imipenem 128
5.2.10. Imipenem survival assay 128
5.2.11. Statistical analysis 128
5.2.12. Data Availability 128
5.3. Results and Discussion 128
5.3.1. Outer membrane vesicle characterization 128
5.3.2. OMV proteome analyses 130
5.3.3. OMV-borne proteins associated with antimicrobial resistance 132
5.3.4. OMV-associated carbapenemase activity 133
5.3.5. OMV-mediated protection 135
5.4. Concluding Remarks 138
5.5. References 140
5.6. Supplemental Material 145

Chapter 6. Genomic and proteomic analyses of mobile genetic elements from recent outbreak-associated carbapenem- and tetracycline-resistant *A. baumannii* clinical isolates 147

Abstract 148
6.1. Introduction 149
6.2. Materials and Methods 150
6.2.1. Bacterial strains 150
6.2.2. OMV purification 150
6.2.3. Transmission electron microscopy (TEM) 151
6.2.4. Dynamic light scattering (DLS) 151
6.2.5. LDS-PAGE 151
6.2.6. LC-MS/MS sample preparation 151
6.2.7. Proteome data analysis 152
6.2.8. Statistical analysis 153

6.2.9. Data Availability 153
6.3. Results 153
6.3.1. Mobile genetic element characterization 154
6.3.2. Outer membrane vesicle characterization 158
6.3.3. Proteomic analysis of OMVs produced by clinical isolates 159
6.3.4. Functional analysis of OMV proteins 161
6.3.5. Virulence- and fitness-related OMV-derived proteins 163
6.4. Concluding Remarks 170
6.5. References 172
6.6. Supplemental Material 142
Chapter 7. General conclusions and future perspectives 180
7.1. General conclusions 181
7.2. Future perspectives 183
7.3. References 185

LIST OF ABBREVIATIONS

AceI - Acitenobacter chlorhexidine efflux protein

AMR - Antimicrobial resistance

ARG - Antibiotic Resistance Gene

Bap - Biofilm-associated proteins

BapAb - Biofilm-associated protein of Acinetobacter baumannii

BLAST - Basic Local Alignment Search Tool

BMD - Broth Microdilution

CARD - Comprehensive Antibiotic Resistance Database

CarO - Carbapenem susceptibility porin

CDS - Protein coding sequences

CFU - Colony-forming unit

CIM - Carbapenem inhibition method

COG - Cluster of Orthologous Gene

CP - Conjugative Plasmids

CpaA - Glycan-specific adamalysin-like protease

CR - Carbapenem-Resistant

CRAb - Carbapenem-Resistant *Acinetobacter baumannii*

Csu - Chaperon/usher pilus system

CSV - Comma-separated Values

DGE - Differential Gene Expression

DLS - Dynamic Light Scattering

DMEM - Dulbecco's Modified Eagle Medium

DMS - DNA Modification System

DNA - Deoxyribonucleic Acid

GCN - Graph Convolutional Network

HemO - Heme oxygenase

HGT - Horizontal gene transfer

HMM - Hidden-Markov Model

HNH - His-Me finger endonuclease

ICE - Integrative Conjugative Elements

ICTV - International Committee on Taxonomy of Viruses

ICU - Intensive care unit

IM - Inner membrane

LB - Lysogeny Broth

LDS - Lithium Dodecyl Sulfate

LPS - Lipopolysaccharide

MDR - Multidrug-resistance

MFS - Major facilitator superfamily

MIC - Minimal inhibitory concentration

MMC - Mitomycin C

MST - Minimum spanning tree

MUSCLE - Multiple Sequence Comparison by Log-Expectation

NCBI - National Center for Biotechnology Information

NDM - New Delhi Metallo-beta-lactamases

NGS - Next-Generation Sequencing

OMP - Outer Membrane Protein

OMV - Outer membrane vesicles

OprD - Outer membrane porin D

ORF - Open Reading Frames

OriT - Origin of Transfer

OriV – Origin of vegetative replication

OXA - Oxacilinases

PADLOC - Prokaryotic Antiviral Defence Locator

PBP - Penicillin-binding protein

PBS - Phosphate Buffered Saline

PCR - Polymerase chain reaction

PDC - Phage-defense candidate system

PFU - Plaque-forming unit

PG - Peptidoglycan

PHASTEST - PHage Search Tool with Enhance Sequence Translation

PilA - Pilus protein A

PMB - Polymyxin B

PNAG - Poly-beta-1,6-N-acetyglucosamine

PP - Phage-Plasmids

ProphAnTool - Phophage Analysis Tool

R - Relaxase

RM - Restriction-modification

RNA - Ribonucleic Acid

RNAseq - RNA sequencing

ROS - Reactive Oxygen Species

RPS-BLAST - Reverse Position-Specific BLAST

RTX - Repeats-in-Toxins

SEM - Standard error of the mean

sgRNA -Single-guided RNAseq

SMC - Structural maintenance of chromosome

sRNA - Small RNA

ssDNA - Single-stranded DNA

SVM - Support Vector Machine module

TA - Toxin-antitoxin

TCA - Trichloroacetic Acid

TEM - Transmission Electron Microscopy

VFDB - Virulence Factors Database

wgMLST - Whole-genome multiple-locus sequence type

WGS - Whole genome sequencing

WHO - World Health Organization

LIST OF FIGURES

Chapter 1

Figure 1.1. Schematic representation of the most relevant virulence factors associated *with A. baumannii*. AceI, *Acinetobacter* chlorhexidine efflux protein; BapAb, biofilm-associated protein of *A. baumannii*; CarO, carbapenem susceptibility porin; CpaA, glycan-specific adamalysin-like protease; Csu, chaperon/usher pilus system; LPS, lipopolysaccharide; Omp, outer membrane protein; PNAG, poly-β-1,6-N-acetylglucosamine; T2SS, type II secretion system; T6SS, type VI secretion system. 3

Figure 1.2. Schematic representation of different types of protein secretion systems encountered in Gram-negative bacteria. Note that the type III system has not been identified in *A. baumannii* 8

Figure 1.3. Mechanisms of horizontal gene transfer (HGT). HGT may take place through natural transformation, transduction, conjugation and OMV delivery 11

Figure 1.4. Graphical representation of horizontal gene transfer through generalized, specialized, and lateral transduction 12

Figure 1.5. Schematic representation of plasmid mobilization through HGT. Conjugative and mobilizable plasmids can be transferred by conjugation. Non-mobilizable plasmids can only rely on either the transduction or transformation for their transfer to a new host cell 14

Figure 1.6. Graphical representation of outer membrane vesicle biogenesis. OMV structures are formed from the bacterial outer membrane. They can harbor different types of cargo, such as DNA, RNA, toxins, and other proteins, which will interact with other cells. OMVs can also protect bacteria against phages. IM, inner membrane; PG, peptidoglycan; OM, outer membrane; LPS, lipopolysaccharides 16

Figure 1.7. Graphical representation of the bacteriophage lytic and lysogenic cycles 18

Chapter 2

Figure 2.1. ProphAnTool workflow overview 38

Figure 2.2. Prophage prevalence within *A. baumannii* genomes. On the left, the prevalence of total prophages, "intact" prophage regions, defective prophages, more than one intact prophage, and more than one defective prophage. Defective prophages include both incomplete and questionable. Plasmid sequences were not considered for this plot. On the right, boxplot with prophage frequency per bacterial genome within prophage-containing genomes. Only genomes and plasmid sequences with prophage regions were considered. Error bars represent the maximum and minimum values, and the single dots represent the outliers 42

Figure 2.3. Distribution of the average number of prophages among a) bacterial sequences and b) plasmid sequences. Left graphs, average number of any prophage region per genome size; Middle graphs, average number of intact prophage regions per genome size; Right graphs,

average number of defective (incomplete and questionable) prophage regions per genome size. Error bars represent standard deviation. 43

Figure 2.4. Taxonomy classification of all intact prophages detected in the dataset 45

Figure 2.5. Intact prophage regions taxonomy and size variation 45

Figure 2.6. Frequency of phages that shared the most homology with intact prophages....46

Figure 2.7. Phylogenetic tree with intact prophages encoded by plasmid sequences. Prophage sequences were aligned using MUSCLE. The tree was built with a bootstrap set to 100. Tree branches are proportional to the branch length (branch length = 0, identical; branch length = 1 no similarity) 47

Figure 2.8. Heatmap with intact prophage regions that harbor antibiotic-resistance genes. The first number in each sequence name means the prophage region within the host genome, which is codified by the GCA code that comes next. Green color indicates the presence of a specific gene within a prophage 49

Figure 2.9. Phylogenetic tree showing the diversity between ARG-harboring intact prophages. Sequences were aligned using MUSCLE. Tree was built with a bootstrap set to 100. Tree branches are proportional to the branch length (branch length = 0, identical; branch length = 1 no similarity). Prophage-predicted families are identified in colors: Green, *Peduoviridae*; Blue, *Chaseviridae*; Purple, *Drexlerviridae*; Orange, *Mesyanzhinovviridae*; Pink, *Herelleviridae*; Brown, *Autographiviridae*, Red, Unknown 50

Figure 2.10. General and functional categories attributed based on COG classification of all CDSs found among intact prophages (mobilome-related CDSs excluded). 1, functional categories belonging to Cellular Processes and Signaling; 2, functional categories belonging to Information Storage and Processing; 3, functional categories belonging to Metabolism; 4, functional categories poorly categorized 53

Figure 2.11. Defense systems found frequency within intact prophage sequences 55

Figure S2.1. Taxonomic family classification of all intact prophages detected in the dataset, corrected for a score >0.90 (n= 560) 63

Figure S2.2. General and functional categories attributed based on COG classification of all CDSs found among intact prophages. 1, functional categories belonging to Cellular Processes and Signaling; 2, functional categories belonging to Information Storage and Processing; 3, functional categories belonging to Metabolism; 4, functional categories poorly categorized 64

Chapter 3

Figure 3.1. Volcano plot visualizing the differentially expressed genes between the WT and *ddrR* mutant in the absence of MMC. Values represent log2-fold changes. Green points – prophage intact-1 encoded genes; Orange points – prophage intact-2 encoded genes; Blue points – prophage intact-3 encoded genes; Grey points – non-prophage encoded genes.....73

Figure 3.2. Proportion of genes a) regulated during the early SOS response induced by MMC treatment in WT and *ddrR* mutant *A. baumannii* ATCC 17978; b) regulated during the early SOS response in WT and *ddrR* mutant *A. baumannii* ATCC 17978, but excluding prophage genes;

and c) encoded by prophages in the WT and *ddrR* mutant *A. baumannii* ATCC 17978 under SOS response 74

Figure 3.3. Mitomycin C (MMC) effect on colony-forming unit (CFU) counts as measured for the *A. baumannii* ATCC 17978 (WT) and 17978::*ddrR* mutant after 30 min of incubation. 17978_C (blue) – untreated WT control culture; 17978_MMC (purple) – MMC-treated WT culture; 17978::*ddrR*_C (pink) – untreated *ddrR* control culture; 17978::*ddrR*_MMC (green) – MMC-treated *ddrR* culture. Statistically significant differences are represented by ** ($p<0.05$) 79

Figure 3.4. Electron micrograph of *A. baumannii* ATCC 17978 WT phage particles after prophage induction at 100,000 × magnification. Black arrows indicate two potentially different capsid structures of the visualized phages 82

Figure 3.5. Quantification of prophages by PFU-counting using lysates obtained upon induction of each of the prophage-free mutants 17978::Pro1, 17978::Pro2 or 17978::Pro1. Pro1_C – 17978::Pro1 control lysate; Pro1_MMC – 17978::Pro1 MMC-induced lysate; Pro2_C – 17978::Pro2 control lysate; Pro2_MMC – 17978::Pro2 MMC-induced lysate; Pro3_C – 17978::Pro3 control lysate; Pro3_MMC – 17978::Pro3 MMC-induced lysate; The color coding of the bars indicates which indicator bacteria were plated to generate the lawn needed for PFU-counting 83

Figure 3.6. Phage concentrations determined by PFU-counting after treatment of *A. baumannii* 17978 or 17978::*ddrR* with MMC (3 μg/mL) for 0 h, 3 h, and 24 h. Control_WT– phage concentration on the control of WT; Control_*ddrR* – phage concentration of the control of *ddrR*; MMC – mitomycin C-induced culture; Pro1 – intact-1; Pro3 – intact-3. Intact-2 was never detected, therefore it was omitted from the graph for simplification 84

Chapter 4

Figure 4.1. Timeline of cultures and preventive measures. Chronological display of sequential infection prevention measures (green) and culture and discharge/transfer data of patient 1 (blue), patient 2 (yellow) and patient 3 (red) 95

Figure 4.2. CRAb1 plasmid map showing the relative positions of antibiotic-resistance genes (red) and virulence-related genes (dark blue). Other genes are not shown for simplification .102

Figure 4.3. Coding sequences of the integron containing Genomic Island 1 and Genomic Island 3. Mobile elements-related genes (blue) and antibiotic resistance genes *tet(x)3*, bla_{NDM1} and *sul2* (red) are marked. Hypothetical proteins (yellow) are not labeled.....103

Figure S4.1. Inhibitory effect of tetracycline class antibiotics against *A. baumannii* clinical isolates and reference strains: (a) Tetracycline, (b) Eravacycline, and (c) Omadacycline.....110

Figure S4.2. Phylogenetic tree of *A. baumannii* plasmids based on sequences submitted to Genbank, showing that the plasmid of the CRAb1 and CRAb2 isolates (highlighted in yellow) is unique (analysis performed in September 2021) 111

Figure S4.3. BLASTn of the bla_{NMD-1} and *tet(x)3* carrying integron. Both the bla_{NMD-1} and *tet(x)3* genes located within genomic islands 3 and 1, respectively, have been described before, but the

plasmids identified in the present outbreak are unique in combining these resistance genes in one integron 112

Chapter 5

Figure 5.1. TEM images of OMVs from the three *A. baumannii* study isolates. A) Ab1; B) CRAb1; C) CRAb2 129

Figure 5.2. Predicted localization of OMV-associated proteins from the Ab1, CRAb1 and CRAb2 isolates 131

Figure 5.3. Venn diagram showing the numbers of common and uniquely identified proteins in OMVs from the Ab1, CRAb1, and CRAb2 study isolates.....132

Figure 5.4. CarbaNP test with isolated OMVs from the CRAb1 and CRAb2 isolates. Tubes from left to right show: 1 - negative control, PBS; 2 - negative control, PBS with imipenem; 3 - CRAb1 OMVs, negative control without imipenem; 4 - CRAb1 OMVs with imipenem; 5 - CRAb2 OMVs, negative control without imipenem; 6 - CRAb2 OMVs with imipenem.....134

Figure 5.5. Visualization of carbapenem inactivation by OMVs from CRAb1 and CRAb2 study isolates using the CIM test. The carbapenem-susceptible strain used was A. baumannii 17978. Control PBS, imipenem diffusion disk incubated with PBS only. Control Ab1, CRAb1, and CRAb2, imipenem diffusion disks incubated with biomass from the respective bacterial isolate resuspended in PBS. OMVs Ab1, CRAb1, and CRAb2, imipenem diffusion disks incubated with OMVs from the respective bacterial isolate resuspended in PBS.....135

Figure 5.6. Protection of the carbapenem-sensitive *A. baumannii* ATCC 17978 strain against growth inhibition by imipenem upon imipenem pretreatment with OMVs of the CRAb2 isolate. Imipenem (0.125 μg/mL) was mixed with OMVs (40 μg) or PBS, and subsequently mixed with pre-cultured bacteria. Bacterial growth was measured by optical density readings at 600 nm for 6 h. As a control, pre-cultured bacteria without additions were mixed with LB.....136

Figure 5.7. *A. baumannii* ATCC 17978 and *E. coli* ATCC 25922 survival in the presence of imipenem, ampicillin, or ciprofloxacin facilitated by OMVs from the CRAb2 isolate. Bacterial growth was assayed by optical density readings (top) and CFU counting (bottom). LB, Control without antibiotic nor OMVs; IMP, imipenem at 0.5 μg/mL; AMP, ampicillin at 256 μg/mL; CIP, Ciprofloxacin at 0.5 μg/mL. UDL, Under limit of detection. Asterisks indicate statistical significance for $p<0.05$ 138

Figure S5.1. Predicted subcellular localization of identified OMV-associated proteins from the Ab1, CRAb1, CRAb2 isolates. Percentages are related to the number of proteins in each localization.....145

Figure S5.2. Spectral scanning upon CarbNP tests with OMVs from the CRAb2 isolate. OMVs were mixed with IMP or PBS. Spectral scans ranging from 300 nm to 700 nm were recorded using a Biotek microplate reader. Incubation of imipenem with the OMVs results in a shift from the red color peak (560 nm) to the yellow color peak (430 nm), which is indicative of imipenem hydrolysis and acidification of the solution. IMP, imipenem 146

Chapter 6

Figure 6.1. Induction curve of Ab1, CRAb1, and CRAb2 A. baumannii isolates using MMC at 3 μg/mL added at T0 155

Figure 6.2. TEM images of phages produced by the MMC-induced a) Ab1, b) CRAb1, and c) CRAb2 isolates 156

Figure 6.3. Numbers of identified OMV-associated proteins from the Ab1, CRAb1, and CRAb2 isolates and their predicted subcellular or extracellular localization. OMVs were collected from bacteria grown in LB or DMEM 161

Figure 6.4. Functional annotation of OMV-borne proteins from isolates Ab1, CRAb1, and CRAb2, grown in LB or DMEM by the cluster of orthologous groups (COG). Each plot shows a comparison of the numbers of proteins assigned to each COG attributed between LB and DMEM 162

Figure 6.5. Venn diagrams with numbers of OMV-associated proteins produced by the Ab1, CRAb1 and CRAb2 isolates grown in LB or DMEM. The bottom diagram was plotted using the common proteins from LB and from DMEM.....164

Figure 6.6. Heatmap with virulence genes identified within OMVs of the Ab1, CRAb1, and CRAb2 isolates upon growth in LB or DMEM. White squares mean the absence of a protein. 169

LIST OF TABLES

Chapter 1

Table 1.1. Overview of studies addressing HGT and the transfer of antimicrobial resistance (AMR) genes in *A. baumannii* 12

Chapter 3

Table 3.1. Comparison of the expression of SOS-related genes in *A. baumannii* ATCC 17978 WT and the respective *ddrR* mutant upon SOS induction with MMC 75

Table 3.2. List of prophage intact-1, -2, and -3 genes and the corresponding fold-changes influenced by the *ddrR* gene deletion in the absence of induced DNA damage..... 77

Table S3.1. Primers and ssDNA donor used in this study 89

Table S3.2. Functional analysis results from FUNAGE-Pro. COG, Cluster of Ontology Genes; GO, Gene Ontology; IPR, InterPro; KEGG, Kyoto Encyclopedia of Genes and Genomes; Pfam, Protein families database..... 90

Chapter 4

Table 4.1. Description of the antibiotic susceptibility and resistome of the isolates in the outbreak. MICs of E. coli and *A. baumannii* reference strains were tested in parallel with the clinical isolates on the gradient strip method and BMD antimicrobial susceptibility testing. No discrepancies were detected compared to EUCAST and CLSI reference MICs 100

Table S4.1. SNP analysis of the plasmid sequence of CRAb1 compared to the plasmid sequence of CRAb2..... 113

Table S4.2. Complete annotation of the CRAb1 plasmid 114

Chapter 5

Table 5.1. Antibiotic resistance genes encoded by the large pCRAb1 and pCRAb2 plasmids in the CRAb1 and CRAb2 isolates 124

Table 5.2. DLS measurements on OMVs from the *A. baumannii* study isolates Ab1, CRAb1 and CRAb2. Two different intensity peaks were detected that correspond to differently sized OMVs, denoted as Peak 1 and Peak 2. PdI refers to the polydispersity index, which indicates how homogeneous the respective sample is 129

Table 5.3. Antimicrobial resistance proteins identified in the OMVs of the Ab1, CRAb1 and CRAb2 isolates. Each protein sequence was inspected by CARD 133

Chapter 6

Table 6.1. Mobile genetic elements carried by the *A. baumannii* isolates Ab1, CRAb1, and CRAb2, and their respective sizes. Prophage regions were detected using the PHASTER tool 153

Table 6.2. Proteins of interest encoded by the intact prophages of the clinical *A. baumannii* isolates Ab1, CRAb1, and CRAb2, and their functions 157

Table 6.3. DLS measurement of OMVs from the AB1, CRAb1, and CRAb2 isolates grown in LB or DMEM 159

Table 6.4. Comparison of the proportions of OMV-associated proteins with a particular predicted subcellular localization for OMVs collected from the Ab1, CRAb1, and CRAb2 isolates grown in LB or DMEM 161

Table 6.5. Virulence-related proteins identified in OMVs from the *A. baumannii* isolates Ab1, CRAb1 and CRAb2, and their clustered orthologous groups (COGs) 167

SCIENTIFIC OUTPUTS

Papers in peer-reviewed journals:

- D.T. Talsma, **R. Monteiro**, R.C.F.Vallejo, M. Heuvelmans, T.N. Le, A.P.A. Hendrickx, S. Rosema, I. Maat, J.M. van Dijl, E. Bathoorn, "Nosocomial transmission of *tet(x3)*, bla_{NDM-1}, and bla_{OXA-97}-carrying Acinetobacter baumannii conferring resistance to eravacycline and omadacycline, the Netherlands, March-August 2021," *Eurosurveillance*, Apr. 2024. Accepted for publication
- **R. Monteiro**, B.S. Alcantud, S. Piersma, A.P.A. Hendrickx, S. Maaß, D.Becher, J. Azeredo, E. Bathoorn, and J.M. van Dijl, "Outer membrane vesicles of clinical *tet(x3)*, bla_{NDM-1}, and bla_{OXA-97}-carrying *Acinetobacter baumannii* isolates contribute to carbapenem resistance". April 2024 – under submission

Posters in conferences:

- **R. Monteiro**, M. Vieira, J. Erdmann, S. Häussler,J. Azeredo "*Pseudomonas aeruginosa* prophages: a new and simplified bioinformatic analysis". Paper presented in 25th Biennial Evergreen International Phage Meeting, August 2023, Washington, USA.
- **R. Monteiro**, B. Santamarina, A.P.A. Hendrickx, E. Bathoorn, J. Azeredo, J.M. Van Dijl. "Carbapenemases (NDM-1) in outer membrane vesicles from clinical Acinetobacter baumannii isolates, a way to bacterial persistence". Paper presented in the 10th Congress of European Microbiologists, FEMS 2023, July 2023, Hamburg, Germany.
- **R. Monteiro**, L.D.R. Melo, R. Domingues, H. Oliveira, J.M. Van Dijl, J. Azeredo. "The *Acinetobacter baumannii* SOS gene ddrR is crucial for prophage maintenance and induction". Viruses of Microbes 2022 – Book of abstracts: Poster MoIM.254(PS3-R4.16), July 2022, Guimarães, Portugal.
- **R. Monteiro**, L.D.R. Melo, J.M. Van Dijl, J. Azeredo. "Different stress conditions lead to different prophage responses changing the phenotype of *Acinetobacter baumannii*". Paper presented in 32nd ECCMID, European Congress of Clinical Microbiology and Infectious Diseases, April 2022, Lisbon, Portugal.

OBJECTIVE AND STRUCTURE OF THE THESIS

The aim of the work described in this thesis was to investigate the evolution of *Acinetobacter baumannii* clinical isolates in terms of virulence and antibiotic resistance, focusing on the roles of horizontal gene transfer agents, such as plasmids, outer membrane vesicles (OMVs), and prophages. To achieve this, a comprehensive approach involving genomics, transcriptomics, and proteomics was employed. Accordingly, this thesis is structured in seven chapters describing the scientific work developed to accomplish the proposed goal.

Chapter 1 serves as a general introduction, offering an overview of the biological context of *Acinetobacter baumannii* and how this species became a serious pathogen in healthcare settings, and shedding light on the role of the various virulence factors that have contributed to its 'success' as a pathogen. Furthermore, the chapter delves into the concept of horizontal gene transfer, with a focus on plasmids, OMVs, and prophages, which have been implicated in bacterial evolution in general, and the emergence of antibiotic resistance in particular, as evidenced by the reported studies.

Chapter 2 presents an extensive analysis of all complete *A. baumannii* genomes deposited in the National Center for Biotechnology Information (NCBI) database, which is part of the United States National Library of Medicine. This analysis was focused on the search for prophages to understand their roles in the virulence of *A. baumannii*. Moreover, to perform the analysis, a new bioinformatic tool (ProphAnTool) was developed, which builds on different publicly available tools used for genome analyses. The ProphAnTool facilitates the automated search for, and characterization of identified prophages.

Chapter 3 presents a transcriptomic analyses of *A. baumannii* cells during early stress responses, with a particular focus on prophage induction. Utilizing RNA sequencing (RNAseq), genome-wide gene expression was assessed in cells exposed to mitomycin C to identify genes potentially associated with prophage induction, as well as genes related to fitness and virulence. Moreover, the role of DdrR protein was studied and correlated with prophage induction. In addition, three prophages from the *A. baumannii* strain employed for transcriptome analysis were characterized.

Chapter 4 describes an outbreak of *A. baumannii* that occurred in a hospital in The Netherlands. Three newly isolated strains were characterized through sequencing and antibiotic resistance, including two highly carbapenem- and tetracycline-resistant isolates.

The studies presented in **Chapter 5** build on the *A. baumannii* clinical isolates described in Chapter 4. Here, the focus was placed on the extracellular carbapenemase activity. Proteomics analyses showed that the carbapenemases were associated with OMVs. The activity of the OMV-associated

carbapenemases was characterized by various methods, including the CarbNP and CIM tests. In addition, the protection against carbapenem activity provided by the OMVs was measured and it was observed that the OMV-associated carbapenemases can provide protection against carbapenems not only to *A. baumannii* but also to other bacterial species.

In **Chapter 6** the mobile genetic elements of the *A. baumannii* clinical isolates described in the previous thesis chapters are described. To this end, the isolates were grown in different media, namely Lysogeny Broth (LB) or the cell culture medium DMEM. Subsequently, the OMVs produced by the isolates were collected from culture supernatants and characterized by proteomics. Furthermore, the studies investigated the plasmids and prophages that the three isolates harbor, and prophage induction was evaluated.

Chapter 7 presents a general discussion of the main conclusions that can be drawn from the studies described in this thesis. Furthermore, perspectives for future investigations are outlined.

Chapter 1

General Introduction

1.1. *Acinetobacter baumannii*

Infectious diseases are emerging as a global healthcare threat due to widespread antibiotic resistance (1). A group of bacterial pathogens named ESKAPE, which includes *Enterococcus faecium*, *Staphylococcus aureus*, *Klebsiella pneumoniae*, *Acinetobacter baumannii*, *Pseudomonas aeruginosa,* and *Enterobacter* species (2), is of particular concern in hospital environments due to high levels of resistance. In 2017, the World Health Organization (WHO) placed some of the ESKAPE pathogens on a priority list for the development of new drugs, and one of the top priority pathogens is Carbapenem-Resistant (CR) *Acinetobacter baumannii* (CRAb) (3).

A. baumannii is an aerobic Gram-negative coccobacillus responsible for opportunistic infections of the skin, the urinary and respiratory tracts, and the bloodstream (4,5). This pathogen is considered a global threat due to its ability to acquire/develop multidrug resistance (4,5). Several reports have shown that this pathogen developed resistance against many different antibiotics, such as fluoroquinolones, aminoglycosides, colistin, and β-lactams. This is mostly due to the action of efflux pumps, aminoglycoside-modifying enzymes, and various targeted mutations (6–8). A recent survey of hospital-acquired *A. baumannii* infections, showed that more than 20 % of all nosocomial infections in intensive care units (ICUs) were caused by this pathogen (9). Furthermore, this species seems to be widespread across the globe, mostly in Africa, with a prevalence rate of up to 67 % (9). In the post-COVID-19 era, *A. baumannii* was one of the most frequently detected pathogens among ICU patients in Chinese hospitals, where it especially affected patients with long stays in these units (10). Also, other countries, like Spain, France, Japan, Egypt, Iran and Italy, witnessed *A. baumannii* outbreaks amongst long-stay ICU patients that were treated for COVID-19 (11).

CRAb strains are particularly problematic due to their broad spectrum of antibiotic resistance, including their resistance to carbapenems, which are considered as the last resort antibiotics for treating infections (12,13). The emergence of antibiotic resistance is mainly driven by the misuse of antibiotics, which potentiates the transmission of resistance genes between cells through horizontal gene transfer (HGT) (14). It has been predicted that, by the year 2050, around 10 million deaths will occur due to antimicrobial resistance (15). Consistent with this view, the incidence of infections caused by antimicrobial-resistant pathogens has increased after the COVID-19 pandemic (16). The persistence of *A. baumannii* in hospital environments relates to its ability to form biofilms on biotic and abiotic surfaces (5,17). Besides, some intrinsic characteristics allow *A. baumannii* to resist desiccation, disinfection and oxidative stresses, making outbreaks caused

by this bacterium difficult to stop and turning it into one of the nowadays most dangerous pathogens that can colonize hospital environments (18).

1.1.1. *Acinetobacter baumannii* virulence factors

There are several highly relevant studies that have explored the virulence of *A. baumannii* regarding antibiotic resistance and pathogenicity in general (5,6,17,19,20). Figure 1 represents the most important virulence factors of *A. baumannii.* These can be related to protein secretion (21,22), biofilm formation (23,24), capsule formation (5,25), lipopolysaccharide (LPS) biosynthesis (5,24), and metal acquisition (24,26,27). In addition, there are several other important features that contribute to the virulence of *A. baumannii*, such as quorum sensing (24,28), the formation of outer membrane vesicles (OMVs) (29–31), factors related to the cell membrane (24,32,33), and adhesion (24,34). The so-called SOS response to DNA-damaging stresses must also be considered as a virulence determinant, because it facilitates bacterial adaptation by inducing mutations when environmental stresses are sensed (35,36).

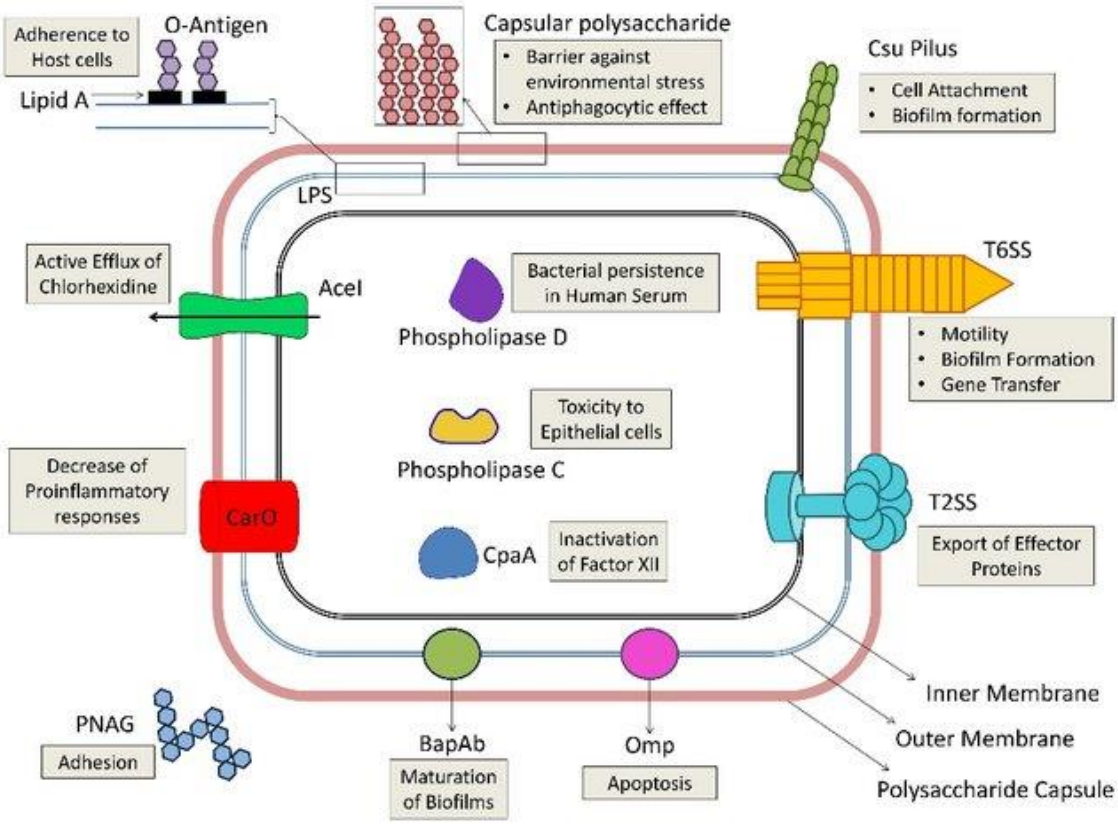


Figure 1.1 Schematic representation of the most relevant virulence factors associated with *A. baumannii*. AceI, *Acinetobacter* chlorhexidine efflux protein; BapAb, biofilm-associated protein of *A. baumannii*; CarO, carbapenem susceptibility porin; CpaA, glycan-specific adamalysin-like protease; Csu, chaperon/usher pilus system; LPS, lipopolysaccharide; Omp, outer membrane

protein; PNAG, poly-β-1,6-N-acetylglucosamine; T2SS, type II secretion system; T6SS, type VI secretion system. Adapted from (20).

1.1.1.1. Outer membrane proteins

Outer membrane proteins (OMPs) are mostly β-barrel-shaped proteins that are localized in the Gram-negative bacterial outer membrane. These proteins are worrisome virulence factors. In *A. baumanni* OMPs are involved in bacterial attachment for biofilm formation, host colonization, induction of host cell apoptosis, chemical compound diffusion, antibiotic resistance, as well as pH and salt tolerance (11,37–41). The outer membrane protein A (OmpA) is one of the most abundant porins in the outer membrane of *A. baumannii*. Besides being involved in host cell adhesion, invasion, and apoptosis, OmpA can also be involved in antibiotic resistance (33,37,39). Naturally, this OMP is present in secreted outer membrane vesicles in high amounts, thereby increasing the pathogenicity of *A. baumannii* (37).

Another important OMP is the carbapenem susceptibility porin (CarO). This OMP mediates the uptake of the amino acids glycine and ornithine, and it has been implicated in carbapenem resistance (38,40,42). Glycine is an essential amino acid that, in excess, was shown to induce morphological changes in the outer membrane of bacteria, thereby enhancing bacterial membrane vesicle production (43). Additionally, CarO facilitates colonization, as was shown for a *carO* deletion strain in a mouse infection model (44). Furthermore, the outer membrane porin D (OprD) forms an outer membrane carboxylate channel (Occ). The Occ channel is involved in the transport of small molecules, such as amino acids, due to its small pore size (45). Moreover, OprD is associated with a hypervirulent *A. baumannii* phenotype, which is known to contribute to the development of antibiotic resistance due to its potential to facilitate the entry of antibiotics (46). In this respect, it is noteworthy that *A. baumannii* can modify its cell envelope permeability in response to environmental changes to enhance bacterial survival (47). Other OMPs such as OmpW and Omp33-36 were shown to be involved in both antibiotic resistance and host cell colonization through their contributions to adhesion and invasion. Specifically, OmpW facilitates iron uptake, and it has a colistin-binding site (48). When this OMP is present in OMVs, it will serve as an antibiotic decoy to protect the host (48,49). Omp33-36, on the other hand, has been associated with host colonization through apoptosis induction and is implicated in carbapenem resistance, similar to the CarO porin (32,50). Lastly, the *A. baumannii* OMPs AbuO and DcaP are involved in pH and salt tolerance (51), and in the transport of phthalates (52), respectively. An AbuO *A. baumannii* mutant was shown to display increased sensitivity to high osmolarity and oxidative

stress, as well as to several antibiotics, proving its importance for bacterial fitness and virulence (51). DcaP was suggested to be involved in the uptake of certain β-lactamase inhibitors due to its preference for negatively charged molecules (52). Besides, the authors found DcaP to be the most abundant channel during host cell infection in mice, which might indicate a role in facilitating colonization.

1.1.1.2. Pili

Pili are structures that extrude from the bacterial surface, playing a critical role in biotic and abiotic surface attachment. In addition, they facilitate biofilm formation and motility, as well as conjugation. These structures can be divided into five different classes: 1) chaperone-usher pili; 2) type IV pili; 3) conjugative type IV secretion pili; 4) curli fibers; and 5) type V pili (53). Only the latter class was never found in *A. baumannii*. The chaperone/usher (Csu) gene cluster encodes the CsuA/B, CsuA, CsuB, and CsuE proteins, which are assembled by CsuC and CsuD into the actual pili system (54,55). This structure was recently unveiled by cryo-electron microscopy, showing a structure that differs from the structure of the classical type I pili. In *A. baumannii*, this structure displays a higher mechanical stability and superelasticity due to a clinch formation at the bacterial surface, which induces pilus secretion-improving adhesion (56). Type IV pili are small bacterial appendages composed of pilins that are assembled into helical fibers. These small structures are important for twitching motility, DNA uptake, and biofilm formation (57). They can be divided into three subtypes, namely Type IVa, type IVb, and type IVc. Type IVa is the most common subtype that is widely encountered in bacteria, whereas type IVb is present mostly in enteric bacteria. Type IVc pili are *Archaea*-derived, but they seem to be widely distributed in bacteria (58,59). The type IVa pilus protein PilA from *A. baumannii* was shown to favor twitching motility and biofilm formation (57) as well as DNA uptake (60). Similar to the pilus structures, curli fibers encoded by the *csgA* operon, facilitate surface adherence, host invasion, and colonization (61). These fibers may stimulate the immune response in the host, allowing the bacterial cells to disseminate deeper into tissues. Likewise, the curli fibers slow down clotting factors, thereby inducing sepsis (61). In *A. baumannii* the curli fibers were shown to be crucial for biofilm formation (62). The conjugative type IV secretion pili have a structure that makes contact with a recipient bacterial cell, which is needed for the exchange of genetic material, mostly in the form of plasmids. Therefore, this system has a critical role in HGT, facilitating the spread of antibiotic-resistance genes (63).

1.1.1.3. Capsule and LPS

The capsule is one of the most important virulence factors of *A. baumannii*. It consists of a highly variable group of packed oligosaccharide subunits forming a protective layer on the bacterial surface (64). This layer protects bacteria against the host immune system helping them to evade it. Moreover, it enhances antimicrobial resistance and facilitates desiccation resistance (25,64,65). Similarly, the LPS associated with the outer membrane is a major virulence factor, which is involved in serum resistance and colonization. Together with pili, the LPS also promotes adherence to host cells before colonization (66). LPS is composed of three structural domains, namely lipid A, the core oligosaccharide, and the O antigen. Lipid A has a hydrophobic character that prevents hydrophilic molecules from passing through the outer membrane. On the other hand, both the core oligosaccharide and the O antigen in LPS provide a hydrophilic structure that renders the outer membrane also impermeable to hydrophobic compounds (67).

1.1.1.4. Metal ion acquisition

Iron is an essential micronutrient for bacterial survival and in environments where its accessibility is limited, such as the human body, the effective acquisition of iron becomes critically important. Accordingly, *A. baumannii* has different metal acquisition systems that help to improve the respective micronutrient uptake. One way for this species to gain access to iron during infection is by secreting hemolytic proteins, such as phospholipase C, which disrupt erythrocytes and release the iron-rich hemoglobin (68). At least eight gene clusters encoding iron acquisition systems were thus far identified in *A. baumannii*. These systems are composed of a conserved ferrous iron acquisition system (*feoABC*), two heme uptake clusters (cluster 1 and cluster 2), and five siderophore biosynthesis clusters (69,70). Heme uptake cluster 1 consists of a TonB-dependent outer membrane receptor, a periplasmic heme-binding protein, and an inner membrane ATP-binding cassette. The heme uptake cluster 2 involves a TonB-dependent receptor, an extracytoplasmic function sigma factor and its anti-sigma factor, and a heme oxygenase (HemO). To import the free iron, the *A. baumannii* cells release a hemophore (HphA) which binds hemoglobin and collects free heme (69,70). After collecting the iron source, HphA transfers it to HphR, an outer membrane receptor that incorporates hemoglobin-bound iron into the cells. According to the literature, this heme uptake system is required for survival and/or dissemination of *A. baumannii* during pulmonary infection in a mouse model (71).

A. baumannii encodes for several siderophores that are responsible for gathering free iron from the environment. These iron chelators can be classified into acinetobactins, fimsbactins and

baumannoferrins (70). Acinetobactin is considered the major siderophore produced by *A. baumannii*. There are two known isomers, pre-acinetobactin or acoinetobactin, depending on the pH. The pre-acinetobactin is prevalent in acidic conditions and acinetobactin is prevalent in neutral/basic conditions (69). According to the literature, expression of this siderophore is required for a successful *A. baumannii* infection in different animal models (72,73). Both the baumannoferrins and fimsbactins do not seem to be required for virulence. Besides, fimsbactins are found in just a few *A. baumannii* genomes, which is in accordance with its lower significance for pathogenesis (70).

Transport of iron across the outer membrane to the periplasm is actively facilitated by the TonB-ExbB-ExbD complex. Three TonB-encoding genes were identified in *A. baumannii*, *tonB1*, *tonB2*, and *tonB3* (74). The iron-regulated *tonB3* gene is crucial for the survival of *A. baumannii* in iron-limiting conditions, as well as for virulence in different animal models (75,76). Furthermore, Feo is the main transport system for ferrous iron in Gram-negative bacteria, and the FeoAB proteins are well-conserved among *A. baumannii* (77). The FeoAB system is regulated by FeoC and composed of the cytoplasmic FeoA protein and the FeoB protein that facilitates active transport of ferrous iron across the cytoplasmic membrane (78). The relevance of this system is underscored by the observation that it is needed for growth of *A. baumannii* in human serum (75). Lastly, the intracellular iron-binding NfuA protein was also shown to be crucial for iron acquisition by contributing to the bacterial iron metabolism (79).

1.1.1.5. Protein secretion

Protein secretion allows bacterial cells to interact with the environment and other hosts through the release of several effectors. In particular, protein secretion can facilitate host colonization, adhesion to surfaces, or the killing of other bacterial cells. In *A. baumannii* the most important secretion systems are the Type I (T1SS), Type II (T2SS), Type IV (T4SS), Type V (T5SS), and Type VI (T6SS) systems (63). Figure 1.2 shows a schematic representation of each of these systems.

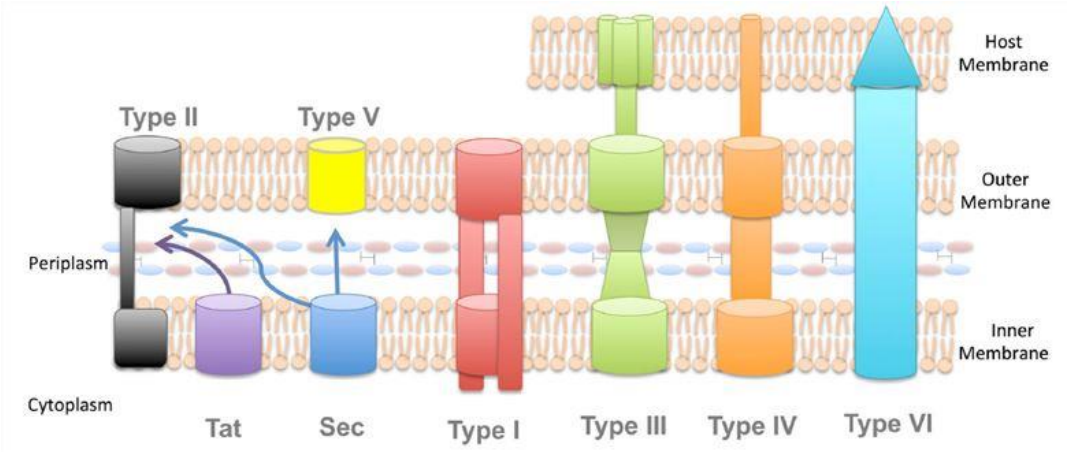


Figure 1.2. Schematic representation of different types of protein secretion systems encountered in Gram-negative bacteria. Note that the type III system has not been identified in *A. baumannii* (Adapted from (80)).

The T1SS is highly conserved in *A. baumannii.* It is composed of three proteins, namely TolC, HlyB, and HlyD. Together, these proteins form a channel through the bacterial membrane, facilitating the secretion of proteins from the cytoplasm to the environment, such as Repeats-in-Toxins (RTX) and biofilm-associated proteins (Bap). This system is implicated in bacterial adhesion and biofilm formation (63). The T2SS is a more complex system, composed of several proteins divided into four parts: an outer membrane complex, the periplasmic pseudopilus, an inner membrane complex, and a cytoplasmic ATPase. The T2SS secretes mostly degradative enzymes and toxins, such as lipases (LipA, LipH, LipAN), proteases (CpaA), and lipoproteins (InvL) that improve the fitness of *A. baumannii* in different environments (63). The T4SS can be subdivided into three different groups, namely IVA, IVB, and GI. This system is dedicated to the conjugation between cells. Additionally, group IVA can be further subdivided into the types F and P. In *A. baumannii* this system is not well characterized even though the F-type was shown to be encoded by the *tra* operon (63). The T5SS can be divided into five different subclasses, denoted Va to Ve. However, only the Vb and Vc subclasses were identified in *A. baumannii* (63). The T5SS is localized exclusively in the outer membrane. It is composed of three structural features, namely a signal sequence, an extracellular secreted passenger and a β-barrel transporter. Type Vb SSs, such as AbFhaB/FhaC or CdiA/CdiB, are involved in the bacterial attachment to host cells as well as biofilm formation. The Type Vc SS, such as the autotransporter Ata, is commonly encountered in clinical isolates, where it is critically associated with both biofilm formation and survival during infection *in vivo* (63). Lastly, the T6SS is the most complex system, since it forms a tubular structure within the cytoplasm. This system can be divided into three parts: a membrane complex (located in the

periplasm/outer membrane), a cytoplasmic baseplate, and a contractile tail tube. This tubular structure similar to a phage tube, can be extruded to make contact with other bacterial cells and to inject toxic effectors in order to outcompete competitors (63). This system was found to be highly prevalent in clinical isolates and multidrug-resistant strains, suggesting that it provides a competitive advantage over other pathogens (81,82). Besides, this system can also promote biofilm formation, and host colonization (81,83).

1.1.1.6. SOS response

The SOS response is a broadly conserved mechanism that allows bacteria to survive when DNA-damage is induced by ionizing radiation, ultraviolet (UV) light, or a mutagenic agent. Once DNA damage has occurred, the host activates a set of error-prone polymerases that will repair it. This repair will introduce several mutations improving the chances of bacterial survival (84). As a system that can lead to deleterious mutations, it needs to be activated only in a last-case scenario. To this end, *Escherichia coli* and most other bacteria utilize the RecA and LexA proteins (84). When DNA damage leads to an accumulation of single-stranded DNA fragments, they will bind to RecA. In the presence of nucleoside triphosphate, RecA then changes into its activated form, the RecA* nucleoprotein filament. Activated RecA* will interact with the LexA repressor protein that is bound to so-called SOS boxes. In the absence of DNA damage, the LexA binding to SOS boxes will keep the respective genes repressed. However, the interaction with RecA* triggers LexA self-cleavage, thereby lowering its DNA-binding affinity and releasing the repression exerted at the SOS box (84,85). The thereby induced SOS genes entail a wide variety of functions to counteract the effects of the DNA damage. These include genes related to DNA repair, homologous recombination, translesion DNA replication, cell division arrest, and others with an as yet unknown function (86,87). In addition, this mechanism can regulate genes related to virulence, fitness, or mobile genetic elements (88,89).

Interestingly, in *A. baumannii* the SOS system has not yet been fully characterized. Despite the similarities with SOS systems in other bacteria, it involves a different set of proteins to regulate it. Besides RecA, the *A. baumannii* SOS system is regulated by the UmuDAb and DdrR proteins, which work in a different way than was shown for other species (35,90–92). Here, RecA acts as a sensor for DNA damage and, as with LexA, the activated RecA* will interact with UmuDAb, thereby stimulating its self-cleavage (93). DdrR on the other hand, binds to UmuDAb to increase its DNA-binding affinity and to facilitate the repression of several SOS genes, such as the error-prone polymerases (91,92,94). The pair UmuDAb/DdrR and RecA regulate all SOS-related genes and

other, not DNA-damage-related genes, such as phage-encoded genes (92,95,96). As was shown for other bacterial species, RecA of *A. baumannii* can contribute to the resistance to desiccation, heat shock, and oxidative stress. Additionally, together with the error-prone polymerases it can induce specific mutations that increase genetic variability, leading to the emergence of antibiotic-resistant variants, as was shown for rifampicin resistance (97,98). Therefore, the SOS response can drive *A. baumannii* evolution, either through mutations and consequently the emergence of variants that are better adapted to particular environments, or by activating mobile genetic elements to stimulate genetic exchanges.

1.1.1.7. Other virulence factors and antibiotic resistance mechanisms

Other proteins and mechanisms, such as antibiotic degrading enzymes or efflux pumps, greatly contribute to bacterial virulence, mostly by promoting antimicrobial resistance. Virulence regulators, such as the BfmRS system, which regulate OmpW and pilus expression, are important for the virulence of *A. baumannii*. Another virulence factor commonly produced by this bacterium is the phospholipase D. This phospholipase plays an important role in virulence, as was shown in a *Galleria mellonella* infection model and a human lung epithelial cell invasion model (99). Furthermore, a variety of resistance mechanisms has been described for *A. baumannii*. These include the production of β-lactamases of the OXA (oxacilinases) and NDM (New Delhi Metallo-beta-lactamases) types (100–102), permeability defects caused by altered porin (OprD) characteristics (103,104), aminoglycoside modification by acetyltransferases, phosphotransferases or nucleotidyltransferases (105), target site alteration through penicillin-binding protein (PBP) modification (105,106), activation of efflux pumps such as AdeABC, AdeFGH, and Tet(A) (107–109), and others (110,111). Many of these mechanisms have been acquired from other bacteria through horizontal gene transfer.

1.1.2. Horizontal gene transfer and virulence spread among *A. baumannii*

Horizontal gene transfer (HGT) is considered one of the main evolutionary mechanisms that allow for a constant adaptation of microorganisms. There are four different mechanisms of gene transfer known, as shown in Figure 1.3: i) bacterial conjugation, ii) natural transformation, iii) genetic transfer through outer membrane vesicles (OMVs), and iv) transduction (112,113). These mechanisms mainly involve three molecular vehicles, namely plasmids, OMVs and phages.

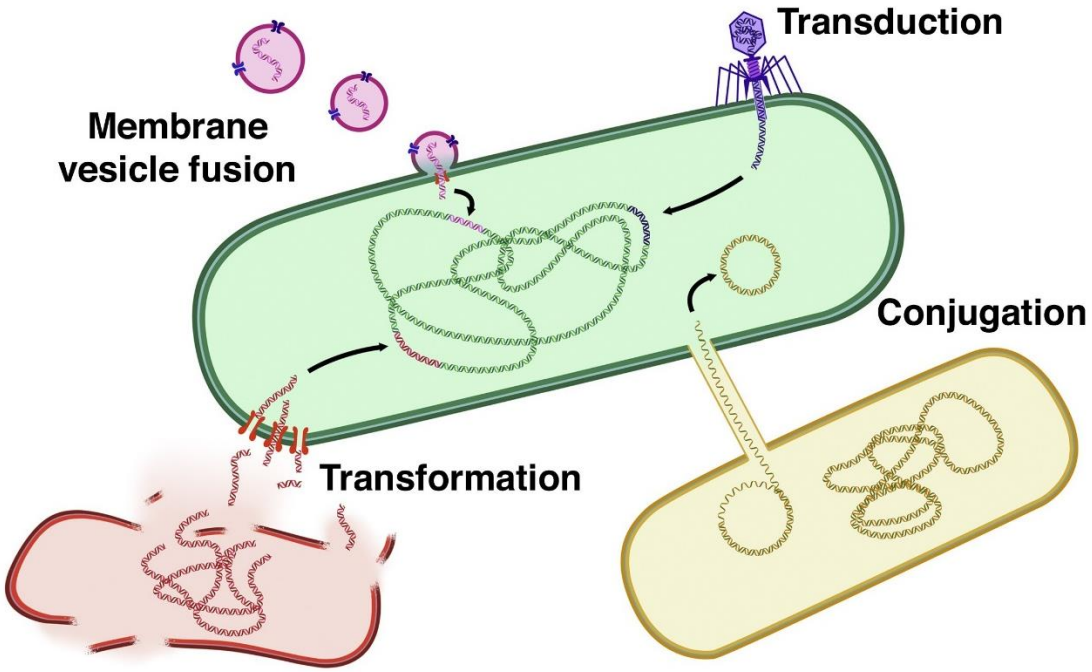


Figure 1.3. Mechanisms of horizontal gene transfer (HGT). HGT may take place through natural transformation, transduction, conjugation and OMV delivery. Adapted from (114).

Bacterial conjugation occurs when two cells exchange genetic material by direct cell-to-cell contact, and it is believed to be the major mechanism responsible for the spread of AMRs (112,115). This type of interaction occurs by transferring a mobile element, usually a plasmid, through a pilus to the recipient cell (T4SS). Natural transformation requires the so-called competence of the cell, meaning that it can bind and internalize DNA fragments from the environment and integrate them into its genome, through homologous recombination (116). HGT through OMVs occurs when OMVs are released by a bacterial cell with a certain cargo including DNA and subsequently absorbed by a neighboring cell. These vesicular structures are commonly excreted by Gram-negative bacteria and have been shown to transport different types of effectors (31,104,117–119). Lastly, transduction refers to phage-mediated gene transfer (Figure 1.4). It follows when bacterial DNA is packed into a phage and the released phage injects it into another cell (120). This mechanism of HGT can be subdivided into generalized, specialized, and lateral transduction (112,113). By acquiring external DNA from other bacteria, *A. baumannii* has increased its fitness, as exemplified by the acquisition of kanamycin resistance genes (121). Other reports showed the potential of this bacterium to acquire fragments from other species' genomes available in the environment. According to these studies, such fragments were related to mobile genetic elements, such as prophages and genes conferring resistance to antibiotics, such as

carbapenems, sulfonamides, aminoglycosides, and others (122,123). The most recent and relevant studies on HGT and antimicrobial resistance in *A. baumannii* are listed in Table 1.1.

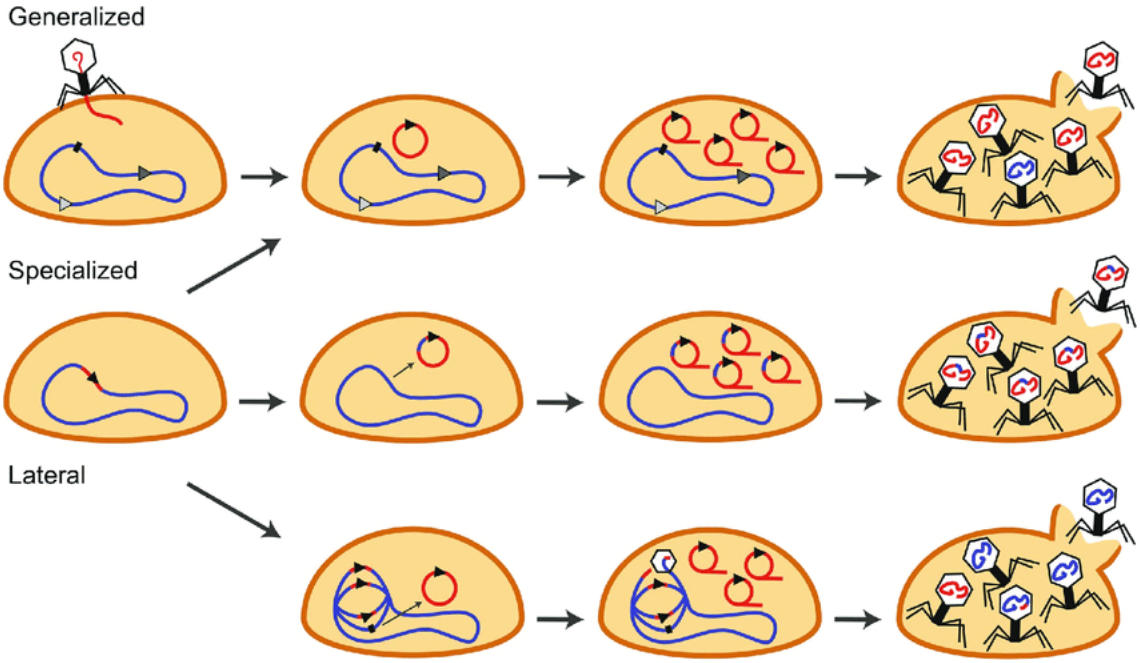


Figure 1.4. Graphical representation of horizontal gene transfer through generalized, specialized, and lateral transduction (Adapted from (124)).

Table 1.1. Overview of studies addressing HGT and the transfer of antimicrobial resistance (AMR) genes in *A. baumannii*

HGT	*A. Baumannii* Strains	AMR gene transferred	Resistances	Ref.
Natural transformation	A118	*sul1, qacEΔ1, aac(6')-Ib-cr, efflux pumps, bla_{TEM-1}, bla_{OXA-23}, strA, strB, aadA1, sat2, dfrA1*	Sulfonamides, quaternary ammonium compound (QAC), aminoglycosides, beta-lactams, streptothricins	(122)
	AYE, 27024	*bla_{OXA-23}*	Carbapenems	(123)
Transduction	R2090; CIP 70.10	*bla_{NDM-1}*	Carbapenems	(125)
	NU-60; ATCC 17978	*ArmA, GyrA-81-L*	Aminoglycosides, fluoroquinolones	(126)
Conjugation	SGH0823	*Tet(39), msr(E)-mph(E)*	Tetracycline, macrolides	(127)
	Ab242	*bla_{OXA-58}, aphA6*	Carbapenems, aminoglycosides	(128)
	597A	*mcr-4.3*	Colistin	(129)
	DETAB-P2	*bla_{OXA-58}, bla_{NDM-1}, ble_{MBL}, sul2, aac(3')-IId, tet(39), msr(E)-mph(E), mer, RND efflux systems*	Carbapenems, macrolides, sulfonamides, aminoglycosides, mercury	(130)
	ICU29; ICU40; Ab19; Ab40; Ab119	*sul2, aph(3')-Via, ant(2')-Ia, aadB*	Sulfonamides, aminoglycosides	(131)

	Ale9; Ale10; Ale18; Ale20; Ale21; Ale26	*bla*$_{PER-7}$, *bla*$_{OXA-23}$, *bla*$_{GES-like}$, *aph(3')-VIa, aac(6')-Lb, dfrA7, sul1, sul2, tet(B), mph(E)-msr(E), cmlA5, arr-2, strA, armA, strB, qacEΔ1*	β-lactams, aminoglycosides, sulfonamides, diaminopyrimidines, tetracyclines, macrolides, chloramphenicol, rifampicin, quaternary ammonium compound (QAC)	(132)
	CMUL CI107	*aacA1, aacC2, sul2, strA, strB, tetA(B)*	Aminoglycosides, sulfonamides, streptothricins, tetracyclines	(133)
	D36	*sul2, aphA1a, mer, aadB*	Sulfonamides, aminoglycosides, mercury	(134)
	E-072658	*mcr-4.7, sul2*	Colistin, sulfonamides	(135)
	CRAb1; CRAb2	*bla*$_{NDM-1}$, *bla*$_{OXA-23}$, *tet(x3), ant(2'')-Ia, aph(3'')-Ib, aph(3')-Ia, aph(6)-Id, ant(3'')-IIa, mph(E), msr(E), abaF*	Carbapenems, tetracyclines, aminoglycosides, macrolides	(136)
	XDR-AB; NDM-AB; AB364	*bla*$_{OXA-23}$, *bla*$_{PER-1}$, *aphA6*	Carbapenems, aminoglycosides	(29)
OMV-mediated	AbH12O-A2; AbH12O-CU3	*bla*$_{OXA-24}$	Carbapenems	(119)
	A_115	*bla*$_{NDM-1}$	Carbapenems	(31)

1.1.2.1. Plasmids

Plasmids are among the most common vehicles for gene transfer, which involves mostly antimicrobial resistance genes. This type of transmission can occur by conjugation or mobilization. Conjugative plasmids (CP) and integrative conjugative elements (ICE), encode the proteins needed for the DNA transfer, called the MOB module, and for mating pair formation, which are called the MPF module (137,138). The MOB module is composed of an origin of transfer (OriT), a relaxase (R), and a Type-IV coupling protein (T4CP). The MPF module, on the other hand, is formed by the T4SS that establishes the connection between two cells. Plasmids that lack the T4SS and only have the MOB module are called mobilizable plasmids and need a co-resident CP to be transmissible as depicted in Figure 1.5 (138). A plasmid that lacks both the MOB and MPF modules, harboring only their origin of vegetative replication (OriV), is considered non-mobilizable, and its transmission only occurs through transduction or transformation (138). The difference between a CP and an ICE is the ability of the CP to self-replicate due to the presence of a replication gene (*rep*), which is absent from an ICE (114,137). Antibiotic-resistance genes harbored by ICE are frequently surrounded by specific short DNA sequences, which are recognized by a new host's site-specific tyrosine recombinases XerC and XerD, leading to the integration of these elements within the genome, as was also shown for *A. baumannii* (128,139).

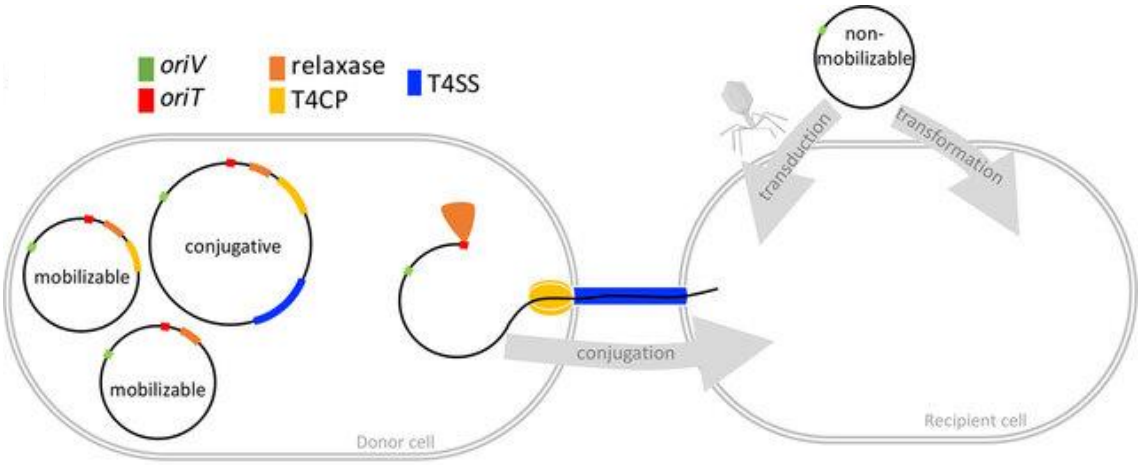


Figure 1.5. Schematic representation of plasmid mobilization through HGT. Conjugative and mobilizable plasmids can be transferred by conjugation. Non-mobilizable plasmids can only rely on either the transduction or transformation for their transfer to a new host cell (adapted from (140)).

In *A. baumannii* CPs allowed the dissemination of antimicrobial resistance genes that confer resistance to, for example, colistin (141), ticarcillin and kanamycin (29), and β-lactams (142,143). The most problematic resistances are those against β-lactams or polymyxins, such as colistin, which often represent the last resort treatments available (128,129,136,144,145). Besides, there are reports of tetracycline and macrolide resistance genes conferred by *A. baumannii* plasmids, as well as resistance genes against sulfonamides, chloramphenicol, colistin, and aminoglycosides (127–136,146). Furthermore, two carbapenem-resistant *A. baumannii* strains were recently isolated during a hospital outbreak that harbored a completely new CP, which encoded several antibiotic resistance genes, such as *tet(x3)*, and bla_{NDM-1} (136). This plasmid was probably acquired during the outbreak through HGT since it was not present in the first *A. baumannii* from the index patient and it was subsequently identified in different strains. Interestingly, some *A. baumannii* plasmids also harbor genes involved in the resistance to quaternary ammonium compounds, which are chemicals used in disinfectants to kill microorganisms (132). CPs may also incur certain fitness tradeoffs. For instance, some encode for regulators that repress a T6SS which, after plasmid loss, leads to the activation of the system that serves to outcompete other bacteria by secretion of a toxin (146). Elements to preserve CP maintenance can also code for toxin-antitoxin (TA) systems, that besides keeping the plasmid within the host, may help the host to survive in harsh environments (147). Recently, an extensive analysis of 450 complete *A. baumannii* genomes revealed a high prevalence of plasmids (80%). The authors found that there is a correlation between the type of plasmid and the type of genes encoded. For

instance, they observed a tendency for R1 plasmids (harboring replication gene Rep_1) to lack antimicrobial resistance genes, whereas R3 plasmids carry important genes that confer resistance (25.3%) to, for example, carbapenems and macrolides. Additionally, RP-type plasmids (encoding a repPriCT_1 gene) were found to be involved in the dissemination of both aminoglycoside and carbapenem resistance genes. Among plasmids with unknown replication genes, almost two-thirds harbored antimicrobial resistance genes and some of them were classified as CPs. In the end, it was concluded that carbapenemase genes were commonly carried by more than one type of plasmids (R3, RP, and without replication gene) (148).

1.1.2.2. Outer membrane vesicles

Outer membrane vesicles (OMVs) are spherical structures released into the environment by extrusion from the outer membrane of Gram-negative bacteria (119,149–153). As depicted in Figure 1.6, these structures are usually composed of the same layers as the bacterial surface, having an inner membrane, periplasm, and an outer membrane (154). OMVs can facilitate epithelial cell colonization, support adhesion and biofilm formation (30,37,155–157), disseminate quorum sensing or other effectors (158), transfer genetic material such as ARGs or mobile elements (159,160), and protect against stresses as imposed by antibiotics of different classes (161–164). Besides, due to the identical outer membrane composition between OMVs and their host, they can serve as decoys against bacteriophages that will attach and inject their DNA into the OMVs without affecting the host (118). Therefore, these vesicles are regarded as crucial virulence determinants that are also important for bacterial survival.

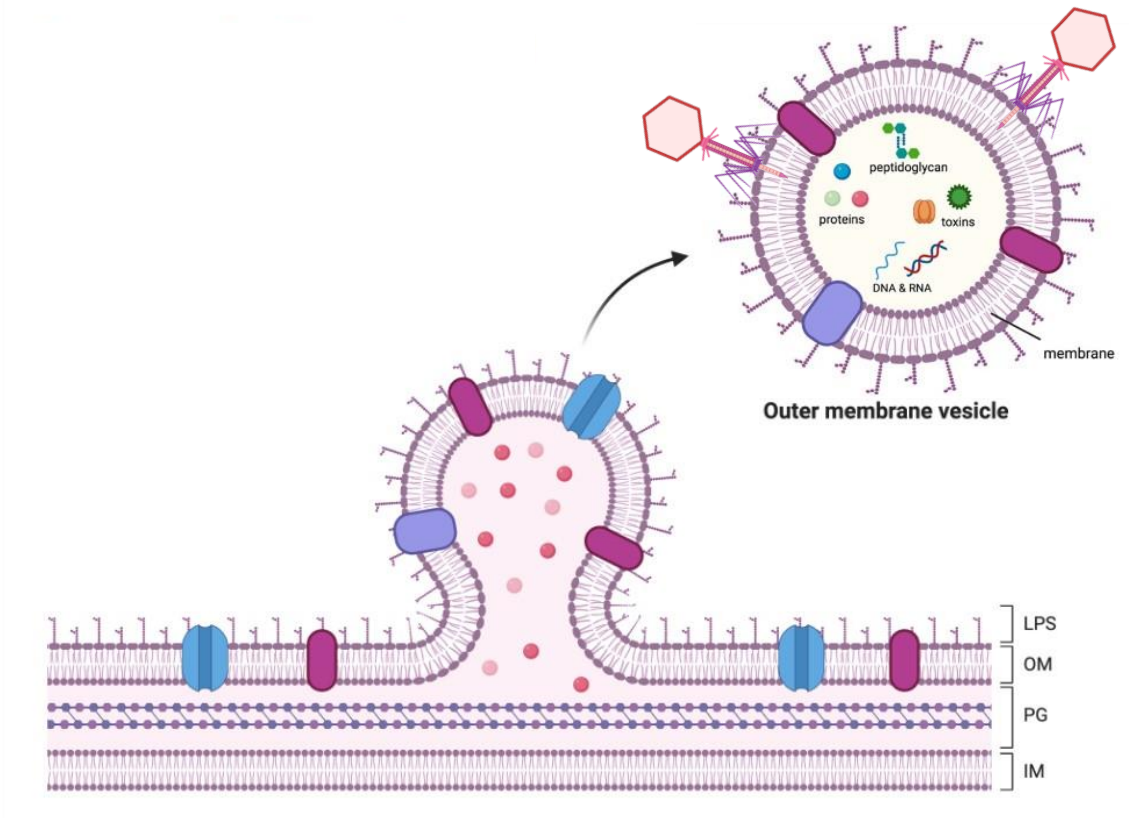


Figure 1.6. Graphical representation of outer membrane vesicle biogenesis. OMV structures are formed from the bacterial outer membrane. They can harbor different types of cargo, such as DNA, RNA, toxins, and other proteins, which will interact with other cells. OMVs can also protect bacteria against phages. IM, inner membrane; PG, peptidoglycan; OM, outer membrane; LPS, lipopolysaccharides (Adapted from Biorender).

OMVs can be considered as the 'swiss army knife' of Gram-negative bacteria. For instance, OMVs of *A. baumannii* were shown to have crucial roles in pathogenicity and the horizontal transfer of β-lactams resistance genes, like $bla_{\text{OXA-24}}$ and $bla_{\text{NDM-1}}$, to other cells, thereby rendering them antibiotic resistance. Thus, OMVs contribute to the resistance spread in *A. baumannii* (31,119). Unfortunately, there is still much information lacking on the OMV-mediated genetic exchange by this pathogen. In addition to DNA, OMVs were shown to also carry virulence effectors both internally and in the outer membrane. For example, toxic polysaccharides were found to be enriched in these vesicles, thereby contributing to *A. baumannii*'s cytotoxicity, survival, and host colonization (17). Outer membrane proteins, like OmpA or Omp33, are usually highly represented in the *A. baumannii* OMVs to facilitate bacterial adhesion and host colonization (37,39,50). *A. baumannii* OMVs may also improve iron uptake with the aid of TonB transporters selectively enriched within their membranes (152). Furthermore, other bacterial species were shown to be protected against different classes of antibiotics such as β-lactams and polymyxins by the released OMVs of *A.*

baumannii strains (49,165,166). This protection is usually accomplished by either degrading/inactivating an antibiotic or by binding the antibiotic with specific receptors present in the membrane of the vesicles. Although the mechanisms by which OMVs are formed or how the DNA and protein cargo are selected still remain unknown, it has been shown how β-lactamases can be selectively enriched within the OMVs. In intact bacterial cells, these periplasmic enzymes are anchored to the outer membrane, and when an OMV is being formed, they are therefore selectively entrapped within the periplasm of these OMVs (166).

Owing to the variety of functions that OMVs have, they have been evaluated as potential vaccines to immunize patients against a specific pathogen, namely *A. baumannii,* and as nanoparticles for drug delivery (167–172). A study with engineered OMVs was performed using modified OMVs produced in *E. coli*, which contained the most abundant *A. baumannii* outer membrane protein OmpA. These engineered OMVs were administrated to mice that were thus successfully immunized against *A. baumannii* (170). Another report used purified OMVs from *A. baumannii* to directly immunize mice, and the results showed a rapid production of IgGs reaching high levels for a long time. This successful immunization protected the mice against *A. baumannii* infection and reduced the bacterial burden in several tissues (173). Following this report, as the authors observed a high production of anti-OMV antibodies, they used immunization to produce and collect polyclonal antibodies. These antibodies, together with antibiotics, were then applied *in vitro* to treat *A. baumannii* cells. This innovative experimental approach resulted in a more efficient antibiotic therapy due to the cell aggregation caused by the antibodies, allowing the antibiotic to reach cells rapidly and in high intracellular concentrations (172). Regarding the possibility of drug delivery through OMVs, a report in which an *A. baumannii* strain was treated with an antibiotic, showed an increased OMV production and an increase in the number of proteins harbored by the OMVs. However, the most interesting result was the presence of the antibiotic within the released OMVs, which actually improved the drug stability (168). Following this, the authors isolated the different antibiotic-loaded vesicles and assessed the bacterial killing efficacy of these structures against different species such as *E. coli*, *P. aeruginosa*, and *K. pneumoniae*. All bacteria were eradicated by the antibiotic-loaded OMVs, showing that they could be used to increase drug efficacy (168).

1.1.2.3. Prophages

Prophages result from the lysogenic cycle of a temperate phage upon infecting a susceptible host (Figure 1.7). These temperate phages can then opt for a lytic life cycle, like virulent

phages, replicating into several phage particles that are released to the environment at the end of the cycle, or they can opt for a lysogenic life cycle by integrating their DNA into the host genome. Once their DNA is integrated into the host genome, the phages are referred to as prophages. Prophages can remain in a dormant state until an external stimulus induces them to excise from the host genome and enter the lytic pathway, thereby lysing the host cell releasing new phage particles. These new virions will search and infect a new host cell and, eventually, integrate into its genome (174). A cell that carries prophages in its DNA is called a lysogen, which is usually immune to superinfection by the same phage.

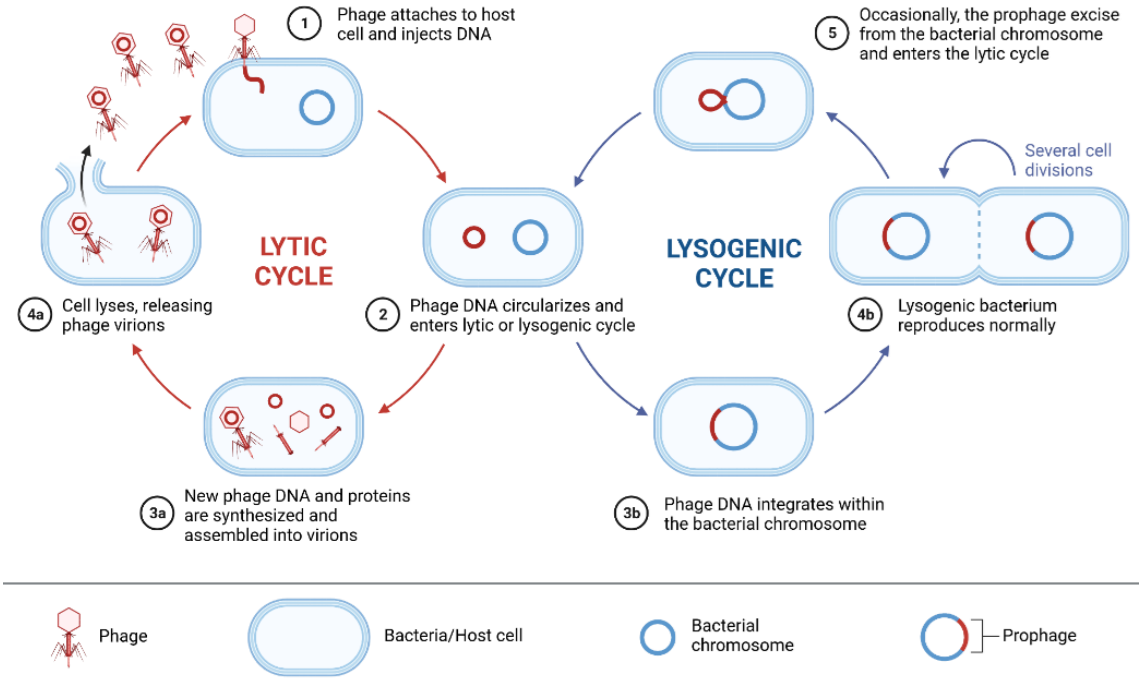


Figure 1.7. Graphical representation of the bacteriophage lytic and lysogenic cycles (Adapted from Biorender).

If an infective phage does not integrate into the host DNA and starts the replication process, it can create so-called transducing particles. These particles are released at the end of the lytic cycle and will infect a new host. This mechanism is called generalized transduction (120). During the production of mature phages, some transducing particles are formed by packaging bacterial DNA into the procapsids, with or without viral DNA. This occurs due to an error in the packaging system. To process the DNA into the capsids, a phage-specific packaging site is recognized by a small terminase that will form hetero-oligomers with a large terminase. Depending on which type of terminase is acting, it can make a nonspecific cut (pac-type) after the capsid capacity is reached,

or it can require a second *cos* site to cleave in a precise and specific way (cos-type) (113). Usually, these transducing particles can infect a new host without replication due to the absence or defectiveness of viral DNA. On the other hand, specialized transduction can only be performed by prophages. This mechanism relates to an abnormal excision event where the prophage DNA 'pulls' bacterial genes, which are adjacent to the integration site of the prophage, into the nascent phage (120). A recent study reported a new type of transduction called lateral transduction (113). This mechanism was discovered during the study of an *S. aureus* prophage that does not excise during its DNA replication. Instead, prophage DNA replication occurs while remaining integrated, resulting in the generation of several copies. Subsequently, some of this phage DNA is excised to continue the lytic cycle. However, this process is erratic and creates capsids with prophage DNA, with a mixture of prophage DNA and host DNA, or with host DNA only (113). Since it was first reported, this phenomenon has been described also for other phages and mobile elements, such as the so-called pathogenicity islands (175–177).

There are many reports showing transduction events with different phages and bacterial species (120). Regarding *A. baumannii,* there are examples of the transfer of antimicrobial resistance genes through generalized transduction, but there is still a significant knowledge gap about such transduction events (125,126). The first *A. baumannii* transducing phage was reported in 1973 by Herman and Juni (178). At that time, the authors isolated a temperate phage that was able to perform generalized transduction by converting the mutant host (an auxotroph of the donor strain) into the wild-type through transfer of the essential allele (178). Following Herman and Juni's findings, it was shown that *A. baumannii* prophages could transfer also antimicrobial resistance genes, such as bla_{NDM-1} (β-lactam resistance) (125), *armA* (aminoglycoside resistance) (126), and *gyrA-81L* (nalidixic acid resistance) (126). These genetic transfers increased the virulence of previously susceptible strains through generalized transduction, agreeing with observations on other bacterial species (179–181).

While lysogenic, prophages establish a symbiotic relationship with the host through the expression of virulence/fitness-related phage-encoded genes. This interaction improves the survival chances of both the phage and the host, and they are under the control of specific host regulators (120). According to the literature, prophages account on average for about 7% of the *A. baumannii* genome (182–186). Most of these studies also demonstrated that *A. baumannii* prophages could harbor a significant number of antimicrobial resistance- and virulence-related genes that can increase this species' pathogenicity. These include genes for antibiotic-degrading enzymes and

efflux pumps (185–188), a phosphoethanolamine transferase associated with polymyxin resistance (189), and other genes for a zinc-dependent hydrolase, or diacylglycerol kinase (190). Besides, there are a few detected prophage genes encoding membrane-associated proteins that could increase bacterial fitness, such as a fimbrial usher protein, lipoproteins, and adhesins. Lastly, prophages were found to encode transporters that can facilitate iron acquisition and resistance to toxic compounds, or genes for UmuD (98) and the RTX toxin (186) that can increase bacterial persistence.

Prophages were also found to be integrated in *A. baumannii* plasmids, which can increase their mobility or induce recombination events (183,191). The possibility of integration of prophages into plasmids would allow for increased mobility even across different species. Indeed, it was recently shown that such prophage-containing plasmids, called phage-plasmids (PPs), represent between 5 to 7% of all sequenced plasmids and phages (191). PPs can propagate through viral particles, as normal phages, or vertically as regular plasmids during the cell cycle. Curiously, *Acinetobacter* has small subgroups of associated PPs with most of them found only in *A. baumannii*, a fact that may contribute to this species' clinical relevance (191).

Integrated prophages are also subjected to genetic pressures from the host that may lead to the inactivation of crucial genes for phage replication. These mutations can result in defective prophages, in a process called pervasive domestication (120,192). This process allows bacteria to inactivate the prophages, thereby inhibiting their lytic capabilities and keeping genes that may improve fitness and virulence. Therefore, despite being defective, these prophages can still influence the bacterial behavior. A well-known mechanism by which prophages are regulated is the SOS response, that regulates prophage induction. In general, prophage induction relies on a balance between two main repressors, CI and Cro. While the first ensures the repression of lytic genes, the second causes repression of CI and, consequently, the derepression of the lytic genes. This allows a prophage to switch to the lytic cycle and start replicating. The CI repressor has a similar active site as LexA. Thus, when RecA is activated, it will also cause the self-cleavage of CI, which derepresses Cro and activates the lytic cycle (193). Since the SOS response in *A. baumannii* differs from that of other bacterial species, such as *E. coli*, the precise way in which prophage induction is regulated in *A. baumannii* is also expected to differ from that in other species. Unfortunately, this mechanism is thus far unknown. Nevertheless, it has been demonstrated that the SOS response is also a prophage inducer in *A. baumannii* (95). This means that there must be an interaction depending on the RecA, UmuDAb, and/or DdrR proteins for prophage induction to

occur. For instance, a recent study showed that DdrR could also bind a prophage repressor of an *A. baumannii* strain. Furthermore, others showed that the expression of prophage genes was dependent on one of the three SOS regulators. However, no molecular or genomic characterization was made to further define these potential interactions (91,92,95,194).

1.2. Concluding remarks

The way *A. baumannii* emerged as a priority pathogen raises many questions on how an environmental non-pathogenic bacterial species evolved into one of the major threats for hospital environments. Multiple studies have revealed that the virulence of *A. baumannii* has seen an uptick, largely attributable to external factors. However, this species possesses several different intrinsic virulence factors that provide ways for it to survive and resist harsh environments, ultimately conducing to its persistence in clinical settings. External factors, such as mobile genetic elements, have contributed greatly to this pathogen's evolution. Particularly, plasmids and prophages have been shown to significantly contribute to pathogenicity by facilitating genetic exchanges, which increase the bacterial arsenal against antimicrobials. Similarly, OMVs were shown to represent critical virulence determinants as well, since they can act as virulence effectors vehicles for HGT or facilitators of infection and colonization. Despite the many studies on *A. baumannii* HGT that have so far been published, there is still missing information about the different elements involved. For instance, how both OMVs and prophages are influenced by the SOS response, or how the OMVs are formed and how the host selects their cargo. With the increase of *A. baumannii* virulence, it has become crucial to better understand these elements, so that this knowledge can be used for infection prevention or the development of targeted treatments against *A. baumannii*. In this respect, a promising example is the use of OMVs, either as vaccines or as nanoparticles for drug delivery.

1.3. REFERENCES

1. Brown ED, Wright GD. Antibacterial drug discovery in the resistance era. Nature. 2016;529(7586):336–43.
2. Rice LB. Federal Funding for the Study of Antimicrobial Resistance in Nosocomial Pathogens: No ESKAPE. J Infect Dis. 2008;197(8):1079–81.
3. Tacconelli E, Carrara E, Savoldi A, Harbarth S, Mendelson M, Monnet DL, *et al.* Discovery, research, and development of new antibiotics: the WHO priority list of antibiotic-resistant bacteria and tuberculosis. Lancet Infect Dis. 2018;18(3):318–27.
4. Peleg AY, Seifert H, Paterson DL. *Acinetobacter baumannii*: Emergence of a successful pathogen. Clin Microbiol Rev. 2008;21(3):538–82.
5. Harding CM, Hennon SW, Feldman MF. Uncovering the mechanisms of *Acinetobacter baumannii* virulence. Nat Rev Microbiol. 2018;
6. Chakravarty B. Genetic mechanisms of antibiotic resistance and virulence in *Acinetobacter baumannii*: background, challenges and future prospects. Mol Biol Rep. 2020 May 1;47(5):4037–46.
7. López-Rojas R, Jiménez-Mejías ME, Lepe JA, Pachón J. *Acinetobacter baumannii* resistant to colistin alters its antibiotic resistance profile: A case report from Spain. Journal of Infectious Diseases. 2011;204(7):1147–8.
8. Doi Y, Murray GL, Peleg AY. *Acinetobacter baumannii*: Evolution of antimicrobial resistance-treatment options. Semin Respir Crit Care Med. 2015;36(1):85–98.
9. Ayobami O, Willrich N, Harder T, Okeke IN, Eckmanns T, Markwart R. The incidence and prevalence of hospital-acquired (carbapenem-resistant) *Acinetobacter baumannii* in Europe, Eastern Mediterranean and Africa: a systematic review and meta-analysis. Emerg Microbes Infect. 2019;8(1):1747–59.
10. Yang S, Hua M, Liu X, Du C, Pu L, Xiang P, *et al.* Bacterial and fungal co-infections among COVID-19 patients in intensive care unit. Microbes Infect. 2021 May 1;23(4–5):104806.
11. Kyriakidis I, Vasileiou E, Pana ZD, Tragiannidis A. *Acinetobacter baumannii* Antibiotic Resistance Mechanisms. Pathogens 2021, Vol 10, Page 373. 2021 Mar 19;10(3):373.
12. Kröger C, Kary SC, Schauer K, Cameron ADS. Genetic regulation of virulence and antibiotic resistance in *Acinetobacter baumannii*. Genes (Basel). 2017;8(1).
13. Poirel L, Nordmann P. Carbapenem resistance in *Acinetobacter baumannii*: Mechanisms and epidemiology. Clinical Microbiology and Infection. 2006;12(9):826–36.
14. Roy S, Chowdhury G, Mukhopadhyay AK, Dutta S, Basu S. Convergence of Biofilm Formation and Antibiotic Resistance in *Acinetobacter baumannii* Infection. Front Med (Lausanne). 2022 Mar 24;9:793615.
15. Tackling drug-resistant infectious globally: Final report and recommendations the review on Antimicrobial resistance chaired by Jim O'Neill. 2016;
16. Lai CC, Chen SY, Ko WC, Hsueh PR. Increased antimicrobial resistance during the COVID-19 pandemic. Int J Antimicrob Agents. 2021 Apr 1;57(4):106324.
17. Lee CR, Lee JH, Park M, Park KS, Bae IK, Kim YB, *et al.* Biology of *Acinetobacter baumannii*: Pathogenesis, antibiotic resistance mechanisms, and prospective treatment options. Front Cell Infect Microbiol. 2017;7(MAR).
18. Roca I, Espinal P, Vila-Fanés X, Vila J. The *Acinetobacter baumannii* oxymoron: Commensal hospital dweller turned pan-drug-resistant menace. Front Microbiol. 2012 Apr 23;3(APR):18713.

19. Skariyachan S, Taskeen N, Ganta M, Venkata Krishna B. Recent perspectives on the virulent factors and treatment options for multidrug-resistant *Acinetobacter baumannii*. Crit Rev Microbiol. 2019;45(3):315–33.
20. Moubareck CA, Halat DH. Insights into *Acinetobacter baumannii*: A Review of Microbiological, Virulence, and Resistance Traits in a Threatening Nosocomial Pathogen. Antibiotics 2020, Vol 9, Page 119. 2020 Mar 12;9(3):119.
21. Harding CM, Kinsella RL, Palmer LD, Skaar EP, Feldman MF. Medically Relevant *Acinetobacter* Species Require a Type II Secretion System and Specific Membrane-Associated Chaperones for the Export of Multiple Substrates and Full Virulence. PLoS Pathog. 2016;
22. Harding CM, Pulido MR, Di Venanzio G, Kinsella RL, Webb AI, Scott NE, *et al.* Pathogenic *Acinetobacter* species have a functional type i secretion system and contact-dependent inhibition systems. Journal of Biological Chemistry. 2017;
23. Di Domenico EG, Farulla I, Prignano G, Gallo MT, Vespaziani M, Cavallo I, *et al.* Biofilm is a major virulence determinant in bacterial colonization of chronic skin ulcers independently from the multidrug resistant phenotype. Int J Mol Sci. 2017;
24. Vijayashree Priyadharsini J, Smiline Girija AS, Paramasivam A. In silico analysis of virulence genes in an emerging dental pathogen *A. baumannii* and related species. Arch Oral Biol. 2018;94(June):93–8.
25. Geisinger E, Isberg RR. Antibiotic Modulation of Capsular Exopolysaccharide and Virulence in *Acinetobacter baumannii*. PLoS Pathog. 2015;
26. Juttukonda LJ, Chazin WJ, Skaar EP. *Acinetobacter baumannii* coordinates urea metabolism with metal import to resist host-mediated metal limitation. mBio. 2016;
27. Nairn BL, Lonergan ZR, Wang J, Braymer JJ, Zhang Y, Calcutt MW, *et al.* The Response of *Acinetobacter baumannii* to Zinc Starvation. Cell Host Microbe. 2016;
28. López M, Mayer C, Fernández-García L, Blasco L, Muras A, Ruiz FM, *et al.* Quorum sensing network in clinical strains of *A. baumannii*: AidA is a new quorum quenching enzyme. PLoS One. 2017;
29. Leungtongkam U, Thummeepak R, Tasanapak K, Sitthisak S. Acquisition and transfer of antibiotic resistance genes in association with conjugative plasmid or class 1 integrons of *Acinetobacter baumannii*. PLoS One. 2018;13(12):1–12.
30. Jha C, Ghosh S, Gautam V, Malhotra P, Ray P. In vitro study of virulence potential of *Acinetobacter baumannii* outer membrane vesicles. Microb Pathog. 2017;111:218–24.
31. Chatterjee S, Mondal A, Mitra S, Basu S. *Acinetobacter baumannii* transfers the blaNDM-1 gene via outer membrane vesicles. Journal of Antimicrobial Chemotherapy. 2017 Aug 1;72(8):2201–7.
32. Novović K, Mihajlović S, Dinić M, Malešević M, Miljković M, Kojić M, *et al. Acinetobacter* spp. porin Omp33-36: Classification and transcriptional response to carbapenems and host cells. PLoS One. 2018;
33. Iyer R, Moussa SH, Durand-Réville TF, Tommasi R, Miller A. *Acinetobacter baumannii* OmpA Is a Selective Antibiotic Permeant Porin. ACS Infect Dis. 2018;
34. Pérez A, Merino M, Rumbo-Feal S, Álvarez-Fraga L, Vallejo JA, Beceiro A, *et al.* The FhaB/FhaC two-partner secretion system is involved in adhesion of *Acinetobacter baumannii* AbH12o-A2 strain. Virulence. 2017;8(6):959–74.
35. Geisinger E, Vargas-Cuebas G, Mortman NJ, Syal S, Dai Y, Wainwright EL, *et al.* The landscape of phenotypic and transcriptional responses to ciprofloxacin in *Acinetobacter baumannii*: Acquired resistance alleles modulate drug-induced sos response and prophage replication. mBio. 2019;10(3):1–19.

36. Jara LM, Cortés P, Bou G, Barbé J, Aranda J. Differential roles of antimicrobials in the acquisition of drug resistance through activation of the SOS response in *Acinetobacter baumannii*. Antimicrob Agents Chemother. 2015 Jul 1;59(7):4318–20.
37. Tiku V, Kofoed EM, Yan D, Kang J, Xu M, Reichelt M, *et al.* Outer membrane vesicles containing OmpA induce mitochondrial fragmentation to promote pathogenesis of *Acinetobacter baumannii*. Sci Rep. 2021 Dec 1;11(1).
38. Uppalapati SR, Sett A, Pathania R. The Outer Membrane Proteins OmpA, CarO, and OprD of *Acinetobacter baumannii* Confer a Two-Pronged Defense in Facilitating Its Success as a Potent Human Pathogen. Vol. 11, Frontiers in Microbiology. Frontiers Media S.A.; 2020.
39. Gaddy JA, Tomaras AP, Actis LA. The *Acinetobacter baumannii* 19606 OmpA protein plays a role in biofilm formation on abiotic surfaces and in the interaction of this pathogen with eukaryotic cells. Infect Immun. 2009;77(8):3150–60.
40. Zhu LJ, Chen XY, Hou PF. Mutation of CarO participates in drug resistance in imipenem-resistant *Acinetobacter baumannii*. J Clin Lab Anal. 2019 Oct 1;33(8):e22976.
41. Lei H, Yiyuan G, Yuqing L, Siyu Y, Shuyan Z, Sirui Z, *et al.* An Outer Membrane Protein YiaD Contributes to Adaptive Resistance of Meropenem in *Acinetobacter baumannii*. Microbiol Spectr. 2022 Apr 4;10(2):e00173-22.
42. Siroy A, Molle V, Lemaître-Guillier C, Vallenet D, Pestel-Caron M, Cozzone AJ, *et al.* Channel formation by CarO, the carbapenem resistance-associated outer membrane protein of *Acinetobacter baumannii*. Antimicrob Agents Chemother. 2005;49(12):4876–83.
43. Hirayama S, Nakao R. Glycine significantly enhances bacterial membrane vesicle production: a powerful approach for isolation of LPS-reduced membrane vesicles of probiotic Escherichia coli. Microb Biotechnol. 2020 Jul 1;13(4):1162–78.
44. Labrador-Herrera G, Pérez-Pulido AJ, Álvarez-Marín R, Casimiro-Soriguer CS, Cebrero-Cangueiro T, Morán-Barrio J, *et al.* Virulence role of the outer membrane protein CarO in carbapenem-resistant *Acinetobacter baumannii*. Virulence. 2020 Dec 31;11(1):1727–37.
45. Dupont M, Pagès JM, Lafitte D, Siroy A, Bollet C. Identification of an OprD homologue in *Acinetobacter baumannii*. J Proteome Res. 2005 Nov;4(6):2386–90.
46. Hua M, Liu J, Du P, Liu X, Li M, Wang H, *et al.* The novel outer membrane protein from OprD/Occ family is associated with hypervirulence of carbapenem-resistant *Acinetobacter baumannii* ST2/KL22. Virulence. 2021 Dec 31;12(1):1–11.
47. Asai S, Umezawa K, Iwashita H, Ohshima T, Ohashi M, Sasaki M, *et al.* An outbreak of blaOXA-51-like- and blaOXA-66-positive *Acinetobacter baumannii* ST208 in the emergency intensive care unit. J Med Microbiol. 2014 Nov 1;63(Pt 11):1517.
48. Catel-Ferreira M, Marti S, Guillon L, Jara L, Coadou G, Molle V, *et al.* The outer membrane porin OmpW of *Acinetobacter baumannii* is involved in iron uptake and colistin binding. FEBS Lett. 2016 Jan 1;590(2):224–31.
49. Park J, Kim M, Shin B, Kang M, Yang J, Lee TK, *et al.* A novel decoy strategy for polymyxin resistance in *Acinetobacter baumannii*. Elife. 2021 Jun 1;10.
50. Carlos R, María T, Esteban FM, Cruz SN, Micaela C, Elena S, *et al.* The *Acinetobacter baumannii* Omp33-36 Porin Is a Virulence Factor That Induces Apoptosis and Modulates Autophagy in Human Cells. Infect Immun. 2014 Oct 7;82(11):4666–80.
51. Bharathi SV, Vasanth V, Govindan R. AbuO, a TolC-Like Outer Membrane Protein of *Acinetobacter baumannii*, Is Involved in Antimicrobial and Oxidative Stress Resistance. Antimicrob Agents Chemother. 2015 Jan 27;59(2):1236–45.
52. Bhamidimarri SP, Zahn M, Prajapati JD, Schleberger C, Söderholm S, Hoover J, *et al.* A Multidisciplinary Approach toward Identification of Antibiotic Scaffolds for *Acinetobacter baumannii*. Structure. 2019 Feb 5;27(2):268-280.e6.

53. Hospenthal MK, Costa TRD, Waksman G. A comprehensive guide to pilus biogenesis in Gram-negative bacteria. Nat Rev Microbiol. 2017 Jun 1;15(6):365–79.
54. Tomaras AP, Dorsey CW, Edelmann RE, Actis L a. Attachment to and biofilm formation on abiotic surfaces by *Acinetobacter baumannii*: Involvement of a novel chaperone-usher pili assembly system. Microbiology (N Y). 2003;149(12):3473–84.
55. Eijkelkamp BA, Stroeher UH, Hassan KA, Paulsen IT, Brown MH. Comparative analysis of surface-exposed virulence factors of *Acinetobacter baumannii*. BMC Genomics. 2014 Nov 25;15(1):1–12.
56. Pakharukova N, Malmi H, Tuittila M, Dahlberg T, Ghosal D, Chang YW, *et al.* Archaic chaperone–usher pili self-secrete into superelastic zigzag springs. Nature. 2022 Sep 8;609(7926):335.
57. Ronish LA, Lillehoj E, Fields JK, Sundberg EJ, Piepenbrink KH. The structure of PilA from *Acinetobacter baumannii* AB5075 suggests a mechanism for functional specialization in *Acinetobacter* type IV pili. J Biol Chem. 2019 Jan 1;294(1):218.
58. Ellison CK, Kan J, Dillard RS, Kysela DT, Ducret A, Berne C, *et al.* Obstruction of pilus retraction stimulates bacterial surface sensing. Science (1979). 2017 Oct 27;358(6362):535–8.
59. Whitfield GB, Brun Y V. The type IVc pilus: just a Tad different. Curr Opin Microbiol. 2024 Jun 1;79:102468.
60. Vesel N, Blokesch M. Pilus production in *Acinetobacter baumannii* is growth phase dependent and essential for natural transformation. J Bacteriol. 2021 Apr;203(8).
61. Barnhart MM, Chapman MR. Curli biogenesis and function. Annu Rev Microbiol. 2006;60:131–47.
62. Saishree Anchana R, Smiline Girija AS, Gunasekaran S, Vijayashree Priyadharsini J. Detection of csgA gene in carbapenem-resistant *Acinetobacter baumannii* strains and targeting with Ocimum sanctum biocompounds. Iran J Basic Med Sci. 2021 May 1;24(5):690.
63. Li P, Zhang S, Wang J, Al-Shamiri MM, Han B, Chen Y, *et al.* Uncovering the Secretion Systems of *Acinetobacter baumannii*: Structures and Functions in Pathogenicity and Antibiotic Resistance. Antibiotics. 2023 Jan 17;12(2):195.
64. Singh JK, Adams FG, Brown MH. Diversity and Function of Capsular Polysaccharide in *Acinetobacter baumannii*. Front Microbiol. 2019;9.
65. Russo TA, Luke NR, Beanan JM, Olson R, Sauberan SL, MacDonald U, *et al.* The K1 capsular polysaccharide of *Acinetobacter baumannii* strain 307-0294 is a major virulence factor. Infect Immun. 2010;
66. Haseley SR, Pantophlet R, Brade L, Holst O, Brade H. Structural and Serological Characterisation of the O-Antigenic Polysaccharide of the Lipopolysaccharide from *Acinetobacter* Junii Strain 65. Eur J Biochem. 1997 Apr 1;245(2):477–81.
67. Bertani B, Ruiz N. Function and biogenesis of lipopolysaccharides. EcoSal Plus. 2018 Dec 31;8(1).
68. Fiester SE, Arivett BA, Schmidt RE, Beckett AC, Ticak T, Carrier M V., *et al.* Iron-Regulated phospholipase C Activity contributes to the cytolytic activity and virulence of *Acinetobacter baumannii*. PLoS One. 2016;
69. Sheldon JR, Skaar EP. *Acinetobacter baumannii* can use multiple siderophores for iron acquisition, but only acinetobactin is required for virulence. PLoS Pathog. 2020 Oct 19;16(10).
70. Cook-Libin S, Sykes EME, Kornelsen V, Kumar A. Iron Acquisition Mechanisms and Their Role in the Virulence of *Acinetobacter baumannii*. Infect Immun. 2022 Oct 1;90(10).

71. Bateman TJ, Shah M, Ho TP, Shin HE, Pan C, Harris G, *et al.* A Slam-dependent hemophore contributes to heme acquisition in the bacterial pathogen *Acinetobacter baumannii*. Nature Communications 2021 12:1. 2021 Nov 1;12(1):1–13.
72. Penwell WF, Arivett BA, Actis LA. The *Acinetobacter baumannii* entA Gene Located Outside the Acinetobactin Cluster Is Critical for Siderophore Production, Iron Acquisition and Virulence. PLoS One. 2012 May 3;7(5).
73. Gaddy JA, Actis LA, Arivett BA, Mcconnell MJ, Rafael LR, Pachón J. Role of Acinetobactin-mediated iron acquisition functions in the interaction of *Acinetobacter baumannii* strain ATCC 19606T with human lung epithelial cells, Galleria mellonella caterpillars, and mice. Infect Immun. 2012;
74. Zimbler DL, Arivett BA, Beckett AC, Menke SM, Actis LA. Functional features of TonB energy transduction systems of *Acinetobacter baumannii*. Infect Immun. 2013;81(9):3382–94.
75. Federica R, Valentina G, Emanuela F, Giordano R, Livia L, Massimiliano L, *et al.* Contribution of Active Iron Uptake to *Acinetobacter baumannii* Pathogenicity. Infect Immun. 2019 Mar 25;87(4):10.1128/iai.00755-18.
76. Eijkelkamp BA, Hassan KA, Paulsen IT, Brown MH. Investigation of the human pathogen *Acinetobacter baumannii* under iron limiting conditions. BMC Genomics. 2011 Feb 23;12(1):1–14.
77. Antunes LCS, Imperi F, Towner KJ, Visca P. Genome-assisted identification of putative iron-utilization genes in *Acinetobacter baumannii* and their distribution among a genotypically diverse collection of clinical isolates. Res Microbiol. 2011 Apr 1;162(3):279–84.
78. Lau CKY, Krewulak KD, Vogel HJ. Bacterial ferrous iron transport: the Feo system. FEMS Microbiol Rev. 2016 Mar 1;40(2):273–98.
79. Zimbler DL, Park TM, Arivett BA, Penwell WF, Greer SM, Woodruff TM, *et al.* Stress response and virulence functions of the *Acinetobacter baumannii* NfuA Fe-S scaffold protein. J Bacteriol. 2012;
80. R GE, Joan M. Bacterial Secretion Systems: An Overview. Microbiol Spectr. 2016 Feb 26;4(1):10.1128/microbiolspec.vmbf-0012–2015.
81. Repizo GD, Gagné S, Foucault-Grunenwald ML, Borges V, Charpentier X, Limansky AS, *et al.* Differential Role of the T6SS in *Acinetobacter baumannii* Virulence. PLoS One. 2015 Sep 24;10(9):e0138265.
82. Dong JF, Liu CW, Wang P, Li L, Zou QH. The type VI secretion system in *Acinetobacter baumannii* clinical isolates and its roles in antimicrobial resistance acquisition. Microb Pathog. 2022 Aug 1;169:105668.
83. Kim J, Lee JY, Lee H, Choi JY, Kim DH, Wi YM, *et al.* Microbiological features and clinical impact of the type VI secretion system (T6SS) in *Acinetobacter baumannii* isolates causing bacteremia. Virulence. 2017 Oct 3;8(7):1378–89.
84. Sassanfar M, Roberts JW. Nature of the SOS-inducing signal in Escherichia coli. The involvement of DNA replication. J Mol Biol. 1990 Mar 5;212(1):79–96.
85. Little JW, Mount DW. The SOS regulatory system of Escherichia coli. Cell. 1982 May 1;29(1):11–22.
86. Fernández De Henestrosa AR, Ogi T, Aoyagi S, Chafin D, Hayes JJ, Ohmori H, *et al.* Identification of additional genes belonging to the LexA regulon in Escherichia coli. Mol Microbiol. 2000;35(6):1560–72.
87. Courcelle J, Khodursky A, Peter B, Brown PO, Hanawalt PC. Comparative Gene Expression Profiles Following UV Exposure in Wild-Type and SOS-Deficient *Escherichia coli*. Genetics. 2001 May 1;158(1):41–64.

88. Kelley WL. Lex marks the spot: the virulent side of SOS and a closer look at the LexA regulon. Mol Microbiol. 2006 Dec;62(5):1228–38.
89. Hochschild A, Lewis M. The bacteriophage lambda CI protein finds an asymmetric solution. Curr Opin Struct Biol. 2009 Feb;19(1):79–86.
90. Aranda J, Poza M, Shingu-Vázquez M, Cortés P, Boyce JD, Adler B, *et al.* Identification of a DNA-Damage-Inducible regulon in *Acinetobacter baumannii*. J Bacteriol. 2013;195(24):5577–82.
91. Pavlin A, Bajc G, Fornelos N, Browning DF, Butala M. The Small DdrR Protein Directly Interacts with the UmuDAb Regulator of the Mutagenic DNA Damage Response in *Acinetobacter baumannii*. J Bacteriol. 2022 Mar 1;204(3).
92. Cook D, Flannigan MD, Candra BV, Compton KD, Hare JM. The DdrR Coregulator of the *Acinetobacter baumannii* Mutagenic DNA Damage Response Potentiates UmuDAb Repression of Error-Prone Polymerases. J Bacteriol. 2022 Oct 4;204(11):e00165-22.
93. Hare JM, Adhikari S, Lambert K V., Hare AE, Grice AN. The *Acinetobacter* regulatory UmuDAb protein cleaves in response to DNA damage with chimeric LexA/UmuD characteristics. FEMS Microbiol Lett. 2012 Sep;334(1):57–65.
94. Cook D, Carrington J, Johnson K, Hare J. Homodimerization and heterodimerization requirements of *Acinetobacter baumannii* sos response coregulators umudab and ddrr revealed by two-hybrid analyses. Can J Microbiol. 2021;67(5):358–71.
95. Hare JM, Ferrell JC, Witkowski TA, Grice AN. Prophage induction and differential RecA and UmuDAb transcriptome regulation in the DNA damage responses of *Acinetobacter baumannii* and *Acinetobacter baylyi*. PLoS One. 2014 Apr 7;9(4).
96. Peterson MA, Grice AN, Hare JM. A corepressor participates in LexA-independent regulation of error-prone polymerases in *Acinetobacter*. Microbiology (Reading). 2020 Feb 1;166(2):212–26.
97. Aranda J, Bardina C, Beceiro A, Rumbo S, Cabral MP, Barbé J, *et al. Acinetobacter baumannii* reca protein in repair of DNA damage, antimicrobial resistance, general stress response, and virulence. J Bacteriol. 2011 Aug;193(15):3740–7.
98. Norton MD, Spilkia AJ, Godoy VG. Antibiotic resistance acquired through a DNA damage-inducible response in *Acinetobacter baumannii*. J Bacteriol. 2013 Mar;195(6):1335–45.
99. Stahl J, Bergmann H, Göttig S, Ebersberger I, Averhoff B. *Acinetobacter baumannii* virulence is mediated by the concerted action of three phospholipases D. PLoS One. 2015;
100. Voulgari E, Politi L, Pitiriga V, Dendrinos J, Poulou A, Georgiadis G, *et al.* First report of an NDM-1 metallo-beta-lactamase-producing *Acinetobacter baumannii* clinical isolate in Greece. Vol. 48, International journal of antimicrobial agents. Netherlands; 2016. p. 761–2.
101. Kumar M. Identification of a Novel NDM Variant, blaNDM-3, From a Multidrug-Resistant *Acinetobacter baumannii*. Vol. 37, Infection control and hospital epidemiology. United States; 2016. p. 747–8.
102. Gonzalez-Villoria AM, Tamayo-Legorreta E, Garza-Ramos U, Barrios H, Sanchez-Pérez A, Rodríguez-Medina N, *et al.* A multicenter study in mexico finds *Acinetobacter baumannii* clinical isolates belonging to clonal complexes 636B (113B) and 92B harboring OXA-72, OXA-239, and OXA-469. Antimicrobial Agents and Chemotherapy. 2016.
103. Wu X, Chavez JD, Schweppe DK, Zheng C, Weisbrod CR, Eng JK, *et al.* In vivo protein interaction network analysis reveals porin-localized antibiotic inactivation in *Acinetobacter baumannii* strain AB5075. Nat Commun. 2016;

104. Jin JS, Kwon SO, Moon DC, Gurung M, Lee JH, Kim S Il, *et al. Acinetobacter baumannii* secretes cytotoxic outer membrane protein a via outer membrane vesicles. PLoS One. 2011;6(2).
105. Bakour S, Alsharapy SA, Touati A, Rolain JM. Characterization of *Acinetobacter baumannii* clinical isolates carrying blaOXA-23 carbapenemase and 16S rRNA methylase armA genes in Yemen. Microbial Drug Resistance. 2014;
106. Arroyo LA, Herrera CM, Fernandez L, Hankins J V., Trent MS, Hancock REW. The pmrCAB operon mediates polymyxin resistance in *Acinetobacter baumannii* ATCC 17978 and clinical isolates through phosphoethanolamine modification of lipid A. Antimicrob Agents Chemother. 2011;
107. Sun JR, Jeng WY, Perng CL, Yang YS, Soo PC, Chiang Y Sen, *et al.* Single amino acid substitution Gly186Val in AdeS restores tigecycline susceptibility of *Acinetobacter baumannii*. Journal of Antimicrobial Chemotherapy. 2016;
108. Sharma A, Sharma R, Bhattacharyya T, Bhando T, Pathania R. Fosfomycin resistance in *Acinetobacter baumannii* is mediated by efflux through a major facilitator superfamily (MFS) transporter-AbaF. Journal of Antimicrobial Chemotherapy. 2017;
109. Li L, Hassan KA, Brown MH, Paulsen IT. Rapid multiplexed phenotypic screening identifies drug resistance functions for three novel efflux pumps in *Acinetobacter baumannii*. Journal of Antimicrobial Chemotherapy. 2016;
110. Trebosc V, Gartenmann S, Royet K, Manfredi P, Tötzl M, Schellhorn B, *et al.* A novel genome-editing platform for drug-resistant *Acinetobacter baumannii* reveals an AdeR-unrelated tigecycline resistance mechanism. Antimicrob Agents Chemother. 2016;
111. Knight D, Dimitrova DD, Rudin SD, Bonomo RA, Rathera PN. Mutations decreasing intrinsic β-lactam resistance are linked to cell division in the nosocomial pathogen *Acinetobacter baumannii*. Antimicrob Agents Chemother. 2016;
112. Thomas CM, Nielsen KM. Mechanisms of, and barriers to, horizontal gene transfer between bacteria. Nat Rev Microbiol. 2005;3(9):711–21.
113. Chen J, Quiles-Puchalt N, Chiang YN, Bacigalupe R, Fillol-Salom A, Chee MSJ, *et al.* Genome hypermobility by lateral transduction. Science (1979). 2018 Oct 12;362(6411):207 LP – 212.
114. McInnes RS, McCallum GE, Lamberte LE, van Schaik W. Horizontal transfer of antibiotic resistance genes in the human gut microbiome. Curr Opin Microbiol. 2020 Feb 1;53:35–43.
115. Von Wintersdorff CJH, Penders J, Van Niekerk JM, Mills ND, Majumder S, Van Alphen LB, *et al.* Dissemination of antimicrobial resistance in microbial ecosystems through horizontal gene transfer. Frontiers in Microbiology. 2016.
116. Mell JC, Redfield RJ. Natural competence and the evolution of DNA uptake specificity. J Bacteriol. 2014;196(8):1471–83.
117. Domingues S, Nielsen KM. Membrane vesicles and horizontal gene transfer in prokaryotes. Curr Opin Microbiol. 2017;38:16–21.
118. Manning AJ, Kuehn MJ. Contribution of bacterial outer membrane vesicles to innate bacterial defense. BMC Microbiol. 2011;11.
119. Rumbo C, Fernández-Moreira E, Merino M, Poza M, Mendez JA, Soares NC, *et al.* Horizontal transfer of the OXA-24 carbapenemase gene via outer membrane vesicles: A new mechanism of dissemination of carbapenem resistance genes in *Acinetobacter baumannii*. Antimicrob Agents Chemother. 2011;55(7):3084–90.
120. Birge EA. Bacterial Bacteriophage and Genetics. 5th ed. Springer New York; 2006. XX, 578.

121. Wilharm G, Piesker J, Laue M, Skiebe E. DNA Uptake by the nosocomial pathogen *Acinetobacter baumannii* occurs during movement along wet surfaces. J Bacteriol. 2013;195(18):4146–53.
122. Traglia GM, Place K, Dotto C, Fernandez JS, Montaña S, Bahiense C dos S, *et al.* Interspecies DNA acquisition by a naturally competent *Acinetobacter baumannii* strain. Int J Antimicrob Agents. 2019;53(4):483–90.
123. Godeux AS, Svedholm E, Barreto S, Potron A, Venner S, Charpentier X, *et al.* Interbacterial Transfer of Carbapenem Resistance and Large Antibiotic Resistance Islands by Natural Transformation in Pathogenic *Acinetobacter*. mBio. 2022 Feb 1;13(1).
124. Chiang YN, Penadés JR, Chen J. Genetic transduction by phages and chromosomal islands: The new and noncanonical. PLoS Pathog. 2019;15(8):e1007878.
125. Krahn T, Wibberg D, Maus I, Winkler A, Bontron S, Sczyrba A, *et al.* Intraspecies transfer of the chromosomal *Acinetobacter baumannii* blaNDM-1 carbapenemase gene. Antimicrob Agents Chemother. 2016;60(5):3032–40.
126. Wachino J ichi, Jin W, Kimura K, Arakawa Y. Intercellular transfer of chromosomal antimicrobial resistance genes between *Acinetobacter baumannii* strains mediated by prophages. Antimicrob Agents Chemother. 2019;63(8):1–16.
127. Blackwell GA, Hall RM. The tet39 determinant and the msrE-mphE genes in *Acinetobacter* plasmids are each part of discrete modules flanked by inversely oriented pdif (XerC-XerD) sites. Antimicrob Agents Chemother. 2017 Aug 1;61(8).
128. Cameranesi MM, Morán-Barrio J, Limansky AS, Repizo GD, Viale AM. Site-Specific Recombination at XerC/D Sites Mediates the Formation and Resolution of Plasmid Co-integrates Carrying a blaOXA-58- and Tn aphA6-Resistance Module in *Acinetobacter baumannii*. Front Microbiol. 2018 Jan 26;9(JAN).
129. Martins-Sorenson N, Snesrud E, Xavier DE, Cacci LC, Iavarone AT, McGann P, *et al.* A novel plasmid-encoded mcr-4.3 gene in a colistin-resistant *Acinetobacter baumannii* clinical strain. Journal of Antimicrobial Chemotherapy. 2020 Jan 1;75(1):60–4.
130. Liu H, Moran RA, Chen Y, Doughty EL, Hua X, Jiang Y, *et al.* Transferable *Acinetobacter baumannii* plasmid pDETAB2 encodes OXA-58 and NDM-1 and represents a new class of antibiotic-resistance plasmids. Journal of Antimicrobial Chemotherapy. 2021 Apr 13;76(5):1130–4.
131. Ababneh Q, Al Sbei S, Jaradat Z, Syaj S, Aldaken N, Ababneh H, *et al.* Extensively drug-resistant *Acinetobacter baumannii*: role of conjugative plasmids in transferring resistance. PeerJ. 2023 Jan 25;11.
132. Sánchez-Urtaza S, Ocampo-Sosa A, Rodríguez-Grande J, El-Kholy MA, Shawky SM, Alkorta I, *et al.* Plasmid content of carbapenem-resistant *Acinetobacter baumannii* isolates belonging to five International Clones collected from hospitals of Alexandria, Egypt. Front Cell Infect Microbiol. 2023 Jan 9;13:1332736.
133. Rafei R, Koong J, Osman M, Atrouni A Al, Hamze M, Hamidian M. Analysis of pCI107 a large plasmid carried by an ST25 *Acinetobacter baumannii* strain reveals a complex evolutionary history and links to multiple antibiotic resistance and metabolic pathways. FEMS Microbes. 2022 Nov 25;3.
134. Hamidian M, Hall RM. Genetic structure of four plasmids found in *Acinetobacter baumannii* isolate D36 belonging to lineage 2 of global clone 1. PLoS One. 2018 Sep 1;13(9):e0204357.
135. Prity FT, Tobin LA, Maharajan R, Paulsen IT, Cain AK, Hamidian M. The evolutionary tale of eight novel plasmids in a colistin-resistant environmental *Acinetobacter baumannii* isolate. Microb Genom. 2023 May 12;9(5):001010.

136. Talsma DT, Monteiro R, Flores-Vallejo R del C, Heuvelmans M, Le TN, Hendrickx APA, *et al.* Nosocomial transmission of tet(x3), blaNDM-1, and blaOXA-97-carrying *Acinetobacter baumannii* conferring resistance to eravacycline and omadacycline, the Netherlands, March-August 2021. Eurosurveillance. 2024 Apr; Accepted for publication
137. Koraimann G, Wagner MA. Social behavior and decision making in bacterial conjugation. Front Cell Infect Microbiol. 2014;4(APR).
138. Smillie C, Garcillán-Barcia MP, Francia MV, Rocha EPC, de la Cruz F. Mobility of Plasmids. Microbiology and Molecular Biology Reviews. 2010 Sep;74(3):434–52.
139. Da Silva G, Domingues S. Insights on the Horizontal Gene Transfer of Carbapenemase Determinants in the Opportunistic Pathogen *Acinetobacter baumannii*. Microorganisms. 2016;4(3):29.
140. Kothari A, Wu YW, Chandonia JM, Charrier M, Rajeev L, Rocha AM, *et al.* Large circular plasmids from groundwater plasmidomes span multiple incompatibility groups and are enriched in multimetal resistance genes. mBio. 2019 Jan 1;10(1).
141. Ma F, Shen C, Zheng X, Liu Y, Chen H, Zhong L, *et al.* Identification of a novel plasmid carrying mcr-4.3 in an *Acinetobacter baumannii* strain in China. Antimicrob Agents Chemother. 2019;
142. Lee YT, Kuo SC, Chiang MC, Yang SP, Chen CP, Chen TL, *et al.* Emergence of carbapenem-resistant non-baumannii species of *Acinetobacter* harboring a blaOXA-51-like gene that is intrinsic to *A. baumannii*. Antimicrob Agents Chemother. 2012;
143. Liu K, Myers ARR, Pisithkul T, Claas KRR, Satyshur KAA, Amador-Noguez D, *et al.* Molecular Mechanism and Evolution of Guanylate Kinase Regulation by (p)ppGpp. Mol Cell. 2015 Oct 13;57(4):735–49.
144. Pagano M, Martins AF, Barth AL. Mobile genetic elements related to carbapenem resistance in *Acinetobacter baumannii*. Brazilian Journal of Microbiology. 2016;47(4):785–92.
145. Partridge SR, Kwong SM, Firth N, Jensen SO. Mobile genetic elements associated with antimicrobial resistance. Clin Microbiol Rev. 2018;31(4):1–61.
146. Weber BS, Ly PM, Irwin JN, Pukatzki S, Feldman MF. A multidrug resistance plasmid contains the molecular switch for type VI secretion in *Acinetobacter baumannii*. Proc Natl Acad Sci U S A. 2015 Jul 28;112(30):9442–7.
147. Armalyte J, Jurenas D, Krasauskas R, Čepauskas A, Sužiedeliene E. The higBA toxin-antitoxin module from the opportunistic pathogen *Acinetobacter baumannii* - Regulation, activity, and evolution. Front Microbiol. 2018 Apr 12;9(APR).
148. Lam MMC, Hamidian M. Examining the role of *Acinetobacter baumannii* plasmid types in disseminating antimicrobial resistance. npj Antimicrobials and Resistance 2024 2:1. 2024 Jan 5;2(1):1–10.
149. Li ZT, Zhang RL, Bi XG, Xu L, Fan M, Xie D, *et al.* Outer membrane vesicles isolated from two clinical *Acinetobacter baumannii* strains exhibit different toxicity and proteome characteristics. Microb Pathog. 2015 Apr 1;81:46–52.
150. Kwon SO, Gho YS, Lee JC, Kim S il. Proteome analysis of outer membrane vesicles from a clinical *Acinetobacter baumannii* isolate. FEMS Microbiol Lett. 2009 Aug;297(2):150–6.
151. Kesavan D, Vasudevan A, Wu L, Chen J, Su Z, Wang S, *et al.* Integrative analysis of outer membrane vesicles proteomics and whole-cell transcriptome analysis of eravacycline induced *Acinetobacter baumannii* strains. BMC Microbiol. 2020 Feb 11;20(1).
152. Dhurve G, Madikonda AK, Jagannadham MV, Siddavattam D. Outer Membrane Vesicles of *Acinetobacter baumannii* DS002 Are Selectively Enriched with TonB-Dependent Transporters and Play a Key Role in Iron Acquisition . Microbiol Spectr. 2022 Apr 27;10(2).

153. Agarwal B, Karthikeyan R, Gayathri P, RameshBabu B, Ahmed G, Jagannadham M v. Studies on the mechanism of multidrug resistance of *Acinetobacter baumannii* by proteomic analysis of the outer membrane vesicles of the bacterium. J Proteins Proteom. 2019 Mar;10(1):1–15.
154. Toyofuku M, Nomura N, Eberl L. Types and origins of bacterial membrane vesicles. Vol. 17, Nature Reviews Microbiology. Nature Publishing Group; 2019. p. 13–24.
155. Cañas MA, Fábrega MJ, Giménez R, Badia J, Baldomà L. Outer Membrane Vesicles From Probiotic and Commensal *Escherichia coli* Activate NOD1-Mediated Immune Responses in Intestinal Epithelial Cells. Front Microbiol. 2018;9.
156. Bielaszewska M, Marejková M, Bauwens A, Kunsmann-Prokscha L, Mellmann A, Karch H. Enterohemorrhagic *Escherichia coli* O157 outer membrane vesicles induce interleukin 8 production in human intestinal epithelial cells by signaling via Toll-like receptors TLR4 and TLR5 and activation of the nuclear factor NF-κB. International Journal of Medical Microbiology. 2018;308(7):882–9.
157. Thomas B, Stefanie S, Jana S, Martin von B, Frank S, Y WL, *et al.* Membrane Vesicle Formation as a Multiple-Stress Response Mechanism Enhances *Pseudomonas putida* DOT-T1E Cell Surface Hydrophobicity and Biofilm Formation. Appl Environ Microbiol. 2012 Sep 1;78(17):6217–24.
158. Mashburn LM, Whiteley M. Membrane vesicles traffic signals and facilitate group activities in a prokaryote. Nature. 2005;437(7057):422–5.
159. Marchant P, Carreño A, Vivanco E, Silva A, Nevermann J, Otero C, *et al.* "One for All": Functional Transfer of OMV-Mediated Polymyxin B Resistance From *Salmonella enterica* sv. *Typhi* ΔtolR and ΔdegS to Susceptible Bacteria. Front Microbiol. 2021 May 5;12.
160. Fulsundar S, Harms K, Flaten GE, Johnsen PJ, Chopade BA, Nielsen KM. Gene transfer potential of outer membrane vesicles of *Acinetobacter baylyi* and effects of stress on vesiculation. Appl Environ Microbiol. 2014;80(11):3469–83.
161. Kim SW, Park S Bin, Im SP, Lee JS, Jung JW, Gong TW, *et al.* Outer membrane vesicles from β-lactam-resistant *Escherichia coli* enable the survival of β-lactam-susceptible *E. coli* in the presence of β-lactam antibiotics. Sci Rep. 2018 Dec 1;8(1).
162. González LJ, Bahr G, Nakashige TG, Nolan EM, Bonomo RA, Vila AJ. Membrane anchoring stabilizes and favors secretion of New Delhi metallo-β-lactamase. Nat Chem Biol. 2016 Jul 1;12(7):516–22.
163. Lee J, Lee EY, Kim SH, Kim DK, Park KS, Kim KP, *et al.* Staphylococcus aureus extracellular vesicles carry biologically active β-lactamase. Antimicrob Agents Chemother. 2013 Jun;57(6):2589–95.
164. Aktar S, Okamoto Y, Ueno S, Tahara YO, Imaizumi M, Shintani M, *et al.* Incorporation of Plasmid DNA Into Bacterial Membrane Vesicles by Peptidoglycan Defects in *Escherichia coli*. Front Microbiol. 2021 Nov 29;12.
165. Martínez MMB, Bonomo RA, Vila AJ, Maffía PC, González LJ. On the Offensive: The Role of Outer Membrane Vesicles in the Successful Dissemination of New Delhi Metallo-b-lactamase (NDM-1). mBio. 2021 Oct 1;12(5).
166. López C, Prunotto A, Bahr G, Bonomo RA, González LJ, Peraro MD, *et al.* Specific Protein-Membrane Interactions Promote Packaging of Metallo-β-Lactamases into Outer Membrane Vesicles. Antimicrob Agents Chemother. 2021 Oct 1;65(10)
167. Jain S, Pillai J. Bacterial membrane vesicles as novel nanosystems for drug delivery. Int J Nanomedicine. 2017 Aug 29;12:6329–41.

168. Huang W, Zhang Q, Li W, Yuan M, Zhou J, Hua L, *et al.* Development of novel nanoantibiotics using an outer membrane vesicle-based drug efflux mechanism. Journal of Controlled Release. 2020 Jan 10;317:1–22.
169. Wang S, Gao J, Wang Z. Outer Membrane Vesicles (OMVs) for Vaccination and Targeted Drug Delivery. Wiley Interdiscip Rev Nanomed Nanobiotechnol. 2019 Mar 1;11(2):e1523.
170. Huang W, Wang S, Yao Y, Xia Y, Yang X, Li K, *et al.* Employing *Escherichia coli*-derived outer membrane vesicles as an antigen delivery platform elicits protective immunity against *Acinetobacter baumannii* infection. Scientific Reports 2016 6:1. 2016 Nov 16;6(1):1–12.
171. Ansari H, Tahmasebi-Birgani M, Bijanzadeh M, Doosti A, Kargar M. Study of the immunogenicity of outer membrane protein A (ompA) gene from *Acinetobacter baumannii* as DNA vaccine candidate in vivo. Iran J Basic Med Sci. 2019 Jun 1;22(6):669–75.
172. Huang W, Zhang Q, Li W, Chen Y, Shu C, Li Q, *et al.* Anti-outer membrane vesicle antibodies increase antibiotic sensitivity of pan-drug-resistant *Acinetobacter baumannii*. Front Microbiol. 2019 Jun 18;10(JUN):463576.
173. Huang W, Yao Y, Long Q, Yang X, Sun W, Liu C, *et al.* Immunization against Multidrug-Resistant *Acinetobacter baumannii* Effectively Protects Mice in both Pneumonia and Sepsis Models. PLoS One. 2014 Jun 23;9(6):e100727.
174. Davies E V., Winstanley C, Fothergill JL, James CE. The role of temperate bacteriophages in bacterial infection. FEMS Microbiol Lett. 2016;363(5):1–10.
175. Chee MSJ, Serrano E, Chiang YN, Harling-Lee J, Man R, Bacigalupe R, *et al.* Dual pathogenicity island transfer by piggybacking lateral transduction. Cell. 2023 Aug 3;186(16):3414-3426.e16.
176. Humphrey S, Fillol-Salom A, Quiles-Puchalt N, Ibarra-Chávez R, Haag AF, Chen J, *et al.* Bacterial chromosomal mobility via lateral transduction exceeds that of classical mobile genetic elements. Nature Communications 2021 12:1. 2021 Nov 8 ;12(1):1–13.
177. Fillol-Salom A, Bacigalupe R, Humphrey S, Chiang YN, Chen J, Penadés JR. Lateral transduction is inherent to the life cycle of the archetypical *Salmonella* phage P22. Nature Communications 2021 12:1. 2021 Nov 8;12(1):1–12.
178. Herman NJ, Juni E. Isolation and Characterization of a Generalized Transducing Bacteriophage for *Acinetobacter*. J Virol. 1974;13(1):46–52.
179. Brown-Jaque M, Oyarzun LR, Cornejo-Sánchez T, Martín-Gómez MT, Gartner S, de Gracia J, *et al.* Detection of bacteriophage particles containing antibiotic resistance genes in the sputum of cystic fibrosis patients. Front Microbiol. 2018;
180. Fillol-Salom A, Alsaadi A, de Sousa JAM, Zhong L, Foster KR, Rocha EPC, *et al.* Bacteriophages benefit from generalized transduction. PLoS Pathog. 2019;
181. Quirós P, Colomer-Lluch M, Martínez-Castillo A, Miró E, Argente M, Jofre J, *et al.* Antibiotic resistance genes in the bacteriophage DNA fraction of human fecal samples. Antimicrob Agents Chemother. 2014;
182. Adams MD, Chan ER, Molyneaux ND, Bonomo RA. Genomewide analysis of divergence of antibiotic resistance determinants in closely related isolates of *Acinetobacter baumannii*. Antimicrob Agents Chemother. 2010;54(9):3569–77.
183. Wright MS, Haft DH, Harkins DM, Perez F, Hujer KM, Bajaksouzian S, *et al.* New insights into dissemination and variation of the healthcare-associated pathogen *Acinetobacter baumannii* from genomic analysis. mBio. 2014;
184. Di Nocera PP, Rocco F, Giannouli M, Triassi M, Zarrilli R. Genome organization of epidemic *Acinetobacter baumannii* strains. BMC Microbiol. 2011;11:224.

185. Gallagher LA, Ramage E, Weiss EJ, Radey M, Hayden HS, Held KG, *et al.* Resources for genetic and genomic analysis of emerging pathogen *Acinetobacter baumannii*. J Bacteriol. 2015;197(12):2027–35.
186. Costa AR, Monteiro R, Azeredo J. Genomic analysis of *Acinetobacter baumannii* prophages reveals remarkable diversity and suggests profound impact on bacterial virulence and fitness. Sci Rep. 2018;8(1):15346.
187. López-Leal G, Santamaria RI, Cevallos MÁ, Gonzalez V, Castillo-Ramírez S. Prophages Encode Antibiotic Resistance Genes in *Acinetobacter baumannii*. Microbial Drug Resistance. 2020;00(00):10–2.
188. Loh B, Chen J, Manohar P, Yu Y, Hua X, Leptihn S. A Biological Inventory of Prophages in *A. baumannii* Genomes Reveal Distinct Distributions in Classes, Length, and Genomic Positions. Front Microbiol. 2020;11(December):1–13.
189. Thai VC, Stubbs KA, Sarkar-Tyson M, Kahler CM. Phosphoethanolamine Transferases as Drug Discovery Targets for Therapeutic Treatment of Multi-Drug Resistant Pathogenic Gram-Negative Bacteria. Antibiotics. 2023 Sep 1;12(9).
190. Traglia G, Chiem K, Quinn B, Fernandez JS, Montaña S, Almuzara M, *et al.* Genome sequence analysis of an extensively drug-resistant *Acinetobacter baumannii* indigo-pigmented strain depicts evidence of increase genome plasticity. Sci Rep. 2018;8(1):1–15.
191. Pfeifer E, Moura De Sousa JA, Touchon M, Rocha EPC. Bacteria have numerous distinctive groups of phage–plasmids with conserved phage and variable plasmid gene repertoires. Nucleic Acids Res. 2021 Mar 18;49(5):2655–73
192. Bobay LM, Touchon M, Rocha EPC. Pervasive domestication of defective prophages by bacteria. Proc Natl Acad Sci U S A. 2014;111(33):12127–32.
193. Little JW. Lysogeny, Prophage Induction, and Lysogenic Conversion. In: Phages. American Society of Microbiology; 2005. p. 37–54.
194. Cook D, Flannigan MD, Chariker JH, Hare JM. DNA damage response coregulator ddrR affects many cellular pathways and processes in *Acinetobacter baumannii* 17978. Front Cell Infect Microbiol. 2023;13.

Chapter 2

Acinetobacter baumannii prophages, a bioinformatic update

- **R. Monteiro**, M.F. Vieira, J.M. van Dijl, J. Azeredo

Abstract

Temperate bacteriophages (phages) play an important role in bacterial virulence by encoding and regulating the expression of virulence factors and influencing host-pathogen interactions. Temperate phages are bacterial viruses that have the ability to integrate their genetic material into bacterial chromosomes, in a lysogenic life cycle. While integrated, the phage DNA is called prophage. Prophages are able to propagate with the bacterial host genome until a stimulus induces them to excise and start a lytic cycle. *Acinetobacter baumannii* is a Gram-negative bacterium that critically affects hospitals by nosocomial infections in immunocompromised patients. The way it rapidly adapts and creates antibiotic-resistant variants makes it a true challenge to treat. One of the mechanisms by which this pathogen can easily adapt is associated with mobile genetic elements, such as prophages that promote genetic exchanges. Indeed, in a previous study of hundreds of *A. baumannii* genomes deposited in NCBI, we found a high prevalence of prophages. These prophages encoded a variety of genes, like antibiotic-resistance genes, therefore increasing the virulence potential of this species. Experimental studies also confirmed that prophages can transfer genes through horizontal gene transfer. Since several new *A. baumannii* genomes were deposited since our last study, an update on these results was needed with a main focus on complete genome sequences. Therefore, we developed the ProphAnTool (Prophage Analysis Tool) to search and analyze large bacterial genome datasets in an automated way. This tool consists of a compilation of several publicly available tools in a single pipeline that generates all results in one go.

Keywords: *A. baumannii*; Bioinformatic tools; MGEs; Prophages; Virulence

2.1. INTRODUCTION

Bacteriophages are the natural predators of bacteria and are considered the most abundant entity in the biosphere (1). These viruses can be present freely in the environment, regulating bacterial communities through infection and kill cycles, or be integrated as DNA within the bacterial cells establishing a symbiotic relationship with their host. Phages can be virulent or temperate according to their life cycles. Virulent phages have strictly lytic life cycles, where they infect the host, inject their DNA, and produce several new phage particles, released through cell lysis. On the other hand, temperate phages besides a lytic cycle, can integrate their DNA into the host genome, potentially altering bacterial phenotype without cell destruction. This is called a lysogenic cycle (1–3). Temperate phage DNA, while integrated within the host, is referred to as a prophage. Owing to their mobility prophages are considered mobile genetic elements that can be responsible for a phenomenon called horizontal gene transfer (HGT) (2). Over the past two decades, research on prophages has increased significantly, with numerous studies highlighting their critical roles in bacterial growth, survival, and pathogenicity (1,4).

The increased awareness of the importance of prophages has motivated the development of bioinformatics tools designed to detect prophages in bacterial genomes, like PHASTEST (5), ProphageHunter (6), Phage_Finder (7), and PPR-Meta (8). Besides, the fact that Next Generation Sequencing became affordable expanded the opportunity for sequencing a greater number of bacterial genomes, thereby increasing the pool of potential sequences available for prophage detection. Regrettably, despite the availability of various tools, prophage analysis often needs manual extraction of prophage DNA and predicted proteins, followed by analysis with different bioinformatic tools, such as BLAST (9), HHPRED (10), CARD (11), VFDB (12), PADLOC (13), and others. In many cases, proficient bioinformatic skills are required to use these tools efficiently. In addition, the analysis of large sets of genes escalates the workload and complexity of the process.

Given the clinical significance of *A. baumannii* species, we have previously conducted a comprehensive analysis of hundreds of *A. baumannii* genomes deposited in the NCBI database. The aim was to elucidate the prevalence and potential roles of prophages within this species (14). However, as the number of deposited genomes continues to rise and *A. baumannii* remains clinically relevant, it led to the necessity to expand our previous work to extract additional insights from the encoded prophages. Previously, genome curation was done manually, prompting us to develop a pipeline to expedite the analysis. ProphAnTool (Prophage Analysis Tool) combines different publicly available bioinformatic tools to automate the analysis of large datasets of genome

sequences with a few clicks, which was applied to a large dataset of complete *A. baumannii* genome sequences from NCBI.

2.2. MATERIALS AND METHODS

2.2.1. General overview of the pipeline

PHASTEST (PHAge Search Tool with Enhance Sequence Translation) is an online platform developed for the systematic identification, annotation, and visualization of prophage sequences within bacterial genomes and plasmids. The annotation process integrates Prodigal for the accuracy and speed of Open Reading Frames (ORF) identification and BLAST+ for aligning phage sequences against a curated database of 420,000 phage proteins, while Diamond BLAST is employed for the bacterial sequence alignment. Prophage identification within PHASTEST involves a scoring mechanism based on several criteria to classify them into intact, questionable, or incomplete categories (5). This mechanism involves three methods:

- Method 1: If a specific phage organism comprises 100% or more of the total number of coding sequences (CDS) in a given region, it receives a total score of 150. If this condition is not fulfilled, methods 2 and 3 are implemented for scoring.
- Method 2: If a certain phage organism constitutes >50% of the total CDS in the region, it is considered the major potential phage.
- Method 3: Presence of phage-related keywords (‘capsid’, ‘head’, ‘integrase’, ‘plate’, ‘tail’, ‘fiber’, ‘coat’, ‘transposase’, ‘portal’, ‘terminase’, ‘protease’ or ‘lysin’) increases the score by 10 each. If the size of the region is greater than 30 kb, the score will be increased by 10. If there are at least 40 proteins in the region, the score will be increased by 10. If all of the phage-related proteins and hypothetical proteins constitute more than 70% of the total number of proteins in the region, the score will be increased by 10.

The region’s total score is determined by comparing the scores of methods 2 and 3, selecting the higher one. If <70, it is marked incomplete; if 70-90, questionable; if >90, intact.

Despite the comprehensive information yielded by the PHASTEST results, there is valuable information that can be added. To address this, we introduce ProphAnTool, a command-line pipeline (Figure 2.1) tailored for processing and analyzing data output from PHASTEST. ProphAnTool was built with Snakemake (15), a Python-based workflow engine that uses Make language, to ensure reproducible and scalable data analysis. Within the Snakemake framework, rules are pivotal, defining specifications for inputs, outputs, commands (including calls to

command line tools and Python scripts), conda environments, and additional parameters, thereby facilitating a structured and efficient analysis pipeline.

The ProphAnTool pipeline comprises six main workflows, including PHASTEST result extraction, as well as workflows for domain-based annotation, detection of virulence genes, taxonomic classification, detection of defense mechanisms, and phylogenetic analysis (Figure 2.1). The main workflow, PHASTEST result extraction, plays a fundamental role by extracting pertinent information and generating input files for subsequent steps. Subsequent workflows utilize output files from the initial extracted results to organize data into desired formats or graphical representations. Domain-based annotation produces a table with annotations, while virulence gene detection generates a heatmap indicating the presence or absence of virulence genes within prophage regions, leveraging several databases. Taxonomic classification yields a pie chart depicting the percentage of families, and defense mechanisms detection results in a barplot illustrating the occurrence of different defense mechanisms across prophage regions. Lastly, phylogenetic analysis culminates in the construction of a phylogenetic tree, encapsulating the evolutionary relationships among the analyzed sequences.

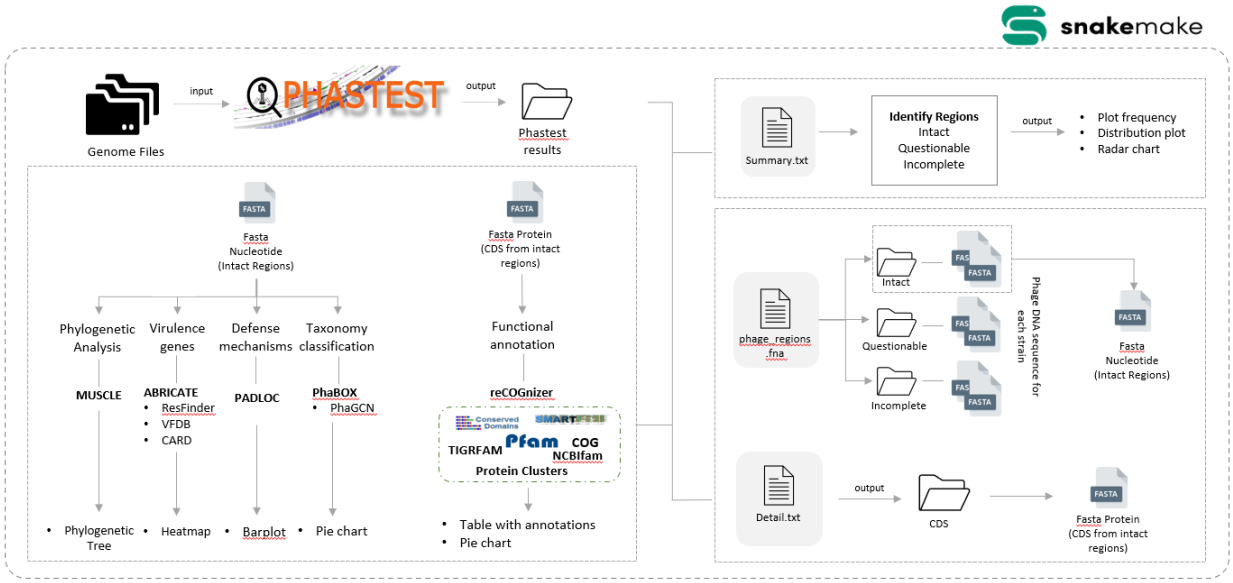


Figure 2.1. ProphAnTool workflow overview.

2.2.2. PHASTEST results extraction workflow

The framework systematically processes genetic data using the PHASTEST (5) tool, organizing the output into structured folders, each representing a distinct genome. These folders contain several files, with the "summary" and "detail" text files serving as key components for the analysis.

The summary file provides an overview of prophage regions, detailing scoring criteria, length, specific keywords, and other relevant information, such as the most similar phage to each region. In contrast, the detail file provides insight into CDSs within identified prophage regions, including their respective BLAST HIT, e-value, protein sequence, and additional contextual information. Additionally, two auxiliary JSON files are included, providing information about predicted genes and predicted phage regions, and offering detailed insights found in the afore-mentioned files.

After processing the referred files, the data is extracted. During the extraction phase, the summary text file undergoes parsing to generate structured outputs. These outputs encompass a Comma Separated Values (CSV) file detailing prophage counts (intact, incomplete, and questionable) alongside the corresponding sizes of the bacterial genomes. Additionally, graphical representations illustrating prophage frequency, distribution relative to bacterial genome size, and the percentage of prophages are generated. Simultaneously, an auxiliary JSON file is generated, containing genome information and associated prophage regions, serving as a reference for subsequent analysis. Additionally, information regarding the most common phages within each region is extracted for further analysis.

Following the extraction of prophage region information, the pipeline proceeds to the data refinement step, which extracts the DNA sequence from intact prophage regions that is delimited by the attachment sites (atts), if such sites are present, compiling them into a single fasta file.

Finally, the subsequent step involves processing both the JSON file obtained in the initial phase and the detail text file to generate a fasta file containing all CDS from the detected intact prophage regions, delimited by atts as described before.

2.2.3. Domain-based annotation workflow

For the domain-based annotation, the fasta file comprising CDSs serves as the input for *reCOGnizer* (16), a tool employed for domain-based annotation using *RPS-BLAST* with the *COG* database as a reference. *RPS-BLAST* uses Hidden-Markov Models (HMMs) for protein identification instead of local sequence alignment, providing an alternative methodology to protein identification. *reCOGnizer* organizes the information obtained with *RPS-BLAST*, obtaining the corresponding *COG* IDs and respective categories to build a functional profile. This tool generates an Excel file containing all the results generated.

2.2.4. Virulence genes detection workflow

Another step in the study involves employing the Abricate (17) tool, which takes as input a fasta file containing DNA sequences from intact prophage regions. Abricate integrates multiple databases such as VFDB (Virulence Factor Database), CARD (Comprehensive Antibiotic Resistance Database), and ResFinder, to identify virulence genes within bacterial genomes. These databases are essential resources that catalog genetic information associated with bacterial virulence factors, antibiotic resistance genes, and resistance determinants, respectively.

VFDB (18) (Virulence Factor Database): VFDB is a comprehensive repository that specializes in virulence factors present in pathogenic bacteria. It encompasses a wide range of genetic determinants responsible for bacterial pathogenicity, facilitating the identification and understanding of these critical elements in bacterial genomes.

CARD (19) (Comprehensive Antibiotic Resistance Database): CARD serves as a valuable resource for identifying antibiotic-resistance genes in bacterial strains. It contains a diverse collection of genes and mutations associated with antibiotic resistance mechanisms, allowing researchers to assess the potential drug resistance profile of bacterial isolates.

Resfinder (20): Resfinder is another database that focuses on resistance determinants in bacteria. It enables the detection of genes responsible for antibiotic resistance, including those related to various classes of antibiotics.

The outcome of this analysis yields a heatmap illustrating the virulence genes detected within specific prophage regions across all previously described databases. Since these databases generate overlapping results, to avoid duplicated data, the locations of the detected genes from each database were compared and the genes with different locations were kept.

2.2.5. Taxonomic classification workflow

For taxonomic classification, PhaGCN (21), a component of PhaBOX (22), plays a central role. PhaBOX is a comprehensive web server designed for thorough phage identification and analysis, and it integrates a suite of four distinct tools: PhaMER (23), PhaTYP (24), PhaGCN, and CHERRY (25). These tools are specifically dedicated to phage identification, lifestyle prediction, taxonomy classification, and host prediction, respectively. Using a Graph Convolutional Network (GCN)-based model, PhaGCN employs a deep learning classifier to discern species-specific features, thus enabling the taxonomic classification of novel phages. The output of this workflow is visualized through a pie chart representing the percentage distribution of families identified within all intact prophages.

2.2.6. Defense Mechanisms workflow

For the defense mechanisms detection PADLOC was used (13), a tool designed to detect antiviral defense mechanisms within prokaryotic genomes. PADLOC operates by scanning genomes against a database of HMMs and employs systematic classification to discern and annotate defense systems based on sequence similarity and genetic structure. The outcome of this step is presented through a bar plot, effectively visualizing the prevalence of diverse defense mechanisms within prophage regions.

2.2.7. Phylogeny workflow

The final step of ProphAnTool consists of using the fasta file containing DNA sequences from intact prophages with detected virulence genes to submit in MUSCLE (26) (Multiple Sequence Comparison by Log-Expectation) alignment. MUSCLE is a widely used tool among bioinformatics for conducting multiple sequence alignments. It aligns multiple sequences to identify homologous regions, which helps in understanding evolutionary relationships, functional similarities, and conserved motifs among sequences. MUSCLE employs a progressive algorithm that constructs the alignment iteratively, refining it to achieve the best possible alignment. Subsequently, the resulting alignment file is preserved, and a phylogenetic tree is constructed based on this alignment, employing 100 bootstrap replications to enhance robustness and accuracy.

2.2.8. Data Availability

ProphAnTool's source code is available at GitHub (https://github.com/mfernandasvieira/ProphAnTool), where detailed instructions on installation and usage are also provided. All Supplemental Tables are available at (LINK).

2.3. RESULTS

2.3.1. Prophage prevalence analysis in *A. baumannii* genomes

A total of 1502 sequences, including plasmids (n= 896), were extracted from the NCBI database and submitted to our pipeline, which returned 2520 prophage regions distributed by 1987 "intact" regions, 277 "questionable" regions, and 256 "incomplete" regions. Among *A. baumannii* genomes, 595 had intact prophages, 167 had incomplete, and 199 had questionable prophage regions. On the other hand, regarding the 896 plasmids, 115 sequences had intact prophage regions, 54 had incomplete, and 21 harbored questionable regions. There was a low prevalence of prophages among plasmids, with only 131 plasmid sequences harboring at least one prophage region (14.62%). Conversely, prophages were highly prevalent within bacterial

genomes, with 99.5% of the strain sequences having at least one prophage region (Figure 2.2). Among the bacterial sequences analyzed, only three did not contain any prophage region or plasmids capable of harboring them. All this data can be verified in Supplemental Table S2.1. ProphAnTool generates both a radar plot and a box plot, presented in Figure 2.2, for an overview of prophage prevalence. As Figure 2.2 (left) shows, there is a high prevalence of intact prophages, with 98% of *A. baumannii* strains harboring intact regions, 91% of which encode more than one intact prophage region. Regarding the frequency of each type of prophage region, Figure 2.2 (right) shows an average of 2.7 intact prophages per bacterial/plasmid sequence and 3.7 total (including plasmids) prophage regions. Of note, we found a low prevalence of defective prophages, either incomplete or questionable. This was to some extent expected, because we used only complete genomes in our analysis, thereby reducing the likelihood of prophage regions being fragmented across different contigs. On the other hand, the low prevalence of defective prophages implies a low level of prophage domestication, as bacterial evolution suggests (27,28).

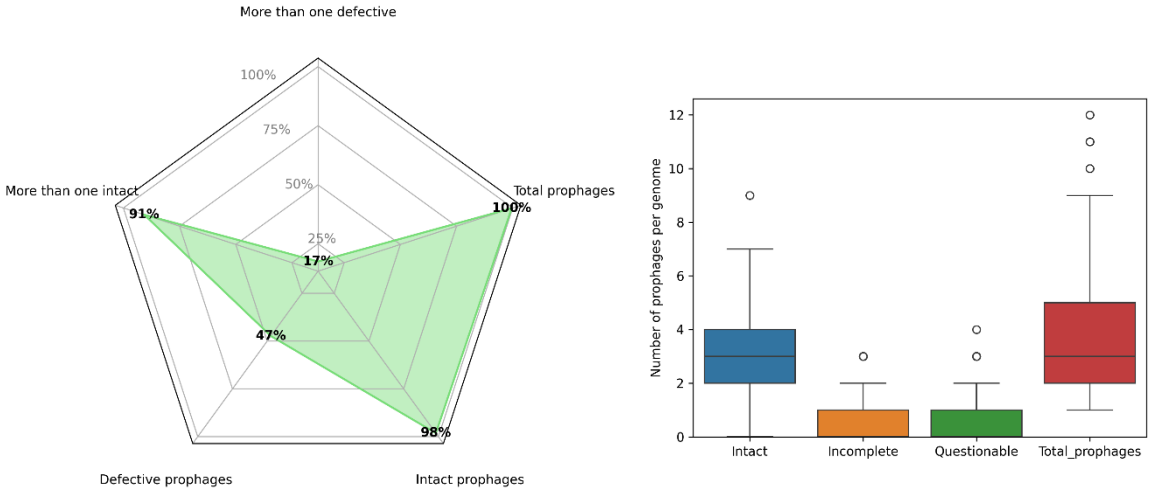


Figure 2.2. Prophage prevalence within *A. baumannii* genomes. On the left, the prevalence of total prophages, intact prophage regions, defective prophages, more than one intact prophage, and more than one defective prophage is plotted. Defective prophages include both incomplete and questionable prophages. Plasmid sequences were not considered for this plot. On the right, a boxplot summarizes the prophage frequency per bacterial genome within prophage-containing genomes. Only genomes and plasmid sequences with prophage regions were considered. Error bars represent the maximum and minimum values, and the single dots represent the outliers.

2.3.2. Prophage distribution within *A. baumannii* strains

Among the 606 genomic and 896 plasmid sequences, we investigated the distribution of prophages, taking into account the size of each sequence. On this dataset, the *A. baumannii* genome sizes range between 2.9 Mb and 4.3 Mb and plasmid sizes are between 1.5 kb and 658

kb. This workflow plots the distribution of the average numbers of prophages to make the data easier to assess (Figure 2.3) through a division into three separate graphs that distinguish the type of prophage region to analyze. As expected, there is a correlation between the increase in genome size and the number of prophages detected. However, this trend is not observed in plasmid sequences (Figure 2.3b). There are four bacterial genomes with more than 10 prophage regions, and one of them has even 12 prophage regions from which 9 are classified as intact regions, showing a high propensity for horizontal gene transfer. Regarding plasmid sequences, our analysis showed a large plasmid (>600 kb) harboring three prophage regions from which only one was considered intact. Interestingly, the sizes of most prophage-harboring plasmids are between 90 kb and 116 kb, including two to three prophage regions. Intriguingly, plasmids with higher sizes mostly do not encode prophages, whereas of the smaller-sized plasmids just a few encode a single prophage region (intact or defective). This shows an opposite trend compared to the bacterial genomes, where the number of prophage regions increases with the sequence size of the host genome.

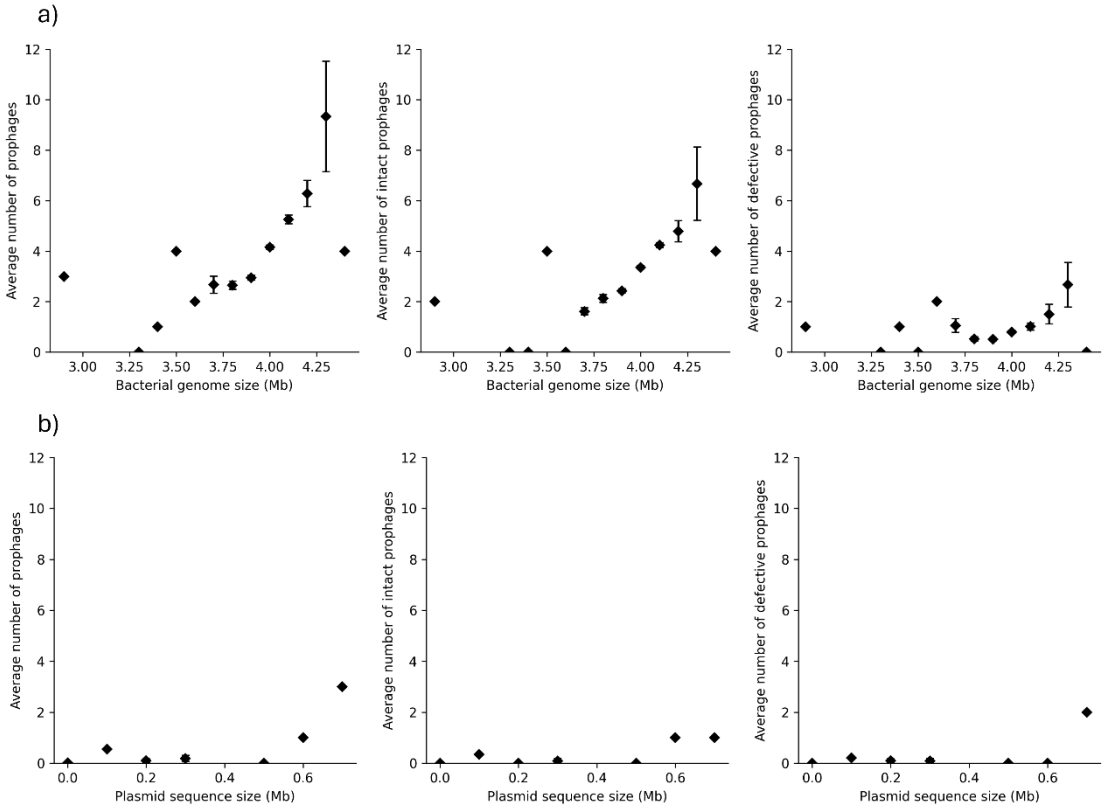


Figure 2.3. Distribution of the average number of prophages among a) bacterial sequences and b) plasmid sequences. Left graphs, average number of any prophage region per genome size; middle graphs, average number of intact prophage regions per genome size; right graphs, average number of defective (incomplete and questionable) prophage regions per genome size. Error bars represent standard deviation.

2.3.3. Prophage taxonomy reveals a highly predominant family

Intact prophages found on our dataset (n = 1987) were grouped for further analysis. Using the PhaGCN tool that was embedded within our pipeline, intact prophages were classified regarding their taxonomy. As a result, a graph was generated with the percentages of each family present on the dataset. Figure 2.4 shows the distribution of the different taxonomic families found. Clearly, the most prevalent family in our dataset is that of the *Chaseviridae* (75.29%) followed by the *Mesyanzhinovviridae* (17.16%) and the *Peduoviridae* (4.83%). Other prophages belonged to other less prevalent families such as the *Drexlerviridae* (0.55%), *Autographiviridae* (0.45%), *Herelleviridae* (0.20%), *Casjensviridae* (0.10%), *Ackermannviridae* (0.05%, n= 1), and *Schitoviridae* (0.05%, n=1). For this analysis, ProphAnTool also generates an Excel file containing a table with all the taxonomic results that can be consulted in Supplemental Table S2.2. PhaGCN predicts taxonomic families and attributes a confidence score between 0.00 and 1.00. If a threshold of 0.90 is established these proportions change drastically as shown in Supplemental Figure S2.1. From the 1963 predicted intact prophages, only 561 have a score higher than 0.90, which is significantly lower. Among these, the *Mesyanzhinovviridae* family (60.78%) is the most prevalent followed by *Chaseviridae* (18.89%) and *Peduoviridae* (13.37%) families. A noteworthy number of predicted families have scores between 0.50 and 0.90 (n= 1357), which would need manual curation to confirm predictions. Looking into the average genome sizes of phages from each family reported in the literature, and comparing them with our dataset, we observed that the genome sizes of the intact prophages identified by our pipeline are generally smaller. For instance, phages of the *Chaseviridae* family are expected to have an average genome size between 52-56 kb, whereas the sizes of our identified prophage genomes ranged between 33 kb and 55 kb with an average of 44 kb (Figure 2.5). The biggest gap between the reported genome size and the actual size observed in our dataset concerned the *Ackermannviridae* prophages. For this prophage family, we determined a size of 33 kb, whereas the *Ackermannviridae* have an average size of 155 kb according to the International Committee on Taxonomy of Viruses (ICTV), a five-fold difference (29).

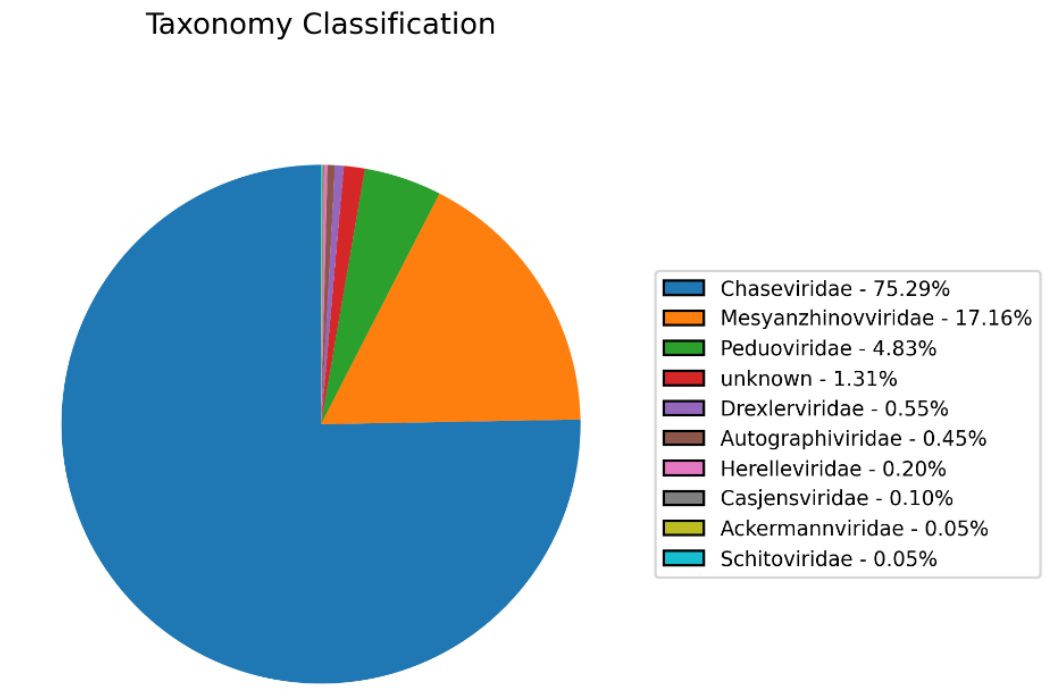


Figure 2.4. Taxonomy classification of all intact prophages detected in the *A. baumannii* dataset.

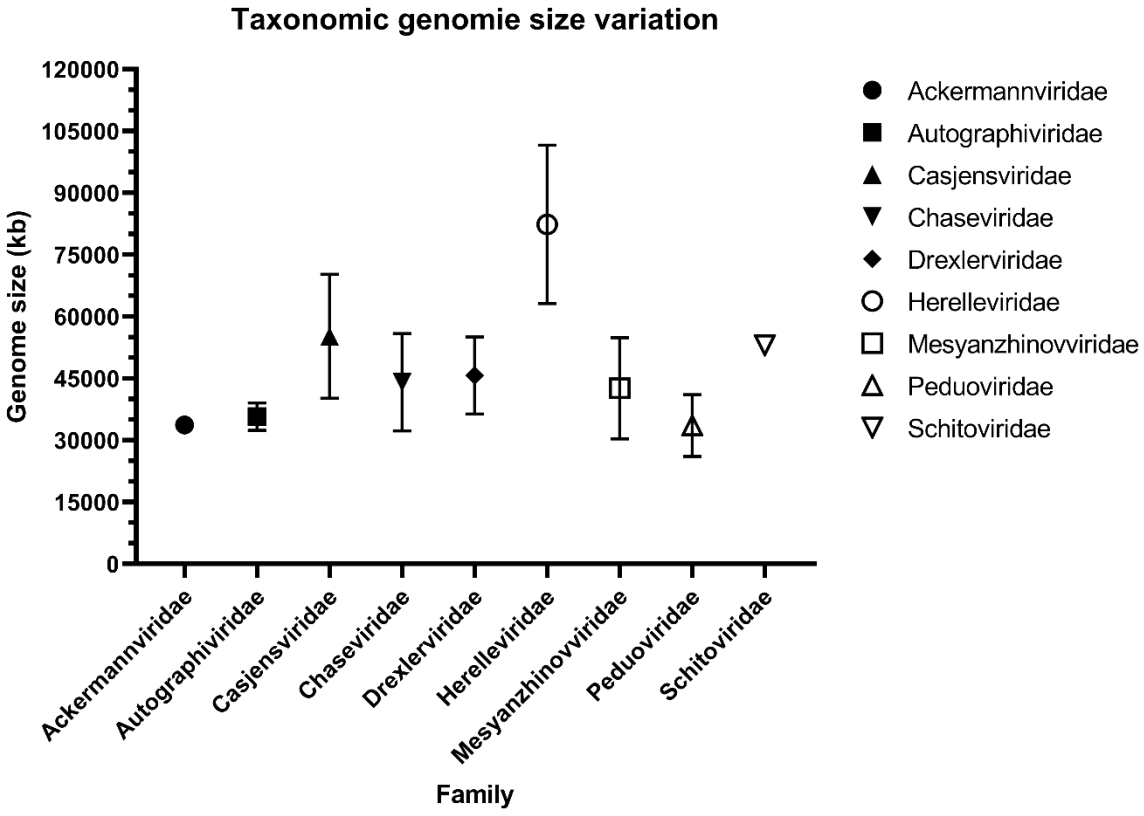


Figure 2.5. Taxonomy of intact prophage regions and their size variation. Please note that this plot was created with Graphpad (ver 7.0) and does not represent a direct output from ProphAnTool.

One of the files generated by PHASTEST contains a list of phages that have a higher number of similar CDSs to each predicted prophage region. The most similar phage found to each intact prophage was then extracted to Supplemental Table S2.3. Thirty-eight different phages were similar to predicted intact prophages, with the *Acinetobacter* phage Bphi_B1251 being the most, by far, commonly found phage (47%), followed by other two phages, YMC11/11/R3177 (14%) and vB_AbaS_TRS1 (12%) (Figure 2.6). These are the phages with which intact prophages shared the most CDS similarities. Curiously, we encountered phages from species other than *A. baumannii*, such as the *Salmonella* phages SEN34 and SSU5, and the *Pseudomonas* phage Dobby.

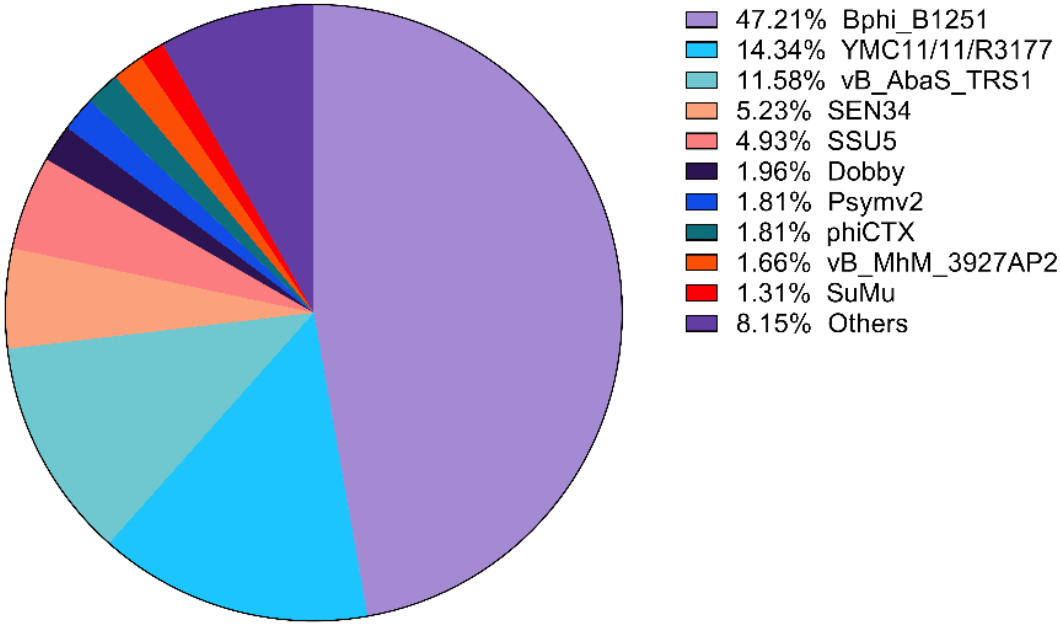


Figure 2.6. Frequency of phages that shared the most similarity with intact prophages. Please note that this plot was created with Graphpad (ver 7.0) and does not represent a direct output from ProphAnTool.

To verify the genomic diversity among intact prophages within plasmids (n= 119), a phylogenetic tree was generated from a MUSCLE alignment as shown in Figure 2.7. The calculated distance matrix is also made available and can be consulted in Supplemental Table S2.4. As the tree shows, there is a group of identical prophages (branch length = 0), which are divergent from the remaining dataset and should represent mostly the same phage. These are predicted *Chaseviridae* phages (despite the score <0.7), with homology to the *Salmonella* phage SSU5. The other sequences are divided into two major clusters, with the bigger cluster divided into several subclusters, all with branch lengths close to zero. This tree shows that the prophages encoded by the plasmids seem to descend from a common ancestor that evolved, which would probably be a SSU5-like phage.

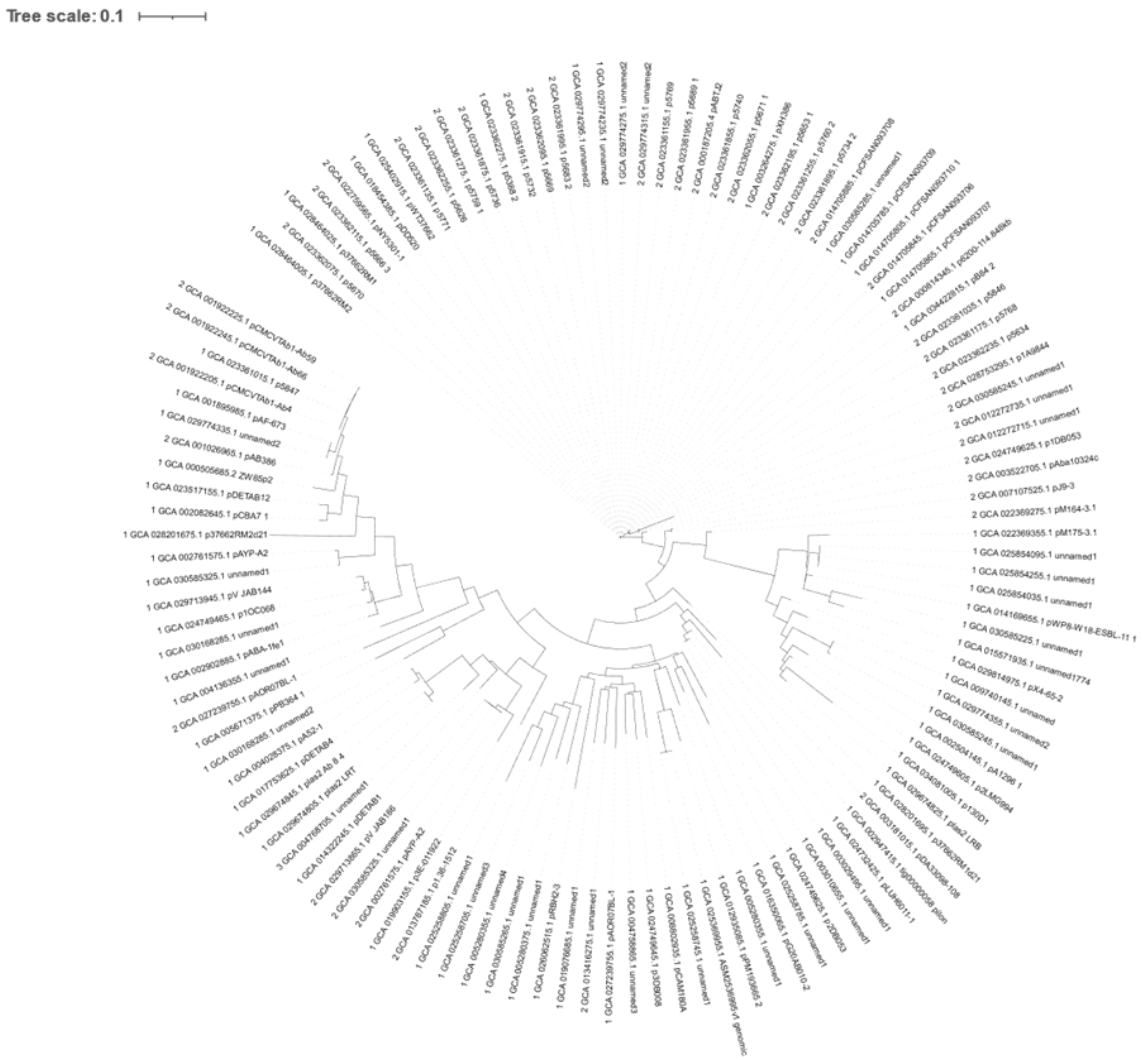


Figure 2.7. Phylogenetic tree with intact prophages encoded by plasmid sequences. Prophage sequences were aligned using MUSCLE. The tree was built with a bootstrap set to 100. Tree branches are proportional to the branch length (branch length = 0, identical; branch length = 1 no similarity). The phylogenetic tree was graphically represented using iTOL *(30)*.

2.3.4. Prophage-associated virulence

To understand the role of prophages in host virulence, the ProphAnTool workflow searches for antibiotic-resistance genes using three different databases (CARD, ResFinder, and VFDB), producing a heatmap as shown in Figure 2.8. Since these three databases yield overlapping results, a filtering process was performed to eliminate duplicate results, based on the predicted positions of each gene. Nevertheless, one of these duplicated genes was still present due to small differences in predicted gene position between the three databases. Therefore, this output should still be manually curated before the final analysis. In the heatmap generated, all prophage regions, that harbor intact prophages encoding for antibiotic resistance genes (ARGs), are represented. In our

dataset, 39 ARGs were found among 38 intact prophages, representing 2% of the predicted intact prophages, and these are marked with green color in the heatmap below. A significant number of the ARGs found are related to aminoglycoside resistance, such as the acetyltransferase genes *aac(3)-Ia/ aac(6')-Ib/ aac(3)-IIa/ aac(6')-Iaf*, the nucleotidyltransferase genes *ant(3'')-IIa/ aadA17/ aadA2/ ant(2'')-Ia*, the phosphotransferase genes *aph(3'')-Ib/ aph(3'')-Ia/ aph(6)-Id*, the 16S rRNA methyltransferase gene *armA*, and the *adeR* gene for an *adeABC* efflux system regulator; others ARGs related to macrolide resistance, including the efflux pump gene *abeS*, the phosphotransferase genes *mphE*, and *msrE*; fluoroquinolone- and tetracycline resistance, such as the efflux pump genes *adeFGH* and the corresponding regulator *adeL*, and the tetracycline efflux pump *tet(A)*; the chloramphenicol resistance genes *catB*, *catI*, and *cmlA5*; genes for β-lactam/carbapenem and cephalosporin resistance, such as the β-lactamase genes bla_{IMP-19}, bla_{OXA-10}, bla_{OXA-23}, bla_{PER-1}, bla_{SCO-1}, bla_{TEM-10}, and bla_{TEM-12}; and sulfonamide resistance, such as the *sul1* and *sul2* genes. In addition, the regulator gene *adeN* whose inactivation may lead to resistance to a wide variety of antibiotic classes was also found. Bacteria producing β-lactamases are widely spread across the globe and the detected bla_{OXA-23} gene is one of the most commonly observed β-lactamase-encoding genes (31). In our present analysis, as Figure 2.8 shows, the most prevalent ARGs among the identified prophages were related to sulfonamide resistance (45% of the prophages carry *sul1*), as well as aminoglycoside resistance (*aph(3')-Ia*, 34%), and the β-lactam resistance (bla_{TEM-12}, 32%). Interestingly, aminoglycoside, sulfonamide, and β-lactam resistance genes have been found previously in prophages of *A. baumannii*, which might indicate a propensity for transduction of these genes between different strains (14,32). However, genes related to aminoglycoside resistance altogether were the most frequently found. According to our results, some prophages are harboring multiple copies of the same antibiotic-resistance gene. For example, the prophage 3_GCA_023361115.1_ASM2336111v1_genomic carries three copies of the *aph(3')-Ia* gene and two copies of the bla_{TEM-12} gene. Curiously, two intact prophages harbored by two plasmids, pPB364 and p1.36, encoded the *mphE* and *msrE* genes, and *sul2* gene respectively. The table with the dataframe used for the heatmap generation is available in Supplemental Table S2.5. It presents the merged results of the CARD, ResFinder, and VFDB analyses. The results files from each database analysis are also made available for the user.



Figure 2.8. Heatmap with intact prophage regions that harbor antibiotic-resistance genes. The first number in each sequence name refers to the prophage region within the host genome, which is codified by the 'GCA' code that comes next. Green color indicates the presence of a specific gene within a prophage.

To understand the prophage phylogenetic relationship between ARG-containing prophages (n= 38), a phylogenetic tree was generated (Figure 2.9), as well as its corresponding distance matrix (see Supplemental Table S2.6). As Figure 2.9 shows, the most prevalent family among these prophages is the *Peduoviridae* family, followed by the *Chaseviridae*. Among the *Peduoviridae*, the most common homologous phage was the *Acinetobacter* Bphi_B1251 phage. Prophages are distributed among three main clusters with one having several subclusters composed of the prophages from other predicted families. There is a tendency for prophages from the same family

to cluster together. As tree branch lengths are close to zero, it seems that prophages show a relatively low genetic diversity.

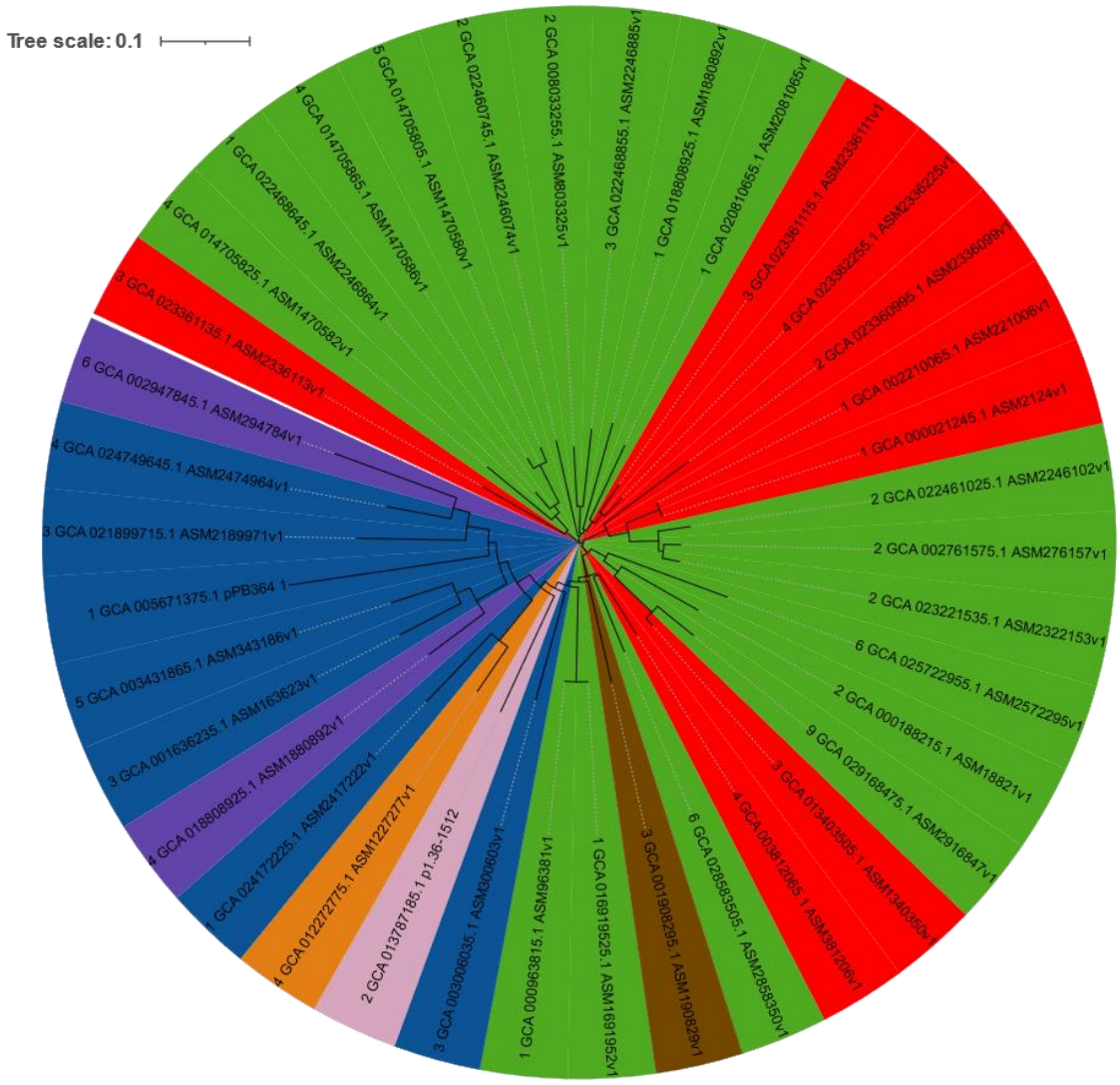


Figure 2.9. Phylogenetic tree showing the diversity between ARG-harboring intact prophages. Sequences were aligned using MUSCLE. The tree was built with a bootstrap set to 100. Tree branches are proportional to the branch length (branch length = 0, identical; branch length = 1, no similarity). Prophage-predicted families are identified in colors: Green, *Peduoviridae*; Blue, *Chaseviridae*; Purple, *Drexlerviridae*; Orange, *Mesyanzhinovviridae*; Pink, *Herelleviridae*; Brown, *Autographiviridae*, Red, Unknown. The phylogenetic tree was graphically represented using iTOL *(30)*.

2.3.5. Prophages strongly influence the *A. baumannii* lifestyle

Prophages can have other roles within their host besides transferring and expressing antibiotic-resistance genes. To identify to what extent this influence goes, the ProphAnTool workflow searches for fitness-related CDSs using the Cluster of Orthologous Genes (COGs) classification to group them

and create an overview of this influence. As expected, a significant number of CDSs were classified as belonging to the mobilome, such as typical phage genes that encode capsid or tail fiber proteins. Therefore, these CDSs were filtered out for this analysis (please see Supplemental Figure S2.2). As Figure 2.10 shows, upon filtering out mobilome-related CDSs, the CDSs found were equally distributed between cellular processes and signaling (33.8%), information storage and processing (31.2%), and poorly characterized (28.4%). Interestingly, only 6.6% belonged to metabolism processes. Functional categories show in detail the potential roles of these CDSs found within each general category. For instance, cellular processes include sub-categories like cell cycle control and cell wall biogenesis as the two most prevalent categories. Within this category, we detected the chromosome segregation ATPases Smc, phosphoethanolamine transferases OpgE, and the periplasmic proteins TonB and TolC. OpgE for instance catalyses the transfer of a phosphoethanolamine group to an osmoregulated periplasmic glucan (33). Both TonB and TolC are important virulence factors, of which the first is crucial for iron uptake and the second is important to combat antimicrobials and oxidative stress (34–36). It should be noted that most of the CDSs found within this category are typical host lysis CDSs, such as murein hydrolases and other similar proteins that are used by phages. Moreover, two other functional categories, namely defense mechanisms which will be explored further, and signal transduction mechanisms, were also represented. Signal transduction includes CDSs like the sRNA-binding carbon storage regulator CsrA that can be involved in iron acquisition (37), and invasion (38), as well as in biofilm formation and cell motility (39,40), and the cyclic di-GMP protein, which regulates several bacterial processes such as virulence gene expression (41). Despite being less prevalent, the post-translational modification sub-category includes an important CDS for protection against strong oxidation stress, such as the chaperedoxin CnoX. This chaperedoxin prevents the effects of chlorination, protecting chaperone degradation and preventing irreversible oxidation (42). Other less represented functional categories are related to cell motility, extracellular structures, and intracellular trafficking. These include CDSs like the outer membrane usher protein FimD/PapC and PapD important for the pilus assembly/secretion (43), and a type II secretion ATPase involved in protein secretion. Additionally, a significant number of replication- and transcription-related CDSs were found in the information and storage category. For example, the DNA polymerase DinP, important for DNA mutagenesis/repair (44), DNA-binding transcriptional regulators like Lrp, MarR, and FrmR that regulate virulence, antibiotic resistance, and quorum sensing (45–47), DNA methylases, and others were highly relevant. As for the previous categories, a significant part of CDSs from the

identified categories were also typical for prophages, such as SOS-response repressors, helicases, and a few transcriptional regulators (2). Within the metabolism category, most CDS were attributed to amino acid, coenzyme, and inorganic ion transport and metabolism. This includes an outer membrane receptor protein (for Fe transport), a glutamine amidotransferase (48), a Zn-dependent dehydrogenase (49), and the cobalamin biosynthesis cobaltochelatase CobT (50) as the most prevalent CDSs. As mentioned above, poorly characterized CDSs account for about a third of the total predicted CDSs, with most of these CDSs being of unknown function, or belonging to the lysozyme family, which is an expected phage CDS as well. There were a few predicted ATPases and other CDSs with conserved domains of the YgiM protein, which is predicted to be a membrane protein as well as YjbI, which are among the most prevalent. The YgiM protein has been implicated in the onset of sepsis providing *A. baumannii* with resistance against macrophages, as described for *E. coli* and *K. pneumoniae* species (51,52). The complete list with all the CDS classifications is presented in Supplemental Table S2.7.

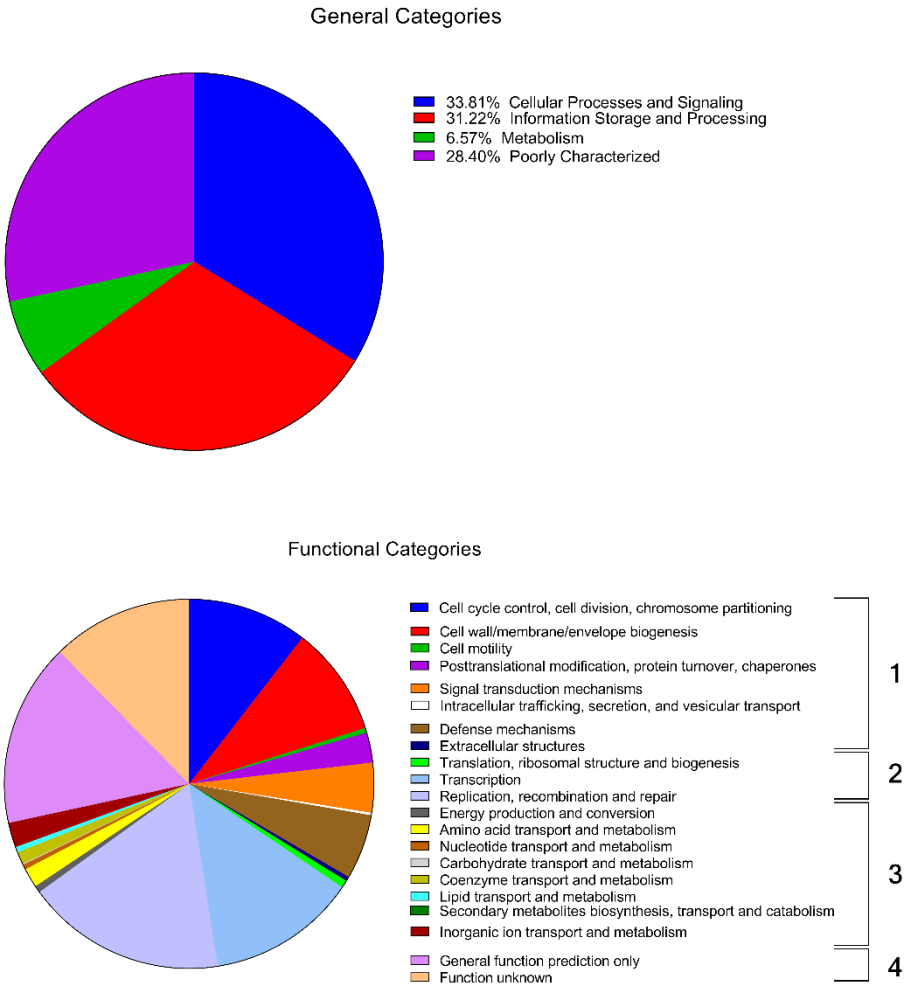


Figure 2.10. General and functional categories based on COG classification attributed to all CDSs found among intact prophages (mobilome-related CDSs excluded). 1, functional categories belonging to Cellular Processes and Signaling; 2, functional categories belonging to Information Storage and Processing; 3, functional categories belonging to Metabolism; 4, functional categories poorly categorized. The color code legend defines the respective sub-categories represented in the pie charts. Please note that this plot was created with Graphpad (ver 7.0) and does not represent a direct output from ProphAnTool.

2.3.6. Prophage regions specifying defense mechanisms

In the ongoing arms race between bacteria and phages, bacteria have evolved defense mechanisms, while phages have developed anti-defense strategies to continue infecting their host. Since prophages are symbiotic parasites that "live" within the host chromosome, they can also employ defense mechanisms to prevent the acquisition of foreign DNA by their host, including that from other phages. In recent years, an increasing number of new defense systems has been discovered. Consequently, this feature has been integrated into the workflow. As mentioned above, a significant number of CDSs with a function that relates to defense mechanisms was detected

within our intact prophage dataset. To better understand how many and which of these systems are present, a specific tool for this task called PADLOC (13), was implemented. With it, the ProphAnTool workflow searches for defense mechanisms within the predicted intact prophage regions, and it generates a bar graph as presented in Figure 2.11, which summarizes the frequency at each of the systems is found. It also generates an Excel file (Supplemental Table S2.8) that specifies the prophages and hosts that contain these systems. The results showed the presence of genes for defense mechanisms in 138 intact prophage regions, representing 6.89% of the total intact prophage regions. This implies that such systems are not widely spread. Among the small set of intact prophages that specify defense systems, there is on average one defense system encoded per intact prophage. Only two prophages encode two different systems, and one of them is integrated within a plasmid (pZW85p2). As Figure 2.11 shows, the most commonly found defense system is the PDC-S33. This is a so far uncharacterized phage-defense candidate system (PDC) that is present in more than 35 prophage sequences. The second most prevalent system is the RosmerTA system, which was detected in more than 25 prophage sequences. This is a toxin-antitoxin (TA) system that was recently characterized (53). Other defense systems found, are the BstA system, which is an abortive infection protein providing host immunity against infections from the same phage (54); a DNA modification system (DMS); the Lamassu system that uses structural maintenance of chromosome (SMC) proteins to protect against foreign DNA replication (55); restriction-modification (RM) type I and type II systems that cleave specific DNA sequences (56); the SoFic protein that can ligate AMP onto proteins (AMPylase) (57); the darTG system, which is a TA system that provides strong phage protection (58); the ietAS of which the mode of action is still to be described (59); and a septu type I that is composed of an ATPase and a His-Me finger (HNH) nuclease (59).

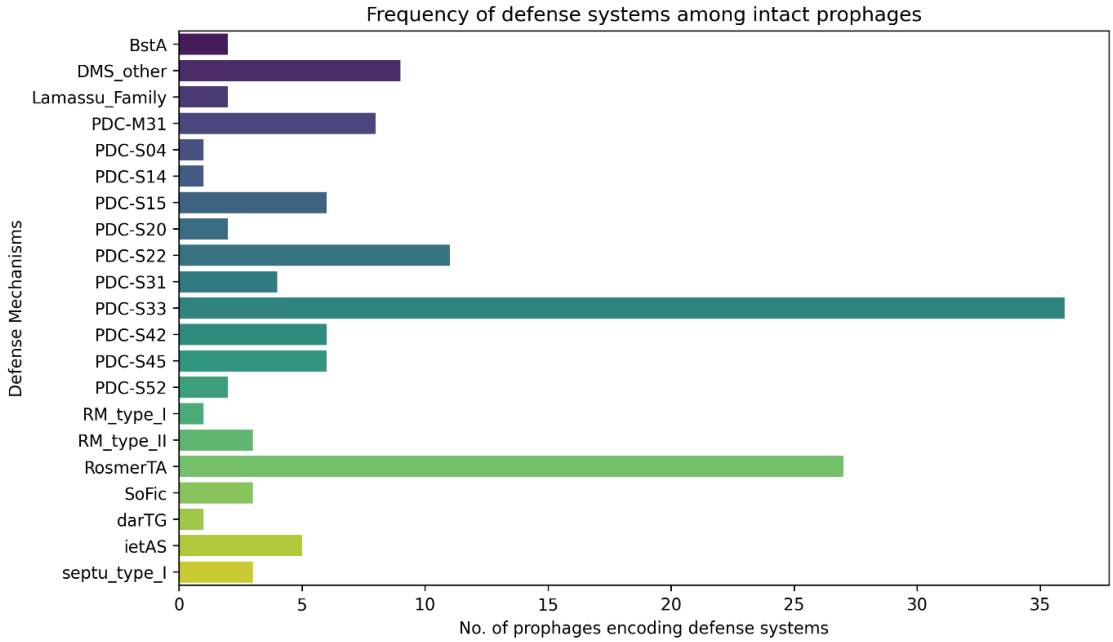


Figure 2.11. Frequencies of defense systems within identified intact prophage sequences.

2.4. Discussion

Prophages have been attracting considerable attention from the research community and, accordingly, the number of publications on prophages have increased substantially over the last two decades. The interest in prophages relies on their importance for host biology dynamics and their involvement in bacterial pathogenesis. On the other hand, prophages have raised interest as they are being considered for phage therapy due to a lack of available lytic phages against certain pathogens (60–62). In a previous study, we analyzed 795 *A. baumannii* genomes that were deposited in the NCBI database and found a significant prevalence of prophages (14). One of the drawbacks of this study was the high number of draft genomes with only a few genome sequences being complete. This biased the results, since many potentially intact regions could be split and therefore considered defective regions. Following this study, other studies have emerged to shed light on the biological functions of *Acinetobacter* prophages (32,63–66). To minimize wrong prophage prediction, we have now used all complete *A. baumannii* genomes deposited in NCBI. Indeed, looking at the number of prophages that we predicted, it is clear that intact prophages are significantly more prevalent than reported previously. Interestingly, we also found several plasmids with an average size of around 100 kb encoding up to two mostly intact prophages, as observed previously (67). Prophages integrated within plasmids have been discovered before and referred to phage-plasmids (PPs), being able to function as phages or plasmids (68). At this point, we can neither exclude nor confirm the possibility that these predicted prophages are PPs. Among the

most prevalent prophages that inserted into plasmids is the *Salmonella* phage SSU5 which, curiously, is part of one of the largest groups of PPs. This can indicate that at least the plasmids encoding SSU5 are PPs (67). In contrast to what was observed for prophages in the bacterial genomes, the plasmid sizes did not correlate with the number of the encoded prophages (14,63).

The taxonomic analysis of intact prophages revealed interesting features. Since ICTV reviewed/re-organized phage families, extinguishing myo/podo/siphoviridae families, only few studies have been conducted using the updated nomenclature. Three-quarters of the intact prophages in our dataset were attributed to the *Chaseviridae* family, which was previously assigned to the myoviruses family. Furthermore, according to the literature, most prophages are siphoviruses (14,32). Nevertheless, a study on *Acinetobacter pittii* prophages indicated that phages of the *Myoviridae* family (old terminology) represent the most common family among intact prophages (65). Surprisingly, the average genome size of intact prophages from each family was below the size reported in the ICTV reports (29). The most striking differences were observed for prophages belonging to *Ackermannviridae* (n= 1) and *Herelleviridae* (n= 4) families, for which the reported sizes are 155 kb and 106-170 kb respectively, whereas the actual determined average size turned out to be 33 kb and 82 kb ± 22 kb. Some reports have indicated smaller prophage sizes compared to those assigned to their respective families, possibly resulting from size optimization while integrated into the chromosome (14,32,69). This reduction in prophage genome size may have been induced by several mutations through recombination events. Additionally, processes such as prophage domestication can lead to mutations that deactivate or reduce the prophage genome (27,28,70). As previously mentioned, PhaGCN predictions are accompanied by a confidence score. The fact that a significant number of predicted prophage families has a score below 0.80 may lead to biased results on this matter. Among the most commonly identified phages, there was one highly prevalent, sharing CDSs with almost half of the intact prophages. This concerned the Bphi_B1251 phage which, together with YMC11/11/R3177 and vB_AbaS_TRS1, are the most prevalent among *A. baumannii* prophages according to the literature (32,65). Prophages encoded by plasmids displayed a relatively low diversity suggesting a common SSU5-like phage ancestor, which would not be surprising since this is part of a relevant PP group as mentioned above.

In our dataset, prophages containing ARGs represent a small subset of sequences. However, the observation that these genes are frequently present within prophages of this species raises the question of whether prophages might play a significant role in the transduction and dissemination of antibiotic-resistance genes (14,32,63–65). Despite the low prevalence of prophages harboring

ARGs, there were cases where these ARGs were present in multiple copies within the same sequence. The presence of these ARGs does not mean that they are necessarily expressed, because some regulators might be missing, but they can potentially be used. Recently, the presence of duplicated ARGs was studied in *E. coli* and it was shown that they increase the severity of the resistance encoded. Besides it was found that this phenomenon is potentiated by mobile genetic elements, such as plasmids or phages through horizontal gene transfer (71).

Bacterial parasites such as prophages, which live in a symbiotic relationship with their host, may also bring fitness advantages. Indeed, in our present dataset, intact prophages were found to encode several fitness- and some potentially virulence-related genes. Some identified genes encoded proteins involved in iron uptake, host colonization, and survival, giving prophages a crucial role in improving the host fitness and pathogenicity across different environments, as was also observed previously (14). Furthermore, it was interesting to notice that several transcriptional regulators encoded in intact prophages are potential regulators of virulence, antibiotic resistance, and fitness, corroborating the theory that prophages can shape their host's behavior and influence pathogenicity. Interestingly, contrary to previous reports, metabolism-related genes comprised less than 7% of the total annotated genes in our present study. This suggests that prophages might have a limited influence on metabolic processes in the host, or that there is a small selective pressure for the transduction of these genes. It should be noted that the methodology used for annotation, based on COG classification, was completely different from the methods used in other previous studies, which may explain some of the differences observed.

Prophages can be sources of defense systems providing their host with a fitness advantage by protecting against phage infection as discussed by Patel and Maxwell (72). However, in our present dataset, these systems were not highly prevalent, being detected in only 6% of the intact prophage sequences. Despite the diversity of defense mechanisms predicted, most of them have so far remained poorly characterized.

2.5. Concluding remarks

With the ProphAnTool, we have automated prophage analysis particularly for large sets of data, integrating several publicly available tools. This approach aims to facilitate a comprehensive analysis of prophage functions and their relevance. We applied this automated methodology to a substantial set of *A. baumannii* genomes, all complete genomes available in the NCBI database, to expand and update the results from previous studies. Here it was shown that prophages are shaping *A. baumannii* pathogenicity, both by potentially transducing specific ARGs and influencing

bacterial gene expression with several transcriptional regulators, suggesting that prophages are important drivers for this pathogen's success. Finally, the ProphAnTool is accessible to the scientific community and can be utilized for analyzing other genome and prophage databases. It allows for easy analysis of large datasets, leading to rapid results. This capability to efficiently handle substantial datasets will accelerate the research on prophages and their implications for bacterial fitness and virulence.

2.6. REFERENCES

1. Fortier LC, Sekulovic O. Importance of prophages to evolution and virulence of bacterial pathogens. Virulence. 2013;4(5):354–65.
2. Canchaya C, Proux C, Fournous G, Bruttin A, Brüssow H. Prophage genomics. Microbiol Mol Biol Rev. 2003;67(2):238–76.
3. Casjens S. Prophages and bacterial genomics: what have we learned so far? Mol Microbiol [Internet]. 2003;49(2):277–300.
4. Hargreaves KR, Otieno JR, Thanki A, Blades MJ, Millard AD, Browne HP, *et al.* As Clear as Mud? Determining the Diversity and Prevalence of Prophages in the Draft Genomes of Estuarine Isolates of Clostridium difficile. Genome Biol Evol. 2015;7(7):1842–55.
5. Wishart DS, Han S, Saha S, Oler E, Peters H, Grant JR, *et al.* PHASTEST: faster than PHASTER, better than PHAST. Nucleic Acids Res. 2023 Jul 5;51(W1):W443–50.
6. Song W, Sun HX, Zhang C, Cheng L, Peng Y, Deng Z, *et al.* Prophage Hunter: an integrative hunting tool for active prophages. Nucleic Acids Res. 2019 May 22;47(W1):W74–80.
7. Fouts DE. Phage_Finder: Automated identification and classification of prophage regions in complete bacterial genome sequences. Nucleic Acids Res. 2006 Nov 24;34(20):5839–51.
8. Fang Z, Tan J, Wu S, Li M, Xu C, Xie Z, *et al.* PPR-Meta: a tool for identifying phages and plasmids from metagenomic fragments using deep learning. Gigascience. 2019 Jun 1;8(6):1–14.
9. Altschul SF, Madden TL, Schäffer AA, Zhang J, Zhang Z, Miller W, *et al.* Gapped BLAST and PSI-BLAST: A new generation of protein database search programs. Vol. 25, Nucleic Acids Research. 1997. p. 3389–402.
10. Zimmermann L, Stephens A, Nam SZ, Rau D, Kübler J, Lozajic M, *et al.* A Completely Reimplemented MPI Bioinformatics Toolkit with a New HHpred Server at its Core. J Mol Biol. 2018;430(15):2237–43.
11. Alcock BP, Raphenya AR, Lau TTY, Tsang KK, Bouchard M, Edalatmand A, *et al.* CARD 2020: antibiotic resistome surveillance with the comprehensive antibiotic resistance database. Nucleic Acids Res. 2020 Jan;48(D1):D517–25.
12. Liu B, Zheng D, Jin Q, Chen L, Yang J. VFDB 2019: a comparative pathogenomic platform with an interactive web interface. Nucleic Acids Res. 2019 Jan;47(D1):D687–92.
13. Payne LJ, Todeschini TC, Wu Y, Perry BJ, Ronson CW, Fineran PC, *et al.* Identification and classification of antiviral defence systems in bacteria and archaea with PADLOC reveals new system types. Nucleic Acids Res. 2021 Nov 8;49(19):10868–78.
14. Costa AR, Monteiro R, Azeredo J. Genomic analysis of *Acinetobacter baumannii* prophages reveals remarkable diversity and suggests profound impact on bacterial virulence and fitness. Sci Rep. 2018;8(1):15346.
15. Köster J, Rahmann S. Snakemake—a scalable bioinformatics workflow engine. Bioinformatics [Internet]. 2018 Oct 15,34(20):3600–3600.
16. Sequeira JC, Rocha M, Alves MM, Salvador AF. UPIMAPI, reCOGnizer and KEGGCharter: Bioinformatics tools for functional annotation and visualization of (meta)-omics datasets. Comput Struct Biotechnol J. 2022 Jan 1;20:1798–810.
17. Seemann T, Abricate, Github https://github.com/tseemann/abricate
18. Chen L, Zheng D, Liu B, Yang J, Jin Q. VFDB 2016: hierarchical and refined dataset for big data analysis–10 years on. Nucleic Acids Res. 2016;44(D1):D694–7.
19. Jia B, Raphenya AR, Alcock B, Waglechner N, Guo P, Tsang KK, *et al.* CARD 2017: expansion and model-centric curation of the comprehensive antibiotic resistance database. Nucleic Acids Res. 2017 Jan 1;45(D1):D566–73.

20. Zankari E, Hasman H, Cosentino S, Vestergaard M, Rasmussen S, Lund O, *et al.* Identification of acquired antimicrobial resistance genes. J Antimicrob Chemother. 2012 Nov;67(11):2640–4.
21. Shang J, Jiang J, Sun Y. Bacteriophage classification for assembled contigs using graph convolutional network. Bioinformatics. 2021 Jul 12;37(Supplement_1):i25–33.
22. Shang J, Peng C, Liao H, Tang X, Sun Y. PhaBOX: a web server for identifying and characterizing phage contigs in metagenomic data. Bioinformatics Advances. 2023 Jan 5;3(1).
23. Shang J, Tang X, Guo R, Sun Y. Accurate identification of bacteriophages from metagenomic data using Transformer. Brief Bioinform. 2022 Jul 18;23(4):1–11.
24. Shang J, Tang X, Sun Y. PhaTYP: predicting the lifestyle for bacteriophages using BERT. Brief Bioinform. 2023 Jan 19 [cited 2024 Apr 19];24(1):1–11.
25. Shang J, Sun Y. CHERRY: a Computational metHod for accuratE pRediction of virus–pRokarYotic interactions using a graph encoder–decoder model. Brief Bioinform. 2022 Sep 20;23(5):1–16.
26. Edgar RC. MUSCLE: multiple sequence alignment with high accuracy and high throughput.
27. Bobay LM, Touchon M, Rocha EPC. Pervasive domestication of defective prophages by bacteria. Proc Natl Acad Sci U S A. 2014;111(33):12127–32.
28. Ramisetty BCM, Sudhakari PA. Bacterial "grounded" prophages: Hotspots for genetic renovation and innovation. Front Genet. 2019;10(FEB):1–17.
29. Anany H, Mahadevan P, Turner D, Adriaenssens EM, Kropinski AM. ICTV Virus Taxonomy Profile: Chaseviridae 2022. Journal of General Virology. 2022 Apr 13;103(4):001715.
30. Letunic I, Bork P. Interactive Tree of Life (iTOL) v6: recent updates to the phylogenetic tree display and annotation tool. Nucleic Acids Res. 2013;1(1256879):13–4.
31. Hamidian M, Nigro SJ. Emergence, molecular mechanisms and global spread of carbapenem-resistant *Acinetobacter baumannii*. Microb Genom. 2019 Oct 1;5(10):e000306.
32. Loh B, Chen J, Manohar P, Yu Y, Hua X, Leptihn S. A Biological Inventory of Prophages in *A. baumannii* Genomes Reveal Distinct Distributions in Classes, Length, and Genomic Positions. Front Microbiol. 2020;11(December):1–13.
33. Bontemps-Gallo S, Cogez V, Robbe-Masselot C, Quintard K, Dondeyne J, Madec E, *et al.* Biosynthesis of Osmoregulated periplasmic glucans in *Escherichia coli*: The phosphoethanolamine transferase is encoded by opgE. Biomed Res Int. 2013;2013.
34. Bharathi SV, Vasanth V, Govindan R. AbuO, a TolC-Like Outer Membrane Protein of *Acinetobacter baumannii*, Is Involved in Antimicrobial and Oxidative Stress Resistance. Antimicrob Agents Chemother. 2015 Jan 27;59(2):1236–45.
35. Abdollahi S, Rasooli I, Mousavi Gargari SL. The role of TonB-dependent copper receptor in virulence of *Acinetobacter baumannii*. Infection, Genetics and Evolution. 2018;60:181–90.
36. Dhurve G, Madikonda AK, Jagannadham MV, Siddavattam D. Outer Membrane Vesicles of *Acinetobacter baumannii* DS002 Are Selectively Enriched with TonB-Dependent Transporters and Play a Key Role in Iron Acquisition. Microbiol Spectr. 2022 Apr 27;10(2).
37. Pourciau C, Pannuri A, Potts A, Yakhnin H, Babitzke P, Romeo T. Regulation of iron storage by CsrA supports exponential growth of *Escherichia coli*. mBio. 2019 Jul 1;10(4).
38. Altier C, Suyemoto M, Lawhon SD. Regulation of *Salmonella enterica* serovar *typhimurium* invasion genes by *csrA*. Infect Immun. 2000;68(12):6790–7.
39. Jackson DW, Suzuki K, Oakford L, Simecka JW, Hart ME, Romeo T. Biofilm formation and dispersal under the influence of the global regulator CsrA of *Escherichia coli*. J Bacteriol. 2002;184(1):290–301.

40. Wei BL, Brun-Zinkernagel AM, Simecka JW, Prüß BM, Babitzke P, Romeo T. Positive regulation of motility and flhDC expression by the RNA-binding protein CsrA of *Escherichia coli*. Mol Microbiol. 2001 Apr 1;40(1):245–56.
41. Tamayo R, Pratt JT, Camilli A. Roles of cyclic diguanylate in the regulation of bacterial pathogenesis. Annu Rev Microbiol. 2007 Oct 13;61(Volume 61, 2007):131–48.
42. Goemans C V., Vertommen D, Agrebi R, Collet JF. CnoX Is a Chaperedoxin: A Holdase that Protects Its Substrates from Irreversible Oxidation. Mol Cell. 2018 May 17;70(4):614-627.e7.
43. Huang Y, Smith BS, Chen LX, Baxter RHG, Deisenhofer J. Insights into pilus assembly and secretion from the structure and functional characterization of usher PapC. Proc Natl Acad Sci U S A. 2009 May 5;106(18):7403–7.
44. Kim SR, Maenhaut-Michel G, Yamada M, Yamamoto Y, Matsui K, Sofuni T, *et al.* Multiple pathways for SOS-induced mutagenesis in *Escherichia coli*: An overexpression of dinB/dinP results in strongly enhancing mutagenesis in the absence of any exogenous treatment to damage DNA. Proc Natl Acad Sci U S A. 1997 Dec 9;94(25):13792–7.
45. Ziegler CA, Freddolino PL. The leucine-responsive regulatory proteins/feast-famine regulatory proteins: an ancient and complex class of transcriptional regulators in bacteria and archaea. Crit Rev Biochem Mol Biol. 2021;56(4):373–400.
46. Molina-Henares AJ, Krell T, Eugenia Guazzaroni M, Segura A, Ramos JL. Members of the IclR family of bacterial transcriptional regulators function as activators and/or repressors. FEMS Microbiol Rev. 2006 Mar 1;30(2):157–86.
47. Deochand DK, Grove A. MarR family transcription factors: dynamic variations on a common scaffold. Crit Rev Biochem Mol Biol. 2017 Nov 2;52(6):595–613.
48. Li Q, Tao QY, Teixeira JS, Shu-Wei Su M, Gänzle MG. Contribution of glutaminases to glutamine metabolism and acid resistance in *Lactobacillus reuteri* and other vertebrate host adapted lactobacilli. Food Microbiol. 2020 Apr 1;86:103343.
49. Newman EB, Kapoor V, Potter R. Role of L-Threonine Dehydrogenase in the Catabolism of Threonine and Synthesis of Glycine by *Escherichia coli*. J Bacteriol. 1976;1245–9.
50. Debussche L, Couder M, Thibaut D, Cameron B, Crouzet J, Blanche' F, *et al.* Assay, purification, and characterization of cobaltochelatase, a unique complex enzyme catalyzing cobalt insertion in hydrogenobyrinic acid a,c-diamide during coenzyme B12 biosynthesis in *Pseudomonas denitrificans*. J Bacteriol. 1992;174(22):7445.
51. Maddalo G, Stenberg-Bruzell F, Götzke H, Toddo S, Björkholm P, Eriksson H, *et al.* Systematic analysis of native membrane protein complexes in *Escherichia coli*. J Proteome Res. 2011 Apr 1;10(4):1848–59.
52. Han M, Chen Z, He P, Li Z, Chen Q, Tong Z, *et al.* YgiM may act as a trigger in the sepsis caused by *Klebsiella pneumoniae* through the membrane-associated ceRNA network. Front Genet. 2022 Sep 23;13:973145.
53. Ernits K, Saha CK, Brodiazhenko T, Chouhan B, Shenoy A, Buttress JA, *et al.* The structural basis of hyperpromiscuity in a core combinatorial network of type II toxin–antitoxin and related phage defense systems. Proceedings of the National Academy of Sciences. 2023 Aug 15;120(33):e2305393120.
54. Owen S V., Wenner N, Dulberger CL, Rodwell E V., Bowers-Barnard A, Quinones-Olvera N, *et al.* Prophages encode phage-defense systems with cognate self-immunity. Cell Host Microbe. 2021 Nov 10;29(11):1620-1633.e8.
55. Doron S, Melamed S, Ofir G, Leavitt A, Lopatina A, Keren M, *et al.* Systematic discovery of antiphage defense systems in the microbial pangenome. Science. 2018 Mar 2;359(6379):eaar4120.

56. Kommireddy V, Valakunja N. Diverse Functions of Restriction-Modification Systems in Addition to Cellular Defense. Microbiology and Molecular Biology Reviews. 2013 Mar 7;77(1):53–72.
57. Millman A, Melamed S, Leavitt A, Doron S, Bernheim A, Hör J, *et al.* An expanded arsenal of immune systems that protect bacteria from phages. Cell Host Microbe. 2022 Nov 9;30(11):1556-1569.e5.
58. LeRoux M, Srikant S, Teodoro GIC, Zhang T, Littlehale ML, Doron S, *et al.* The DarTG toxin-antitoxin system provides phage defence by ADP-ribosylating viral DNA. Nat Microbiol. 2022 Jul 1;7(7):1028–40.
59. Gao L, Altae-Tran H, Böhning F, Makarova KS, Segel M, Schmid-Burgk JL, *et al.* Diverse enzymatic activities mediate antiviral immunity in prokaryotes. Science. 2020 Aug 28;369(6507):1077–84.
60. González de Aledo M, Blasco L, Lopez M, Ortiz-Cartagena C, Bleriot I, Pacios O, *et al.* Prophage identification and molecular analysis in the genomes of *Pseudomonas aeruginosa* strains isolated from critical care patients . mSphere. 2023 Aug 24;8(4).
61. Nale JY, Thanki AM, Rashid SJ, Shan J, Vinner GK, Dowah ASA, *et al.* Diversity, Dynamics and Therapeutic Application of *Clostridioides difficile* Bacteriophages. Viruses. 2022 Dec 1;14(12):2772.
62. Monteiro R, Pires DP, Costa AR, Azeredo J. Phage Therapy : Going Temperate ? Trends Microbiol. 2018;xx:1–11.
63. Kondo K, Kawano M, Sugai M. Distribution of Antimicrobial Resistance and Virulence Genes within the Prophage-Associated Regions in Nosocomial Pathogens. mSphere. 2021 Aug 25;6(4).
64. López-Leal G, Santamaria RI, Cevallos MÁ, Gonzalez V, Castillo-Ramírez S. Letter to the Editor: Prophages Encode Antibiotic Resistance Genes in *Acinetobacter baumannii*. Vol. 26, Microbial Drug Resistance. Mary Ann Liebert Inc.; 2020. p. 1275–7.
65. Zhu R, Mathur V. Prophages Present in *Acinetobacter pittii* Influence Bacterial Virulence, Antibiotic Resistance, and Genomic Rearrangements. PHAGE: Therapy, Applications, and Research. 2022 Mar 1;3(1):38–49.
66. Álvarez VE, Quiroga MP, Galán AV, Vilacoba E, Quiroga C, Ramírez MS, *et al.* Crucial Role of the Accessory Genome in the Evolutionary Trajectory of *Acinetobacter baumannii* Global Clone 1. Front Microbiol. 2020 Mar 18;11:465735.
67. Brovedan MA, Cameranesi MM, Limansky AS, Morán-Barrio J, Marchiaro P, Repizo GD. What do we know about plasmids carried by members of the *Acinetobacter* genus? World Journal of Microbiology and Biotechnology 2020 36:8. 2020 Jul 13;36(8):1–15.
68. Pfeifer E, Moura De Sousa JA, Touchon M, Rocha EPC. Bacteria have numerous distinctive groups of phage–plasmids with conserved phage and variable plasmid gene repertoires. Nucleic Acids Res. 2021 Mar 18;49(5):2655–73.
69. López-Leal G, Camelo-Valera LC, Hurtado-Ramírez JM, Verleyen J, Castillo-Ramírez S, Reyes-Muñoz A. Mining of Thousands of Prokaryotic Genomes Reveals High Abundance of Prophages with a Strictly Narrow Host Range. mSystems. 2022 Aug 30;7(4).
70. Abedon ST. Domestication of Phage Genes. Bacteriophages as Drivers of Evolution. 2022;193–203.
71. Maddamsetti R, Yao Y, Wang T, Gao J, Huang VT, Hamrick GS, *et al.* Duplicated antibiotic resistance genes reveal ongoing selection and horizontal gene transfer in bacteria. Nature Communications 2024 15:1. 2024 Feb 16;15(1):1–15.
72. Patel PH, Maxwell KL. Prophages provide a rich source of antiphage defense systems. Curr Opin Microbiol. 2023 Jun 1;73:102321.

2.7. SUPPLEMENTARY MATERIAL

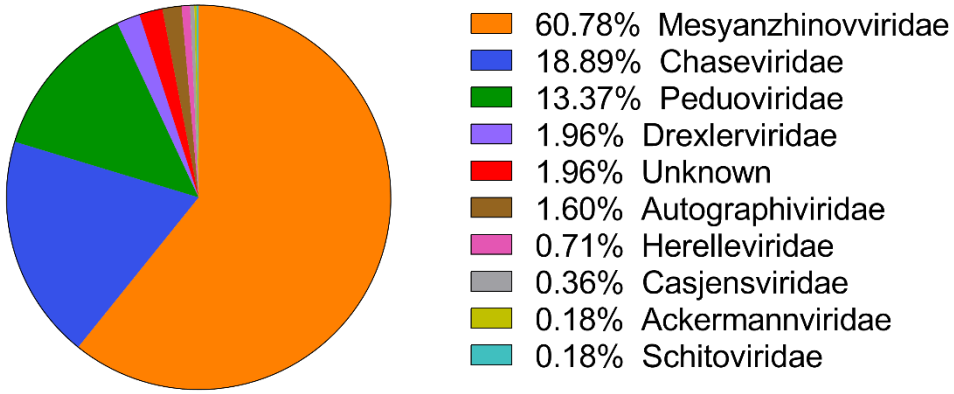


Figure S2.1. Taxonomic family classification of all intact prophages detected in the dataset, corrected for a score >0.90 (n= 560).

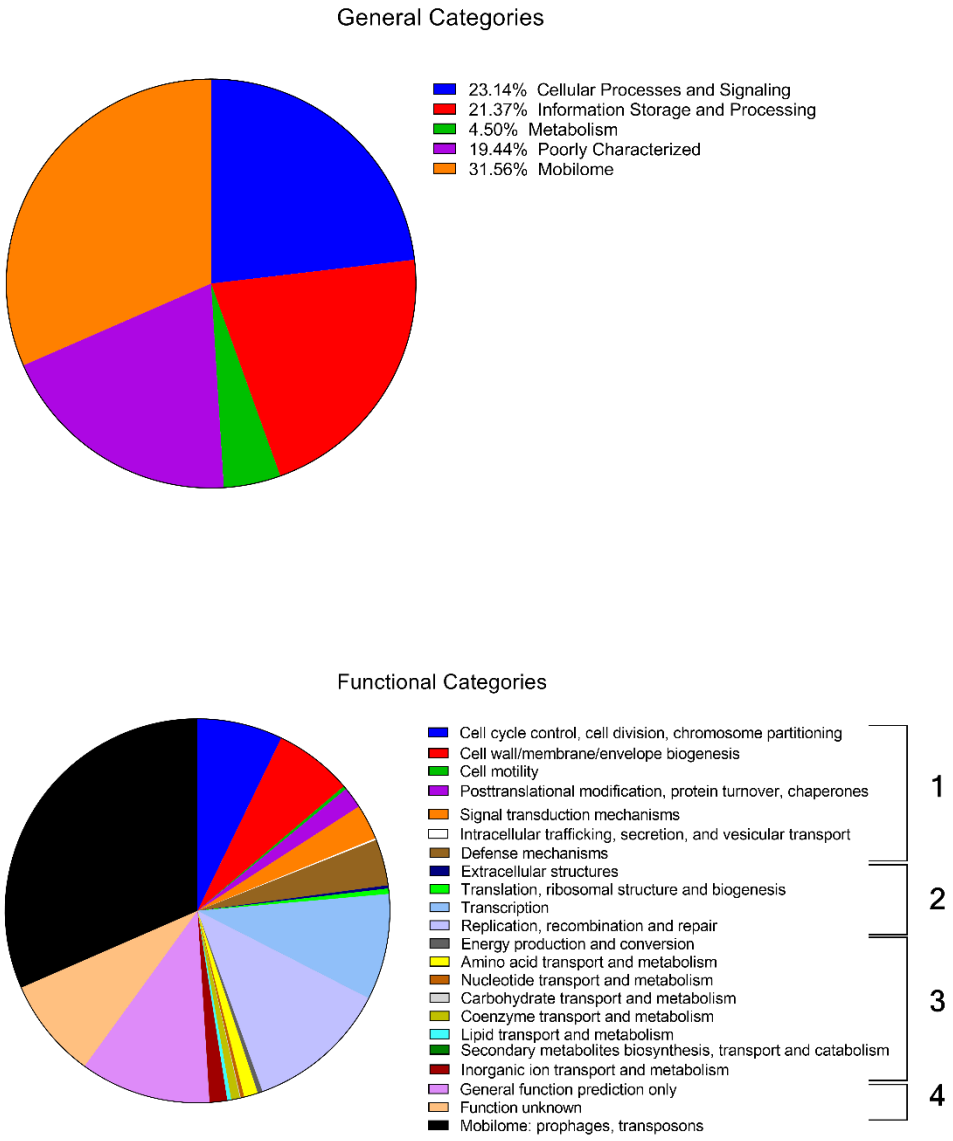


Figure S2.2. General and functional categories attributed based on COG classification of all CDSs found among intact prophages. 1, functional categories belonging to Cellular Processes and Signaling; 2, functional categories belonging to Information Storage and Processing; 3, functional categories belonging to Metabolism; 4, functional categories poorly categorized.

Chapter 3

Prophage induction control by DdrR in *A. baumannii* during early stages of the SOS response

---

- **R. Monteiro**, R. Domingues, H. Oliveira, A. de Jong, E. Bathoorn, J.M. van Dijl, J. Azeredo

Abstract

Acinetobacter baumannii is a critical Gram-negative bacterial pathogen that evolved by mutation and horizontal gene transfer, thereby acquiring resistance to a range of different antimicrobials. Recent studies have started to unveil how the SOS response works in *A. baumannii*, with known central roles for the RecA, UmuDAb, and DdrR proteins. Nevertheless, the DdrR protein still has undefined features in the regulation of non-DNA-damage-inducible genes, which include mobile elements such as prophages. Therefore, our present study was aimed at understanding how DdrR regulates differences in bacterial gene expression, with particular focus on prophage gene expressions. To this end, genomics and transcriptomics approaches were applied. A deletion strain lacking the *ddrR* gene was constructed for the transcriptomics experiments, as well as three mutants lacking individual prophages. Our results show that the absence of DdrR influences several virulence genes in the absence of an SOS response. More interestingly, prophage gene expression seemed significantly deregulated with late genes being overexpressed. Similarly, upon exposure to mitomycin C, prophage genes were highly induced. One particular prophage-borne gene, coding for protein Q, was affected by the absence of the *ddrR* gene in all prophages. Although all prophages seemed activatable, we could only detect the induction of two of them. Our present study shows that the DdrR, besides influencing bacterial virulence expression, is indeed influencing prophage induction, by an unknown mechanism that still needs to be characterized.

Keywords: A. baumannii; Phage induction; Prophages; SOS response; Virulence

3.1. INTRODUCTION

A. baumannii, a Gram-negative bacterium, has become a feared pathogen due to its resistance to last-generation antibiotics like the carbapenems. For this reason, it is nowadays regarded as a top-priority pathogen for the development of new drugs by the World Health Organization (1,2). The development of multidrug resistance in this organism is mainly related to its high genomic plasticity, which allowed it to mutate, as well as acquire external DNA by horizontal gene transfer (HGT). These two mechanisms also contributed to its evolution from a soil bacterium to a bacterium that has adapted to the human niche. In addition, the so-called SOS system of *A. baumannii* plays a crucial role in its adaptation and survival strategies (3,4). This system is well-conserved among bacteria, featuring the RecA/LexA proteins with a central role. In particular, the SOS response of *A. baumannii* relies on three main proteins, namely RecA, DdrR, and UmuDAb (5–8). The *ddrR* gene is a unique feature *of A. baumannii*, with no homology to any other bacterial gene. Accordingly, its function was explored only recently (7–12). The studies so far showed that the DdrR protein functions as a co-regulator of SOS genes together with the UmuDAb protein to which it can bind (11). The DdrR-UmuDAb complex was shown to interact with different operons, for instance the one encoding the error-prone DNA polymerases, keeping them tightly repressed (8,10). Peterson and colleagues observed that nine DNA damage-inducible genes were activated by the DdrR-UmuDAb complex, in addition to genes that were regulated independently by DdrR (10). DdrR-dependently expressed genes were found to be related to DNA replication and repair, as well as other bacterial processes like solute transport or transcriptional regulation.

The SOS response in *A. baumannii* significantly influences HGT mediated by mobile genetic elements, such as plasmids and prophages. Upon antibiotic stress, the SOS response triggers the lytic cycle of prophages that ends with bacterial death and the release of multiple virion particles that will look for a new host to infect and insert their DNA. Eventually, the virions will also transfer extra genetic information from the previous host to newly infected bacteria (12–14). Genome sequencing has revealed a high prevalence of prophages in *A. baumannii* genomes, many of which carry virulence/fitness-related genes that can potentially be transferred (15–17). Recent studies showed that prophage genes can be induced or repressed in the presence or absence of the DdrR protein (10). Moreover, it was also shown that this protein could directly bind to a phage repressor, indicating that it may be involved in prophage regulation, including prophage induction (7,8,11). Recently, Cook *et al.* revisited one of the previous studies, which revealed that the *ddrR* gene influences not only bacterial fitness and virulence but also the induction of two phage repressors (7). Despite these studies, the mechanism by which the DdrR protein modulates prophage induction or the expression of virulence is still unknown. Yet, a better

understanding of DdrR function can be helpful in the development of new strategies to address infections caused by *A. baumannii*. Therefore, the present study was aimed at exploring the relevance of the *ddrR* gene both for virulence expression and prophage induction through the use of genomics and transcriptomics approaches.

3.2. MATERIALS AND METHODS

3.2.1. Bacterial strains and growth conditions

For RNAseq experiments, *A. baumannii* strain ATCC 17978 and its derivative 17978::*ddrR* were grown overnight by incubation at 37 °C and under agitation at 120 rpm in Dulbecco's Modified Eagle Medium (DMEM High Glucose, GlutaMAX™ supplement, Gibco). For phage induction experiments, the *A. baumannii* strain ATCC 17978 and its prophage-free derivatives 17978::Pro1, 17978::Pro2, and 17978::Pro3 were grown in Lysogeny Broth (LB, NZytech). When required, LB was supplemented with 50 µg/mL kanamycin (NZytech) and 100 µg/mL apramycin (Alfaesar). LB agar plates contained 1.2 % agar and LB top agar contained 0.2 % agar.

3.2.2. Whole-genome sequencing of *A. baumannii* ATCC 17978

Because of the variability of *A. baumannii* ATCC 17978 sequences archived in the GeneBank database (NCBI), we decided to re-sequence the *A. baumannii* ATCC 17978 strain from our collection and the respective *ddR* deletion mutant using both Illumina Miseq and Nanopore MinION platforms followed by hybrid assembly of the strain's genome sequence. To this end, the DNA of both strains was extracted using the Quick-Start Protocol DNeasy UltraClean Microbial Kit (Qiagen, Germany) according to the manufacturer's protocol. The DNA concentrations were determined using a Qubit® 2.0 fluorometer and the dsDNA HS and/or BR assay kit (Life Technologies, Carlsbad, CA, US). Illumina Miseq sequencing was performed as previously described (18). Nanopore MinION sequencing was performed using the rapid barcoding kit (SQK-RBK004) from Oxford Nanopore Technologies according to manufacturers instructions. For post-sequencing processing and short-read-first hybrid assembly of bacterial genomes, we used Trimmomatic (Galaxy version 0.38.1) (19) with default settings for short read Illumina data trimming, the Porechop (version 0.2.4) adapter trimmer for Oxford Nanopore reads, and Unicycler (version 0.4.8) (20) for assembly of the trimmed Illumina reads (R1 and R2) and the Nanopore (porechopped) long reads. The sequences resulting from the hybrid assembly are available at (LINK). Annotation of the sequenced genomes was performed with PROKKA (21,22) from the Galaxy web platform.

3.2.3. Prophage detection, phage induction and phage quantification

The determined *A. baumannii* ATCC 17978 sequences were submitted to the PHASTEST webserver for prophage detection and pre-annotation (23). Complete prophage annotation was performed using BLASTp (24), HHPred (25,26), VirFAM (27), and PhANNs (28). For prophage induction during growth in LB or DMEM, 3 µg/mL of mitomycin C (MMC, ThermoFisher) was added to the cultures, followed by an overnight incubation with shaking at 37 °C. Transmission Electron Microscopy (TEM) was used to visualize phage particles liberated from the resulting cell lysates. TEM samples were prepared as previously described (29). Briefly, phages were collected by centrifugation at 20,000 × g and washed with water twice, then the phages were pipetted onto copper grids with carbon-coated Formvar films and stained with 5 % uranyl acetate (pH=4). Subsequently, images were collected using a Talos F200i electron microscope at 80 kV. Phage quantification was performed using the double-layer agar technique. To this end, 100 µL of overnight cultures of the prophage-free strains 17978::Pro1, 17978::Pro2, 17978::Pro3 were mixed with 0.2 % molten LB agar and plated on regular LB with 1.2 % agar. In parallel, phage lysates were 10-fold serially diluted and filtered through a 0.22 µm filter. Following solidification of the top agar, 10 µL drops of each phage lysate dilution were pipetted onto the lawn and left to dry prior to incubation at 37 °C for 16 h. Subsequently, plaque-forming units (PFUs) were counted.

3.2.4. Construction of the different mutants

A. baumannii ATCC 17978 mutants were generated using the CRISPR-Cas system previously described for this species (30). This system involves the use of two different plasmids. The pSGAb-km plasmid encodes the single-guided RNA (sgRNA) as well as the spacer to target the chromosomal region that is to be modified, whereas the pCasAb-apr plasmid encodes the RNA-guided DNA endonuclease Cas9 and the RecAb recombinase to help repair the DNA cut caused by Cas9. First *A. baumannii* bacteria were electroporated with pCasAb-apr, and plasmid-carrying transformed bacteria were selected on LB agar supplemented with apramycin. Subsequently, pCasAb-apr-harboring bacteria were used for electroporation with pSGAb-km, as well as the donor template when required, and plated on LB agar supplemented with kanamycin. For *ddrR* gene deletion, a spacer was inserted in pSGAb-apr by golden gate cloning, using oligonucleotides detailed in Supplemental Material Table S3.1. A single-stranded DNA (ssDNA) template was used as a donor for this modification as specified in Table S3.1. Prophage-free *A. baumannii* variants were generated using spacers targeting integrases of each prophage without a donor template. Prophage-cured bacteria were selected and inspected for the absence of the prophage using primers specified in Table S3.1. Plasmid curation was performed by streaking bacteria on LB agar supplemented with 5 % sucrose, followed by overnight incubation at 37 °C. Plasmid-free bacteria were

subsequently identified by transferring colonies to antibiotic-containing and antibiotic-free LB agar plates and selecting the bacteria that only grew on the antibiotic-free LB agar.

3.2.5. RNAseq experiments and analyses

For RNAseq experiments, 5 mL overnight cultures of *A. baumannii* were diluted 1:100 in 45 mL of fresh DMEM medium and incubated at 37 °C with shaking at 120 rpm until cells reached a density of 3 × 10^8 colony-forming units (CFUs)/mL. Subsequently, the cultures were divided into two flasks with 10 mL of cell culture each. 3 µg/mL of MMC was added to one of the flasks followed by an incubation of 30 min. After this time, 5 mL samples were immediately frozen in liquid nitrogen and stored at -80 °C until RNA extraction. Notably, for each strain/condition, three biological replicates were performed. To isolate RNA, frozen bacterial pellets were thawed on ice and RNA was extracted using a phenol-chloroform protocol adapted from the literature (31). Briefly, thawed bacterial cells were mixed with 1 volume of ice-cold killing buffer (20 mM Tris/HCl [pH 7,5], 5 mM $MgCl_2$, 20 mM NaN_3), vortexed and centrifuged (Avanti J-26S XP, Beckman Coulter Inc., Brea, California, USA) for 15 min at 8,000 × g and 4 °C. The supernatant was discarded, and the bacterial cells were resuspended in 200 µL of killing buffer. The bacteria were then mechanically disrupted by adding a spatula tip of small glass beads (0.1 mm diameter, Scientific Industries Inc., Bohemia, New York, USA) and bead-beating in a Precellys24 tissue homogenizer (Bertin Technologies, Montigny-le-Bretonneux, France). Up to 2 mL of lysis buffer (4 M guanidine thiocyanate, 25 mM sodium acetate [pH 5.2], 0.5% N-laurylsarcosinate [wt/vol]) was then added to each tube. Upon vortex-mixing, 1 mL of the lysate was used for phenol-chloroform extraction. Bacterial lysates were extracted twice with 1 volume of acid phenol, mixed, and centrifuged at 18,500 × g (MIKRO 200, Hettich, Germany) for 5 min at room temperature. Then, the aqueous phase was mixed with chloroform/isoamyl alcohol (24:1), mixed and centrifuged. After collecting the aqueous fraction, 1/10 volume of 3 M sodium acetate (pH 5.2) and 1.2 volume of isopropanol were added, and RNA precipitation was carried out by incubating the samples at -20 °C overnight. The RNA was collected by centrifugation (15 min at 18,500 × g, 4 °C), and washed with 80 % RNAse-free Ethanol. Pelleted RNA was dried for 1 h at room temperature before resuspending it in 100 µL of RNAse-free water. The RNA concentration was measured in a Nanodrop, and its quality was assessed by running a 1% (w/v) agarose gel mixed previously with 1% bleach (v/v). Turbo DNase (Invitrogen) was used to remove any DNA contaminants, followed by RNA cleaning using acid phenol and re-precipitation.

The RiboCop for Bacteria (Lexogen) was used to deplete 800 ng of the extracted total RNA for rRNA. The NEBNext® Ultra™ II Directional RNA Library Prep Kit for Illumina® (New England Biolabs, UK) was used to prepare the library preps for Illumina sequencing. Samples were sequenced on the Illumina

NexSeq 1000 to generate 100 bases single-end reads (100SE) with an average read-depth of 20M reads per sample. The quality of the resulting fastq reads was checked using FastQC (v0.11.9) (Babraham Bioinformatics, Cambridge) and mapped on the reference genome with Bowtie2 (v2.4.2 70) using default settings. The resulting SAM files were converted to BAM using SAMtools (v1.1171), and featuresCounts (v2.0.1 72) was used to obtain the gene counts.

The T-REX pipeline (32) was applied to perform the statistical analysis and determine differential gene expression. Subsequently, the obtained data from the DGEs was analyzed for Functional Analysis and Gene set Enrichment for Prokaryotes using FACoP: Functional Annotation and Classification of Proteins of Prokaryotes (33). Further analysis of identified proteins of interest was done with BlastP (34) and Uniprot (35). The DGE data is available in Supplemental Material Table S3.3 and can be accessed at (LINK).

3.2.6. Statistical analyses

Statistical calculations were made through GraphPad software, version 7.0. All data are expressed as means ± standard error of the mean (SEM) and statistical differences were calculated by two-way ANOVA and Tukey's multiple comparison test. Statistical analysis of the RNAseq results was carried out using the T-REx2 RNA-Seq analysis pipeline. A gene was considered significantly differentially expressed when the fold change was $\geq |2.0|$ and the false discovery rate (FDR) adjusted p-value ≤ 0.05.

3.3. RESULTS AND DISCUSSION

3.3.1. DdrR and its role in bacterial processes including virulence and fitness

At the time of this study, there were several disparities within NCBI on the *A. baumannii* ATCC 17978 genome sequence with several different sequences available and no closed genomes. As this strain was also in our lab for some time, we chose to sequence it using the Illumina and Nanopore platforms, to obtain a completely closed genome sequence for the generation of more accurate results. Following its annotation, we deleted the *ddrR* gene from our lab strain (17978::*ddrR*), which was used for all subsequent experiments.

Transcriptomic profiles from the 17978 and 17978::*ddrR* strains (respectively referred to as the WT and *ddrR* strains) were determined and compared under the same conditions (with or without MMC) using RNAseq. In particular, a differential gene expression analysis was performed followed by functional analysis and gene set enrichment to identify relevant biological functions influenced by the *ddrR* deletion. Differentially expressed genes between the WT and *ddrR* strains in the absence of MMC were plotted in a Volcano plot (Figure 3.1). The transcriptomic profiles revealed that 183 genes were upregulated, and

100 genes were downregulated in the absence of MMC, showing a strong influence of the *ddrR* deletion on overall gene expression. Among the upregulated genes, the Funage-Pro webserver identified different class IDs related to metabolism (COG: Q – Secondary metabolites biosynthesis, transport, and catabolism) (33). A KEGG pathways analysis showed that upregulated genes belong to a pathway (ko01053) that is related to the biosynthesis of non-ribosomally synthesized peptides from the siderophore group. Furthermore, by analyzing gene ontology classes, it was found that significantly upregulated processes included isochorismatase activity (GO:0008908), organic substance biosynthesis (GO:1901576), 2,3-dihydroxybenzoate-serine ligase activity (GO:0047527), ABC-type transporter activity (GO:0140359), enterobactin biosynthesis (GO:0009239), and others (Supplemental Material Table S3.2). Among the upregulated genes were also some genes related to virulence, specifying for example the NorM protein (AFMDGAFA_00063), the tetracycline resistance protein A (AFMDGAFA_00380), CsuA (36) (AFMDGAFA_01312), the OprD porin (AFMDGAFA_02858), and the copper resistance proteins A and B (AFMDGAFA_03074 and AFMDGAFA_03075). Some of the downregulated genes were also related to fitness and virulence, such as genes for Omp33-36 (AFMDGAFA_00191), the ferric-anguibactin receptor FatA (AFMDGAFA_00952), an MFS transporter (AFMDGAFA_00953), and superoxide dismutase [Fe] (AFMDGAFA_01176). A complete table with all differentially expressed genes is presented in Supplemental Material Table S3.3. Although there are variations between our experimental setup and previous studies, certain genes displayed comparable transcriptional profiles in the absence of *ddrR*. For example, the gene for the ProY permease (AFMDGAFA_00078), the formimidoylglutamase (AFMDGAFA_00080), the Omp33-*36* porin (AFMDGAFA_00191), a hypothetical protein (AFMDGAFA_00215), and the glutamate synthase [NADPH] small chain (AFMDGAFA_00314) were downregulated, as was reported in another study (10).

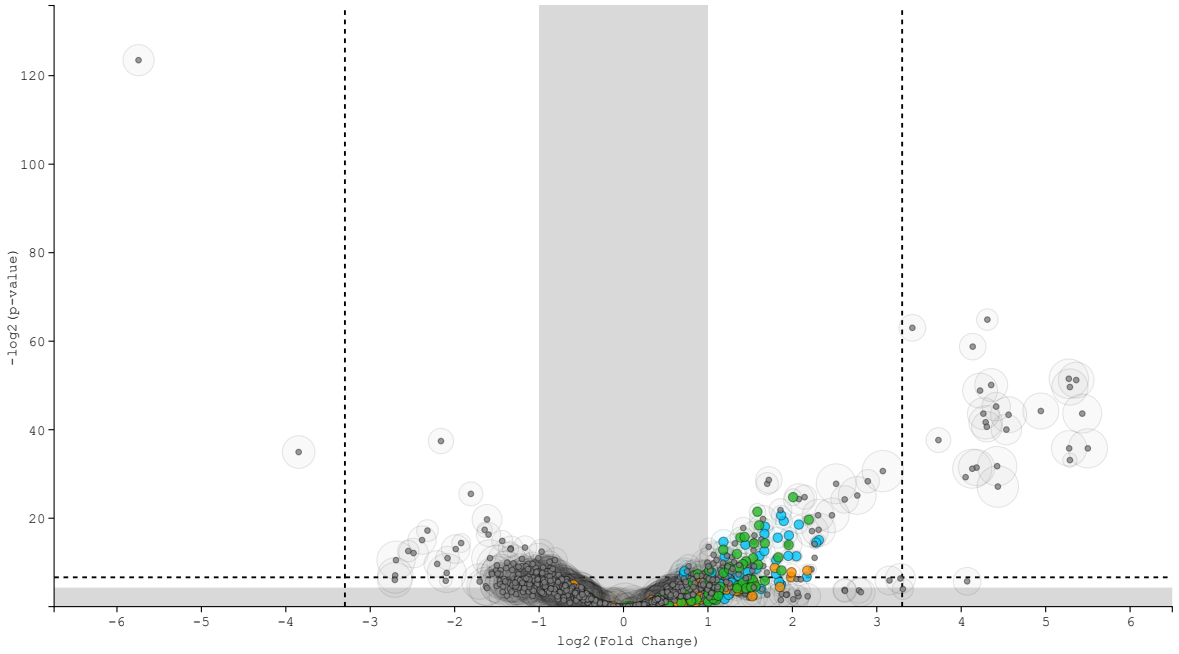


Figure 3.1. Volcano plot visualizing the differentially expressed genes between the WT and *ddrR* mutant in the absence of MMC. Values represent log2-fold changes. Green points – prophage intact-1 encoded genes; Orange points – prophage intact-2 encoded genes; Blue points – prophage intact-3 encoded genes; Grey points – non-prophage encoded genes.

3.3.2. Early SOS response under DNA damage

To investigate the early stages of the SOS response and how *ddrR* might influence them, we treated the *A. baumannii* ATCC 17978 and 17978::*ddrR* strains with MMC. The MMC-induced stress response was stopped by snap-freezing the cells after 30 min of incubation in liquid nitrogen before proceeding with RNA extraction. The subsequent transcriptome analysis revealed a set of 77 and 96 genes that were deregulated compared to the WT and *ddrR* strains, respectively. Figure 3.2-a shows the proportion of these sets of genes between both strains, with both strains having 76 deregulated genes in common, while one gene was only deregulated in the WT strain and 20 were only deregulated in the *ddrR* strain. Among the commonly deregulated genes, typical SOS genes such as *recA*, *ddrR*, *umuD*, *umuC*, and *umuDAb* were induced in both strains (Table 3.1), in accordance with the results from previous studies (5,10,12), even though we used a different experimental setup including different growth media as well as a lower incubation time with MMC. It should be noted that the *ddrR* gene appeared to be overexpressed in the *ddrR* mutant, but this must be attributed to mapping of RNA sequences to the region adjacent to the *ddrR* gene, as the *ddrR* gene knockout was successfully confirmed by Sanger sequencing. Curiously, in both strains, the SOS genes *uvrA* and *uvrC* were induced, whereas the *ruvC* and *holB* genes were not induced. This is contrary to the findings of Hare *et al.* who did not detect any alterations in the expression

of the former two genes and observed repression of the latter pair (12). However, a following study from the same group re-analyzed the same data corroborating our observation (7). Moreover, the *uvrA* gene for example was also shown to be induced in another study with *A. baumannii* (5). This gene, which is part of the UvrABC system involved in DNA repair, was shown to be among the first SOS genes to be induced in *E. coli* after UV irradiation (14). Thus, both *uvrA* and *uvrC* appear to be part of an early SOS response. Regarding our strains, there are a few differences in the SOS genes that are expressed upon MMC treatment, as outlined in Table 3.1. For instance, the *ssb*, *ruvB*, and *ruvA* genes were induced (2.8, 2.2, and 2.1-fold respectively) only in the absence of the *ddrR* gene, which might indicate a role in keeping them regulated. The expression profiles of the *ruvB* and *ruvA* genes were similar to what has been observed previously, where these two genes were among the ones induced after DNA damage only in the mutant strain (10). The *ssb* gene, which is fundamental for several cellular processes like DNA replication and repair in *E. coli*, is SOS-regulated and it shows a high basal expression which further increases only after a stronger SOS induction (37). As an early response, an overexpression of *ssb* would not be expected. Therefore, the fact it was induced only in the *ddrR* mutant, may indicate that DdrR can somehow regulate *ssb* expression by maintaining a basal expression level, and timing its full expression once the DNA damage signal becomes stronger. Besides, DdrR may also keep the *ssb* gene repressed to allow the expression of more error-prone DNA polymerases, which could potentially increase genomic mutations, as suggested by Cook et al. (7).



Figure 3.2. Proportion of genes a) regulated during the early SOS response induced by MMC treatment in WT and *ddrR* mutant *A. baumannii* ATCC 17978; b) regulated during the early SOS response in WT and *ddrR* mutant *A. baumannii* ATCC 17978, but excluding prophage genes; and c) encoded by prophages in the WT and *ddrR* mutant *A. baumannii* ATCC 17978 under SOS response. Venn diagrams were created using InteractiVenn (38).

Table 3.1. Comparison of the expression of SOS-related genes in *A. baumannii* ATCC 17978 WT and the respective *ddrR* mutant upon SOS induction with MMC

Locus tag	gene	WT[a]	*ddrR*[b]
AFMDGAFA_00002	*dnaN*	-	-
AFMDGAFA_00003	*recF*	-	-
AFMDGAFA_00004	*gyrB*	-	-
AFMDGAFA_00193	*uvrA*	2.7	3.5
AFMDGAFA_00201	*ssb*	-	2.8
AFMDGAFA_00404	*recG*	-	-
AFMDGAFA_00930	*ruvB*	-	2.2
AFMDGAFA_00931	*ruvA*	-	2.1
AFMDGAFA_01016	*uvrB*	-	-
AFMDGAFA_01564	*umuC*	9.6	7.2
AFMDGAFA_01622	*recA*	3.6	4.8
AFMDGAFA_01856	*uvrA*	-	-
AFMDGAFA_02029	*hupB*	-	-
AFMDGAFA_02141	*holB*	-	-
AFMDGAFA_02188	*ruvC*	-	-
AFMDGAFA_02316	*umuDAb*	15.9	20.5
AFMDGAFA_02317	*ddrR*	30	7.3*
AFMDGAFA_02563	*umuD*	23.8	30.9
AFMDGAFA_02564	*rumB*	21.1	14.8
AFMDGAFA_02713	*dnaQ*	-	-
AFMDGAFA_02901	*ftsK*	-	-
AFMDGAFA_03118	*polA*	-	-
AFMDGAFA_03408	*recN*	-	-
AFMDGAFA_03419	*uvrC*	2.6	3.1
AFMDGAFA_03541	*dinB*	-	-
AFMDGAFA_03838	*umuD*	27.9	42.5
AFMDGAFA_03839	*umuC*	13.2	16.5

[a] *Fold change in gene expression between MMC-treated ATCC 17978 WT cells and untreated WT cells.*

[b] *Fold change in gene expression between MMC-treated ATCC 17978::ddrR cells and untreated ddrR cells.*

[*] *The gene ddrR was not present in the genome after the knockout, confirmed by whole-genome sequencing.*

3.3.3. DdrR influences a wide range of genes no-DNA-damage-inducible genes

As mentioned above, DdrR potentially regulates a wide range of genes beyond the SOS core genes upon MMC induction. As shown in Figure 3.2-b, only 23 and 35 genes were deregulated in the WT and *ddrR* strains, respectively. Excluding the canonical SOS genes, there was only one gene repressed in the WT, encoding a hypothetical protein (AFMDGAFA_01302). In contrast, five genes were repressed in the

ddrR strain including genes for a TolC family protein (AFMDGAFA_00281), CzcB/A (AFMDGAFA_00282/ AFMDGAFA_00283), and the copper resistance proteins A/B (AFMDGAFA_03074/AFMDGAFA_03075). The TolC protein, the cation efflux system proteins CzcB and CzcA, and the copper resistance proteins A (CopA) and B (CopB) are related to the virulence and fitness of the host. In particular, TolC is a transmembrane protein that has been implicated in the export of proteins that are toxic to the host, such as antimicrobials, playing a critical role in bacterial pathogenicity (39). CopA and CopB, and CzcB and CzcA are involved in the resistance to copper and cadmium respectively (40–42). On the other hand, 12 genes were upregulated in both strains, meaning that their regulation might be independent of DdrR. Among the latter are genes encoding the DNA topoisomerase subunit B (AFMDGAFA_00126), a putative S-Adenosyl methionine (SAM) protein (AFMDGAFA_00381), a DNA repair protein (AFMDGAFA_00381), a dGTPase (AFMDGAFA_00932), the regulatory RecX protein (AFMDGAFA_01621), SOS-response associated peptidase (SRAP) (AFMDGAFA_02051), a N-acetylmuramidase (AFMDGAFA_02503), the LexA-like regulator (AFMDGAFA_02506), the GstA protein (AFMDGAFA_03323), the DNA topoisomerase subunit A (AFMDGAFA_03533), and a few hypothetical proteins. Most of these genes are related to SOS response, such as the DNA topoisomerase, a DNA repair protein, the RecX protein, the SAM protein, and the LexA-like regulator. The LexA-like regulator is, in fact, a phage repressor and, accordingly, it is expected to be expressed under stress. Furthermore, there were 5 genes upregulated only in the *ddrR* strain, including the esterase YqiA, a ribose-phosphate pyrophosphokinase, a nicotine phosphoribosyltransferase, a TonB-dependent copper receptor, and a hypothetical protein. All but the TonB-dependent copper receptor are involved in bacterial metabolic processes. On the other hand, the copper receptor is an outer membrane protein with a crucial role in *A. baumannii* virulence since it mediates iron acquisition, adherence, and biofilm formation (43,44).

3.3.4. DdrR has a critical regulatory role in prophage gene expression

After carefully analyzing the genomic sequence obtained from the hybrid assembly, three prophage regions were detected through PHASTER as reported by Hare *et al*. (12). However, in our analysis they were detected as intact prophages which we denoted as intact-1, intact-2, and intact-3. These intact prophages were predicted to belong to three different families, namely the *Peduoviridae*, *Autographiviridae* and *Drexlerviridae*, which may correspond to the morphologies presented by myoviruses (intact-1), podoviruses (intact-2), and siphoviruses (intact-3) respectively.

In the absence of stress, prophage-encoded genes of *ddrR* strain accounted for a quarter (24.4%) of the deregulated genes, which implies a potentially strong influence of DdrR on prophage gene expression. These genes are identified by different colors in the volcano plot shown in Figure 3.1 and

listed in Table 3.2. They encode mostly structural phage proteins, such as the major capsid, portal, or tail fiber proteins. In addition, they encode a few transcriptional regulators responsible for the lytic-lysogenic switch, such as the Cro protein, a DNA-binding protein, or the antitermination protein Q. Both the Cro and Q proteins are considered important regulators of the prophage lifecycle. Cro acts as a lytic cycle activator, allowing the phage to start the replication cycle, and the protein Q acts at a certain point of the lytic cycle, allowing the switch from early/middle to late gene expression (45). These findings may indicate a possible correlation between DdrR and late prophage gene expression by influencing the expression of the antitermination protein Q gene.

Table 3.2. List of prophage intact-1, -2, and -3 genes and the corresponding fold-changes influenced by the *ddrR* gene deletion in the absence of induced DNA damage

Locus Tag	Product	Fold change
Intact-1		
AFMDGAFA_01497	DNA-binding protein	2.9
AFMDGAFA_01509	Cro/CI family transcriptional regulator	3.6
AFMDGAFA_01510	Putative DNA-binding protein/regulatory protein	3.6
AFMDGAFA_01516	Hypothetical protein	2.8
AFMDGAFA_01518	Hypothetical protein	3.5
AFMDGAFA_01527	VSR endonuclease	4.5
AFMDGAFA_01528	Transposase	2.4
AFMDGAFA_01530	Terminase large subunit	3.2
AFMDGAFA_01531	Portal	4.2
AFMDGAFA_01532	Minor capsid protein	2.7
AFMDGAFA_01534	Hypothetical protein	2.3
AFMDGAFA_01535	Hypothetical protein	2.2
AFMDGAFA_01536	Telomere regulation protein	3.2
AFMDGAFA_01537	Major capsid protein	2.3
AFMDGAFA_01538	Stress-responsive nuclear envelope protein	3.7
AFMDGAFA_01539	Head-tail joint	2.6
AFMDGAFA_01540	Glutamate 5-kinase	3
AFMDGAFA_01541	Peptidase	2.8
AFMDGAFA_01542	Putative tail completion protein	2.1
AFMDGAFA_01546	Hypothetical protein	3.1
AFMDGAFA_01547	Tail fiber	3.5
AFMDGAFA_01548	Phage tail tube protein	3.6
AFMDGAFA_01549	Tail assembly chaperone	3.9
AFMDGAFA_01555	Putative minor tail protein	5
AFMDGAFA_01556	Minor tail protein	3.2
AFMDGAFA_01557	Minor tail protein	4.9
AFMDGAFA_01558	Host specificity factor TipJ family phage tail protein	2.3
AFMDGAFA_01559	Holin	4.1
AFMDGAFA_01560	Lysozyme	3.9
AFMDGAFA_01561	Hypothetical protein	3.5
Intact-2		
AFMDGAFA_02067	Hypothetical protein	3.5
AFMDGAFA_02068	Lysozyme; glycoside hydrolase family protein	4
AFMDGAFA_02069	Holin	2.8
AFMDGAFA_02080	Major tail subunit	2.9

AFMDGAFA_02082	Neck	2.4
AFMDGAFA_02089	Large subunit terminase	4.5
AFMDGAFA_02096	Hypothetical protein	2.9
AFMDGAFA_02105	Replicative DNA helicase	4
AFMDGAFA_02108	Cro protein	3.6
Intact-3		
AFMDGAFA_02567	N-acetylmuramidase	4.6
AFMDGAFA_02568	Ammonia monooxygenase/methane monooxygenase	4.6
AFMDGAFA_02569	Phage tail protein	4.6
AFMDGAFA_02571	Hypothetical protein	4.6
AFMDGAFA_02572	Sialate O-acetylesterase	4.6
AFMDGAFA_02574	Hypothetical protein	4.6
AFMDGAFA_02575	Tail protein	4.6
AFMDGAFA_02577	Hypothetical protein	4.6
AFMDGAFA_02579	Major tail protein	2.9
AFMDGAFA_02580	Tail completion protein	3
AFMDGAFA_02581	Neck	2.7
AFMDGAFA_02582	Hypothetical protein	3.9
AFMDGAFA_02583	Major capsid protein (Adaptor)	2.7
AFMDGAFA_02584	Hypothetical protein	3
AFMDGAFA_02585	Major capsid protein	2.6
AFMDGAFA_02586	Hypothetical protein	2.7
AFMDGAFA_02587	Putative head protein	3
AFMDGAFA_02588	Hypothetical protein	3.2
AFMDGAFA_02589	Hypothetical protein	2.6
AFMDGAFA_02591	Minor capsid protein	2.9
AFMDGAFA_02592	Portal	2.4
AFMDGAFA_02593	Phage terminase large subunit	4
AFMDGAFA_02594	Hypothetical protein	3.6
AFMDGAFA_02595	Putative metallopeptidase	2.6
AFMDGAFA_02599	Phage antitermination protein Q	2.2
AFMDGAFA_02600	Hypothetical protein	2.8
AFMDGAFA_02606	Type II methyltransferase M.PspPI	2.7
AFMDGAFA_02608	XRE family transcriptional regulator (cII protein)	2.9
AFMDGAFA_02611	Hypothetical protein	3
AFMDGAFA_02613	Hypothetical protein	2.9

To ascertain whether the observed expression of prophage genes would lead to the release of phages from bacterial hosts, bacterial growth was followed under MMC stress (Figure 3.3). The data shows that after 30 min of incubation with MMC, the number of the *ddrR* mutant bacteria was reduced by one order of magnitude, which usually is an indication of prophage induction (Figure 3.3). Conversely, the MMC-treated WT culture maintained an essentially constant cell count, whereas the untreated culture exhibited growth. As discussed above, in the absence of MMC, few prophage genes were overexpressed in the *ddrR* mutant, and these include mostly structural phage genes, such as the portal, minor and major capsid genes, the tail fiber gene, and others considered as late genes. During the SOS response, most of the induced genes belong to the three prophage regions (70 % and 64 % from the WT and *ddrR* transcriptomes, respectively). For instance, in the WT strain several prophage genes were induced by

MMC (intact-1 – 17/71 genes; intact-2 – 16/54 genes; intact-3 –21/60 genes), most of them being genes for transcriptional regulators, such as Cro, XRE, the phage repressor CI, and the YdaU repressor, and a few encoding hypothetical proteins. Curiously, the three prophages harbor genes for methyltransferases that were highly induced by MMC. Possibly, these enzymes protect the phage DNA from restriction-modification (R-M) systems upon infection of a bacterial host cell. The intact-2 prophage was the only one with an annotated excisionase, which was also induced by MMC (6.3-fold). Thus, during the first 30 min of MMC induction of WT cells, prophages seemed to be activated. Furthermore, SOS-response genes, such as *umuC* and *umuD* encoded by intact-1 and intact-3 were also induced, as already discussed above.

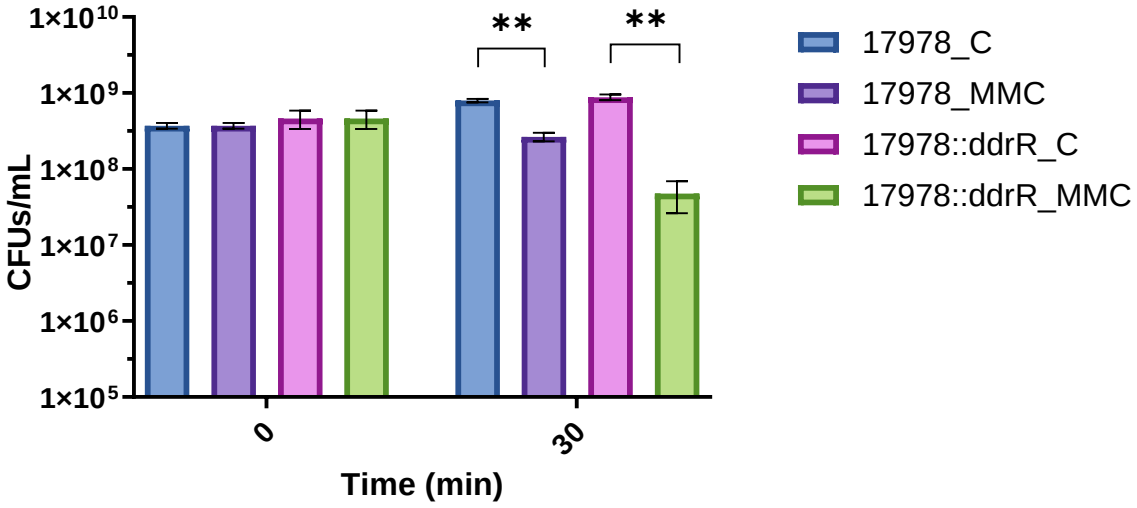


Figure 3.3. Mitomycin C (MMC) effect on colony-forming unit (CFU) counts as measured for the *A. baumannii* ATCC 17978 (WT) and 17978::*ddrR* mutant after 30 min of incubation. 17978_C (blue) – untreated WT control culture; 17978_MMC (purple) – MMC-treated WT culture; 17978::*ddrR*_C (pink) – untreated *ddrR* control culture; 17978::*ddrR*_MMC (green) – MMC-treated *ddrR* culture. Statistically significant differences are represented by ** ($p<0.05$).

The transcriptome of the *ddrR* mutant under MMC-induced SOS stress exhibited a profile similar to that of the WT. Even though these profiles shared similarities, the *ddrR* mutant showed a slight increase in the number of overexpressed genes upon MMC treatment. As can be inferred from the Venn diagram in Figure 3.2-c, DdrR potentially regulates the expression of seven prophage genes. Of these, five belong to the intact-1 prophage, and two belong to intact-2 and intact-3 prophages. Amongst the intact-1 prophage genes, there were genes for a putative DNA transcription activator (AFMDGAFA_01515), a HNH endonuclease (AFMDGAFA_01517), a putative endodeoxyribonucease I (AFMDGAFA_01519), a phage antitermination protein Q (AFMDGAFA_01520), and a hypothetical protein (AFMDGAFA_01518)

induced by MMC, which were not induced in the WT strain. Amongst genes of the prophages intact-2 and intact-3, there was only the gene for the antitermination protein Q (AFMDGAFA_02101 and AFMDGAFA_02599 respectively) induced by MMC in the *ddrR* mutant. It is therefore tempting to propose that DdrR may regulate gene *q* expression by an unknown mechanism, keeping late genes under the host's control to avoid uncontrolled prophage induction and subsequent cell lysis. Since DdrR is not known to have any DNA-binding properties, this regulatory mechanism should involve a second protein. Gene *q,* which produces the antitermination protein Q that modifies RNA polymerase to ignore several terminator sites leading to gene transcription, is directly repressed by the transcriptional activator CII. The CII protein, on the other hand, activates several promotors including the pAQ promoter that transcribes an antisense RNA aQ in order to inhibit gene *q* expression and keep blocking late gene expression (45,46). As CII has these properties, this regulation might be influenced by DdrR, which would interact with it by increasing DNA binding in the same way as it does with UmuDAb to keep error-prone DNA polymerases under tight control (8,11). From the prophage perspective, having protein Q regulated by DdrR would help to efficiently reach optimal phage particle production with a timed late gene expression. This tighter control would favor prophage stability, which would in turn be beneficial for both parties: on the one hand, the host would be able to better control prophage induction and, on the other hand, as the prophage needs gene expression to be in sync, it would have a way to sense the host's SOS response, just like the Cro/CI pair works together with the LexA/RecA pair in *E. coli*. Such an interaction between DdrR and other proteins has been partially studied. It was observed that DdrR could bind to LexA regulators from different species and, given the similarities, this association also occurred with UmuDAb (11). Curiously, the same study showed that DdrR could also form a complex with the phage repressor CI from a prophage equivalent to the intact-1 prophage identified in our present study. Furthermore, Pavlin *et al.* also tested another phage repressor from a prophage equivalent intact-3, but no association with DdrR was observed (11). Regarding CII, an interaction with DdrR has not been proven yet, but such an interaction seems plausible since the temperate phage GIL01 encodes a similar protein (in function) to DdrR, which is named Gp7. The Gp7 protein interacts with the LexA repressor to enhance DNA binding. Because GIL01 lacks a phage repressor, like CI, to mediate prophage lytic/lysogeny cycles, it uses Gp7 for this regulation. This phage establishes lysogeny by increasing LexA binding to its SOS box in the lysogenic promoter P1, which is located in the early genes. The Gp7 complex inhibits LexA auto-cleavage mediated by RecA and keeps the phage lysogenic (47). Moreover, Gp7 can also repress other prophages by delaying their induction to allow phage GIL01 to be induced first. This observation parallels

our present hypothesis regarding the role of the DdrR protein during prophage induction, the main difference being that Gp7 is encoded by the phage GIL01 and not by the host (48).

3.3.5. *A. baumannii* 17978 inducible prophages

To test our hypothesis, we looked further into the prophages encoded by the *A. baumannii* 17978 genome and characterized them. First, we decided to quantify prophage induction accurately and compare the induction levels among the three detected intact prophages. While in their previous study, Hare and colleagues successfully detected prophage induction with MMC using both TEM and PCR, they were unable to quantify or identify which specific prophages were induced (12). This aspect is however crucial to substantiating the formulated theory. In order to validate our induction conditions, and corroborate the results observed from transcriptomics, cells were incubated in LB supplemented with MMC overnight to make sure prophage induction would occur. After being collected and filtered, the lysates were inspected by TEM (Figure 3.4). As shown in Figure 3.4, there was an apparent distinction between two different phages with subtly different capsid shapes, indicated by the black arrows. Furthermore, these phages presented two different tail sizes of 130 nm and 150 nm, respectively which may correspond to intact-1 (Peduoviridae) and intact-3 (Drexlerviridae) prophages, judged by the reported sizes. This validation aligns with the findings of our transcriptome analyses, which indicate prophage induction by treatment with MMC. However, we were unable to definitively confirm the induction of all three prophages by TEM, since their identity could only be approximated based on the morphologies of the phage families to which they are assigned by sequence similarity.

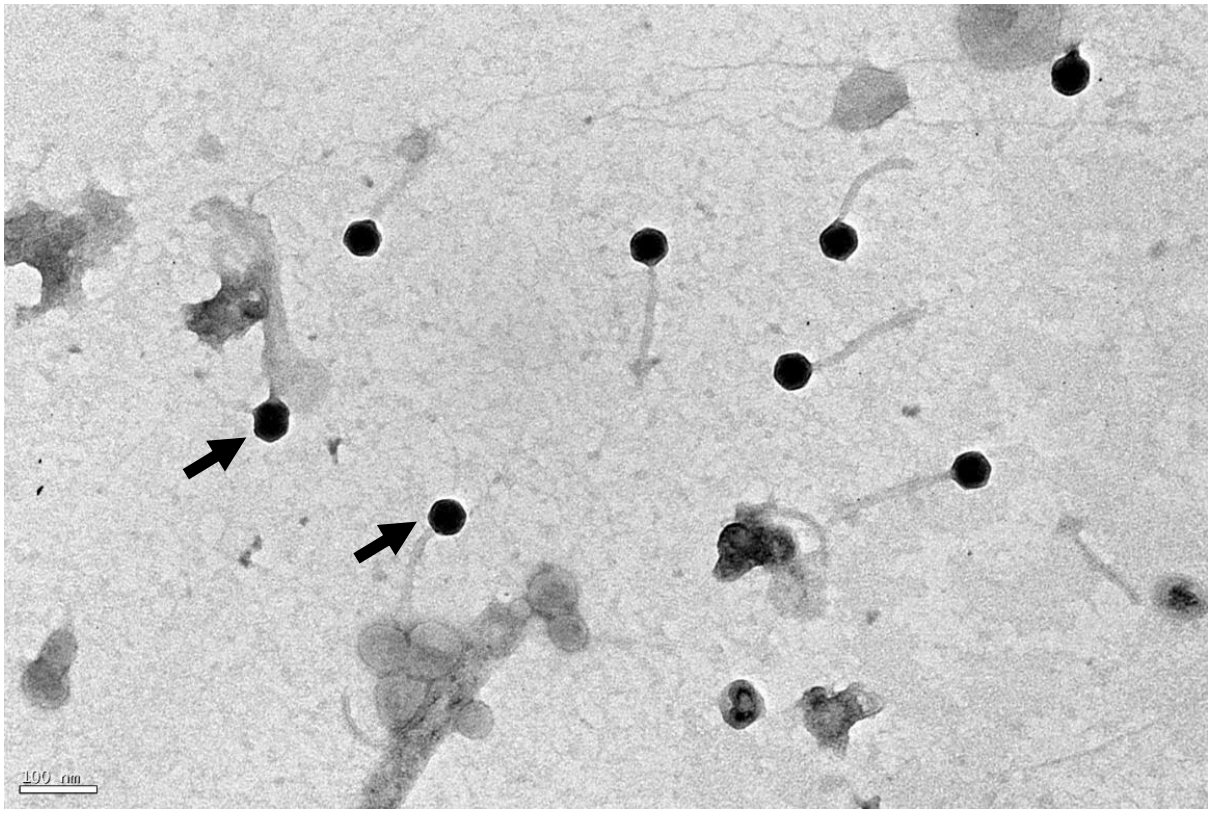


Figure 3.4. Electron micrograph of *A. baumannii* ATCC 17978 WT phage particles after prophage induction at 100,000 × magnification. Black arrows indicate two potentially different capsid structures of the visualized phages.

To identify and quantify which prophages from WT and *ddR* strains are induced by MMC, a collection of three mutant strains was created from the WT strain using the CRISPR-Cas system, with each strain lacking one specific prophage. The resulting strains were named 17978::Pro1 (intact-1 cured strain), 17978::Pro2 (intact-2 cured strain), and 17978::Pro3 (intact-3 cured strain). To validate the prophage deletions, we conducted an induction experiment on each phage-cured mutant to trace possible signs of phage replication. For quantification purposes, although no superinfection exclusion system was detected within any of the three prophage regions, it was assumed that the strain lacking a particular prophage would be specifically infected by that phage. Accordingly, when phages in lysates obtained upon prophage induction were quantified using the different prophage-cured mutants 17978::Pro1, 17978::Pro2 or 17978::Pro3 as indicator strains, phage plaques were observed on lawns formed by 17978::Pro1 and 17978::Pro3 strains, but not on 17978::Pro2 lawns, which indicated that intact-1 and intact-3 had been induced by MMC in contrast to intact-2. As shown in Figure 3.5, lysates from the 17978::Pro1 mutant bacteria, lacking intact-1, presented 1.64×10^8 PFUs/mL only when used to infect the 17978::Pro3 mutant, which lacks intact-3. The same was observed with lysates from the 17978::Pro3 mutant when used to infect 17978::Pro1 mutant bacteria. Interestingly, despite the fact that attempts to induce

prophage intact-2 never yielded phage plaques, it exhibited chromosomal excision, as suggested by the observed overexpression of the excisionase gene. This observation may indicate a probable competition of intact-2 with the other two prophages for the host machinery necessary for phage replication. Such competition suggests that the replication rate of intact-2 might not be sufficiently high to generate phage particles before the burst induced by the two other prophages. Another possibility could be that the intact-2 phage is incapable of infecting or recognizing the capsular type of ATCC 17978, which might have undergone evolution and alteration, as was previously reported in the literature for *A. baumannii* (49,50) and other bacterial species (51–53). Yet another option would be that an unknown host defense mechanism avoids infection by intact-2 phages.

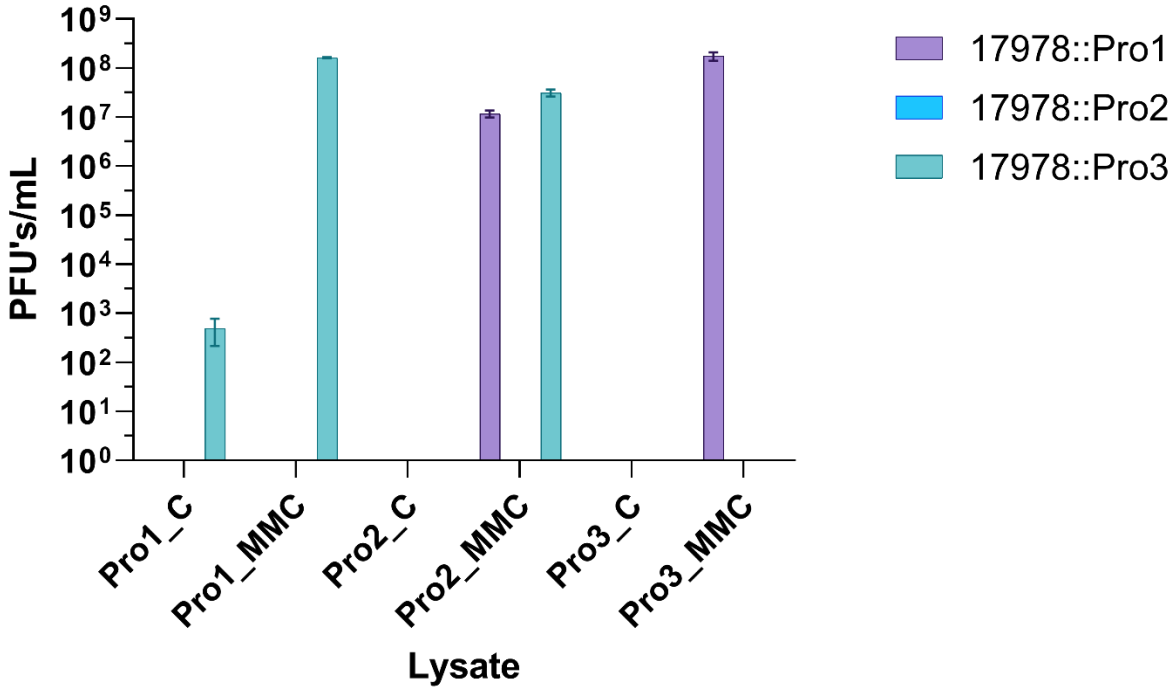


Figure 3.5. Quantification of prophages by PFU-counting using lysates obtained upon induction of each of the prophage-free mutants 17978::Pro1, 17978::Pro2 or 17978::Pro1. Pro1_C – 17978::Pro1 control lysate; Pro1_MMC – 17978::Pro1 MMC-induced lysate; Pro2_C – 17978::Pro2 control lysate; Pro2_MMC – 17978::Pro2 MMC-induced lysate; Pro3_C – 17978::Pro3 control lysate; Pro3_MMC – 17978::Pro3 MMC-induced lysate; The color coding of the bars indicates which indicator bacteria were plated to generate the lawn needed for PFU-counting.

After demonstrating the inducibility of at least two prophages, induction experiments were performed with the WT and *ddrR* strains to assess the differences in prophage induction according to the hypothesis formulated. Both WT and *ddrR* cultures were treated with MMC and the phage concentration was measured after 3 h and 24 h by PFU-counting. Unfortunately, no statistically significant differences in

phage titers were observed, as shown in Figure 3.6. The phage concentration in both lysates was essentially the same, even in the controls where no MMC was added. One of the reasons that might explain this result is the difficulty of counting phage plaques generated by what is believed to be the intact-3 phage. This causes significant variability between different experiments, which was particularly evident in controls where fewer phage plaques were found. Temperate phage plaques are usually difficult to enumerate by PFU-counting, but with a suitable indicator strain, the resolution may in principle be improved. Unfortunately, no compatible strain was available in our collection, which was de facto the reason why we generated the three different prophage deletion strains.

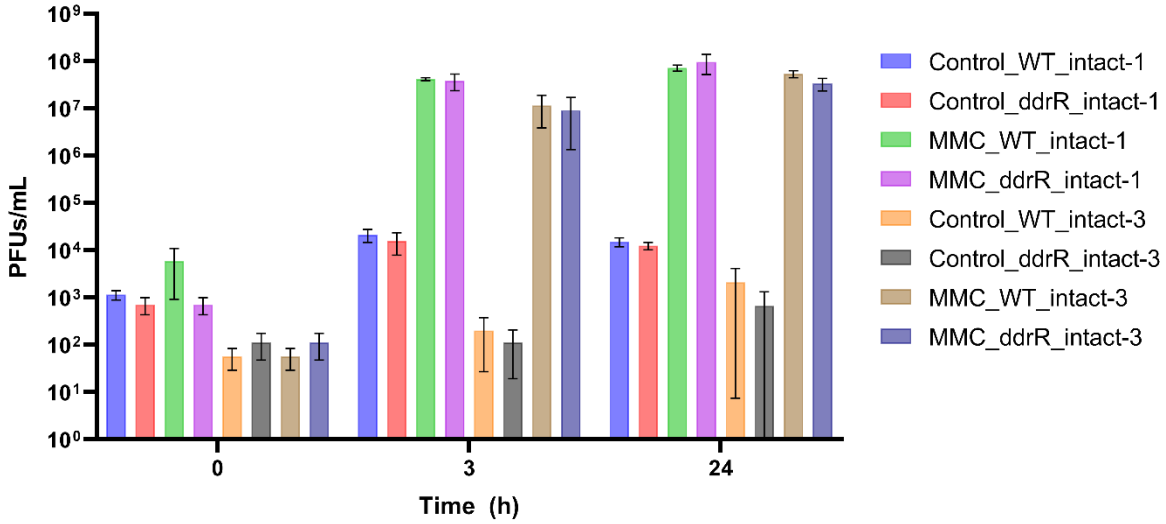


Figure 3.6. Phage concentrations determined by PFU-counting after treatment of *A. baumannii* 17978 or 17978::*ddrR* with MMC (3 µg/mL) for 0 h, 3 h, and 24 h. Control_WT– phage concentration on the control of WT; Control_*ddrR* – phage concentration of the control of *ddrR*; MMC – mitomycin C-induced culture; Pro1 – intact-1; Pro3 – intact-3. Intact-2 was never detected, therefore it was omitted from the graph for simplification.

3.4. CONCLUDING REMARKS

The *Acinetobacter* family has a very unique mechanism to face environmental stresses, which may explain its existence in natural environments before evolving only fairly recently into a critical nosocomial pathogen. This genus possesses an SOS response that operates distinctively from the conventional LexA/RecA system found in *E. coli* and many other microorganisms. This unique SOS response could contribute to *A. baumannii's* remarkable genome plasticity, leading to high levels of antibiotic resistance and virulence. With an SOS response primarily reliant on three proteins, namely RecA, UmuDAb, and DdrR, the prophages within this genus also needed to evolve and adapt to these differences. Therefore, it is not surprising to identify a prophage induction mechanism that works differently from what has been described in the literature for other pathogens.

DdrR has caught some attention in recent years, with a few studies emerging to unveil its function. This small protein was found to be involved in the core SOS response regulation by helping UmuDAb to regulate error-prone polymerases. Our study shows that the *ddrR* gene has a role not only in the SOS response, but also in virulence/fitness and, potentially, in prophage induction. The control of induction may involve an interaction with protein CII to regulate the antitermination protein Q, to avoid early prophage induction. More studies are needed to verify this association, starting with the interaction between the DdrR and CII proteins in order to better understand this mechanism. Moreover, these studies will be crucial to better understand the pathogenicity of the increasingly significant pathogen *A. baumannii*.

3.5. REFERENCES

1. Shadan A, Pathak A, Ma Y, Pathania R, Singh RP. Deciphering the virulence factors, regulation, and immune response to *Acinetobacter baumannii* infection. Front Cell Infect Microbiol. 2023 Feb 23;13:1053968.
2. Antunes LCS, Visca P, Towner KJ. *Acinetobacter baumannii*: Evolution of a global pathogen. Pathog Dis. 2014;71(3):292–301.
3. Little JW, Mount DW. The SOS regulatory system of *Escherichia coli*. Cell. 1982 May 1;29(1):11–22.
4. Baharoglu Z, Mazel D. SOS, the formidable strategy of bacteria against aggressions. Vol. 38, FEMS Microbiology Reviews. Oxford University Press; 2014. p. 1126–45.
5. Aranda J, Poza M, Shingu-Vázquez M, Cortés P, Boyce JD, Adler B, *et al.* Identification of a DNA-Damage-Inducible regulon in *Acinetobacter baumannii*. J Bacteriol. 2013 Dec;195(24):5577–82.
6. Aranda J, López M, Leiva E, Magán A, Adler B, Bou G, *et al.* Role of *Acinetobacter baumannii* UmuD homologs in antibiotic resistance acquired through DNA damage-induced mutagenesis. Antimicrob Agents Chemother. 2014 Mar;58(3):1771–3.
7. Cook D, Flannigan MD, Chariker JH, Hare JM. DNA damage response coregulator ddrR affects many cellular pathways and processes in *Acinetobacter baumannii* 17978. Front Cell Infect Microbiol. 2023;13.
8. Cook D, Flannigan MD, Candra BV, Compton KD, Hare JM. The DdrR Coregulator of the *Acinetobacter baumannii* Mutagenic DNA Damage Response Potentiates UmuDAb Repression of Error-Prone Polymerases. J Bacteriol. 2022 Oct 4;204(11):e00165-22.
9. Cook D, Carrington J, Johnson K, Hare J. Homodimerization and heterodimerization requirements of *Acinetobacter baumannii* sos response coregulators umudab and ddrr revealed by two-hybrid analyses. Can J Microbiol. 2021;67(5):358–71.
10. Peterson MA, Grice AN, Hare JM. A corepressor participates in LexA-independent regulation of error-prone polymerases in *Acinetobacter*. Microbiology. 2020 Feb 1;166(2):212–26.
11. Pavlin A, Bajc G, Fornelos N, Browning DF, Butala M. The Small DdrR Protein Directly Interacts with the UmuDAb Regulator of the Mutagenic DNA Damage Response in *Acinetobacter baumannii*. J Bacteriol. 2022 Mar 1;204(3).
12. Hare JM, Ferrell JC, Witkowski TA, Grice AN. Prophage induction and differential RecA and UmuDAb transcriptome regulation in the DNA damage responses of *Acinetobacter baumannii* and *Acinetobacter baylyi*. PLoS One. 2014 Apr 7;9(4).
13. Nanda AM, Heyer A, Krämer C, Grünberger A, Kohlheyer D, Frunzke J. Analysis of SOS-induced spontaneous prophage induction in *Corynebacterium glutamicum* at the single-cell level. J Bacteriol. 2014;196(1):180–8.
14. Courcelle J, Khodursky A, Peter B, Brown PO, Hanawalt PC. Comparative Gene Expression Profiles Following UV Exposure in Wild-Type and SOS-Deficient *Escherichia coli*. Genetics. 2001 May 1;158(1):41–64.
15. Wachino J ichi, Jin W, Kimura K, Arakawa Y. Intercellular transfer of chromosomal antimicrobial resistance genes between *Acinetobacter baumannii* strains mediated by prophages. Antimicrob Agents Chemother. 2019;63(8):1–16.
16. Loh B, Chen J, Manohar P, Yu Y, Hua X, Leptihn S. A Biological Inventory of Prophages in *A. baumannii* Genomes Reveal Distinct Distributions in Classes, Length, and Genomic Positions. Front Microbiol. 2020;11(December):1–13.
17. Costa AR, Monteiro R, Azeredo J. Genomic analysis of *Acinetobacter baumannii* prophages reveals remarkable diversity and suggests profound impact on bacterial virulence and fitness. Sci Rep. 2018;8(1):15346.

18. Nepal S, Bonn F, Grasso S, Stobernack T, De Jong A, Zhou K, *et al.* An ancient family of mobile genomic islands introducing cephalosporinase and carbapenemase genes in *Enterobacteriaceae*. Virulence. 2018 Jan 1;9(1):1377–89.
19. Bolger AM, Lohse M, Usadel B. Trimmomatic: a flexible trimmer for Illumina sequence data. Bioinformatics. 2014 Aug 1;30(15):2114–20.
20. Wick RR, Judd LM, Gorrie CL, Holt KE. Unicycler: Resolving bacterial genome assemblies from short and long sequencing reads. PLoS Comput Biol. 2017 Jun 8;13(6):e1005595.
21. Cuccuru G, Orsini M, Pinna A, Sbardellati A, Soranzo N, Travaglione A, *et al.* Orione, a web-based framework for NGS analysis in microbiology. Bioinformatics. 2014 Jul 1;30(13):1928–9.
22. Seemann T. Prokka: rapid prokaryotic genome annotation. Bioinformatics. 2014 Jul 15;30(14):2068–9.
23. Wishart DS, Han S, Saha S, Oler E, Peters H, Grant JR, *et al.* PHASTEST: faster than PHASTER, better than PHAST. Nucleic Acids Res. 2023 Jul 5;51(W1):W443–50.
24. Johnson M, Zaretskaya I, Raytselis Y, Merezhuk Y, McGinnis S, Madden TL. NCBI BLAST: a better web interface. Nucleic Acids Res. 2008;36.
25. Zimmermann L, Stephens A, Nam SZ, Rau D, Kübler J, Lozajic M, *et al.* A Completely Reimplemented MPI Bioinformatics Toolkit with a New HHpred Server at its Core. J Mol Biol. 2018;430(15):2237–43.
26. Gabler F, Nam SZ, Till S, Mirdita M, Steinegger M, Söding J, *et al.* Protein Sequence Analysis Using the MPI Bioinformatics Toolkit. Curr Protoc Bioinformatics. 2020 Dec 1;72(1):e108.
27. Lopes A, Tavares P, Petit MA, Guérois R, Zinn-Justin S. Automated classification of tailed bacteriophages according to their neck organization. BMC Genomics. 2014;15(1):1027.
28. Cantu VA, Salamon P, Seguritan V, Redfield J, Salamon D, Edwards RA, *et al.* PhANNs, a fast and accurate tool and web server to classify phage structural proteins. PLoS Comput Biol. 2020 Nov 2;16(11):e1007845-.
29. Melo LDR, Sillankorva S, Ackermann HW, Kropinski AM, Azeredo J, Cerca N. Isolation and characterization of a new *Staphylococcus epidermidis* broad-spectrum bacteriophage. Journal of General Virology. 2014 Feb;95(PART 2):506–15.
30. Wang Y, Wang Z, Chen Y, Hua X, Yu Y, Ji Q. A Highly Efficient CRISPR-Cas9-Based Genome Engineering Platform in *Acinetobacter baumannii* to Understand the H2O2-Sensing Mechanism of OxyR. Cell Chem Biol. 2019 Dec 19;26(12):1732-1742.e5.
31. Nicolas P, Mäder U, Dervyn E, Rochat T, Leduc A, Pigeonneau N, *et al.* Condition-Dependent Transcriptome Reveals High-Level Regulatory Architecture in Bacillus subtilis. Science. 2012 Mar 2;335(6072):1103–6.
32. de Jong A, van der Meulen S, Kuipers OP, Kok J. T-REx: Transcriptome analysis webserver for RNA-seq Expression data. BMC Genomics. 2015;16(1):663.
33. De Jong A, Kuipers OP, Kok J. FUNAGE-Pro: comprehensive web server for gene set enrichment analysis of prokaryotes. Nucleic Acids Res. 2022 Jul 5;50(W1):W330–6.
34. Altschul SF, Madden TL, Schäffer AA, Zhang J, Zhang Z, Miller W, *et al.* Gapped BLAST and PSI-BLAST: A new generation of protein database search programs. Vol. 25, Nucleic Acids Research. 1997. p. 3389–402.
35. Consortium TU, Bateman A, Martin MJ, Orchard S, Magrane M, Ahmad S, *et al.* UniProt: the Universal Protein Knowledgebase in 2023. Nucleic Acids Res. 2023 Jan 6;51(D1):D523–31.
36. Ramezanalizadeh F, Owlia P, Rasooli I. Type I pili, CsuA/B and FimA induce a protective immune response against *Acinetobacter baumannii*. Vaccine. 2020 Jul 22;38(34):5436–46.
37. Feliciello I, Đermić E, Malović H, Ivanković S, Zahradka D, Ljubić S, *et al.* Regulation of ssb Gene Expression in *Escherichia coli*. Int J Mol Sci. 2022 Sep 1;23(18).

38. Heberle H, Meirelles VG, da Silva FR, Telles GP, Minghim R. InteractiVenn: A web-based tool for the analysis of sets through Venn diagrams. BMC Bioinformatics. 2015 May 22;16(1):1–7.
39. Nikaido H. Multidrug efflux pumps of gram-negative bacteria. J Bacteriol. 1996 Oct 1;178(20):5853–9.
40. Solioz M, Odermatt A. Copper and Silver Transport by CopB-ATPase in Membrane Vesicles of *Enterococcus hirae*. Journal of Biological Chemistry. 1995;270(16):9217–21.
41. Rensing C, Pribyl T, Nies DH. New functions for the three subunits of the CzcCBA cation-proton antiporter. J Bacteriol. 1997 Nov 1;179(22):6871–9.
42. Odermatt A, Krapf R, Solioz M. Induction of the Putative Copper ATPases, CopA and Copb, of *Enterococcus hirae* by Ag+ and Cu2+, and Ag+ Extrusion by CopB. Biochem Biophys Res Commun. 1994;202(1):44–8.
43. Abdollahi S, Rasooli I, Mousavi Gargari SL. The role of TonB-dependent copper receptor in virulence of *Acinetobacter baumannii*. Infection, Genetics and Evolution. 2018;60:181–90.
44. Dhurve G, Madikonda AK, Jagannadham MV, Siddavattam D. Outer Membrane Vesicles of *Acinetobacter baumannii* DS002 Are Selectively Enriched with TonB-Dependent Transporters and Play a Key Role in Iron Acquisition. Microbiol Spectr. 2022 Apr 27;10(2).
45. Oppenheim AB, Kobiler O, Stavans J, Court DL, Adhya S. Switches in bacteriophage lambda development. Vol. 39, Annual Review of Genetics. 2005. p. 409–29.
46. Yin Z, Kaelber JT, Ebright RH. Structural basis of Q-dependent antitermination. Proc Natl Acad Sci U S A. 2019 Sep 10;116(37):18384–90.
47. Fornelos N, Butala M, Hodnik V, Anderluh G, Bamford JK, Salas M. Bacteriophage GIL01 gp7 interacts with host LexA repressor to enhance DNA binding and inhibit RecA-mediated auto-cleavage. Nucleic Acids Res. 2015 Jun 5;43(15):7315–29.
48. Pavlin A, Lovše A, Bajc G, Otoničar J, Kujović A, Lengar Ž, *et al.* A small bacteriophage protein determines the hierarchy over co-residential jumbo phage in *Bacillus thuringiensis* serovar israelensis. Commun Biol. 2022 Dec 1;5(1).
49. Arbatsky NP, Kasimova AA, Shashkov AS, Shneider MM, Popova A V., Shagin DA, *et al.* Involvement of a Phage-Encoded Wzy Protein in the Polymerization of K127 Units To Form the Capsular Polysaccharide of *Acinetobacter baumannii* Isolate 36-1454. Microbiol Spectr. 2022 Jun 29;10(3).
50. Timoshina OY, Kasimova AA, Shneider MM, Arbatsky NP, Shashkov AS, Shelenkov AA, *et al.* Loss of a Branch Sugar in the *Acinetobacter baumannii* K3-Type Capsular Polysaccharide Due To Frameshifts in the gtr6 Glycosyltransferase Gene Leads To Susceptibility To Phage APK37.1. Microbiol Spectr. 2023 Feb 14;11(1).
51. Taylor VL, Udaskin ML, Islam ST, Lam JS. The D3 bacteriophage α-polymerase inhibitor (Iap) peptide disrupts O-antigen biosynthesis through mimicry of the chain length regulator Wzz in *Pseudomonas aeruginosa*. J Bacteriol. 2013;195(20):4735–41.
52. Sasaki T, Uchida T, Kurahashi K. Glucosylation of O-Antigen in *Salmonella* Carrying El5 and Es4 Phages*. Vol. 249, The Journal of Biological Chemistry;761-777(3). 1974.
53. Neemuchwala A, Teatero S, Athey TBT, McGeer A, Fittipaldi N. Capsular Switching and Other Large-Scale Recombination Events in Invasive Sequence Type 1 Group B *Streptococcus*. Emerging Infectious Disease journal. 2016;22(11):1941.

3.6.SUPPLEMENTAL MATERIAL

Table S3.1. Primers and ssDNA donor used in this study

Name	Sequence	Description
17978_spaceDdrR_FW	TAGTCTTTCGGCTGCTTCACTTTC	spacer for *ddrR* KO
17978_spaceDdrR_RV	AAACGAAAGTGAAGCAGCCGAAAG	
pSGAb_spaceCheck_FW	ACCTCATTCTATTAGACTCTCG	Check spacer insertion into pSGAb plasmid
pSGAb_spaceCheck_RV	GGAAACAGCTATGACCATGC	
17978_*ddrR*_Donor	ATATGAGTTAGATTCAGTTTTTGGTATGGAGACATGCGAAGTTTAAAATAATAAAAATAAAGGAGGCATAATGCCTCCTT	ssDNA donor for *ddrR* deletion (40 bp homology UP and DW)
17978_*ddrR*_delFW	GGTCGTGGTCAGAACTCTCG	check for *ddrR* KO
17978_*ddrR*_delRV	TGCAATCACAATATCGCCCGA	
Pro1_int_SpaceFW	tagtGAACTCTATCGAGTGACAAT	spacer for int (17978-pro1) KO
Pro1_int_SpaceRV	aaacATTGTCACTCGATAGAGTTC	
Pro2_int_SpaceFW	tagtCTTAGCATCACGAAATTCAT	spacer for int (17978-pro2) KO
Pro2_int_SpaceRV	aaacATGAATTTCGTGATGCTAAG	
Pro3_int_SpaceFW	tagtTGAACAACATGTAATTCCTG	spacer for int (17978-pro3) KO
Pro3_int_SpaceRV	aaacCAGGAATTACATGTTGTTCA	
17978Pro1_FW	CTCTGGTTTGCGTTAGCG	attL region of 17978 Pro1
17978intPro1_RV	TACTGCCTAATTGTTTTTGGTC	
17978intPro1_FW	ATAATGACACGAATGAAACGG	attR region of 17978 Pro1
17978Pro1_RV	TGCCATAAAGTTTCGCCC	
17978Pro2_FW	CGTGCAGTCATTGTCTTTCC	attL region of 17978 Pro2
17978intPro2_RV	CCAGCTAATCTCATCCAGCC	
17978intPro2_FW	TAGAGGGTTCACTGATAGCC	attR region of 17978 Pro2
17978Pro2_RV	GGAGTGGATTACCGTTTACG	
17978Pro3_FW	TGGTTTCTGCATTACAAAAGC	attL region of 17978 Pro3
17978intPro3_RV	TCACCAGCTTTAATTCGTGC	
17978intPro3_FW	GTCAGTTGAAGAAAGAACGC	attR region of 17978 Pro3
17978Pro3_RV	TCAACGTCAGTATAAATTTGGC	

Table S3.2. Functional analysis results from FUNAGE-Pro. COG, Cluster of Ontology Genes; GO, Gene Ontology; IPR, InterPro; KEGG, Kyoto Encyclopedia of Genes and Genomes; Pfam, Protein families database

ClassID	Class	Description
Q	COG	METABOLISM; Secondary metabolites biosynthesis, transport, and catabolism
COG1132	eggNOG_COG	(ABC) transporter
COG1535	eggNOG_COG	Isochorismatase
COG1020	eggNOG_COG	D-alanine [D-alanyl carrier protein] ligase activity
COG3433	eggNOG_COG	Isochorismatase activity
GO:0008908	GO	Isochorismatase activity
GO:0031177	GO	Phosphopantetheine binding
GO:0047527	GO	2,3-dihydroxybenzoate-serine ligase activity
GO:1901576	GO	Organic substance biosynthetic process
GO:0140359	GO	ABC-type transporter activity
GO:0019752	GO	Carboxylic acid metabolic process
GO:0009239	GO	Enterobactin biosynthetic process
GO:0005886	GO	Plasma membrane
GO:0016765	GO	Transferase activity, transferring alkyl or aryl (other than methyl) groups
GO:0019290	GO	Siderophore biosynthetic process
GO:0016874	GO	Ligase activity
IPR000868	IPR	Isochorismatase-like
IPR010071	IPR	Amino acid adenylation domain
IPR003439	IPR	ABC transporter-like, ATP-binding domain
IPR042099	IPR	ANL, N-terminal domain
IPR023213	IPR	Chloramphenicol acetyltransferase-like domain superfamily
IPR036380	IPR	Isochorismatase-like superfamily
IPR045851	IPR	AMP-binding enzyme, C-terminal domain superfamily
IPR036640	IPR	ABC transporter type 1, transmembrane domain superfamily
IPR003593	IPR	AAA+ ATPase domain
IPR025110	IPR	AMP-binding enzyme, C-terminal domain
IPR036736	IPR	ACP-like superfamily
IPR020845	IPR	AMP-binding, conserved site
IPR001242	IPR	Condensation domain
IPR016291	IPR	Isochorismatase
IPR011527	IPR	ABC transporter type 1, transmembrane domain
IPR009081	IPR	Phosphopantetheine binding ACP domain
IPR000873	IPR	AMP-dependent synthetase/ligase domain
IPR027417	IPR	P-loop containing nucleoside triphosphate hydrolase
01053 Biosynthesis of siderophore group nonribosomal peptides [PATH:ko01053]	KEGG	ko01053
Ligase	KEYWORDS	
operon_0566	operons	S1;ID=AFMDGAFA_01137_gene;locus_tag=AFMDGAFA_01137
operon_0565	operons	S1;ID=AFMDGAFA_01131_gene;locus_tag=AFMDGAFA_01131
operon_0567	operons	S1;ID=AFMDGAFA_01139_gene;locus_tag=AFMDGAFA_01139
operon_0921	operons	S1;ID=AFMDGAFA_01895_gene;locus_tag=AFMDGAFA_01895

PF00857	Pfam	Isochorismatase family
PF00005	Pfam	ABC transporter
PF00501	Pfam	AMP-binding enzyme
PF13193	Pfam	AMP-binding enzyme C-terminal domain
PF00668	Pfam	Condensation domain
PF00550	Pfam	Phosphopantetheine attachment site

Chapter 4

Nosocomial transmission of *tet(x3)*, *bla*$_{NDM-1}$, and *bla*$_{OXA-97}$-carrying *Acinetobacter baumannii* conferring resistance to eravacycline and omadacycline, the Netherlands, March-August 2021

This chapter was based on the following scientific article:

- D.T. Talsma, **R. Monteiro**, R.C. Flores-Vallejo, M. Heuvelmans, T. Le, A.P.A. Hendrickx, S. Rosema, I. Maat, J.M. van Dijl, E. Bathoorn, "Nosocomial transmission of tet(x3), blaNDM-1, and blaOXA-97-carrying Acinetobacter baumannii conferring resistance to eravacycline and omadacycline, the Netherlands, March-August 2021," *Eurosurveillance*, Apr. 2024. Accepted for publication.

Abstract

Carbapenem-resistant *Acinetobacter baumannii* (CRAb) is a critically important pathogen causing serious nosocomial infections. Here, we described an outbreak of CRAb on an ICU ward in the Netherlands. During an outbreak of non-resistant *A. baumannii*, while infection prevention control measures were in place, CRAb isolates, carrying highly similar *bla_{NDM-1}*- and *tet(x3)*-encoding plasmids, were isolated from three patients over a period of several months. The chromosomal and plasmid sequences of the CRAb and non-carbapenemase-carrying *A. baumannii* isolates cultured from patient materials were analysed using hybrid assemblies of short-read and long-read sequencing data. Sequencing of the CRAb isolates revealed that the CRAb outbreak consisted of two different strains, carrying similar plasmids. The plasmids contained multiple antibiotic resistance genes including the tetracycline resistance gene *tet(x3),* and the *bla_{NDM-1}* and *bla_{OXA-97}* carbapenemase genes. Minimal inhibitory concentrations (MICs) were determined for thirteen antibiotics, including the newly registered tetracycline antibiotics eravacycline and omadacycline. The CRAb isolates were showing high MICs for tetracycline antibiotics including eravacycline and omadacycline, except for minocycline which showed low MICs. This is the first description of CRAb isolates, carrying *bla_{NDM-1}*, and *bla_{OXA-97}* combined with extended resistance to tetracycline classes conferred by *tet(x3),* from a Dutch hospital.

Keywords: CRAb, outbreak, NDM, tet(x3)

4.1. INTRODUCTION

Carbapenem-resistant *Acinetobacter baumannii* (CRAb) is a critically important pathogen causing serious nosocomial infections with limited treatment options (1). The World Health Organisation ranked CRAb with the highest score on their priority list to guide the development of new drugs (2). *A. baumannii* is a common cause of healthcare- or ventilator-associated pneumonia with an overall mortality rate of 43% (3). The prevalence of CRAb is highly variable across Europe with proportions varying from <2.6% in Northern European countries to 75.5% in Southern European countries (4). In the Netherlands, CRAb has rarely been detected in patients without a history of hospitalisation abroad.

Antibiotics of the tetracycline class are important last-line treatment options in case of CRAb infections (*e.g.,* tigecycline, minocycline, and the recently approved eravacycline and omadacycline) (5). Tetracyclines inhibit bacterial protein synthesis by blocking the aminoacyl-t RNA binding site on the ribosome(6). Unfortunately, acquired resistance to tetracyclines has been found in Gram-negative bacteria. One of the resistance mechanisms in Gram-negative bacteria is based on acquisition of the so-called Tet(x) variants. *Tet(x)* genes code for monooxygenases that degrade a broad spectrum of tetracycline analogues (7). Recent reports from China have described the occurrence of *tet(x)* genes on plasmids of Gram-negative bacteria, conferring high-level resistance to tigecycline (7,8). Also, in carbapenem-resistant *Acinetobacter* species the detection of *tet(x)* genes on plasmids has been reported, and the authors recommended surveillance on the dissemination of *tet(x)* carrying plasmids (9). To date, there have been no reports of *tet(x)* detection in clinical specimens from Europe.

In the present report, we described an outbreak of closely related CRAb in The Netherlands. We characterized the large multidrug-resistance (MDR) plasmids present in both outbreak clones, carrying *tet(x3)*, the two carbapenemase genes *bla*$_{NDM-1}$ and *bla*$_{OXA-97}$, and numerous other resistance genes. We investigated the impact of *tet(x3*) on the susceptibility to antibiotics of the tetracycline class, including eravacycline and omadacycline.

4.1.1. Outbreak detection

In early February 2021, three patients treated for a SARS-CoV-2 infection in an ICU ward of a Dutch hospital tested positive for non-resistant *A. baumannii*. By mid-March, a first patient colonized with CRAb was identified. This index patient (patient 1), without a recent history of traveling abroad, was colonized with a non-resistant *A. baumannii* isolate (denoted Ab1) from day three of his admission, and this isolate was persistently cultured from respiratory material of the patient in the subsequent weeks. Four weeks after the admission of this patient, a first CRAb isolate (denoted CRAb1) was

cultured from a bronchoalveolar lavage fluid of this patient (Figure 4.1). Since the patient had no recent travel history, it was suggested that he had contracted the CRAb in the IC ward. The index patient could be transferred to the regular ward, one week after culturing of the CRAb.

Despite infection prevention measures, a second patient (patient 2) admitted for SARS-CoV-2 infection, presented a CRAb-positive sputum sample on mid-May (solely culture-positive in sputum) (Figure 4.1). The respective isolate was denoted CRAb2. This CRAb2-carrying patient had been admitted to the ICU 1.5 months after discharge of the index patient and had tested negative for *A. baumannii* in multiple rectal screening cultures prior to testing positive for CRAb. This patient passed away 5 days after testing positive for CRAb due to respiratory failure. It remained unclear to what extent this outcome was affected by the CRAb carriage, although treatment consisting of ciprofloxacin 400 mg three times daily combined with nebulized colistin was started when the CRAb was isolated from the patient's respiratory tract. In the following 2.5 months no more wild-type antimicrobial sensitive *A. baumannii* or CRAb isolates were cultured from patient material. However, 2.5 months after the CRAb2-positive patient had passed away, a third patient (patient 3), who had been staying at the ICU for 3 weeks prior to transfer to another hospital tested positive for CRAb in a rectal swab six days after transfer (Figure 4.1). This patient's isolate was denoted CRAb3. Despite extensive culturing, solely rectal colonization was detectable for patient 3. Patient 3 passed away in October due to respiratory failure, which was unrelated to the colonization with the CRAb.

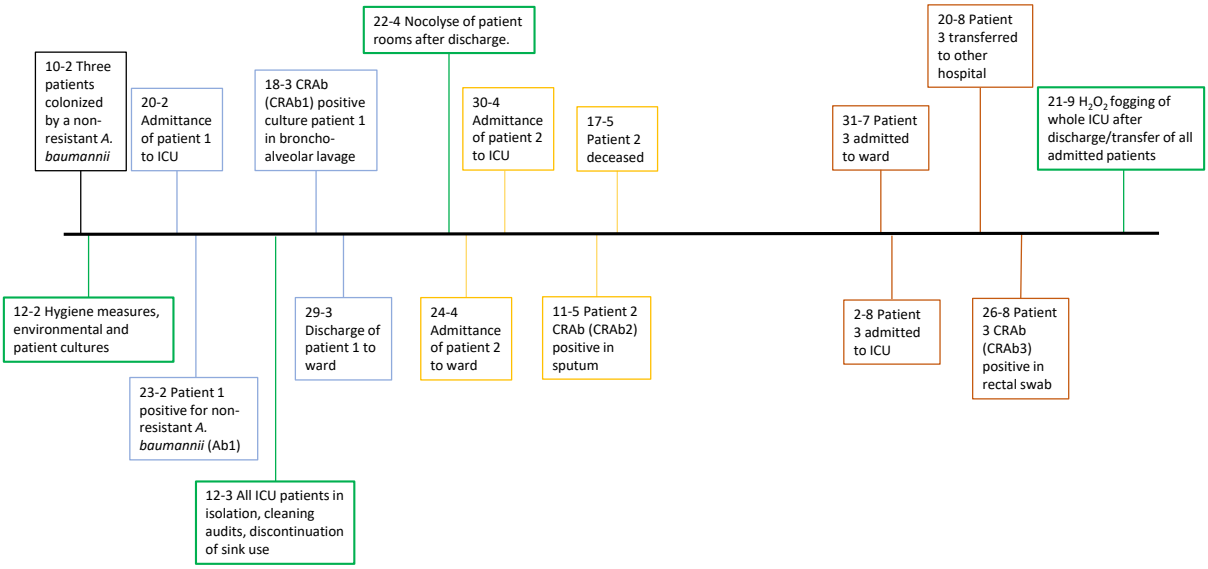


Figure 4.1. Timeline of cultures and preventive measures. Chronological display of sequential infection prevention measures (green) and culture and discharge/transfer data of patient 1 (blue), patient 2 (yellow) and patient 3 (red).

4.2. MATERIALS AND METHODS

4.2.1. Setting and definitions

In this report, we described an outbreak of CRAb in a five-bed intensive care unit (ICU) within a 300-bed regional hospital in the period between March and August 2021. No CRAb isolate had been isolated from patients in this hospital before the outbreak described in this study. A total of three CRAb isolates were collected from three different patients, all admitted to the ICU. All clinical isolates in this study were tested for antibiotic susceptibility using the Becton, Dickinson and Company Phoenix™ automated identification and susceptibility testing system. Carbapenem resistance was confirmed by meropenem gradient strip test (E-test®, bioMerieux®, Amersfoort, The Netherlands). Carbapenemase gene carriage was determined by Next-Generation Sequencing (NGS) as outlined below.

4.2.2. Rectal and environmental culture screening protocol

Rectal swabs were incubated in brain heart infusion broth (Thermofisher®, Waltham, USA) containing 16 mg/L amoxicillin and incubated for 24 h at 35 °C, whereafter 100 µl of broth was used to inoculate Brilliance™ CRE agar (Thermofisher®, Waltham, USA), CHROMID® ESBL agar and CHROMID® Oxa-48 agar (bioMerieux, Amersfoort, the Netherlands). The plates were then incubated for 48 h at 35 °C. Environmental samples were collected when active transmission of *A. baumannii* was suspected, and plated on 5% sheep blood agar (BA) and McConkey agar for 48 h at 35°C.

4.2.3. Additional testing of outbreak strains

For the purpose of this study, additional susceptibility testing and NGS were performed on three isolates involved in the outbreak. This concerned the initial wild-type antibiotic-sensitive *A. baumannii* isolate of the index patient (Ab1), the CRAb isolate of the index patient (CRAb1), and a CRAb isolate of the first consecutive positive patient in the outbreak (CRAb2). The isolate of the third CRAb positive patient in the outbreak was named CRAb3.

4.2.4. Antibiotic susceptibility testing (AST)

AST was performed using Vitek®-2 (card N344), gradient strip tests, and the broth microdilution (BMD) method. For Vitek®-2 testing, the procedure was carried out according to manufacturer's indications. The MICs for meropenem, imipenem, ampicillin/sulbactam and tigecycline were determined using the gradient strip method, performed according to the manufacturer's (bioMerieux®, Amersfoort, the Netherlands) protocol. 0.5 McFarland suspensions in 0.9% (w/v) saline were made from 1-day-old cultures on BA plates. The isolates were inoculated on Mueller Hinton (MH) agar from

Mediaproducts®, Groningen, the Netherlands. All the plates were incubated at 35 °C for 16-20 h after which the Minimum Inhibitory Concentration (MIC) was determined. The MIC was defined as 100% growth inhibition.

Susceptibility testing for minocycline, eravacycline and omadacycline was performed using the BMD method. For minocycline, MICs were determined by BMD in cation-adjusted Mueller-Hinton broth (TREK diagnostic systems/Thermo Fisher), according to the Clinical and Laboratory Standards Institute (CLSI) guidelines. Minocycline MIC was read with 80% inhibition of growth (in comparison to the growth control), when trailing growth occurs. Eravacycline and omadacycline BMD testing was performed according to **ISO 20776-1:2019** using the broth culture method to prepare the inoculum. MICs were interpreted according to the EUCAST guidelines with tetracycline as a control (10,11). The *A. baumannii* ATCC 17978 and *Escherichia coli* ATCC 25922 strains were included as reference and quality control. All the concentrations were tested in triplicates in two independent experiments (n=6). As negative controls, bacteria treated only with MH broth and bacteria treated with the final concentration of dimethyl sulfoxide in the assay (vehicle ≤0.31 % v/v_{final}) were included. The MIC was determined visually by naked-eye inspection and defined as the lowest concentration of antibiotic that completely inhibited bacterial growth (no haze growth, pinpoint growth, or turbidity was seen) upon incubation at 35 °C for 24 h. With the aim of assisting the determination of the MIC with a complementary spectrophotometric method, end-point absorbance measurements ($Abs_{\lambda=600\ nm}$) were done using a Biotek® Epoch-2 reader. The results were graphed using GraphPad Prism® V.8.0.1 according to the following equation: **Eq.1:** Bacterial growth (%) = (mean OD_{600} value of antibiotic-treated bacteria $_{(at\ t=24\ h)}$ - mean OD_{600} value of antibiotic-treated bacteria $_{(at\ t=0h)}$) / (mean OD_{600} value of vehicle-treated bacteria $_{(after\ t=24\ h)}$ - mean OD_{600} value of vehicle-treated bacteria $_{(at\ t=0\ h)}$)*100. In the absence of published EUCAST breakpoints for tetracycline-related antibiotics against *Acinetobacter* species, the interpretation of the MIC was done based on the CLSI guidelines (CLSI, MIC interpretative breakpoints for *Acinetobacter* spp., M100-ED33, 2023).

4.2.5. Whole genome sequencing (WGS)

Illumina short-read sequencing - A total DNA extraction for WGS was performed directly from colonies of the different *A. baumannii* isolates using an Ultraclean Microbial DNA Isolation Kit (MO BIO Laboratories, Carlsbad, CA, US) according to the manufacturer's protocol. DNA concentrations were determined using a Qubit® 2.0 fluorometer and the dsDNA HS and/or BR assay kit (Life Technologies, Carlsbad, CA, US). Subsequently, DNA libraries were prepared using the Nextera XT v2 kit (Illumina,

San Diego, CA, US) according to the manufacturer's instructions. Short-read sequencing was performed with an Illumina MiSeq System, generating paired-end reads of 250 bp. *De novo* assembly of paired-end reads was performed using CLC Genomics Workbench v20.0.4 (QIAGEN, Hilden, Germany) after quality trimming (Qs ≥ 20) establishing a word size of 29.

Nanopore long-read sequencing - High-molecular weight DNA was isolated using an in-house developed protocol (12), and the Oxford Nanopore protocol SQK-LSK109 was followed (Oxford Nanopore Technologies, Oxford, GB/UK). The final library was loaded onto a MinION flow cell (MIN-106 R9.4.1) and a 48-h sequence run was started without live base calling. Once the sequencing run was completed, base-calling, and de-multiplexing were performed using Albacore 2.3.1, and a single FASTA file per isolate was extracted from the FAST5 files using Poretools 0.5.1 (13). Fifty base pairs were trimmed at both sides and only reads larger than 5,000 were used in further analyses.

Hybrid assembly of Illumina and Nanopore DNA sequences - The Nanopore and Illumina sequencing data were used for hybrid genome assembly using Unicycler v0.4.4 (14). The resulting contig files were annotated using Prokka v1.14.6, and they were subsequently loaded into BioNumerics version 7.6.3 (Applied Maths, Sint-Martens-Latem, Belgium) for further comparative analyses (15). Plasmids with ≥95% sequence identity were regarded as highly similar. Lastly, the plasmids were analyzed by using the Basic Local Alignment Search Tool from the National Center for Biotechnology Information.

4.2.6. Sequence data analysis for antimicrobial resistance determinants and plasmids

The antibiotic resistance gene profiles and plasmid replicons of all of sequenced *A. baumannii* isolates were assessed using the AMRFinder version 3.8.4, IslandViewer4 and PlasmidFinder (version 2.0.2) databases available from the Center for Genomic Epidemiology (16,17). For AMRFinder, a 90% identity and a minimum length of 60% threshold were used, whereas for PlasmidFinder, an identity of 95% was utilized. The resulting sequence-derived data, such as resistance genes, replicons, and whole-genome multiple-locus sequence type (wgMLST) profiles were imported into BioNumerics for analyses. For comparative wgMLST analyses, the short-read sequencing data of the *A. baumannii* isolates were used. A minimum spanning tree (MST) was built using BioNumerics as described previously (12). The categorical coefficient was used to calculate the MST, and the MST was based on an in-house *A. baumannii* wgMLST scheme made in SeqSphere software version 6.0.2 (Ridom GmbH, Münster, Germany). The in-house *A. baumannii* wgMLST scheme was based on 3473 genes, including 2390

core genome genes and 1083 accessory genome genes, using the genome of the *A. baumannii* strain ACICU (Genbank accession number NC_010611.1, September 2021) as a reference.

4.2.7. Ethical statement and informed consent

For this study, ethical approval and informed consent were not required since all isolates were cultured as part of routine clinical care. All experiments were performed in accordance with the guidelines of the Declaration of Helsinki and the institutional regulations, and all samples were anonymized. Clinical decision making was not influenced by additional data collected for research purposes.

4.2.8. Data availability statement

The sequence data have been submitted to the NCBI GenBank database under the BioProject number PRJNA1011532.

4.3. RESULTS

4.3.1. Antimicrobial susceptibility testing of the *A. baumannii* outbreak isolates

The results of the AST of the Ab1, CRAb1 and CRAB2 isolates are presented in Table 4.1. NGS showed that the CRAb3 isolate was nearly genetically identical to the CRAb2 isolate, and it was therefore not subject to extensive AST. In particular, the Ab1 isolate showed MICs below the CLSI breakpoint to all tested antibiotics with exception of an intermediate resistance to tetracycline. In contrast, the CRAb1 and CRAb2 isolates showed MICs above the CLSI breakpoint for ampicillin/sulbactam and carbapenems. Moreover, high MICs were observed for most of the tetracycline antibiotics, including tigecycline, as well as eravacycline and omadacycline, as presented in Supplemental Figure S4.1. Interestingly, low MICs were measured for minocycline, both in the Ab1 strain and the CRAb1 and CRAb2 strains. For comparison, the MICs of the reference strains *A. baumannii* ATCC 17978 and *E. coli* ATCC 25922 were tested in parallel but, as expected, they were identical to the reference MICs provided by EUCAST and CLSI (Table 4.1).

Table 4.1 - Description of the antibiotic susceptibility and resistome of the isolates in the outbreak. MICs of E. coli and A. baumannii reference strains were tested in parallel with the clinical isolates on the gradient strip method and BMD antimicrobial susceptibility testing. No discrepancies were detected compared to EUCAST and CLSI reference MICs

Isolate	Previous ICU stay (days)	Isolation date	Susceptibility to CIP[a]/STX[a]/GEN[a]/ TOB[a]	MIC IMI[c]	MIC MERO[c]	MIC AMP/SUL[c]	MIC TET[b]	MIC MINO[c]	MIC TIGE[c]	MIC ERA[b]	MIC OMA[b]	*Bla*-genes[d]	Non *bla*-*resistance genes*[d]
Ab1	3	23/2/2021	I/S/S/S	0.19	0.38	1.0	8	0.12	0.38	0.125	0.5	bla_{ADC-79}, $bla_{OXA-100}$	-
CRAb1	26	18/3/2021	I/R/S/S	>32	>32	48	128	0.12	>4.0	4	16	bla_{ADC-79}, $bla_{OXA-100}$, bla_{NDM-1}, bla_{OXA-97}	*tet(x3), sul2, ant(2")-Ia, aph(3")-Ib, aph(3')-Ia, aph(6)-Id, ant(3")-IIa, mph(E), msr(E)*
CRAb2	12	11/5/2021	I/R/R/S	>32	>32	64	64	0.25	>4.0	2	8	bla_{ADC-79}, $bla_{OXA-100}$, bla_{NDM-1}, bla_{OXA-97}	*tet(x3), sul2, abaF, ant(2")-Ia, aph(3")-Ib, aph(3')-Ia, aph(6)-Id, ant(3")-IIa, mph(E), msr(E)*
***E. coli* ATCC 25922**	NA	NA	NT	0.125	0.023	3.0	1.0	0.50	0.094	0.125	0.5	NT	NT
***A. baumannii* ATCC 17978**	NA	NA	NT	0.19	0.38	1.0	2.0	0.12	0.25	0.063	0.125	NT	NT

MIC in mg/L, CIP, ciprofloxacin; STX, co-trimoxazol; GEN, gentamicin; TOB, tobramycin; TET, tetracycline; IMI, imipenem; MERO, meropenem; AMP/SUL, ampicillin/sulbactam; MINO, minocycline; TIGE, tigecycline; ERA, eravacycline; OMA, omadacycline; NA, not applicable; NT, not tested.

[a] MIC determined by VITEK®-2

[b] MIC determined by BMD

[c] MIC determined using the gradient strip method

[d] Antimicrobial resistance genes as identified with AMRfinder

4.3.2. Genomic analysis of the outbreak A. baumannii isolates

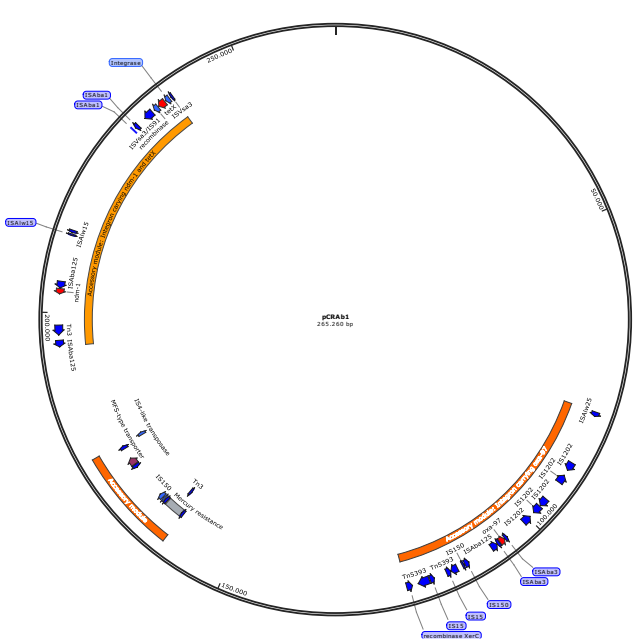
NGS showed that the four *A. baumannii* isolates Ab1 and CRAb1-3 belonged to wgMLST sequence type 32. Furthermore, the wgMLST analysis showed that the outbreak of CRAb was related to two distinct genetic clusters of *A. baumannii*. The wgMLST analysis revealed that the Ab1 isolate and the CRAb1 isolate, which were isolated from the same patient, were the same strain, showing a difference of only one allele. The analysis also revealed that the CRAb2 and CRAb3 isolates from patients 2 and 3, respectively, were the same strain with only 1 allele difference. However, the CRAb2 and CRAb3 belonged to a different MLST cluster than the CRAb1 isolate, with 238 allelic differences between the clusters.

Analysis of the hybrid genome assemblies with AMRFinder revealed the presence of the intrinsic chromosomally-encoded resistance genes of *A. baumannii* in the three sequenced isolates Ab1, CRAb1 and CRAb2. These included amongst others the *bla*$_{OXA-100}$ and *bla*$_{ADC-79}$ genes (Table 4.1). The isolate CRAb2 carried the fosfomycin resistance gene *abaF* chromosomally, whereas the isolate CRAb1 lacked this gene.

4.3.3. Analysis of multidrug resistance plasmids

The isolate CRAb1 was found to harbor highly similar, but not identical resistance gene-carrying plasmid (pCRAb1) compared to the isolate CRAb2 (pCRAb2) and CRAb3 (pCRAb3). pCRAb2 and pCRAb3 were identical plasmids. The length of pCRAb1 was 262 kbp and 265 kbp for pCRAb2 and pCRAb2 displayed 38 SNPs and some insertions and deletions in intergenic regions compared to pCRAb1 which are listed in Supplemental Table S4.1. In addition, pCRAb2 showed extra IS1202 elements resulting in the >3000 bp larger plasmid sequence. These plasmids had not been published before in GenBank as presented in Supplemental Figure S4.2 which shows the phylogenetic tree of *Acinetobacter* plasmids with no known closely related plasmid. Since all plasmids are highly similar, we solely present the analysis of pCRAb1 in more detail. The map of pCRAb1 is shown in Figure 4.2. This is a conjugative plasmid that contains several resistance genes located on three accessory modules, including the beta-lactam resistance genes *bla*$_{NDM-1}$, *bla*$_{OXA-97}$, the tetracycline resistance gene *tet(x3),* the sulphonamide resistance gene *sul2,* the aminoglycoside resistance genes *ant(2")-Ia, aph(3")-Ib, aph(3')-Ia, aph(6)-Id*, and the macrolide resistance genes *mph(E)* and *msr(E).* In addition, the plasmid carries several virulence-related genes, including genes encoding 'major facilitator superfamily (MFS) transporters, iron uptake proteins, lipoproteins, and secretion systems (18–21). Genes responsible for horizontal plasmid mobility, such as *traX*, *dotL*, *dotM*, *dotO*, and a gene encoding a TrbI-like protein

(22–24) are encoded by this plasmid. For more information, please refer to Supplemental Table S4.2, which lists the complete annotation of the pCRAb1. Lastly, the plasmid carries three genomic islands (GI) each harboring antibiotic resistance and virulence-related genes.


pCRAb1
265.260 bp
Integrase
ISAba1
ISAba1
ISAba15
ISAba125
Tn3
ISAba125
ISAba3
ISAba3
ISAba3

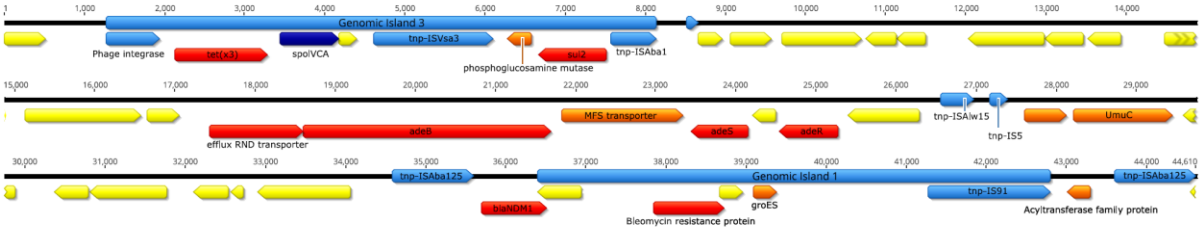


Figure 4.3 - Coding sequences of the integron containing Genomic Island 1 and Genomic Island 3. Mobile elements-related genes (blue) and antibiotic resistance genes *tet(x)3*, *bla*$_{NDM1}$ and *sul2* (red) are marked. Hypothetical proteins (yellow) are not labeled. Integron map generated by Geneious Prime® 2023.2.1.

4.3.4. Outbreak control measures

Prior to the detection of CRAb, outbreak prevention measures were already in place because of an outbreak of non-resistant *A. baumannii* (including isolate Ab1) involving multiple patients. These measures included intensified discharge cleaning of nursing rooms, weekly patient screening by rectal culture on all ICU admitted patients, and environmental screening of inter-patient applied medical devices, tray tables, beds, and sinks. Despite these measures, *A. baumannii* was persistently cultured from patients and their environment. Moreover, all three CRAb-positive patients were admitted to the ICU because of a SARS-CoV-2 infection and were therefore nursed in isolation or by cohort nursing with a negative pressure regime. Medical staff was wearing long-sleeve gowns, gloves, glasses and FFP2 masks. Upon culturing of a CRAb isolate, the respective patients were placed in a single room with negative pressure regime. Medical staff was wearing long-sleeve gowns, gloves, surgical masks, glasses, and hairnets. Patients testing positive for CRAb in clinical samples (e.g. sputum) were tested for confirmation by rectal swab and re-testing of the positive body site. After identification of the CRAb-positive index patient, infection prevention measures were further intensified. To this end, all patients in the ICU ward were nursed in isolation with daily cleaning of rooms and disposal of all unused disposable medical equipment upon discharge of patients, discontinued usage of sinks, special hand hygiene training for nurses and medical staff, and implementation of adenosine triphosphate measurements to aid cleaning of the patient area. Still, due to the continuous identification of non-resistant *A. baumannii* in environmental cultures, nocolysis of nursing rooms was performed after patient discharge. This stopped the transmission of non-resistant *A. baumannii* and also environmental cultures remained negative after the start of nocolysis. Nonetheless, after the start of nocolysis, two more CRAb-positive patients were identified (CRAb2 and CRAb3). Because all possible measures had already been taken before identification of the second CRAb-positive patient, no additional measures

were taken. However, upon identification of the CRAb3 isolate, an admission stop was instigated, and all patients on the respective ICU were either discharged or transferred to other hospitals in the following weeks. Once all patients had been discharged, the entire ICU ward was disinfected and cleaned twice followed by hydrogen peroxide vapor decontamination. Hereafter, no more CRAb-positive patients were identified.

4.4. DISCUSSION

The present study describes an unusual outbreak of CRAb in a Dutch ICU ward, which was caused by two distinct clones of *A. baumannii* that both contain plasmid-borne carbapenemase *bla*$_{OXA-97}$, *bla*$_{NDM-1}$ and tetracycline resistance-conferring *tet(x3)* genes. To our knowledge this concerns the first reported isolation of *bla*$_{NDM-1}$- and *tet(x3)*-positive *A. baumannii* from patients in the Netherlands and, moreover, from Western Europe. The fact that the present CRAb outbreak involved two separate clusters of *A. baumannii* is perhaps even more remarkable, because the isolation of a CRAb from patient-derived materials is still a very rare event in Dutch hospitals. In fact, CRAb had never before been isolated from patients in the hospital in which the outbreak occurred. So far, the isolation of CRAb was essentially always associated with a recent treatment of the respective patients in hospitals outside the Netherlands. Unexpectedly, however, the CRAb-positive patients described in our present study had not visited foreign hospitals in the recent past.

Since no CRAb was identified by environmental sampling, the precise mechanism of transmission remains elusive. In fact, we can also only hypothesize how the described outbreak of CRAb was caused by two different, but closely related wgMLST clusters carrying similar plasmids. The first two patients involved in the outbreak had tested negative for *A. baumannii* prior to being colonized by CRAb suggesting that these patients had acquired CRAb in the ICU. This seems also the most likely scenario for the acquisition of the genetically identical CRAb2 and CRAb3 isolates from patients 2 and 3. The hypothesis that transmission had occurred in the ICU is supported by the fact that vigorous cleaning of the whole ICU ward, including the use of hydrogen peroxide vapor, effectively stopped the outbreak. Two plausible explanations for an outbreak of CRAb consisting of two distinct wgMLST clusters are that CRAb2 evolved from CRAb1 via missing links between the two isolates, or that they share a common ancestor that had persisted in a local reservoir for a longer time period combined with a transfer of the antibiotic resistance-carrying plasmid between CRAb1 and CRAb2/3. Unfortunately, we can only speculate on the exact mechanism of transmission and the relation between the two wgMLST clusters in the outbreak, since no CRAb isolates were recovered from environmental samples.

It is interesting to note that the isogenic Ab1 and CRAb1 isolates were obtained from the index patient 1. This, as discussed above, indicates an introduction of the *bla*$_{NDM-1}$ and *bla*$_{OXA-97}$-carrying plasmid in or in the close vicinity of patient 1, which would be supported by the fact that none of the environmental cultures tested positive for CRAb. Also remarkable is the size of the plasmids (>260 kb), which is due to the acquisition of an extensive accessory genome mediated by insertion sequences and phage integrases (26). The number of plasmid lineages is restricted in *Acinetobacter*, and only some of these lineages include plasmids with multiple antibiotic-resistance genes (27). Such multidrug resistance (MDR) plasmids are often large conjugative plasmids of more than 100 kb (28). Analysis of the genomic islands and the integrase carrying the *bla*$_{NDM-1}$ and *tet(x3)* in the plasmids of our outbreak revealed that the *tet(x3)*-carrying part has been a recent addition to the integrase. The CRAb2 and CRAb3 isolates, belonging to the second wgMLST cluster identified in the outbreak, carry a plasmid that is 98% identical to the plasmid carried by the CRAb1 isolate, which suggests a common recent ancestry.

The *tet(x3)* gene found on the plasmids conveys resistance to a broad range of antibiotics in the tetracycline group. Antibiotics from the tetracycline group are often regarded as a last line treatment for CRAb infections. Tetracycline resistance mediated by *tet(x)* genes was previously described upon the introduction of tigecycline (29,30) and it has been reported for clinical *A. baumannii* isolates in China (31). Chen and colleagues also described the phenotypical resistance patterns for tetracyclines in *tet(x)*-carrying *A. baumannii*, including resistance to tetracycline and tigecycline, as well as high MICs for the new-generation tetracyclines omadacycline (8-16mg/L) and eravacycline (2-8mg/L) (31).

Interestingly, the CRAb isolates described in our present study showed relatively low MICs to minocycline. To date, minocycline MICs in *tet(x3)* carrying *Acinetobacter* have not been described. However, the reported minocycline MIC for an *A. baumannii* isolate carrying *tet(x5)* was 2-8 mg/L, and also in *tet(x3)* or *tet(x4)* carrying *E. coli* isolates the MICs for minocycline were increased compared to a *tet(x)* naïve strain (32,33) These observations suggest that minocycline may be a treatment option for infections caused by some, but certainly not all, *tet(x)*-carrying *A. baumannii*. This makes a precise MIC determination relevant, since it was recently demonstrated that minocycline could be a cornerstone in the treatment of multi- and extremely drug-resistant *A. baumannii* infections due to its synergy with sulbactam (34). Dimitriadis and colleagues showed that the gradient strip method is less reliable compared to automated susceptibility testing for minocycline (35). Moreover, the optimal dosage of minocycline for *A. baumannii* infections is a topic of debate, as recent pharmacokinetic and pharmacodynamic data of minocycline administration suggest that the current breakpoints might be

too high (36). The discussion on the optimal dosing and AST method for minocycline in *A baumannii* might be even more relevant due to the introduction of a *tet(x3)* carrying *A. baumannii* in Europe described in this study.

4.5. CONCLUDING REMARKS

In conclusion, we here report an alert for the emergence of CRAb in the Netherlands with an extended resistance pattern to the last-line tetracycline antibiotics and ampicillin-sulbactam in hospitalized patients with no clinical history abroad. The transmissions were rapidly confirmed by collaborative typing efforts at an academic institution and the National Institute for Public Health and the Environment of the Netherlands. The immediate infection control interventions most likely prevented a large-scale outbreak.

4.6. REFERENCES

1. Piperaki ET, Tzouvelekis LS, Miriagou V, Daikos GL. Carbapenem-resistant Acinetobacter baumannii: in pursuit of an effective treatment. Clinical Microbiology and Infection. 2019 Aug;25(8):951–7.
2. Tacconelli E, Carrara E, Savoldi A, Harbarth S, Mendelson M, Monnet DL, et al. Discovery, research, and development of new antibiotics: the WHO priority list of antibiotic-resistant bacteria and tuberculosis. The Lancet Infectious Diseases. 2018 Mar;18(3):318–27.
3. Mohd Sazlly Lim S, Zainal Abidin A, Liew SM, Roberts JA, Sime FB. The global prevalence of multidrug-resistance among Acinetobacter baumannii causing hospital-acquired and ventilator-associated pneumonia and its associated mortality: A systematic review and meta-analysis. Journal of Infection. 2019 Dec;79(6):593–600.
4. Ayobami O, Willrich N, Suwono B, Eckmanns T, Markwart R. The epidemiology of carbapenem-non-susceptible Acinetobacter species in Europe: analysis of EARS-Net data from 2013 to 2017. Antimicrobial Resistance & Infection Control. 2020 Dec 19;9(1):89.
5. Isler B, Doi Y, Bonomo RA, Paterson DL. New Treatment Options against Carbapenem-Resistant *Acinetobacter baumannii* Infections. Antimicrobial Agents and Chemotherapy. 2019 Jan;63(1).
6. Chopra I, Roberts M. Tetracycline Antibiotics: Mode of Action, Applications, Molecular Biology, and Epidemiology of Bacterial Resistance. Microbiology and Molecular Biology Reviews. 2001 Jun;65(2):232–60.
7. Sun J, Chen C, Cui CY, Zhang Y, Liu X, Cui ZH, et al. Plasmid-encoded tet(X) genes that confer high-level tigecycline resistance in Escherichia coli. Nature Microbiology. 2019 Jun 24;4(9):1457–64.
8. He T, Wang R, Liu D, Walsh TR, Zhang R, Lv Y, et al. Emergence of plasmid-mediated high-level tigecycline resistance genes in animals and humans. Nature Microbiology. 2019 May 27;4(9):1450–6.
9. He T, Li R, Wei R, Liu D, Bai L, Zhang L, et al. Characterization of Acinetobacter indicus co-harbouring tet(X3) and blaNDM-1 of dairy cow origin. Journal of Antimicrobial Chemotherapy. 2020 Sep 1;75(9):2693–6.
10. EUCAST reading guide for broth microdilution. https://www.eucast.org/ast_of_bacteria/mic_determination; 2024.
11. ISO. 2019. ISO 20776-1:2019. Susceptibility testing of infectious agents and evaluation of performance of antimicrobial susceptibility test devices. Part 1: broth micro-dilution reference method for testing the in vitro activity of antimicrobial agents against rapidly growing aerobic bacteria involved in infectious diseases.
12. Hendrickx APA, Landman F, de Haan A, Borst D, Witteveen S, van Santen-Verheuvel MG, et al. Plasmid diversity among genetically related Klebsiella pneumoniae blaKPC-2 and blaKPC-3 isolates collected in the Dutch national surveillance. Scientific Reports. 2020 Oct 8;10(1):16778.
13. Loman NJ, Quinlan AR. Poretools: a toolkit for analyzing nanopore sequence data. Bioinformatics. 2014 Dec 1;30(23):3399–401.
14. Wick RR, Judd LM, Gorrie CL, Holt KE. Unicycler: Resolving bacterial genome assemblies from short and long sequencing reads. PLOS Computational Biology. 2017 Jun 8;13(6):e1005595.
15. Seemann T. Prokka: rapid prokaryotic genome annotation. Bioinformatics. 2014 Jul 15;30(14):2068–9.
16. Bertelli C, Laird MR, Williams KP, Lau BY, Hoad G, Winsor GL, et al. IslandViewer 4: expanded prediction of genomic islands for larger-scale datasets. Nucleic Acids Research. 2017 Jul 3;45(W1):W30–5.

17. Feldgarden M, Brover V, Haft DH, Prasad AB, Slotta DJ, Tolstoy I, et al. Validating the AMRFinder Tool and Resistance Gene Database by Using Antimicrobial Resistance Genotype-Phenotype Correlations in a Collection of Isolates. Antimicrobial Agents and Chemotherapy. 2019 Nov;63(11).
18. Akhtar AA, Turner DPJ. The role of bacterial ATP-binding cassette (ABC) transporters in pathogenesis and virulence: Therapeutic and vaccine potential. Microbial Pathogenesis. 2022 Oct;171:105734.
19. Chang JC, Wilkening R V., Rahbari KM, Federle MJ. Quorum Sensing Regulation of a Major Facilitator Superfamily Transporter Affects Multiple Streptococcal Virulence Factors. Journal of Bacteriology. 2022 Sep 20;204(9).
20. Green ER, Mecsas J. Bacterial Secretion Systems: An Overview. Microbiology Spectrum. 2016 Jan 29;4(1).
21. Kovacs-Simon A, Titball RW, Michell SL. Lipoproteins of Bacterial Pathogens. Infection and Immunity. 2011 Feb;79(2):548–61.
22. Alt-Mörbe J, Stryker JL, Fuqua C, Li PL, Farrand SK, Winans SC. The conjugal transfer system of Agrobacterium tumefaciens octopine-type Ti plasmids is closely related to the transfer system of an IncP plasmid and distantly related to Ti plasmid vir genes. Journal of Bacteriology. 1996 Jul;178(14):4248–57.
23. Christie PJ, Gomez Valero L, Buchrieser C. Biological Diversity and Evolution of Type IV Secretion Systems. In 2017. p. 1–30.
24. Maneewannakul K, Maneewannakul S, Ippen-Ihler K. Characterization of traX, the F plasmid locus required for acetylation of F-pilin subunits. Journal of Bacteriology. 1995 Jun;177(11):2957–64.
25. Siguier P. ISfinder: the reference centre for bacterial insertion sequences. Nucleic Acids Research. 2006 Jan 1;34(90001):D32–6.
26. Desmet S, Nepal S, van Dijl JM, Van Ranst M, Chlebowicz MA, Rossen JW, et al. Antibiotic Resistance Plasmids Cointegrated into a Megaplasmid Harboring the *bla* $_{OXA-427}$ Carbapenemase Gene. Antimicrobial Agents and Chemotherapy. 2018 Mar;62(3).
27. Salgado-Camargo AD, Castro-Jaimes S, Gutierrez-Rios RM, Lozano LF, Altamirano-Pacheco L, Silva-Sanchez J, et al. Structure and Evolution of Acinetobacter baumannii Plasmids. Frontiers in Microbiology. 2020 Jun 18;11.
28. Ghaly TM, Paulsen IT, Sajjad A, Tetu SG, Gillings MR. A Novel Family of Acinetobacter Mega-Plasmids Are Disseminating Multi-Drug Resistance Across the Globe While Acquiring Location-Specific Accessory Genes. Frontiers in Microbiology. 2020 Dec 2;11.
29. Moore IF, Hughes DW, Wright GD. Tigecycline is modified by the flavin-dependent monooxygenase TetX. Biochemistry. 2005;44(35).
30. Yang W, Moore IF, Koteva KP, Bareich DC, Hughes DW, Wright GD. TetX Is a Flavin-dependent Monooxygenase Conferring Resistance to Tetracycline Antibiotics. Journal of Biological Chemistry. 2004 Dec;279(50):52346–52.
31. Chen C, Cui CY, Yu JJ, He Q, Wu XT, He YZ, et al. Genetic diversity and characteristics of high-level tigecycline resistance Tet(X) in Acinetobacter species. Genome Medicine. 2020 Dec 7;12(1):111.
32. He T, Wang R, Liu D, Walsh TR, Zhang R, Lv Y, et al. Emergence of plasmid-mediated high-level tigecycline resistance genes in animals and humans. Nature Microbiology. 2019 May 27;4(9):1450–6.
33. Wang L, Liu D, Lv Y, Cui L, Li Y, Li T, et al. Novel Plasmid-Mediated *tet* (X5) Gene Conferring Resistance to Tigecycline, Eravacycline, and Omadacycline in a Clinical Acinetobacter baumannii Isolate. Antimicrobial Agents and Chemotherapy. 2019 Dec 20;64(1).

34. Chandran S, Manokaran Y, Vijayakumar S, Shankar BA, Bakthavatchalam YD, Dwarakanathan HT, et al. Enhanced bacterial killing with a combination of sulbactam/minocycline against dual carbapenemase-producing Acinetobacter baumannii. European Journal of Clinical Microbiology & Infectious Diseases. 2023 May 11;42(5):645–51.
35. Dimitriadis P, Protonotariou E, Varlamis S, Poulou A, Vasilaki O, Metallidis S, et al. Comparative evaluation of minocycline susceptibility testing methods in carbapenem-resistant Acinetobacter baumannii. Int J Antimicrob Agents. 2016 Sep;48(3):321–3.
36. Tsakris A, Koumaki V, Dokoumetzidis A. Minocycline susceptibility breakpoints for *Acinetobacter baumannii*: do we need to re-evaluate them? Journal of Antimicrobial Chemotherapy. 2019 Feb 1;74(2):295–7.

4.7. SUPPLEMENTAL MATERIAL

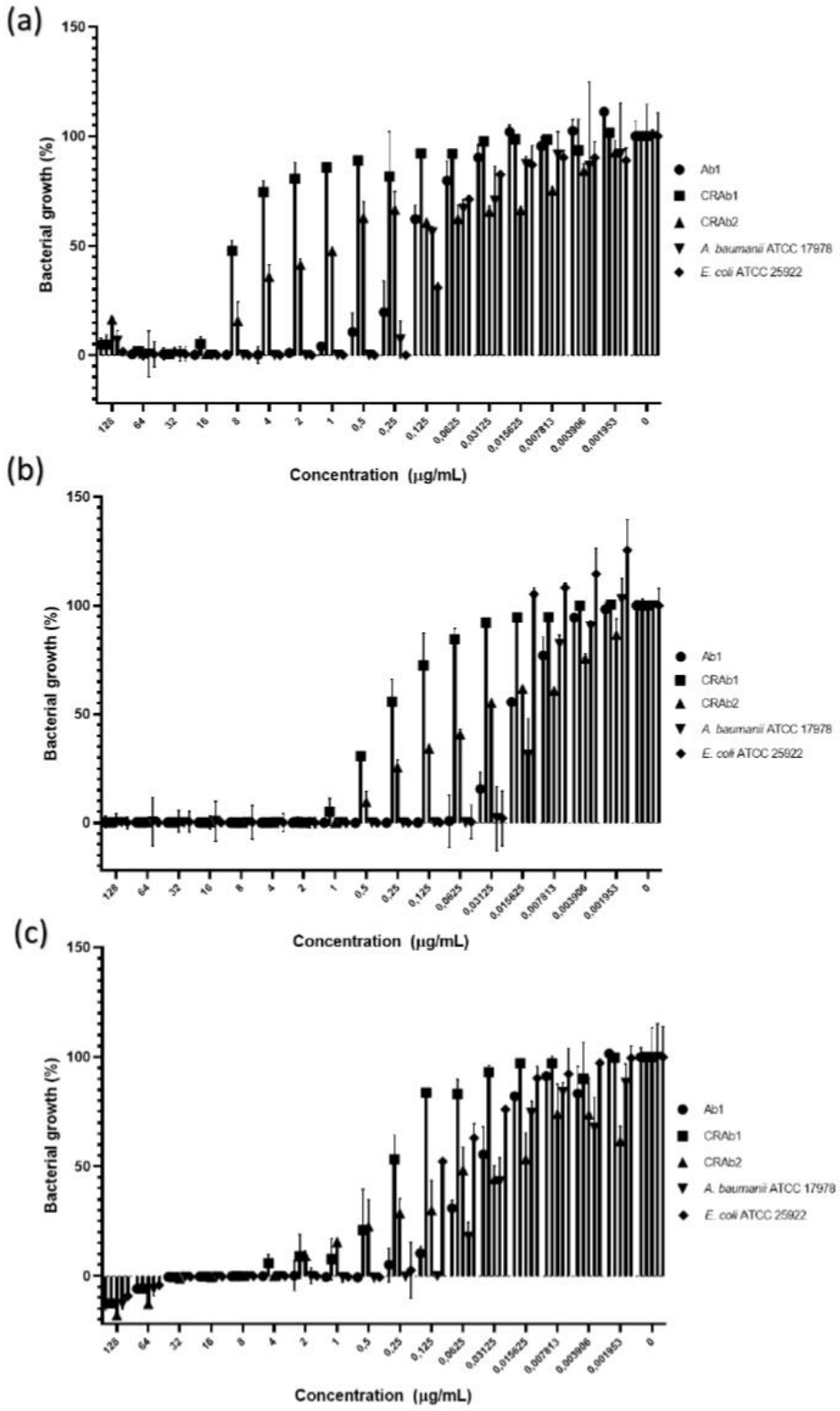


Figure S4.1 - Inhibitory effect of tetracycline class antibiotics against A. baumannii clinical isolates and reference strains: (a) Tetracycline, (b) Eravacycline, and (c) Omadacycline.

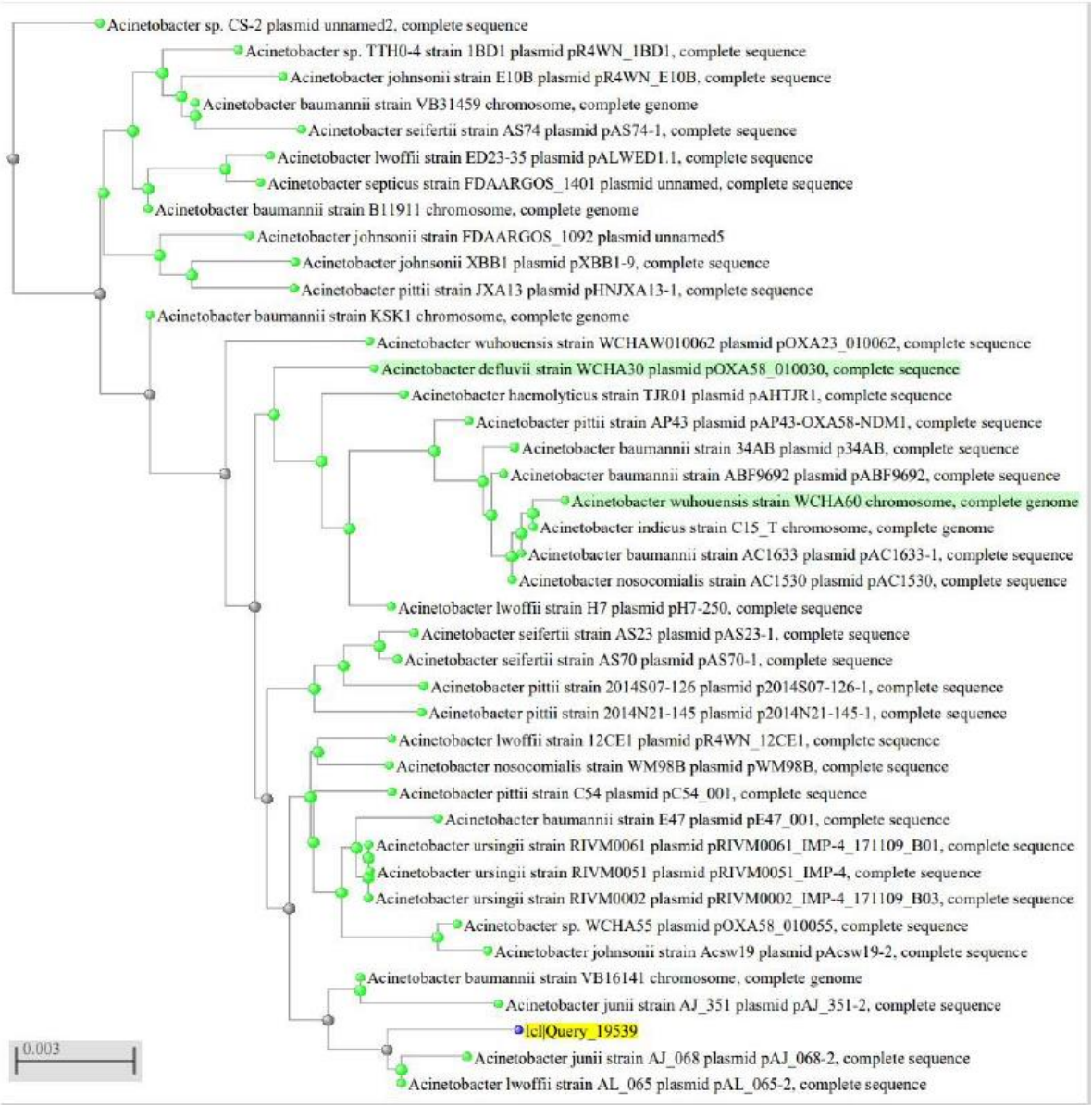


Figure S4.2 - Phylogenetic tree of A. baumannii plasmids based on sequences submitted to Genbank, showing that the plasmid of the CRAb1 and CRAb2 isolates (highlighted in yellow) is unique (analysis performed in September 2021).

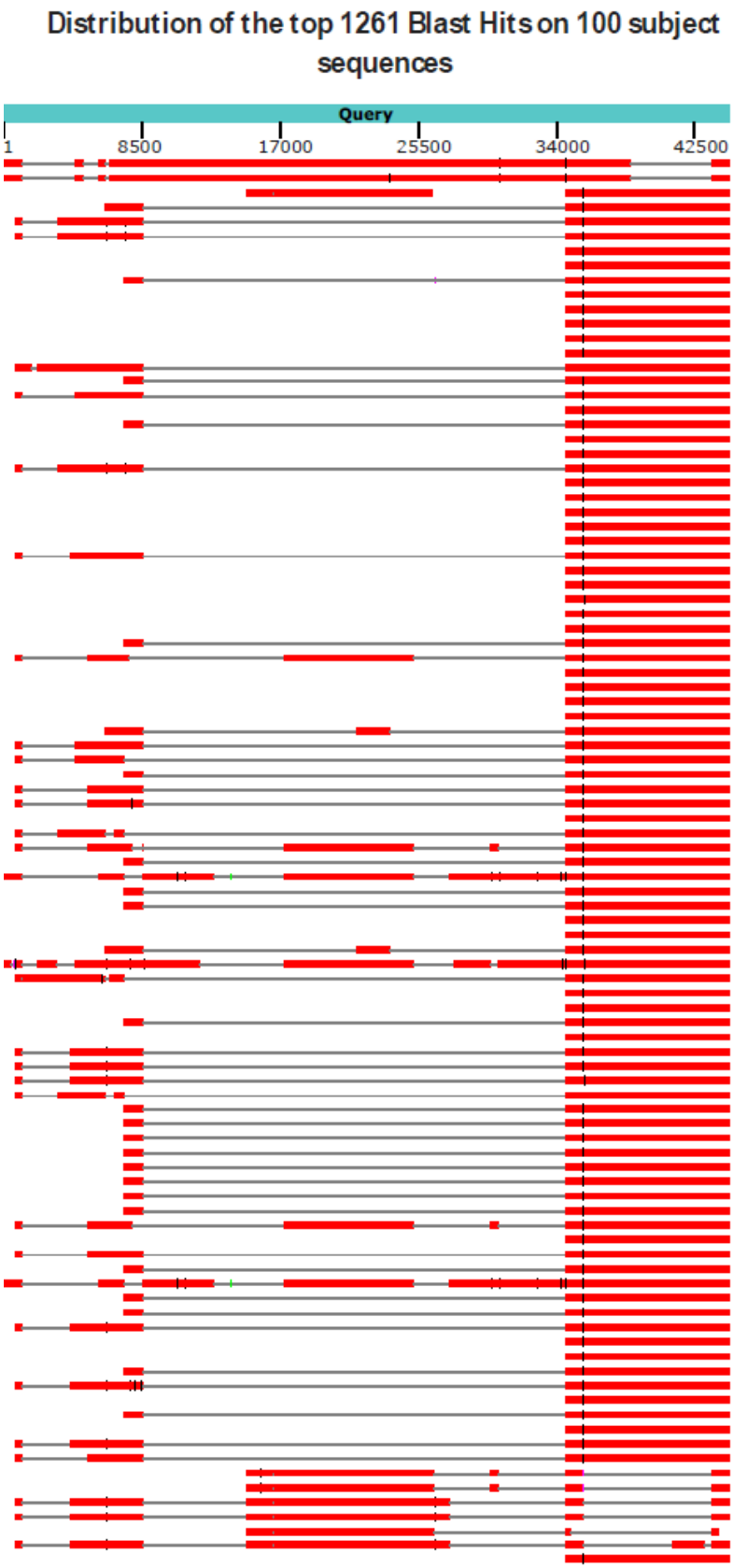


Figure S4.3 - BLASTn of the bla$_{NMD-1}$ *and tet(x)3* carrying integron. Both the bla$_{NMD-1}$ and *tet(x)3* genes located within genomic islands 3 and 1, respectively, have been described before, but the plasmids identified in the present outbreak are unique in combining these resistance genes in one integron.

Table S4.1. SNP analysis of the plasmid sequence of CRAb1 compared to the plasmid sequence of CRAb2

SNP pattern	Sequence	Positions	AA change	Codon		Gene
TC	CRAb2	7994	7994	No	CTT to CTC	ISAba125 family transposase
TC	CRAb2	8084	8084	No	ACT to ACC	ISAba125 family transposase
TC	CRAb2	8087	8087	No	TTT to TTC	ISAba125 family transposase
AC	CRAb2	8273	8273	No	CCA to CCC	ISAba125 family transposase
GT	CRAb2	14389	14389	S to Y	GGA to GTA	phosphohydrolase
GA	CRAb2	43225	43225	No	Intergenic region	
AT	CRAb2	53111	53111	K to STOP	AAG to TAG	DNA methyltransferase
GT	CRAb2	55868	55868	G to C	GGT to TGT	restriction endonuclease subunit R
AT	CRAb2	63505	63505	No (L)	AAG to TAG	Hypothetical protein
GA	CRAb2	78476	78476	No (K)	AAG to AAA	Hypothetical protein
GT	CRAb2	86290	86290	S to L	CGA to CTA	Transposase
GT	CRAb2	89003	89003	R to L	CGA to CTA	IS26 transposase
TC	CRAb2	96474	96474	No (L)	CTT to CTC	tnp-IS30
TC	CRAb2	96564	96564	No (T)	ACT to ACC	tnp-IS30
TC	CRAb2	96567	96567	No(F)	TTT to TTC	tnp-IS30
AC	CRAb2	96753	96753	No (P)	CCA to CCC	tnp-IS30
GA	CRAb2	96789	96789	No (L)	CTG to CTA	tnp-IS30
AG	CRAb2	99488	99488	No	Intergenic region	
TG	CRAb2	116693	116693	F to Q	TTT to TTG	LysR family transcriptional regulator
CG	CRAb2	143183	143183	No	Intergenic region	
TA	CRAb2	168599	168599	No (A)	GCT to GCA	LPD1 domain-containing protein
GA	CRAb2	173427	173427	No	Intergenic region	
TC	CRAb2	196031	196031	H to R	GTG to GCG	Hypothetical protein
GA	CRAb2	197758	197758	No (Y)	GTA to ATA	Hypothetical protein
CA	CRAb2	200511	200511	No	Intergenic region	
GA	CRAb2	200517	200517	No	Intergenic region	
AG	CRAb2	200610	200610	No	Intergenic region	
GA	CRAb2	211490	211490	No (S)	TCG to TCA	putative outer membrane core complex of type IVb secretion system
GA	CRAb2	211795	211795	G to E	CGA to GAA	putative outer membrane core complex of type IVb secretion system
TA	CRAb2	217496	217496	L to I	TTA to ATA	Hypothetical protein
CA	CRAb2	220425	220425	P to Q	CCA to CAA	Hypothetical protein
TC	CRAb2	225355	225355	Y to H	TAT to CAT	DUF6685 domain-containing protein
AG	CRAb2	254368	254368	Stop to W	TAG to TGG	translesion error-prone DNA polymerase V autiproteolytic subunit
TC	CRAb2	255495	255495	M to T	ATG to ACG	DNA polymerase V subunit
TC	CRAb2	260925	260925	No (L)	CTT to CTC	ISAba126 family transposase
TC	CRAb2	261015	261015	No (T)	ACT to ACC	ISAba126 family transposase
TC	CRAb2	261018	261018	No (F)	TTT to TTC	ISAba126 family transposase
AC	CRAb2	261204	261204	No (P)	CCA to CCC	ISAba126 family transposase
Deletions						
ATGGTTTTAAG	CRAb1	121045	121055		Intergenic regions	repeat region
ACCACGCCAAGGAATCTAAAG CTGT TATCAGTCTGATAATGAAAAA ACCA	CRAb1	200552	200601		Intergenic regions	
A	CRAb1	200546	200546		Intergenic regions	
Insertions						
ACCA	CRAb2	203730	203733		Intergenic regions	
Transposons						
tnp-IS30	CRAb1	171736	172746		Gene disruption	Hypothetical protein

Table S2.2. Complete annotation of the CRAb1 plasmid

Locus_tag	Name	Product	Type	Gene start	Gene end	Length	Direction
	traJ-II RNA	traJ-II RNA regulatory	regulatory	116804	116904	101	reverse
LLILAP_18375		LPD1 domain-containing protein	CDS	173636	180862	7227	forward
LLILAP_18380		Hypothetical protein	CDS	180872	181303	432	forward
LLILAP_18385		Hypothetical protein	CDS	181576	182148	573	forward
LLILAP_18390		Hypothetical protein	CDS	182102	182890	789	forward
LLILAP_18395		Hypothetical protein	CDS	182899	183381	483	forward
LLILAP_18400		Hypothetical protein	CDS	183479	185335	1857	forward
LLILAP_18405		Hypothetical protein	CDS	185384	185785	402	reverse
LLILAP_18410		Hypothetical protein	CDS	185835	186248	414	reverse
LLILAP_18415	*dotA/traY*	DotA/TraY family protein	Plasmid backbone	186515	189520	3006	forward
LLILAP_18420		Hypothetical protein	CDS	189582	190076	495	reverse
LLILAP_18425		Peptidase family M23	Virulence related	190320	192332	2013	forward
LLILAP_18430		Hypothetical protein	CDS	192355	192765	411	forward
LLILAP_18435		Hypothetical protein	CDS	192780	193205	426	forward
LLILAP_18440		Hypothetical protein	CDS	193258	193902	645	reverse
LLILAP_18445		ATP-dependent helicase	Plasmid backbone	193895	195451	1557	reverse
LLILAP_18450		Hypothetical protein	CDS	195455	196012	558	reverse
LLILAP_18455		Hypothetical protein	CDS	196012	196581	570	reverse
LLILAP_18460		Hypothetical protein	CDS	196594	197268	675	reverse
LLILAP_18465		Hypothetical protein	CDS	197281	198186	906	reverse
LLILAP_18470	*icmP/dotM*	Type IV secretion system protein IcmP/DotM	Plasmid backbone	198309	199838	1530	reverse
LLILAP_18475		NUBPL iron-transfer P-loop NTPase	Virulence related	201241	202077	837	forward
LLILAP_18480	*parB*	ParB domain-containing protein	Virulence related	202087	203148	1062	forward
LLILAP_18485		Hypothetical protein	CDS	203194	204021	828	reverse
LLILAP_18490	*stbA*	StbA protein	Virulence related	204018	205124	1107	reverse
LLILAP_18495		Hypothetical protein	CDS	205151	205420	270	reverse
LLILAP_18500		Type II/IV secretion system protein	Virulence related	205430	206725	1296	reverse
LLILAP_18505		Type IV secretory system, conjugal DNA-protein transfer	Plasmid backbone	206753	207562	810	reverse
LLILAP_18510	*dotD/traH*	DotD/TraH family lipoprotein	Plasmid backbone	207600	208046	447	reverse
LLILAP_18515		Hypothetical protein	CDS	209131	210354	1224	forward
LLILAP_18520		Hypothetical protein	CDS	210355	210642	288	forward
LLILAP_18525		Type-IV b secretion system, inner-membrane complex component	Plasmid backbone	210653	211336	684	forward
LLILAP_18530		Putative outer membrane core complex of type IVb secretion	Plasmid backbone	211350	212297	948	forward
LLILAP_18535	*trbI*	DotG/IcmE/VirB10 family protein	Plasmid backbone	212319	213830	1512	forward
LLILAP_18540		Hypothetical protein	CDS	213836	214717	882	forward
LLILAP_18545		Hypothetical protein	CDS	214728	215303	576	forward
LLILAP_18550		Hypothetical protein	CDS	215471	215884	414	forward
LLILAP_18555		HNH endonuclease	regulatory	215995	216882	888	forward
LLILAP_18560		Hypothetical protein	CDS	216893	218095	1203	forward
LLILAP_18565	*icmB/dotO*	type IV secretion system protein IcmB/DotO	Plasmid	218153	221335	3183	forward

Locus_tag	Name	Product	Type	Gene start	Gene end	Length	Direction
			backbone				
LLILAP_18570	*dotL*	type IV secretion protein DotL	Plasmid backbone	221458	224250	2793	forward
LLILAP_18575		Hypothetical protein	CDS	224885	225058	174	forward
LLILAP_18580		DUF6685 domain-containing protein	CDS	225145	226233	1089	forward
LLILAP_18585		Hypothetical protein	CDS	226246	226752	507	forward
LLILAP_18590	*int*	Phage integrase family	Mobile genetic elements	227512	228177	666	forward
LLILAP_18595	*tet(X3)*	tetracycline-inactivating monooxygenase Tet(X3)	Antibiotic resistance	228367	229533	1167	forward
LLILAP_18600	*spoIVCA*	resolvase	Plasmid backbone	229682	230419	738	forward
LLILAP_18605		Hypothetical protein	CDS	230416	230640	225	forward
LLILAP_18610	*tnp-ISVsa3*	IS91-like element ISVsa3 family transposase	Mobile genetic elements	230851	232344	1494	forward
LLILAP_18615		phosphoglucosamine mutase	Virulence related	232520	232822	303	reverse
LLILAP_18620	*sul2*	sulfonamide-resistant dihydropteroate synthase Sul2	Antibiotic resistance	232909	233757	849	reverse
LLILAP_18625	*tnp-ISAba1*	IS4 family ISAba1 transposase	Mobile genetic elements	233814	234383	570	forward
LLILAP_18630	*tnp-IS4*	IS4 family transposase	Mobile genetic elements	234766	234903	138	forward
LLILAP_18635		Hypothetical protein	CDS	234900	235205	306	forward
LLILAP_18640		Hypothetical protein	CDS	235303	235812	510	forward
LLILAP_18645		Hypothetical protein	CDS	235952	236938	987	forward
LLILAP_18650		Hypothetical protein	CDS	236994	237371	378	reverse
LLILAP_18655		Hypothetical protein	CDS	237385	237744	360	reverse
LLILAP_18660		Hypothetical protein	CDS	238277	239227	951	reverse
LLILAP_18665		Hypothetical protein	CDS	239239	239709	471	reverse
LLILAP_18670		Hypothetical protein	CDS	239774	240181	408	reverse
LLILAP_18675		Hypothetical protein	CDS	240731	241120	390	forward
LLILAP_18680		Hypothetical protein	CDS	241371	242819	1449	forward
LLILAP_18685		Hypothetical protein	CDS	242897	243301	405	forward
LLILAP_18690		HlyD-D23 domain-containing protein	Antibiotic resistance	243678	244841	1164	forward
LLILAP_18695	*adeB*	multidrug efflux RND transporter permease subunit	Antibiotic resistance	244841	247942	3102	forward
LLILAP_18700		MFS transporter	Virulence related	248069	249583	1515	forward
LLILAP_18705	*AdeS*	two-component sensor histidine kinase AdeS	Antibiotic resistance	249687	250403	717	reverse
LLILAP_18710		Hypothetical protein	CDS	250458	250748	291	reverse
LLILAP_18715	*adeR*	efflux system response regulator transcription factor AdeR	Antibiotic resistance	250792	251520	729	reverse
LLILAP_18720		Hypothetical protein	CDS	251644	252537	894	reverse
LLILAP_18725	*tnp-ISAlw15*	IS5 family ISAlw15 transposase	Mobile genetic elements	252808	253212	405	forward
LLILAP_18730	*tnp-IS5*	IS5 family transposase	Mobile genetic elements	253415	253642	228	forward
LLILAP_18735		Translesion error-prone DNA polymerase V autoproteolytic subunit	Virulence related	253848	254369	522	forward
LLILAP_18740	*umuC*	DNA polymerase V subunit UmuC	Virulence related	254456	255694	1239	forward
LLILAP_18745		Hypothetical protein	CDS	255829	256116	288	reverse
LLILAP_18750		Hypothetical protein	CDS	256606	257034	429	reverse
LLILAP_18755		Hypothetical protein	CDS	257057	258013	957	reverse
LLILAP_18760		Hypothetical protein	CDS	258349	258774	426	reverse

Locus_tag	Name	Product	Type	Gene start	Gene end	Length	Direction
LLILAP_18765		Hypothetical protein	CDS	258813	258968	156	reverse
LLILAP_18770		Hypothetical protein	CDS	259151	260299	1149	reverse
LLILAP_18775	*tnp-ISAba125*	IS30-like element ISAba125 family transposase	Mobile genetic elements	260833	261843	1011	forward
LLILAP_18780	*blaNDM-1*	subclass B1 metallo-beta-lactamase NDM-1	Antibiotic resistance	1	813	813	forward
LLILAP_18785		Hypothetical protein	CDS	694	1245	552	reverse
LLILAP_18790	*ble*	Bleomycin resistance protein	Antibiotic resistance	2142	3023	882	forward
LLILAP_18795		Hypothetical protein	CDS	2968	3258	291	forward
LLILAP_18800	*groES*	co-chaperone GroES	Virulence related	3395	3685	291	forward
LLILAP_18805	*tnp-IS91*	IS91 family transposase	Mobile genetic elements	5570	7099	1530	forward
LLILAP_18810		Acyltransferase family protein	Virulence related	7310	7594	285	reverse
LLILAP_18815	*tnp-ISAba125*	IS30-like element ISAba125 family transposase	Mobile genetic elements	7902	8912	1011	forward
LLILAP_18820		Hypothetical protein	CDS	8847	9374	528	reverse
LLILAP_18825		Hypothetical protein	CDS	9367	10239	873	reverse
LLILAP_18830		Hypothetical protein	CDS	10252	10893	642	reverse
LLILAP_18835		Hypothetical protein	CDS	11114	11644	531	reverse
LLILAP_18840		Hypothetical protein	CDS	11845	12327	483	reverse
LLILAP_18845		DUF6573 domain-containing protein	CDS	12407	12841	435	reverse
LLILAP_18850		cold shock domain-containing protein	Virulence related	12992	13489	498	forward
LLILAP_18855		Hypothetical protein	CDS	13559	13897	339	reverse
LLILAP_18860		phosphohydrolase	Virulence related	14055	15152	1098	reverse
LLILAP_18865		Hypothetical protein	CDS	15329	15805	477	reverse
LLILAP_18870		Hypothetical protein	CDS	15878	16192	315	reverse
LLILAP_18875		Hypothetical protein	CDS	16205	17047	843	reverse
LLILAP_18880		Hypothetical protein	CDS	17299	17829	531	reverse
LLILAP_18885		Hypothetical protein	CDS	17873	18436	564	reverse
LLILAP_18890	*fic/DOC*	Fic/DOC family	Plasmid backbone	18581	19339	759	reverse
LLILAP_18895		Hypothetical protein	CDS	19409	19621	213	reverse
LLILAP_18900		Hypothetical protein	CDS	19819	20274	456	forward
LLILAP_18905		Hypothetical protein	CDS	20377	20913	537	reverse
LLILAP_18910		Hypothetical protein	CDS	21525	22019	495	reverse
LLILAP_18915		Hypothetical protein	CDS	22113	22538	426	reverse
LLILAP_18920		Hypothetical protein	CDS	22580	23473	894	reverse
LLILAP_18925		Hypothetical protein	CDS	23473	23901	429	reverse
LLILAP_18930		Hypothetical protein	CDS	24129	24953	825	reverse
LLILAP_18935		HNS domain-containing protein	CDS	25140	25466	327	forward
LLILAP_18940		Hypothetical protein	CDS	25546	25815	270	reverse
LLILAP_18945		Hypothetical protein	CDS	25815	26159	345	reverse
LLILAP_18950		Hypothetical protein	CDS	26320	26508	189	forward
LLILAP_18955	*tnp-IS4*	IS4 family transposase	Mobile genetic elements	26867	27403	537	reverse
LLILAP_18960	*tnp-IS4*	IS4 family transposase	Mobile genetic elements	27400	27960	561	reverse
LLILAP_18965		Hypothetical protein	CDS	28019	28219	201	forward
LLILAP_18970	*gstA*	glutathione S-transferase	Virulence related	28336	28953	618	forward
LLILAP_18975		Hypothetical protein	CDS	29045	29398	354	forward

Locus_tag	Name	Product	Type	Gene start	Gene end	Length	Direction
LLILAP_18980	*yqaA*	Inner membrane protein YqaA	Virulence related	29395	29823	429	forward
LLILAP_18985		MFS transporter	Virulence related	29859	31112	1254	reverse
LLILAP_18990	*tnp-IS4*	IS4 family transposase	Mobile genetic elements	31229	31789	561	forward
LLILAP_18995	*tnp-IS4*	IS4 family transposase	Mobile genetic elements	31786	32322	537	forward
LLILAP_19000		Hypothetical protein	CDS	32317	33234	918	reverse
LLILAP_19005	*cas6/cse3/casE*	Type I-E CRISPR-associated protein Cas6/Cse3/CasE	Plasmid backbone	33311	34042	732	reverse
LLILAP_19010	*mpr*	zinc metalloproteinase Mpr protein	Virulence related	34335	35513	1179	forward
LLILAP_19015		Hypothetical protein	CDS	35510	35878	369	forward
LLILAP_19020		helicase SNF2	Plasmid backbone	35878	37545	1668	forward
LLILAP_19025		Hypothetical protein	CDS	37556	37672	117	forward
LLILAP_19030	*tnp-IS3*	IS3 family transposase	Mobile genetic elements	37831	38523	693	reverse
LLILAP_19035	*tnp-ISAba14*	IS3 family ISAba14 transposase	Mobile genetic elements	38658	38963	306	reverse
LLILAP_19040		Hypothetical protein	CDS	39030	39518	489	reverse
LLILAP_19045	*merA*	mercury(II) reductase	Antibiotic resistance	39663	41348	1686	reverse
LLILAP_19050		Hypothetical protein	CDS	41435	41845	411	forward
LLILAP_19055	*merR*	mercury resistance transcriptional regulator MerR	Antibiotic resistance	42248	42703	456	forward
LLILAP_19060	*tnp-IS5*	IS5 family transposase	Mobile genetic elements	42710	43135	426	reverse
LLILAP_19065		Hypothetical protein	CDS	43324	43668	345	forward
LLILAP_19070		Hypothetical protein	CDS	43730	43948	219	forward
LLILAP_19075		Hypothetical protein	CDS	44667	45623	957	reverse
LLILAP_19080		Hypothetical protein	CDS	45780	46430	651	forward
LLILAP_19085	*traX*	TraX protein	Plasmid backbone	46406	47197	792	forward
LLILAP_19090		Hypothetical protein	CDS	47266	48012	747	reverse
LLILAP_19095		Hypothetical protein	CDS	48130	48870	741	reverse
LLILAP_19100		Hypothetical protein	CDS	48905	49474	570	reverse
LLILAP_19105		Hypothetical protein	CDS	49525	49947	423	reverse
LLILAP_19110		Hypothetical protein	CDS	50007	50813	807	forward
LLILAP_19115		SLT domain-containing protein	CDS	50815	51669	855	forward
LLILAP_19120		TNase-like domain-containing protein	CDS	51755	52261	507	forward
LLILAP_19125		Hypothetical protein	CDS	52267	52575	309	forward
LLILAP_19130		site-specific DNA-methyltransferase	regulatory	52748	54283	1536	forward
LLILAP_19135		restriction endonuclease subunit R	Plasmid backbone	54299	56986	2688	forward
LLILAP_19140		Hypothetical protein	CDS	57039	59882	2844	reverse
LLILAP_19145		DUF2807 domain-containing protein	CDS	60180	60842	663	forward
LLILAP_19150		virulence-associated e family protein	Virulence related	60987	62666	1680	reverse
LLILAP_19155		Hypothetical protein	CDS	62683	63591	909	reverse
LLILAP_19160		Hypothetical protein	CDS	63660	64913	1254	reverse
LLILAP_19165		Hypothetical protein	CDS	65515	65748	234	forward
LLILAP_19170		Hypothetical protein	CDS	65799	65951	153	reverse
LLILAP_19175		Hypothetical protein	CDS	65951	66472	522	reverse
LLILAP_19180		type I DNA topoisomerase	Plasmid backbone	66828	69491	2664	forward

Locus_tag	Name	Product	Type	Gene start	Gene end	Length	Direction
LLILAP_19185		Hypothetical protein	CDS	69508	70506	999	forward
LLILAP_19190		Hypothetical protein	CDS	70702	70935	234	forward
LLILAP_19195		zinc-ribbon-2 domain-containing protein	CDS	71016	72824	1809	reverse
LLILAP_19200		Hypothetical protein	CDS	73026	73355	330	reverse
LLILAP_19205		H-NS histone family protein	CDS	73598	74059	462	reverse
LLILAP_19210		DUF2726 domain-containing protein	CDS	74171	74689	519	reverse
LLILAP_19215		Hypothetical protein	CDS	74908	75597	690	forward
LLILAP_19220		Hypothetical protein	CDS	75978	76361	384	forward
LLILAP_19225		NERD domain-containing protein	regulatory	76364	77200	837	forward
LLILAP_19230		Hypothetical protein	CDS	77313	78350	1038	reverse
LLILAP_19235		Hypothetical protein	CDS	78462	80378	1917	forward
LLILAP_19240		Hypothetical protein	CDS	80498	81343	846	forward
LLILAP_19245		Hypothetical protein	CDS	81459	82031	573	forward
LLILAP_19250	*int*	Phage integrase family	Mobile genetic elements	82058	82990	933	forward
LLILAP_19255		Hypothetical protein	CDS	83156	83818	663	forward
LLILAP_19260	*tn3*	Tn3 family transposase	Mobile genetic elements	83904	86330	2427	reverse
LLILAP_19265	*aph(3')-Ia*	aminoglycoside O-phosphotransferase APH(3')-Ia	Antibiotic resistance	86932	87795	864	reverse
LLILAP_19270	*ant(2'')-Ia*	aminoglycoside nucleotidyltransferase ANT(2'')-Ia	Antibiotic resistance	87846	88379	534	reverse
LLILAP_19275	*tnp-IS26*	IS6-like element IS26 family transposase	Mobile genetic elements	88516	89220	705	forward
LLILAP_19280	*tn5393*	Transposase of Tn5393-like transposon, N-terminal	Mobile genetic elements	89254	90330	1077	reverse
LLILAP_19285	*spoIVCA*	transposon DNA-invertase	Virulence related	90456	91070	615	forward
LLILAP_19290	*tnp-ISAba14*	IS3 family ISAba14 transposase	Mobile genetic elements	91189	91494	306	forward
LLILAP_19295	*tnp-IS3*	IS3 family transposase	Mobile genetic elements	91629	92321	693	forward
LLILAP_19300	*aph(3'')-Ib*	aminoglycoside O-phosphotransferase APH(3'')-Ib	Antibiotic resistance	92421	93224	804	forward
LLILAP_19305	*aph(6)-Id*	aminoglycoside O-phosphotransferase APH(6)-Id	Antibiotic resistance	93224	94060	837	forward
LLILAP_19310		plasmid replication DNA-binding protein	Plasmid backbone	94217	94669	453	forward
LLILAP_19315		Hypothetical protein	CDS	94691	94834	144	forward
LLILAP_19320		Hypothetical protein	CDS	95033	95491	459	reverse
LLILAP_19325		Hypothetical protein	CDS	95491	96225	735	reverse
LLILAP_19330	*tnp-IS30*	IS30 family transposase	Mobile genetic elements	96382	97392	1011	forward
LLILAP_19335	*tnp-IS1*	IS1 family transposase	Mobile genetic elements	97421	97867	447	reverse
LLILAP_19340	*blaOXA-58*	OXA-58 family carbapenem-hydrolyzing class D beta-lactamase	Antibiotic resistance	98017	98790	774	forward
LLILAP_19345	*tnp-IS1*	IS1 family transposase	Mobile genetic elements	98881	99318	438	forward
LLILAP_19350	*araC*	AraC family transcriptional regulator	regulatory	99761	100588	828	forward
LLILAP_19355	*lysE*	LysE family translocator	regulatory	100638	101243	606	forward
LLILAP_19360	*relE/parE*	addiction module killer protein	Plasmid backbone	101340	101636	297	forward
LLILAP_19365		putative addiction module antidote protein	regulatory	101638	101928	291	forward
LLILAP_19370	*tnp-ISNCY*	ISNCY family transposase	Mobile genetic elements	102031	103365	1335	reverse
LLILAP_19375		Hypothetical protein	CDS	103508	103990	483	forward
LLILAP_19380	*relE/parE*	Type II toxin-antitoxin system RelE/ParE family	Plasmid	104106	104426	321	forward

Locus_tag	Name	Product	Type	Gene start	Gene end	Length	Direction
		toxin	backbone				
LLILAP_19385	*nadS*	NadS family protein	regulatory	104419	104691	273	forward
LLILAP_19390	*tnp-ISNCY*	ISNCY family transposase	Mobile genetic elements	104787	106121	1335	reverse
LLILAP_19395	*msr(E)*	ABC-F type ribosomal protection protein Msr(E)	Antibiotic resistance	106670	108145	1476	forward
LLILAP_19400	*mph(E)*	Mph(E) family macrolide 2'-phosphotransferase	Antibiotic resistance	108201	109085	885	forward
LLILAP_19405		resolvase	Virulence related	109275	109886	612	reverse
LLILAP_19410	*lrp*	DNA-binding transcriptional regulator, Lrp family	Virulence related	110085	110567	483	reverse
LLILAP_19415	*lysE*	Lysine transporter LysE	regulatory	110698	111333	636	forward
LLILAP_19420		Hypothetical protein	CDS	111791	112105	315	reverse
LLILAP_19425		Iron ABC transporter permease	Virulence related	112412	114040	1629	reverse
LLILAP_19430		iron ABC transporter substrate-binding protein	Virulence related	114124	115134	1011	reverse
LLILAP_19435	*fbpC 2*	Fe(3+) ions import ATP-binding protein FbpC 2	Virulence related	115157	116281	1125	reverse
LLILAP_19440	*lysR*	LysR family transcriptional regulator	regulatory	116400	116768	369	reverse
LLILAP_19445		Hypothetical protein	CDS	117074	117409	336	forward
LLILAP_19450	*tnp-ISAlw25*	IS1 family ISAlw25 transposase	Mobile genetic elements	117809	118510	702	reverse
LLILAP_19455		Hypothetical protein	CDS	118834	119079	246	forward
LLILAP_19460		Hypothetical protein	CDS	119155	119583	429	reverse
LLILAP_19465		Hypothetical protein	CDS	119773	120306	534	forward
LLILAP_19470		N-acetylmuramoyl-L-alanine amidase	regulatory	120345	120986	642	reverse
LLILAP_19475		Hypothetical protein	CDS	121157	121909	753	forward
LLILAP_19480		Hypothetical protein	CDS	122297	122542	246	reverse
LLILAP_19485	*pcfJ*	PcfJ-like protein	CDS	122734	124404	1671	reverse
LLILAP_19490		LPD1 domain-containing protein	CDS	124401	126041	1641	reverse
LLILAP_19495		Hypothetical protein	CDS	126060	126443	384	reverse
LLILAP_19500		Hypothetical protein	CDS	126450	127217	768	reverse
LLILAP_19505		Putative lipoprotein	Virulence related	127219	128541	1323	reverse
LLILAP_19510		Hypothetical protein	CDS	128632	129150	519	reverse
LLILAP_19515		Hypothetical protein	CDS	129225	129578	354	forward
LLILAP_19520		Hypothetical protein	CDS	129678	130424	747	reverse
LLILAP_19525		Putative lipoprotein	Virulence related	130485	130847	363	forward
LLILAP_19530		Hypothetical protein	CDS	130997	131890	894	reverse
LLILAP_19535	*loiP*	Metalloprotease LoiP	Virulence related	131906	132685	780	reverse
LLILAP_19540		Hypothetical protein	CDS	132678	133166	489	reverse
LLILAP_19545		Hypothetical protein	CDS	133176	133685	510	reverse
LLILAP_19550		Hypothetical protein	CDS	133691	134113	423	reverse
LLILAP_19555		Hypothetical protein	CDS	134278	134931	654	forward
LLILAP_19560		Hypothetical protein	CDS	134997	135509	513	reverse
LLILAP_19565		Hypothetical protein	CDS	135517	136647	1131	reverse
LLILAP_19570		Hypothetical protein	CDS	137333	138202	870	reverse
LLILAP_19575		Transporter	Virulence related	138304	138903	600	reverse
LLILAP_19580		Hypothetical protein	CDS	138896	140686	1791	reverse
LLILAP_19585		Hypothetical protein	CDS	140854	141330	477	reverse
LLILAP_19590		Hypothetical protein	CDS	143186	144820	1635	forward
LLILAP_19595	*res*	Type III restriction enzyme, res subunit	Plasmid backbone	144852	151484	6633	forward

Locus_tag	Name	Product	Type	Gene start	Gene end	Length	Direction
LLILAP_19600		Hypothetical protein	CDS	151614	151763	150	forward
LLILAP_19605		Hypothetical protein	CDS	151797	156230	4434	forward
LLILAP_19610		Hypothetical protein	CDS	156233	157126	894	forward
LLILAP_19615		Hypothetical protein	CDS	157195	157623	429	forward
LLILAP_19620		Hypothetical protein	CDS	157627	158433	807	forward
LLILAP_19625		Hypothetical protein	CDS	158459	159421	963	forward
LLILAP_19630		Hypothetical protein	CDS	159434	160270	837	forward
LLILAP_19635		Hypothetical protein	CDS	160276	161466	1191	forward
LLILAP_19640		Hypothetical protein	CDS	161479	162720	1242	forward
LLILAP_19645		LPD1 domain-containing protein	CDS	162930	170216	7287	forward
LLILAP_19650		Hypothetical protein	CDS	170300	170959	660	forward
LLILAP_19655		Hypothetical protein	CDS	171132	171683	552	forward
LLILAP_19660	*tnp-IS30*	IS30 family transposase	Mobile genetic elements	171736	172746	1011	forward
LLILAP_19665		Hypothetical protein	CDS	172795	173394	600	forward
	gi2	Genomic island 2	Mobile genetic elements	82058	94060	12003	
	gi3	Genomic island 3	Mobile genetic elements	227510	234383	6874	
	gi1	Genomic island 1	Mobile genetic elements	694	7099	6406	

Chapter 5

Outer membrane vesicles of clinical *tet(x3)*, *bla*$_{NDM-1}$, and *bla*$_{OXA-97}$-carrying *Acinetobacter baumannii* isolates contribute to carbapenem resistance

- **R. Monteiro**, B.S. Alcantud, S. Piersma, A.P.A. Hendrickx, S. Maaß, D. Becher, J. Azeredo, E. Bathoorn, and J.M. van Dijl

R. Monteiro kindly acknowledges Lilly Franzmeyer and Jürgen Bartel for technical support with the proteome analyses.

Abstract

Infections caused by carbapenem-resistant *Acinetobacter baumannii* (CRAb) are associated with high patient morbidity and mortality. The serious threat for human health imposed by CRAb was recently underscored by identification of close-to-untouchable carbapenem- and tetracycline-resistant isolates. Since outer membrane vesicles (OMVs) of Gram-negative bacteria may contribute to antimicrobial resistance, our present study was aimed at investigating OMVs produced by the first two carbapenem- and tetracycline-resistant *A. baumannii* isolates in Europe. These isolates, denoted CRAb1 and CRAb2, contain large, nearly identical plasmids that specify multiple resistances. Both isolates produce OMVs that were analyzed by differential light scattering, transmission electron microscopy and proteomics. By comparison with OMVs from the plasmid-free non-carbapenem-resistant *A. baumannii* isolate Ab1, which is an isogenic ancestor of the CRAb1 isolate, we show that plasmid carriage by the CRAb1 and CRAb2 isolates leads to an increased OMV size that is accompanied by increased diversity of the OMV proteome. Our analyses show that OMVs from CRAb1 and CRAb2 are major reservoirs of proteins involved in antimicrobial resistance, including the plasmid-encoded carbapenemases Bla$_{NDM-1}$, and Bla$_{OXA-97}$. We also show that these OMV-borne carbapenemases hydrolyze imipenem and protect otherwise carbapenem-sensitive *A. baumannii* and *Escherichia coli* isolates against this antibiotic. Altogether, our observations show that OMVs from highly drug-resistant CRAb confer protection against last-resort antibiotics to non-resistant bacterial pathogens.

Keywords: A. baumannii; Antibiotic-Resistance; Carbapenemases; OMV; Virulence

5.1. INTRODUCTION

Acinetobacter baumannii is a Gram-negative bacterium that is notorious for causing life-threatening healthcare- and ventilator-associated pneumonia (1–5). Particularly the emergence of carbapenem-resistant *A. baumannii* (CRAb) variants has raised the alarms due to their ability to resist last-generation β-lactam antibiotics. Combined with the already critical multidrug resistance in *A. baumannii*, the emergence of CRAb has increased the patient morbidity and mortality due to *A. baumannii* infections even further (1,4,6). This led the World Health Organization (WHO) to declare CRAb as a top-priority pathogen for the development of new antimicrobials (7).

The main mechanisms underlying the rapid emergence of multi-drug resistant bacteria in general are: (i) the transfer of antibiotic resistance genes between different strains or species, and (ii) the mutation of specific genes that either lead to their overexpression or silencing, thereby causing increased antibiotic resistance (8,9). In the case of CRAb, resistance is mostly caused by the acquisition of plasmids that carry carbapenemase genes (10,11). Tetracyclines are usually applied to treat CRAb infections but, unfortunately, tetracycline-resistant CRAb isolates have emerged (12,13). Such isolates can even be resistant to important last-line antibiotics such as tigecycline, minocycline, eravacycline and omadacycline (14–17). The resistance to these antibiotics may be conferred by Tet(x) monooxygenases that can degrade tetracyclines (17,18).

Gram-negative bacteria like *A. baumannii* are known to discharge so-called outer membrane vesicles (OMVs) into their environment (19–24). OMVs can help the host to thrive in different environments, providing a huge fitness advantage during the colonization of mammalian cells or surfaces by creating the first layers supporting biofilm formation (25–28). Moreover, these vesicles may be involved in horizontal gene transfer favoring the spread of antibiotic resistance genes and they can also help to disseminate quorum-sensing molecules (21,29,30). OMVs can also serve important functions in bacterial virulence, for instance by neutralizing the host immune defenses (31,32). Lastly, OMVs can provide different types of protection against environmental hazards, for instance by serving as decoys for bacteriophages (33), and by inactivating or binding antibiotics from different classes, like carbapenems (34–36) and polymyxins (37,38).

In the course of a recent *A. baumannii* outbreak in an intensive care unit in the Netherlands, which initially started with carbapenemase-sensitive isolates, two tetracycline-resistant CRAb strains with distinct multi-locus sequence types were isolated from two of the affected patients (39). Whole-genome sequencing showed that these isolates, denoted CRAb1 and CRAb2, carried close-to-identical plasmids of 265 kb with multiple antibiotic resistance genes, including the *bla*$_{NDM-1}$ and *bla*$_{OXA-97}$

carbapenemase genes and the *tet(x3)* tetracycline resistance gene (Table 5.1). The *tet(x3)* gene was shown to confer high-level resistance to last-resort tetracyclines, including the newly registered eravacycline and omadacycline, which made these two isolates highly exceptional for CRAb isolates from Europe. In addition, the plasmids pCRAb1 and pCRAb2 had not been described before. Whole-genome sequencing of the first carbapenemase-sensitive isolate Ab1 from the outbreak's index patient showed that this isolate was isogenic with the CRAb1 isolate that was collected four weeks later from the same patient. The Ab1 and CRAb1 isolates differed only for the presence of the 265-kb plasmid pCRAb1 in the CRAb1 isolate and the absence of a prophage from the CRAb1 isolate. Altogether, the collected data are indicative of inter-bacterial plasmid transfer during the outbreak, although the origin of the pCRAb1 and pCRAb2 plasmids remained unknown (39).

Table 5.1. Antibiotic resistance genes encoded by the large pCRAb1 and pCRAb2 plasmids in the CRAb1 and CRAb2 isolates

Antibiotic resistance genes	**Resistance against**
bla_{ADC-79} *$bla_{OXA-100}$* *bla_{NDM-1}* *bla_{OXA-97}*	*β-lactams/carbapenems*
tet(x3)	*Tetracyclines*
sul2	*Sulphonamides*
ant(2")-Ia *aph(3")-Ib* *aph(3')-Ia* *aph(6)-Id* *ant(3")-IIa*	*Aminoglycosides*
mph(E) *msr(E)*	*Macrolides*

Since previous studies have implicated OMVs in the Gram-negative bacterial resistance to antimicrobial agents, our present study was aimed at investigating whether the two tetracycline-resistant CRAb strains, CRAb1 and CRAb2, produce OMVs that contribute to these traits. To address this question, a proteomics approach was followed and combined with subsequent functional analyses. For comparison, we also analyzed the OMV proteome of the early non-resistant Ab1 isolate.

5.2. MATERIALS AND METHODS

5.2.1. Bacterial strains

The three *A. baumannii* isolates used for this study were denoted Ab1 (*bla*$_{ADC-79}$, *bla*$_{OXA-100}$), (*bla*$_{ADC-79}$, *bla*$_{OXA-100}$, *bla*$_{NDM-1}$, *bla*$_{OXA-97}$, *tet(x3)*, *sul2*, *ant(2'')-Ia*, *aph(3'')-Ib*, *aph(3')-Ia*, *aph(6)-Id*, *ant(3'')-IIa*, *mph(E)*, *msr(E)*), and CRAb2 (*bla*$_{ADC-79}$, *bla*$_{OXA-100}$, *bla*$_{NDM-1}$, *bla*$_{OXA-97}$, *tet(x3)*, *sul2*, *abaF*, *ant(2'')-Ia*, *aph(3'')-Ib*, *aph(3')-Ia*, *aph(6)-Id*, *ant(3'')-IIa*, *mph(E)*, *msr(E)*). The genome sequences of these isolates have been submitted to the NCBI GenBank database and are available under the BioProject number PRJNA1011532. The isolates were routinely grown in Lysogeny Broth (LB, BD Difco™) at 37 °C. The cultures were shaken at 120 rpm using a Multitron Triple Incubator Shaker (Infors HT). LB plates contained 1.2 % agar (BD Difco™).

5.2.2. OMV purification

In order to isolate OMVs, overnight cultures of *A. baumannii* were used to inoculate 250 mL of LB at a 1:100 dilution. Subsequently, the bacteria were cultured for 24 h at 37 °C and 120 rpm. The bacteria were then pelleted by centrifugation at 8,000 × *g* for 20 min at 4 °C, using an Avanti J-26S XP centrifuge (Beckman Coulter Inc., Brea, California, USA). The culture supernatant containing OMVs was filtered through a 0.22 µm polyethersulfone (PES) filter (VWR) and kept at 4 °C. OMVs were collected from the cell-free culture supernatant by ultracentrifugation at 30,000 rpm (150,000 × *g*) for 4 h, at 4 °C, using an OptimaTM XL-80K ultracentrifuge (Beckman Coulter Inc., Brea, California, USA). The supernatant was discarded, and the pellet was washed three times with phosphate-buffered saline (PBS) by ultracentrifugation at 100,000 × *g* for 3 h at 4 °C. OMVs were resuspended in 300-500 µL of PBS for further analysis. Quantification of the OMV protein content was performed using the Pierce™ BCA Protein Assay Kit (ThermoFisher), and 2 % SDS for OMV solubilization (40).

5.2.3. Dynamic light scattering

For dynamic light scattering (DLS) analysis, a Zetasizer Nano ZS (Malvern Panalytical Ltd, UK) was used. To this end, 40 µL of PBS-diluted OMVs (100-200 µg/mL) were submitted to DLS in micro cuvettes (part no. ZEN0040, Malvern Panalytical). The refractory index (RI) was set to 1.45 with an absorption of 0.001 and the dispersant RI was set to 1.335 with a viscosity of 0.8882. The temperature was set to 25 °C. Measurements were performed in triplicate with an equilibration time of 90 s.

5.2.4. Transmission electron microscopy (TEM)

For visualization of OMVs by TEM, negative staining was performed using a solution of 5 % uranyl acetate as previously described (41). A drop of the OMVs was deposited onto a copper grid with carbon-coated Formvar films. After 15 min of incubation, the grids were rinsed with ultrapure water, stained with uranyl acetate, and washed again before visualization using a Talos F200i electron microscope at 80 kV.

5.2.5. LDS-PAGE

OMV samples (20 µg) were precipitated with trichloroacetic acid (TCA) at a final concentration of 10 % by incubation for 18 h at 4 °C. Subsequently, proteins were pelleted at 18,500 × *g*, at 4 °C for 20 min, washed with 1 mL of ice-cold acetone, centrifuged for 10 min, and dried by incubating the pellets at 60 °C for 10 min. Precipitated proteins were resuspended in a gel loading buffer containing NuPAGE 10× sample reducing agent and 4× lithium dodecyl sulfate (LDS) sample buffer (Invitrogen, USA), boiled at 98 °C for 10 min, and separated on 10 % NuPAGE gels (Invitrogen, USA) by LDS polyacrylamide gel electrophoresis (PAGE). After electrophoresis proteins were stained with SimplyBlue SafeStain (Life Technologies, CA) and analyzed.

5.2.6. LC-MS/MS sample preparation

Gel lanes of LDS-gels with OMV samples (three independent biological replicates per strain) were excised in one piece and subjected to trypsin digestion as described earlier (42). For the subsequent LC-MS/MS measurements, the digests were separated by reversed phase column chromatography using an EASY nLC 1000 (Thermo Fisher Scientific) with self-packed columns (OD 360 µm, ID 100 µm, length 20 cm) filled with 3 µm diameter C18 particles (Dr. Maisch, Ammerbuch-Entringen, Germany). Following loading/desalting in 0.1 % acetic acid in water, the peptides were separated by applying a binary non-linear gradient from 1-99 % acetonitrile in 0.1 % acetic acid over 162 min. The LC was coupled online to a LTQ Orbitrap Velos mass spectrometer (Thermo Fisher, Bremen, Germany) with a spray voltage of 2.6 kV. After a survey scan in the Orbitrap (r = 30,000), MS/MS data were recorded for the twenty most intensive precursor ions in the linear ion trap. Singly charged ions were not considered for MS/MS analysis. The lock mass option was enabled throughout all analyses.

After mass spectrometric measurement, a database search was performed using MaxQuant (version 2.0.3.0) with databases of *Acinetobacter baumannii* Ab1, CRAb1, and CRAb2 isolates (3752, 3922, and 4119 entries, respectively) in separate (43). These databases were obtained from Prokka v1.14.6 annotation. For strain CRAb1 also protein sequences encoded by the plasmid (268 entries)

were used for spectrum identification. Common laboratory contaminants and reversed sequences were included by MaxQuant. Search parameters were set as follows: trypsin/P specific digestion with up to two missed cleavages, methionine oxidation, and N-terminal acetylation as variable modification, match between runs with default parameters enabled. The false discovery rates (FDRs) of protein and the peptide spectrum match (PSM) levels were set to 0.01. Two identified unique peptides were required for protein identification. MaxLFQ (44) and iBAQ (45) values were calculated in MaxQuant with default settings as a proxy for protein abundance.

5.2.7. Proteome data analysis

Functions of detected proteins were assessed using BLASTp and manually curated using UniProt webserver (46). COG categories were attributed using eggNOG (ver.6.0.0) (47) and reCOGnizer (ver.1.10.0) (48). The predicted subcellular localization of each identified OMV protein was assessed using PSORTb (ver.3.0) (49) and literature data. For protein comparison across the isolates, VENN diagrams were drawn using InteractiVENN (50). Antibiotic resistance proteins were predicted using CARD (51). Virulence genes were determined by complementing the afore-mentioned tools with the VirulentPred algorithm (ver.1.0) (52), which predicts bacterial virulence factors based on their amino acid composition, the bilayer cascade Support Vector Machine module (SVM), and the Predict Pathogenic Proteins in Metagenomic data sets (MP3) website (53).

5.2.8. Carbapenemase activity assays

Two procedures were applied to assay carbapenemase activity associated with OMVs: the CarbaNP test and the Carbapenem inhibition method (CIM). The CarbaNP test was adapted from a previous study (54) and was performed by mixing 100 µL containing 3.5 mg of OMVs with either solution A (100 µL of an aqueous solution of 0.05 % phenol-red with 10 mM of SO_4Zn), or solution B (solution A supplemented with imipenem at 6 mg/mL), followed by a 2 h incubation at 37 °C. Negative controls with or without imipenem, and with or without OMVs were used to accurately check for color changes. For the CIM analyses, a protocol was adapted from van der Zwaluw *et al.* (55). Briefly, an imipenem diffusion disk (BD BBL™ Sensi-Disc™, BD) was incubated for 2 h at 37 °C in 500 µL PBS with or without 2 mg/mL of OMVs. Afterwards, the disk was placed on an agar plate with a bacterial lawn of the imipenem susceptible indicator strain *A. baumannii* ATCC 17978. Positive controls were also prepared by incubating disks in PBS with the bacterial biomass of each of the strains from which OMVs were derived. Agar plates were incubated overnight at 37 °C and the presence or absence of zones of growth inhibition was inspected.

5.2.9. OMV-mediated protection against imipenem

To evaluate the protection conferred by the OMVs against carbapenems, growth curves were recorded where the imipenem susceptible *A. baumannii* ATCC 17978 strain was incubated with antibiotics at a minimum inhibitory concentration (MIC), with or without CRAb2-derived OMVs. In particular, an overnight pre-inoculum of *A. baumannii* ATCC 17978 in LB was diluted to a cell density of 2×10^5 CFUs/mL and mixed with or without imipenem (0.125 μg/mL) and OMVs (20 μg) in a 96-well plate. The cultures were incubated in an Epoch plate reader (Biotek) for 6 h at 37 °C with continuous shaking (120 rpm) and with 30 min interval optical density measurements at 600 nm (OD_{600}). The experiment was performed in three independent biological replicates.

5.2.10. Imipenem survival assay

Survival assays were performed by incubating *A. baumannii* ATCC 17978 and *E. coli* ATCC 25922, diluted from an overnight LB pre-inoculum to a cell density of 2×10^5 CFUs/mL, with an inhibitory antibiotic concentration (0.5 μg/mL of imipenem, 256 μg/mL of ampicillin) and three different CRAb2 OMV concentrations (10 μg/mL, 25 μg/mL, 50 μg/mL). The assay was carried out in 96-well plates that were incubated for 24 h at 37 °C without shaking. OD_{600} and colony-forming units (CFUs) were measured and compared to non-treated controls. The assay was performed in three different biological replicates.

5.2.11. Statistical analysis

Statistical analyses were performed using GraphPad software, version 7.0. All data are expressed as means ± standard error of the mean (SEM) and statistical differences were calculated by two-way ANOVA and Tukey's multiple comparison tests.

5.2.12. Data Availability

All MS data have been deposited in the PRIDE repository of the ProteomeXchange Consortium (56) with the dataset identifier PXD051698 (Reviewer account details: Username, reviewer_pxd051698@ebi.ac.uk; Password, AYb7LRIF). Supplemental Table 5S1 can be accessed at (LINK).

5.3. RESULTS AND DISCUSSION

5.3.1. Outer membrane vesicle characterization

OMVs from the three *A. baumannii* study isolates Ab1, CRAb1 and CRAb2 were collected after 24 h culturing in LB. This involved subsequent centrifugation, ultracentrifugation and filtering steps after

which the OMVs were resuspended in PBS. A first characterization of the OMVs was performed by DLS and TEM. The DLS measurements revealed that OMVs from all three isolates contained two differently sized populations. As presented in Table 5.2, two distinct peaks were detectable for each sample. OMVs from the Ab1 isolate had, on average, a smaller size than OMVs from the other two isolates. TEM images of the different OMV preparations showed that the smaller-sized population was prevalent, with very few OMVs of the higher size population (Figure 5.1). The latter OMVs, together with some aggregated OMVs that were also detectable, could be responsible for the Peak 1 detected by DLS. These observations suggest that the actual size of OMVs is reflected by Peak 2 in the DLS measurements, which would be in accordance with the results from other studies (19,22,24,57). Of note, Figure 5.1C shows the presence of phage particles on CRAb2 OMVs which may, at least partially, explain the presence of Peak 1.

Table 5.2. DLS measurements on OMVs from the *A. baumannii* study isolates Ab1, CRAb1 and CRAb2. Two different intensity peaks were detected that correspond to differently sized OMVs, denoted as Peak 1 and Peak 2. PdI refers to the polydispersity index, which indicates how homogeneous the respective sample is

***A. baumannii* isolates**	**Peak 1 Average size (nm)**	**Peak 2 Average size (nm)**	**PdI**
Ab1	194.9 ± 81.91	36.15 ± 9.61	0.309
CRAb1	275.5 ± 133.2	48.59 ± 14.89	0.494
CRAb2	266.1 ± 137.5	45.86 ± 13.04	0.409

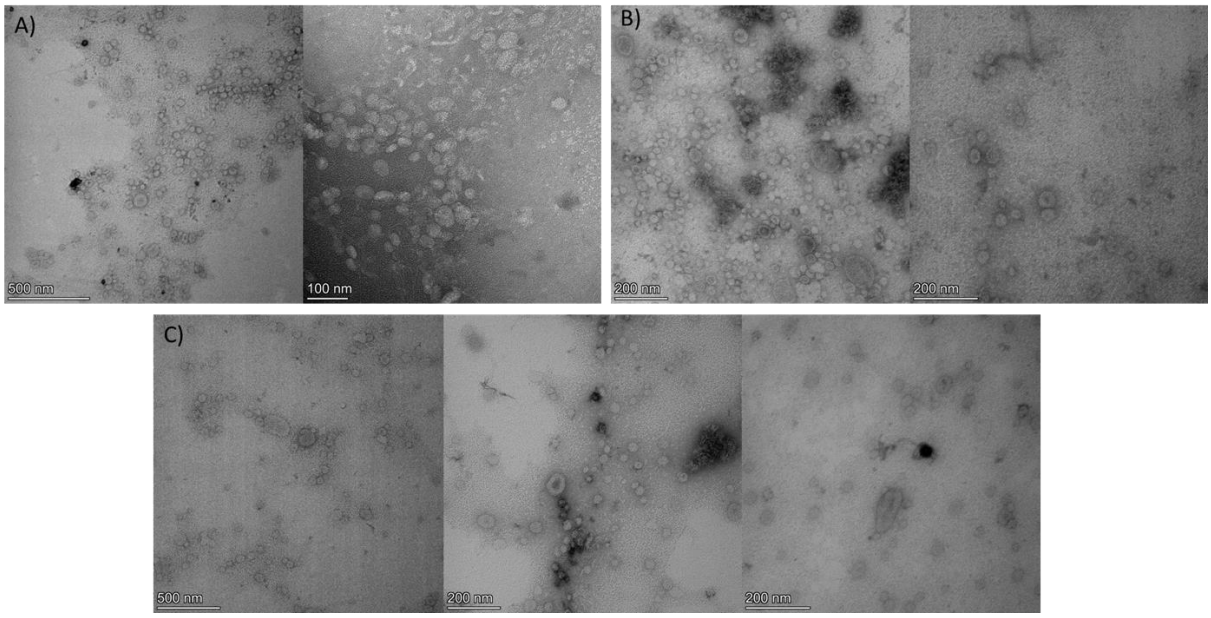


Figure 5.1. TEM images of OMVs from the three *A. baumannii* study isolates. A) Ab1; B) CRAb1; C) CRAb2.

5.3.2. OMV proteome analyses

OMVs from the three study isolates were isolated and analyzed by MS for their protein content (Supplemental Table S5.1). The OMVs from the Ab1 strain presented the lowest protein diversity, with 162 different identified proteins (Figure 5.2). The OMVs from the two CRAb isolates, CRAb1 and CRAb2, displayed significantly more protein diversity with, respectively, 406 and 522 identified proteins (Figure 5.2). Since the Ab1 and CRAb1 strains are isogenic this suggests that the higher protein diversity in OMVs from the CRAb1 isolate is related to the large plasmid that the CRAb1 isolate carries or to the absence of a prophage from the CRAb1 isolate. However, since OMVs of the CRAb2 isolate show a comparably high protein diversity as OMVs from the CRAb1 isolate, it seems most likely that the elevated protein diversity of OMVs from the CRAb1 and CRAb2 isolates is due to the presence of pCRAb1 and pCRAb2, respectively.

As shown in Figure 5.2 and Supplemental Figure S5.1, the largest portion number of OMV proteins from the Ab1 isolate was predicted to be located in the outer membrane (33.33 %), whereas many other proteins were predicted to originate from multiple or unknown locations (19.14 %). The remaining identified OMV proteins from the Ab1 isolate were bioinformatically assigned to the inner membrane (12.96 %), cytoplasm (12.35 %), periplasm (11.73 %), or extracellular milieu (10.49 %). OMVs from the CRAb1 and CRAb2 isolates displayed a similar protein composition with nearly half of them having a predicted cytoplasmic localization (47.29 % and 57.28 %, respectively). This is a higher proportion of predicted cytoplasmic proteins than was observed for OMVs from the Ab1 isolate and could perhaps be related to the larger OMV sizes measured for the CRAb1 and CRAb2 OMVs. Both the CRAb1 and CRAb2 OMVs presented a lower proportion of predicted outer membrane proteins (13.55 % and 10.34 % respectively) compared to the Ab1 OMVs. Furthermore, a similar proportion of predicted inner membrane (15.76 % and 13.41 %), periplasmic (5.91 % and 4.41 %), and extracellular proteins (5.17 % and 2.68 %) was observed in the CRAb1 and CRAb2 OMVs, respectively. Lastly, a significant number of proteins with unknown localization (12.32 % and 11.88 %) was identified in OMVs from both CRAb isolates. Importantly, inspection of the total numbers of identified OMV proteins per predicted subcellular localization (Supplemental Figure S5.1) shows that the main differences between OMVs from the Ab1 versus the CRAb1/CRAb2 proteins relate to proteins with a predicted cytoplasmic or inner membrane localization (Figure 5.2). In contrast, comparable numbers of proteins with a predicted outer membrane, periplasmic, or extracellular localization were identified in OMVs of the three isolates.

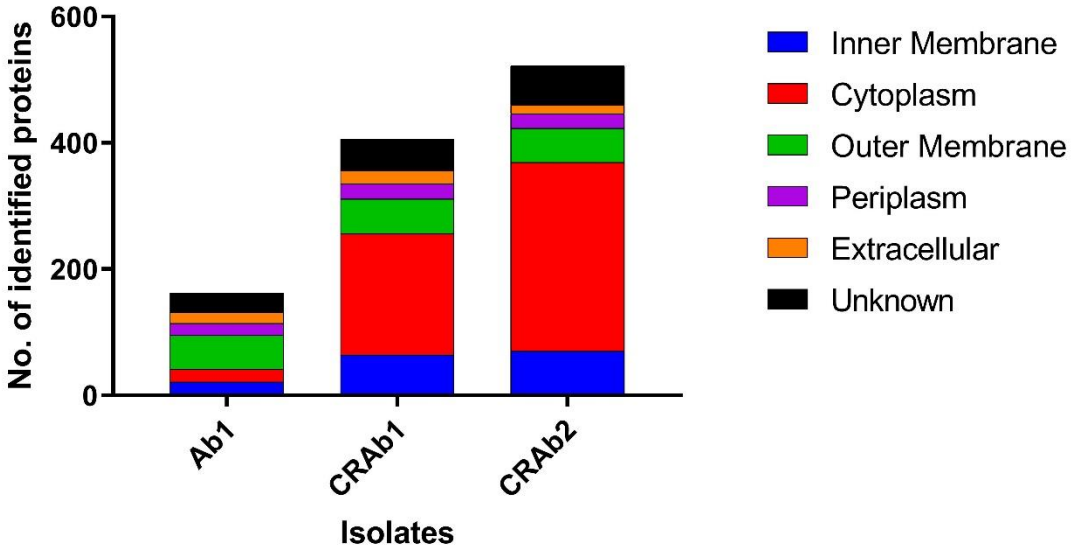


Figure 5.2. Predicted localization of OMV-associated proteins from the Ab1, CRAb1 and CRAb2 isolates.

To assess the similarities and differences in the identified protein content of OMVs from the three *A. baumannii* isolates, a BLASTp analysis was performed and the results are presented in VENN diagrams (Figure 5.3). For this analysis, only proteins with an amino acid sequence with 100 % coverage and greater than 95 % identity were considered to be the same. The VENN diagram shows that, with 129 common proteins, there is a significant overlap in the OMV proteins from the three *A. baumannii* isolates. Yet, there are also clear differences. Specifically, 6 proteins are unique to Ab1 OMVs, 43 proteins to CRAb1 OMVs, and 176 proteins to CRAb2 OMVs. Despite the high genomic similarity between the Ab1 and CRAb1 isolates, there are still 11 OMV proteins from the Ab1 isolate that are not present in OMVs from the CRAb1 isolate, and 255 OMV proteins from the CRAb1 isolate that are absent from OMVs of the Ab1 isolate. None of the 11 unique proteins in Ab1 OMVs relate to the prophage that is absent from the CRAb1 isolate, which suggests that the carriage of plasmid pCRAb1 is largely responsible for the differences in the protein content of the Ab1 and CRAb1 OMVs. If so, the same is probably true for the presence of pCRAb2 in the CRAb2 isolate, which would imply that the plasmid carriage by the CRAb1 and CRAb2 isolates triggers the inclusion of additional cytoplasmic and inner membrane proteins in their OMVs. In this respect, it is noteworthy that in OMVs from the CRAb1 and CRAb2 isolates only four plasmid-encoded proteins were identified of which two were identified in OMVs from both isolates.

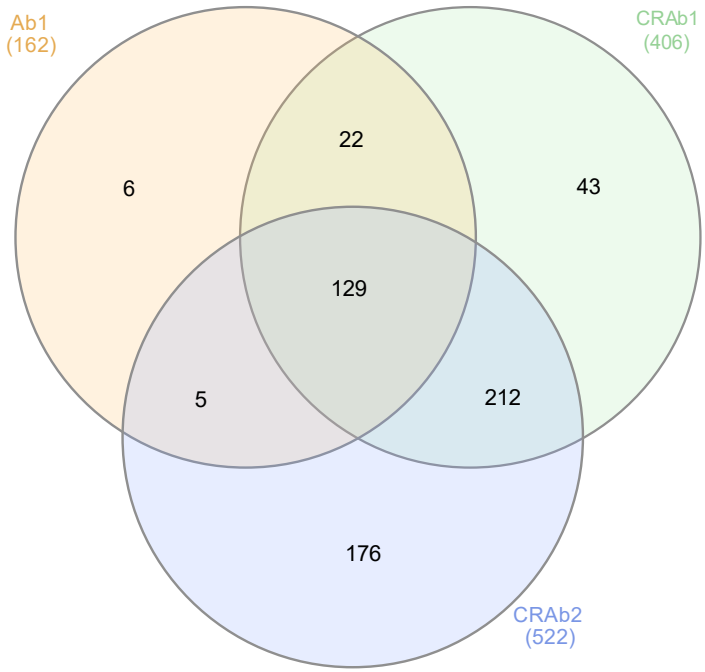


Figure 5.3. Venn diagram showing the numbers of common and uniquely identified proteins in OMVs from the Ab1, CRAb1, and CRAb2 study isolates.

5.3.3. OMV-borne proteins associated with antimicrobial resistance

For functional annotation, proteins were analyzed using a combination of BLASTp, eggNOG, abricate, and manual curation based on UniProt. The analysis revealed that among the 129 common OMV-borne proteins, several were related to antibiotic resistance (AR), including the penicillin-binding protein 1B (58), and the AdeK and AdeT RND-type efflux pumps (59,60). Notably, the Bla$_{OXA-97}$ and Bla$_{NDM-1}$ enzymes, which are carbapenemases encoded by the pCRAb1 and pCRAb2 plasmids, were present in the OMVs of the CRAb1 and CRAb2 isolates. Additionally, we found another ß-lactamase, Bla$_{OXA-100}$, and the efflux pumps AdeJ and AdeI, which are chromosomally encoded and can confer resistance to a wide range of antibiotics (59). Other proteins that potentially have a role in antimicrobial resistance, such as the OmpW family outer membrane β-barrel protein (UniProt - ACIAD2272) (61), the copper resistance protein B (62), the CpaA metalloendopeptidase (63), and the cobalt-zinc-cadmium resistance protein CzcA (64), were also identified. Table 5.3 lists all antibiotic resistance proteins found across the OMVs of the different isolates. These observations show that *A. baumannii* OMVs can be regarded as reservoirs for proteins that confer antibiotic resistance, some of which may protect not only *A. baumannii* but also other bacterial cells against antimicrobials (21,24,29).

Table 5.3. Antimicrobial resistance proteins identified in the OMVs of the Ab1, CRAb1 and CRAb2 isolates. Each protein sequence was inspected by CARD (51)

Common in Ab1, CRAb1, and CRAb2 OMVs			
ID	Protein	Gene	CARD
P0003	AdeT, RND type efflux pump	*adeT*	-
P0009	Cobalt-zinc-cadmium resistance protein CzcA; efflux RND transporter permease subunit	*czcA*	*mexK*
P0169	Outer membrane protein OprM	*oprM*	*adeK*
P0222	Ornithine uptake porin CarO type 1	*carO*	*carO*
P0367	Cell envelope integrity protein TolA	*tolA*	-
P0478	Putative lipoprotein YiaD; OmpA-like	*yiaD*	*
P0522	Copper resistance protein B		*
P0582	Outer membrane protein W	*ompW*	*
Common in Ab1 and CRAb1 OMVs			
ID	Protein	Gene	CARD
P0008	Macrolide export protein MacA	*macA*	*
P0523	Copper resistance protein A; copper resistance system multicopper oxidase		-
P0265	OmpW family outer membrane ß-barrel protein	*omp*	*
Common in CRAb1 and CRAb2 OMVs			
ID	Protein	Gene	CARD
P0170	Multidrug resistance protein MexB; multidrug efflux RND transporter permease subunit AdeJ	*acrB*	*adeJ*
P0171	Multidrug efflux pump subunit AcrA	*acrA*	*adeI*
P0392	ß-lactamase OXA-100	*bla*	*OXA-100*
P0644	ß-lactamase OXA-97	*bla*	*OXA*-97
P0647	Metallo-ß-lactamase type 2 NDM-1	*bla*	*NDM*-1
Unique to CRAb1 OMVs			
ID	Protein	Gene	CARD
P0062	Penicillin-binding protein 1A	*mrcA*	*
Unique to CRAb2 OMVs			
ID	Protein	Gene	CARD
P0495	Colistin resistance protein EmrA; HlyD family secretion protein		*
P0532	Macrolide export protein MacA	*macA*	*

**CARD showed several genes with low identities (<60 %).*

5.3.4. OMV-associated carbapenemase activity

Previous studies have shown that different Gram-negative bacterial species, including *A. baumannii*, secrete β-lactamases in association with OMVs (34,35,65). Furthermore, López *et al.* proposed that carbapenemases, such as NDM-1, are active in the periplasm, but can be packaged into OMVs due to electrostatic interaction with the outer membrane (66). Since we identified the carbapenemases Bla$_{OXA-97}$ and Bla$_{NDM-1}$ in OMVs from the CRAb1 and CRAb2 isolates, we wanted to know whether these enzymes are active and protect the bacteria against bactericidal carbapenem activity.

To assess OMV-associated carbapenemase activity, the CarbaNP test was performed (54). This test involved the mixing of OMVs with a phenol-red solution containing a carbapenem antibiotic. Since hydrolysis of the antibiotic by carbapenemase activity will lead to acidification of the solution, a color change from red to yellow is indicative of carbapenemase activity in the OMVs. Figure 5.4 shows the color change from red to orange/yellow in samples that contained OMVs from the CRAb1 or CRAb2 isolates and imipenem, with a notable difference between the OMV-treated and the negative control samples. This result was further verified by recording the absorption spectra of the solutions, which clearly showed a shift from the red color peak (560 nm) to the yellow color peak (430 nm), with a red/yellow color ratio shift from 1.1 to 0.52 observe for the CRAb2 OMVs (Supplemental Figure S5.2).

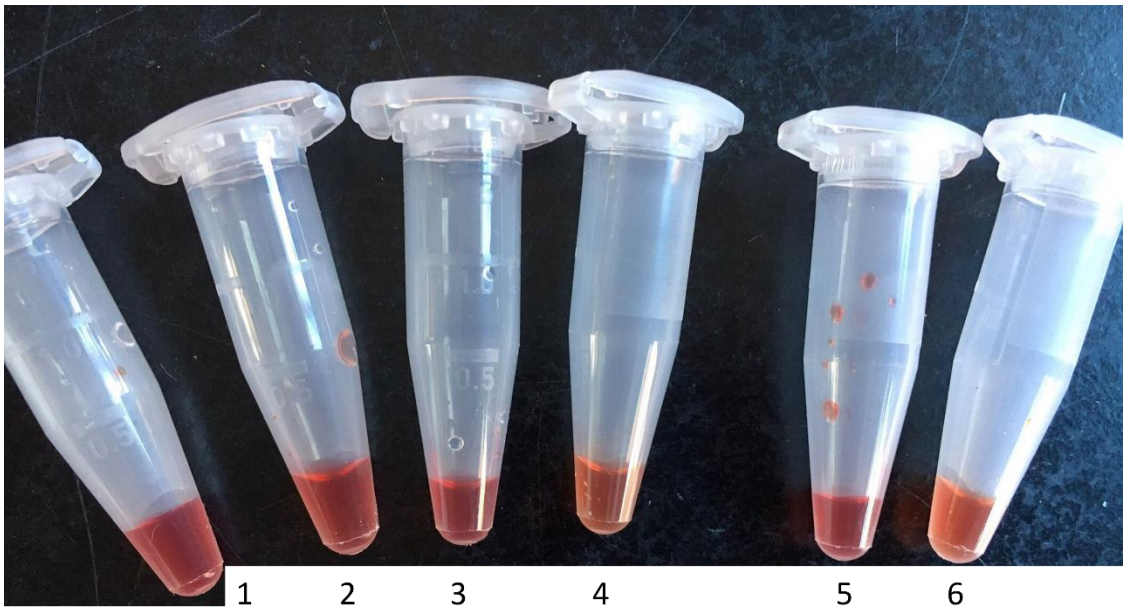


Figure 5.4. CarbaNP test with isolated OMVs from the CRAb1 and CRAb2 isolates. Tubes from left to right show: 1 - negative control, PBS; 2 - negative control, PBS with imipenem; 3 - CRAb1 OMVs, negative control without imipenem; 4 - CRAb1 OMVs with imipenem; 5 - CRAb2 OMVs, negative control without imipenem; 6 - CRAb2 OMVs with imipenem.

To test whether the OMV-associated carbapenemase activity could protect carbapenem-sensitive bacteria against such antibiotics, we applied the carbapenem inhibition method (CIM). This procedure is based on the incubation of a diffusion disk with imipenem in a solution containing OMVs or PBS, and the subsequent use of the incubated disk in a disk diffusion test on a plate with a susceptible strain. Lack of carbapenemase activity in the OMVs would not affect the antibiotic present in the disk and, accordingly, there would be a zone of growth inhibition detectable around the disk upon its usage in the disk diffusion test for carbapenem sensitivity. Conversely, OMV-associated carbapenemase activity would lead to diminished or no growth inhibition around the disk. Indeed, the results of the CIM

showed that OMVs from the CRAb1 and CRAb2 isolates were capable of efficiently inactivating imipenem within the disc, while OMVs from the Ab1 isolate did not inactivate the imipenem in the disc (Figure 5). As expected, the negative control of disk incubation without OMVs showed a clear zone of growth inhibition around the disk, while the positive controls of disk incubation with biomass of the CRAb1 or CRAb2 isolates in PBS resulted in the degradation of imipenem within the disk, as was evidenced by the absence of growth inhibition. Together, these results demonstrated the presence of active carbapenemases in the OMVs and implied that these OMVs can potentially contribute to increased bacterial tolerance to carbapenems.

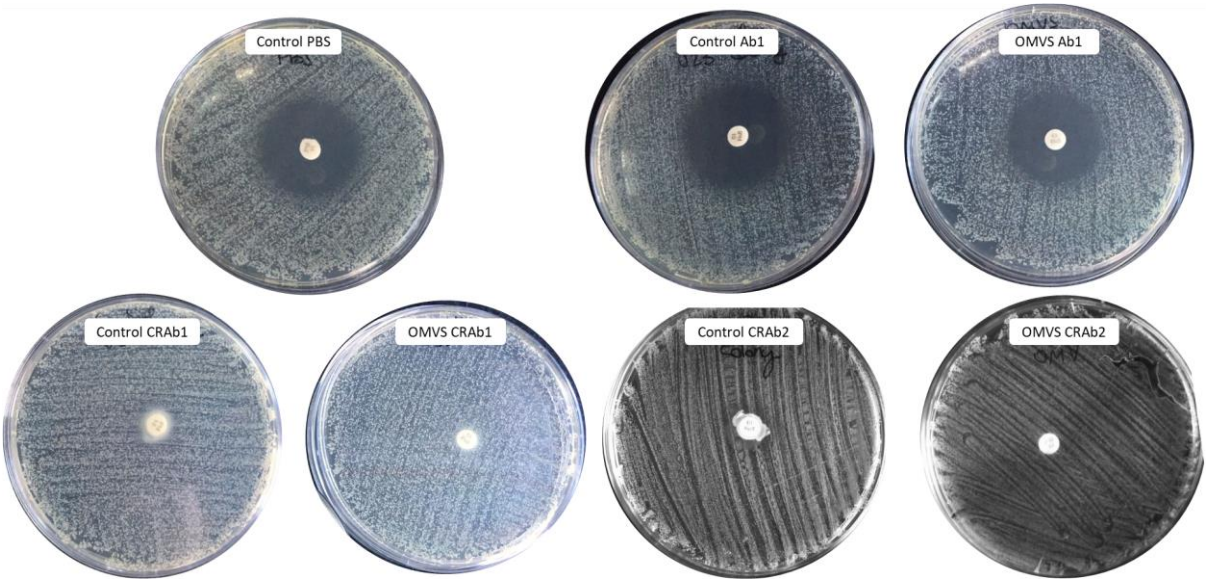


Figure 5.5. Visualization of carbapenem inactivation by OMVs from CRAb1 and CRAb2 study isolates using the CIM test. The carbapenem-susceptible strain used was *A. baumannii* 17978. Control PBS, imipenem diffusion disk incubated with PBS only. Control Ab1, CRAb1, and CRAb2, imipenem diffusion disks incubated with biomass from the respective bacterial isolate resuspended in PBS. OMVs Ab1, CRAb1, and CRAb2, imipenem diffusion disks incubated with OMVs from the respective bacterial isolate resuspended in PBS.

5.3.5. OMV-mediated protection

To assess the protection against carbapenems as conferred by the OMV-borne carbapenemases during bacterial growth, we incubated the carbapenem-susceptible strain *A. baumannii* ATCC 17978 with OMVs from the CRAb2 isolate in the presence or absence of imipenem. Ab1 OMVs were tested as well without any visible effect (data not shown). First, both OMVs (40 μg) and imipenem (0.125 μg/mL) were pre-incubated for 2 h at 37 °C before adding them to an equal volume of culture at OD600 of 0.2 and, subsequently, growth was continued for 6 h. The results are shown in Figure 5.6. During the first 30 min of the incubation, a decrease in the OD600 was observed, which was caused by the dilution of

the culture upon mixing with the mixture of OMVs and imipenem. After 2 h of incubation, the growth rates started to diverge between cultures where imipenem was or was not pre-incubated with OMVs. After 4 h of incubation, the culture with OMV-pre-treated imipenem continued to grow at the same rate as the LB control, whereas the culture with the non-pre-treated imipenem stopped growing and even showed a slightly decreased OD_{600}. This shows that the OMV-associated carbapenemase activity reduced the imipenem concentration to such an extent that the carbapenem-sensitive *A. baumannii* ATCC 17978 strain was able to grow. This observation is consistent with findings from other studies where β-lactamase-carrying OMVs from *E. coli* (34), *Staphylococcus aureus* (36), *Streptococcus pyogenes* (67), or *Stenotrophomonas maltophilia* (68) provided protection to β-lactam-susceptible strains of the same or other species. Furthermore, it was shown that OMVs of A. baumannii could protect a susceptible strain against polymyxin B (PMB) (24,37). However, in the latter case, the OMVs most likely provided protection against PMB by binding this antibiotic and limiting the free PMB level rather than degrading it.

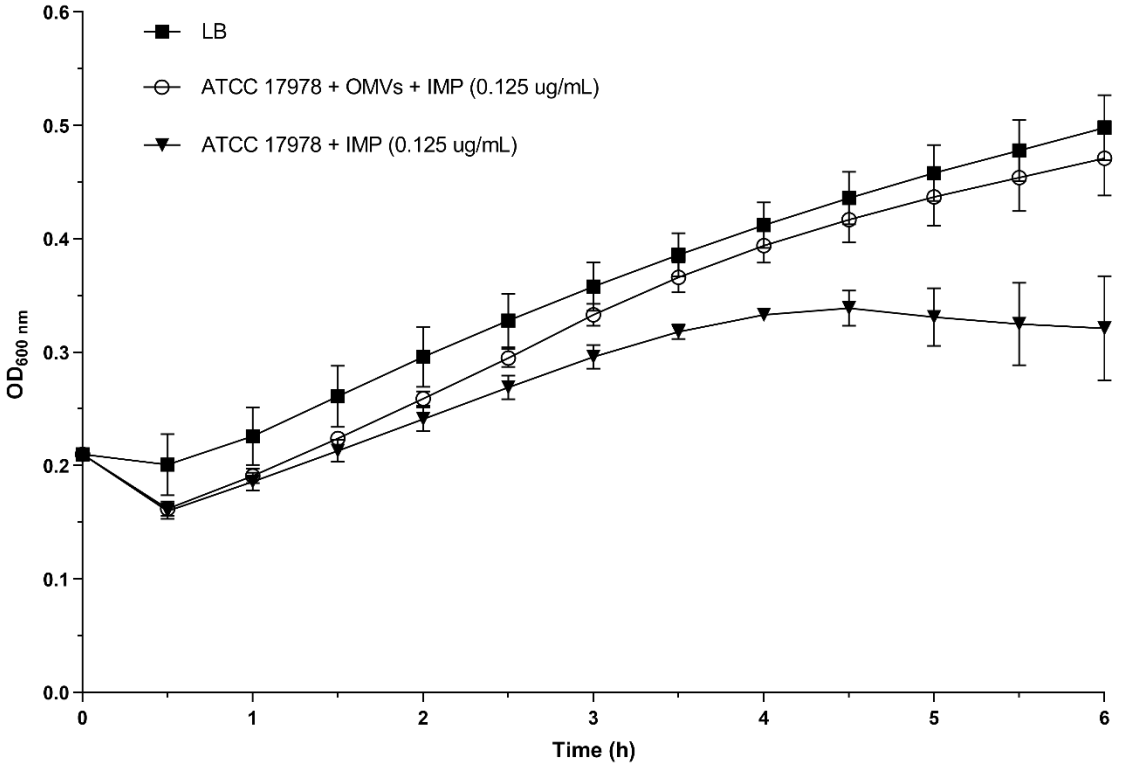


Figure 5.6. Protection of the carbapenem-sensitive *A. baumannii* ATCC 17978 strain against growth inhibition by imipenem upon imipenem pretreatment with OMVs of the CRAb2 isolate. Imipenem (0.125 μg/mL) was mixed with OMVs (40 μg) or PBS, and subsequently mixed with pre-cultured bacteria. Bacterial growth was measured by optical density readings at 600 nm for 6 h. As a control, pre-cultured bacteria without additions were mixed with LB.

Lastly, we wanted to assess the efficiency of the OMV-mediated protection against antibiotics by using different amounts of OMVs and checking for bacterial survival. For these experiments, we used two different antibiotic-susceptible species, namely *A. baumannii* ATCC 17978 and *E. coli* ATCC 25922. These bacteria were incubated with growth-inhibitory concentrations of imipenem, ampicillin or ciprofloxacin, with or without three different concentrations of OMVs from the CRAb2 isolate (10/25/50 μg/mL). Of note, the MIC of ampicillin for the *A. baumannii* ATCC 17978 strain was very high and, therefore, only the *E. coli* ATCC 25922 strain was tested for OMV-medicated protection against this antibiotic. Cultures of *A. baumannii* ATCC 17978 and *E. coli* ATCC 25922 were incubated for 24 h and growth was measured by optical density readings and CFU counting. The results, in Figure 5.7, showed that 10 μg/mL OMVs were enough to facilitate the survival of both bacterial species in the presence of imipenem, or the survival of *E. coli* ATCC 25922 in the presence of ampicillin. This result is consistent with the data of Kim and colleagues, who showed that OMVs from *E. coli* that carry β-lactamases can provide protection against ampicillin at an OMV concentration of at least 5 μg/mL (34). In the case of *A. baumannii* ATCC 17978, the bacterial growth in the presence of imipenem was fully restored at an OMV concentration of 25 μg/mL as was evident from optical density readings and CFU counting. Notably, a lower concentration of OMVs (10 μg/mL) already provided full protection against imipenem to *E. coli* ATCC 25922. This suggests that *E. coli* ATCC 25922 is more tolerant to imipenem than *A. baumannii* ATCC 17978. Similarly, when incubating the *E. coli* ATCC 25922 strain with OMVs and ampicillin, 25 μg/mL of OMVs was needed to fully restore growth to the level of the non-treated control. To verify that the observed OMV-medicated protection against the cell wall biogenesis-targeting antibiotics imipenem and ampicillin was specific, we used the fluoroquinolone antibiotic ciprofloxacin, which targets the topoisomerases II and IV in the bacterial cytoplasm. As shown in Figure 5.7, there was no bacterial growth observed in cultures treated with OMVs and ciprofloxacin, which is consistent with the observation that no ciprofloxacin-resistance-related proteins were detected in the OMVs (38,69). Furthermore, we assessed whether the OMV-mediated protection against imipenem was perhaps due to transfer of plasmid-borne resistance genes from the OMVs of the CRAb2 strain to *A. baumannii* ATCC 17978 or *E. coli* ATCC 25922, similar to what was previously reported for *E. coli* (21,29,70). However, upon plating the cultured bacteria on LB agar with imipenem, no growth of *A. baumannii* ATCC 17978 or *E. coli* ATCC 22975 was observed, showing that the OMVs mediated transient protection against imipenem.

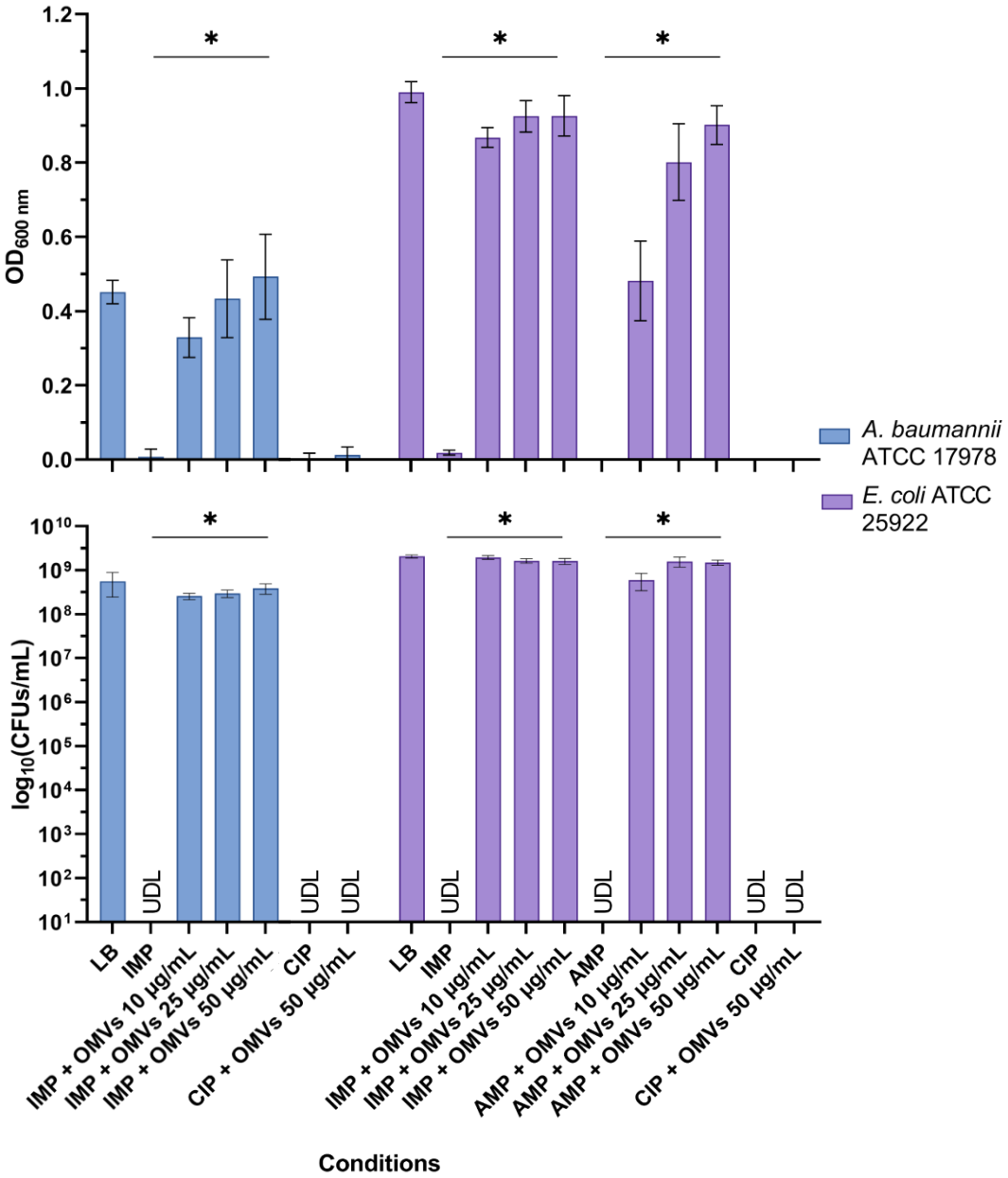


Figure 5.7. *A. baumannii* ATCC 17978 and *E. coli* ATCC 25922 survival in the presence of imipenem, ampicillin, or ciprofloxacin facilitated by OMVs from the CRAb2 isolate. Bacterial growth was assayed by optical density readings (top) and CFU counting (bottom). LB, Control without antibiotic nor OMVs; IMP, imipenem at 0.5 µg/mL; AMP, ampicillin at 256 µg/mL; CIP, Ciprofloxacin at 0.5 µg/mL. UDL, Under limit of detection. Asterisks indicate statistical significance for $p<0.05$.

5.4. CONCLUDING REMARKS

OMVs may play different roles in the life of Gram-negative bacteria. For instance, they can help in the colonization of a host (25–27), the formation of biofilms (28), virulence (31,32), the transfer of DNA or quorum-sensing molecules to neighboring cells (21,29,30), and the protection against phages (33) and antimicrobials (33,34). Here we show that two recently isolated highly drug-resistant clinical

A. baumannii strains secrete OMVs loaded with different antibiotic resistance-related proteins. Among the OMV-borne antibiotic-resistance proteins, two carbapenemases were identified, which were highly active in the degradation of imipenem and provided protection against this antibiotic to other carbapenem-sensitive bacteria. The observed protection against imipenem was transient, meaning that there was no evidence for OMV-mediated carbapenemase gene transfer, despite the fact that several previous studies implicated OMVs from *A. baumannii* in the horizontal transfer of antibiotic resistance genes (21,29). Altogether, our study highlights the possible role of OMVs in conferring protection against potent last-resort antibiotics to otherwise antibiotic-susceptible bacterial pathogens. Importantly, this mechanism of antibiotic resistance, which has been underappreciated for decades, may contribute to the emergence of *A. baumannii* and other opportunistic pathogens, lead to polymicrobial infections by dangerous pathogens, and increase the severity of bacterial infections by marginalizing the efficacy of antibiotic therapy.

5.5. REFERENCES

1. Pogue JM, Zhou Y, Kanakamedala H, Cai B. Burden of illness in carbapenem-resistant *Acinetobacter baumannii* infections in US hospitals between 2014 and 2019. BMC Infect Dis. 2022 Dec 1;22(1).
2. Alrahmany D, Omar AF, Alreesi A, Harb G, Ghazi IM. *Acinetobacter baumannii* Infection-Related Mortality in Hospitalized Patients: Risk Factors and Potential Targets for Clinical and Antimicrobial Stewardship Interventions. Antibiotics. 2022 Aug 1;11(8).
3. Vivo A, Fitzpatrick MA, Suda KJ, Jones MM, Perencevich EN, Rubin MA, *et al.* Epidemiology and outcomes associated with carbapenem-resistant *Acinetobacter baumannii* and carbapenem-resistant Pseudomonas aeruginosa: a retrospective cohort study. BMC Infect Dis. 2022 Dec 1;22(1):1–12.
4. Du X, Xu X, Yao J, Deng K, Chen S, Shen Z, *et al.* Predictors of mortality in patients infected with carbapenem-resistant *Acinetobacter baumannii*: A systematic review and meta-analysis. Am J Infect Control. 2019 Sep 1;47(9):1140–5.
5. Fitzpatrick MA, Suda KJ, Poggensee L, Vivo A, Wirth M, Wilson G, *et al.* Epidemiology and clinical outcomes associated with extensively drug-resistant (XDR) *Acinetobacter* in US Veterans' Affairs (VA) medical centers. Infect Control Hosp Epidemiol. 2021 Mar 1;42(3):305–10.
6. Patel R V., Shah JS, Revathi G, Siika W, Shah R. *Acinetobacter* infections: a retrospective study to determine in hospital mortality rate and clinical factors associated with mortality. Infection Prevention in Practice. 2019 Jun 1;1(2):100010.
7. Tacconelli E, Carrara E, Savoldi A, Harbarth S, Mendelson M, Monnet DL, *et al.* Discovery, research, and development of new antibiotics: the WHO priority list of antibiotic-resistant bacteria and tuberculosis. Lancet Infect Dis. 2018 Mar 1;18(3):318–27.
8. Marchand I, Damier-Piolle L, Courvalin P, Lambert T. Expression of the RND-Type Efflux Pump AdeABC in *Acinetobacter baumannii* Is Regulated by the AdeRS Two-Component System. Antimicrob Agents Chemother. 2004 Sep;48(9):3298.
9. Lee Y, Kim CK, Lee H, Jeong SH, Yong D, Lee K. A Novel Insertion Sequence, ISAba10, Inserted into ISAba1 Adjacent to the blaOXA-23 Gene and Disrupting the Outer Membrane Protein Gene carO in *Acinetobacter baumannii*. Antimicrob Agents Chemother. 2011 Jan;55(1):361.
10. Stéphane C, Laurent P, Thierry N, Henri D, Patrice N. Genetics and Expression of the Carbapenem-Hydrolyzing Oxacillinase Gene blaOXA-23 in *Acinetobacter baumannii*. Antimicrob Agents Chemother. 2007 Apr 1;51(4):1530–3.
11. Beig M, Badmasti F, Solgi H, Nikbin VS, Sholeh M. Carbapenemase genes distribution in clonal lineages of *Acinetobacter baumannii*: a comprehensive study on plasmids and chromosomes. Front Cell Infect Microbiol. 2023;13.
12. He T, Wang R, Liu D, Walsh TR, Zhang R, Lv Y, *et al.* Emergence of plasmid-mediated high-level tigecycline resistance genes in animals and humans. Nat Microbiol. 2019;4(9):1450–6.
13. Burcu I, Yohei D, A BR, L PD. New Treatment Options against Carbapenem-Resistant *Acinetobacter baumannii* Infections. Antimicrob Agents Chemother. 2018 Dec 21;63(1):10.1128/aac.01110-18.
14. Yang JL, Yang CJ, Chuang YC, Sheng WH, Chen YC, Chang SC. Minocycline Susceptibility and tetB Gene in Carbapenem-Resistant *Acinetobacter baumannii* in Taiwan. Infect Drug Resist. 2022;15:2401–8.
15. M LD, Shazad M, Marina W, Neil W. In Vitro Activity of Eravacycline against Carbapenem-Resistant Enterobacteriaceae and *Acinetobacter baumannii*. Antimicrob Agents Chemother. 2016 May 23;60(6):3840–4.

16. R ES, M HA, Hongyu J, B HC, M HK, R MJ, *et al.* Informing Antibiotic Treatment Decisions: Evaluating Rapid Molecular Diagnostics To Identify Susceptibility and Resistance to Carbapenems against *Acinetobacter* spp. in PRIMERS III. J Clin Microbiol. 2016 Dec 28;55(1):134–44.
17. Chen C, Cui CY, Yu JJ, He Q, Wu XT, He YZ, *et al.* Genetic diversity and characteristics of high-level tigecycline resistance Tet(X) in *Acinetobacter* species. Genome Med. 2020;12(1):111.
18. Yang W, Moore IF, Koteva KP, Bareich DC, Hughes DW, Wright GD. TetX Is a Flavin-dependent Monooxygenase Conferring Resistance to Tetracycline Antibiotics*. Journal of Biological Chemistry. 2004;279(50):52346–52.
19. Li ZT, Zhang RL, Bi XG, Xu L, Fan M, Xie D, *et al.* Outer membrane vesicles isolated from two clinical *Acinetobacter baumannii* strains exhibit different toxicity and proteome characteristics. Microb Pathog. 2015 Apr 1;81:46–52.
20. Kwon SO, Gho YS, Lee JC, Kim S il. Proteome analysis of outer membrane vesicles from a clinical *Acinetobacter baumannii* isolate. FEMS Microbiol Lett. 2009 Aug;297(2):150–6.
21. Rumbo C, Fernández-Moreira E, Merino M, Poza M, Mendez JA, Soares NC, *et al.* Horizontal transfer of the OXA-24 carbapenemase gene via outer membrane vesicles: A new mechanism of dissemination of carbapenem resistance genes in *Acinetobacter baumannii*. Antimicrob Agents Chemother. 2011 Jul;55(7):3084–90.
22. Kesavan D, Vasudevan A, Wu L, Chen J, Su Z, Wang S, *et al.* Integrative analysis of outer membrane vesicles proteomics and whole-cell transcriptome analysis of eravacycline induced *Acinetobacter baumannii* strains. BMC Microbiol. 2020 Feb 11;20(1).
23. Dhurve G, Madikonda AK, Jagannadham MV, Siddavattam D. Outer Membrane Vesicles of *Acinetobacter baumannii* DS002 Are Selectively Enriched with TonB-Dependent Transporters and Play a Key Role in Iron Acquisition. Microbiol Spectr. 2022 Apr 27;10(2).
24. Agarwal B, Karthikeyan R, Gayathri P, RameshBabu B, Ahmed G, Jagannadham M v. Studies on the mechanism of multidrug resistance of *Acinetobacter baumannii* by proteomic analysis of the outer membrane vesicles of the bacterium. J Proteins Proteom. 2019 Mar;10(1):1–15.
25. Cañas MA, Fábrega MJ, Giménez R, Badia J, Baldomà L. Outer Membrane Vesicles From Probiotic and Commensal *Escherichia coli* Activate NOD1-Mediated Immune Responses in Intestinal Epithelial Cells. Front Microbiol. 2018;9.
26. Bielaszewska M, Marejková M, Bauwens A, Kunsmann-Prokscha L, Mellmann A, Karch H. Enterohemorrhagic *Escherichia coli* O157 outer membrane vesicles induce interleukin 8 production in human intestinal epithelial cells by signaling via Toll-like receptors TLR4 and TLR5 and activation of the nuclear factor NF-κB. International Journal of Medical Microbiology. 2018;308(7):882–9.
27. Tiku V, Kofoed EM, Yan D, Kang J, Xu M, Reichelt M, *et al.* Outer membrane vesicles containing OmpA induce mitochondrial fragmentation to promote pathogenesis of *Acinetobacter baumannii*. Sci Rep. 2021 Dec 1;11(1).
28. Thomas B, Stefanie S, Jana S, Martin von B, Frank S, Y WL, *et al.* Membrane Vesicle Formation as a Multiple-Stress Response Mechanism Enhances Pseudomonas putida DOT-T1E Cell Surface Hydrophobicity and Biofilm Formation. Appl Environ Microbiol. 2012 Sep 1;78(17):6217–24.
29. Chatterjee S, Mondal A, Mitra S, Basu S. *Acinetobacter baumannii* transfers the blaNDM-1 gene via outer membrane vesicles. Journal of Antimicrobial Chemotherapy. 2017 Aug 1;72(8):2201–7.
30. Mashburn LM, Whiteley M. Membrane vesicles traffic signals and facilitate group activities in a prokaryote. Nature. 2005;437(7057):422–5.

31. Marines du TE, Yanyan F, Demi van der H, Claudia H, Marina LÁ, M ML, *et al.* Coating and Corruption of Human Neutrophils by Bacterial Outer Membrane Vesicles. Microbiol Spectr. 2022 Aug 24;10(5):e00753-22.
32. Gabarrini G, Palma Medina LM, Stobernack T, Prins RC, du Teil Espina M, Kuipers J, *et al.* There's no place like OM: Vesicular sorting and secretion of the peptidylarginine deiminase of *Porphyromonas gingivalis*. Virulence. 2018 Dec 31;9(1):459–67.
33. Manning AJ, Kuehn MJ. Contribution of bacterial outer membrane vesicles to innate bacterial defense. BMC Microbiol. 2011;11.
34. Kim SW, Park S Bin, Im SP, Lee JS, Jung JW, Gong TW, *et al.* Outer membrane vesicles from β-lactam-resistant *Escherichia coli* enable the survival of β-lactam-susceptible *E. coli* in the presence of β-lactam antibiotics. Sci Rep. 2018 Dec 1;8(1).
35. González LJ, Bahr G, Nakashige TG, Nolan EM, Bonomo RA, Vila AJ. Membrane anchoring stabilizes and favors secretion of New Delhi metallo-β-lactamase. Nat Chem Biol. 2016 Jul 1;12(7):516–22.
36. Lee J, Lee EY, Kim SH, Kim DK, Park KS, Kim KP, *et al.* Staphylococcus aureus extracellular vesicles carry biologically active β-lactamase. Antimicrob Agents Chemother. 2013 Jun;57(6):2589–95.
37. Park J, Kim M, Shin B, Kang M, Yang J, Lee TK, *et al.* A novel decoy strategy for polymyxin resistance in *Acinetobacter baumannii*. Elife. 2021 Jun 1;10.
38. Marchant P, Carreño A, Vivanco E, Silva A, Nevermann J, Otero C, *et al.* "One for All": Functional Transfer of OMV-Mediated Polymyxin B Resistance From *Salmonella enterica* sv. Typhi ΔtolR and ΔdegS to Susceptible Bacteria. Front Microbiol. 2021 May 5;12.
39. Talsma DT, Monteiro R, Flores-Vallejo R del C, Heuvelmans M, Le TN, Hendrickx APA, *et al.* Nosocomial transmission of tet(x3), blaNDM-1, and blaOXA-97-carrying *Acinetobacter baumannii* conferring resistance to eravacycline and omadacycline, the Netherlands, March-August 2021. Eurosurveillance. 2024 Apr;
40. Morton RE, Evans TA. Modification of the bicinchoninic acid protein assay to eliminate lipid interference in determining lipoprotein protein content. Anal Biochem. 1992 Aug 1;204(2):332–4.
41. Melo LDR, Sillankorva S, Ackermann HW, Kropinski AM, Azeredo J, Cerca N. Isolation and characterization of a new *Staphylococcus epidermidis* broad-spectrum bacteriophage. Journal of General Virology. 2014 Feb;95(PART 2):506–15.
42. Bonn F, Bartel J, Büttner K, Hecker M, Otto A, Becher D. Picking Vanished Proteins from the Void: How to Collect and Ship/Share Extremely Dilute Proteins in a Reproducible and Highly Efficient Manner. Anal Chem. 2014 Aug 5;86(15):7421–7.
43. Cox J, Mann M. MaxQuant enables high peptide identification rates, individualized p.p.b.-range mass accuracies and proteome-wide protein quantification. Nat Biotechnol. 2008;26(12):1367–72.
44. Rgen Cox J, Hein MY, Luber CA, Paron I, Nagaraj N, Mann M. Accurate Proteome-wide Label-free Quantification by Delayed Normalization and Maximal Peptide Ratio Extraction, Termed MaxLFQ* □ S Technological Innovation and Resources. Molecular & Cellular Proteomics. 2014;13:2513–26.
45. Schwanhäusser B, Busse D, Li N, Dittmar G, Schuchhardt J, Wolf J, *et al.* Global quantification of mammalian gene expression control. Nature. 2011;473(7347):337–42.
46. Consortium TU. UniProt: the Universal Protein Knowledgebase in 2023. Nucleic Acids Res. 2023 Jan 6;51(D1):D523–31.

47. Huerta-Cepas J, Szklarczyk D, Heller D, Hernández-Plaza A, Forslund SK, Cook H, *et al.* eggNOG 5.0: a hierarchical, functionally and phylogenetically annotated orthology resource based on 5090 organisms and 2502 viruses. Nucleic Acids Res. 2019 Jan 8;47(D1):D309–14.
48. Sequeira JC, Rocha M, Alves MM, Salvador AF. UPIMAPI, reCOGnizer and KEGGCharter: Bioinformatics tools for functional annotation and visualization of (meta)-omics datasets. Comput Struct Biotechnol J. 2022 Jan 1;20:1798–810.
49. Yu NY, Wagner JR, Laird MR, Melli G, Rey S, Lo R, *et al.* PSORTb 3.0: improved protein subcellular localization prediction with refined localization subcategories and predictive capabilities for all prokaryotes. Bioinformatics. 2010 Jul 1;26(13):1608–15.
50. Heberle H, Meirelles VG, da Silva FR, Telles GP, Minghim R. InteractiVenn: A web-based tool for the analysis of sets through Venn diagrams. BMC Bioinformatics. 2015 May 22 [cited 2023 Mar 10];16(1):1–7.
51. Jia B, Raphenya AR, Alcock B, Waglechner N, Guo P, Tsang KK, *et al.* CARD 2017: expansion and model-centric curation of the comprehensive antibiotic resistance database. Nucleic Acids Res. 2017 Jan 1 [cited 2023 Mar 10];45(D1):D566–73.
52. Garg A, Gupta D. VirulentPred: A SVM based prediction method for virulent proteins in bacterial pathogens. BMC Bioinformatics. 2008 Jan 28;9(1):1–12.
53. Gupta A, Kapil R, Dhakan DB, Sharma VK. MP3: A Software Tool for the Prediction of Pathogenic Proteins in Genomic and Metagenomic Data. PLoS One. 2014 Apr 15 [cited 2023 Mar 10];9(4):e93907.
54. Pasteran F, Tijet N, Melano RG, Corso A. Simplified protocol for Carba NP test for enhanced detection of carbapenemase producers directly from bacterial cultures. J Clin Microbiol. 2015 Dec 1;53(12):3908–11.
55. Van Der Zwaluw K, De Haan A, Pluister GN, Bootsma HJ, De Neeling AJ, Schouls LM. The Carbapenem Inactivation Method (CIM), a simple and low-cost alternative for the carba NP test to assess phenotypic carbapenemase activity in Gram-negative rods. PLoS One. 2015 Mar 23;10(3).
56. Deutsch EW, Bandeira N, Perez-Riverol Y, Sharma V, Carver JJ, Mendoza L, *et al.* The ProteomeXchange consortium at 10 years: 2023 update. Nucleic Acids Res. 2023 Jan 6 [cited 2024 Apr 29];51(D1):D1539–48.
57. Yun SH, Park EC, Lee SY, Lee H, Choi CW, Yi YS, *et al.* Antibiotic treatment modulates protein components of cytotoxic outer membrane vesicles of multidrug-resistant clinical strain, *Acinetobacter baumannii* DU202. Clin Proteomics. 2018 Aug 31;15(1).
58. Zapun A, Contreras-Martel C, Vernet T. Penicillin-binding proteins and β-lactam resistance. Vol. 32, FEMS Microbiology Reviews. 2008. p. 361–85.
59. Laurence DP, Sophie M, Sylvie B, Thierry L, Patrice C. AdeIJK, a Resistance-Nodulation-Cell Division Pump Effluxing Multiple Antibiotics in *Acinetobacter baumannii*. Antimicrob Agents Chemother. 2008 Feb 1;52(2):557–62.
60. Siroy A, Cosette P, Seyer D, Lemaître-Guillier C, Vallenet D, Van Dorsselaer A, *et al.* Global Comparison of the Membrane Subproteomes between a Multidrug-Resistant *Acinetobacter baumannii* Strain and a Reference Strain. J Proteome Res. 2006 Dec 1;5(12):3385–98.
61. Roterman I, Stapor K, Fabian P, Konieczny L. The functional significance of hydrophobic residue distribution in bacterial beta-barrel transmembrane proteins. Membranes (Basel). 2021 Aug 1;11(8).
62. Völlmecke C, Drees SL, Reimann J, Albers SV, Lübben M. The ATPases CopA and CopB both contribute to copper resistance of the thermoacidophilic archaeon *Sulfolobus solfataricus*. Microbiology (United Kingdom). 2012 Jun 1;158(6):1622–33.

63. Tilley D, Law R, Warren S, Samis JA, Kumar A. CpaA a novel protease from *Acinetobacter baumannii* clinical isolates deregulates blood coagulation. FEMS Microbiol Lett. 2014;356(1):53–61.
64. Nies DH. The Cobalt, Zinc, and Cadmium Efflux System CzcABC from *Alcaligenes eutrophus* Functions as a Cation-Proton Antiporter in *Escherichia coli*. Vol. 177, Journal of Bacteriology. 1995.
65. Ciofu O, Beveridge TJ, Kadurugamuwa J, Walther-Rasmussen J, Høiby N. Chromosomal beta-lactamase is packaged into membrane vesicles and secreted from *Pseudomonas aeruginosa*. J Antimicrob Chemother. 2000 [cited 2023 Mar 27];45(1):9–13.
66. López C, Prunotto A, Bahr G, Bonomo RA, González LJ, Peraro MD, *et al.* Specific Protein-Membrane Interactions Promote Packaging of Metallo-β-Lactamases into Outer Membrane Vesicles. Antimicrob Agents Chemother. 2021 Oct 1;65(10).
67. Bielaszewska M, Daniel O, Nyč O, Mellmann A. In vivo secretion of β-lactamase-carrying outer membrane vesicles as a mechanism of β-lactam therapy failure. Membranes (Basel). 2021 Nov 1;11(11).
68. Devos S, Stremersch S, Raemdonck K, Braeckmans K, Devreese B. Intra-and interspecies effects of outer membrane vesicles from *Stenotrophomonas maltophilia* on β-lactam resistance. Antimicrob Agents Chemother. 2016 Apr 1;60(4):2516–8.
69. Kulkarni HM, Nagaraj R, Jagannadham M V. Protective role of *E. coli* outer membrane vesicles against antibiotics. Microbiol Res. 2015 Dec 1;181:1–7.
70. Yaron S, Kolling GL, Simon L, Matthews KR. Vesicle-Mediated Transfer of Virulence Genes from *Escherichia coli* O157:H7 to Other Enteric Bacteria. Vol. 66, Applied and Environmental Microbiology. 2000.

5.6. SUPPLEMENTAL MATERIAL

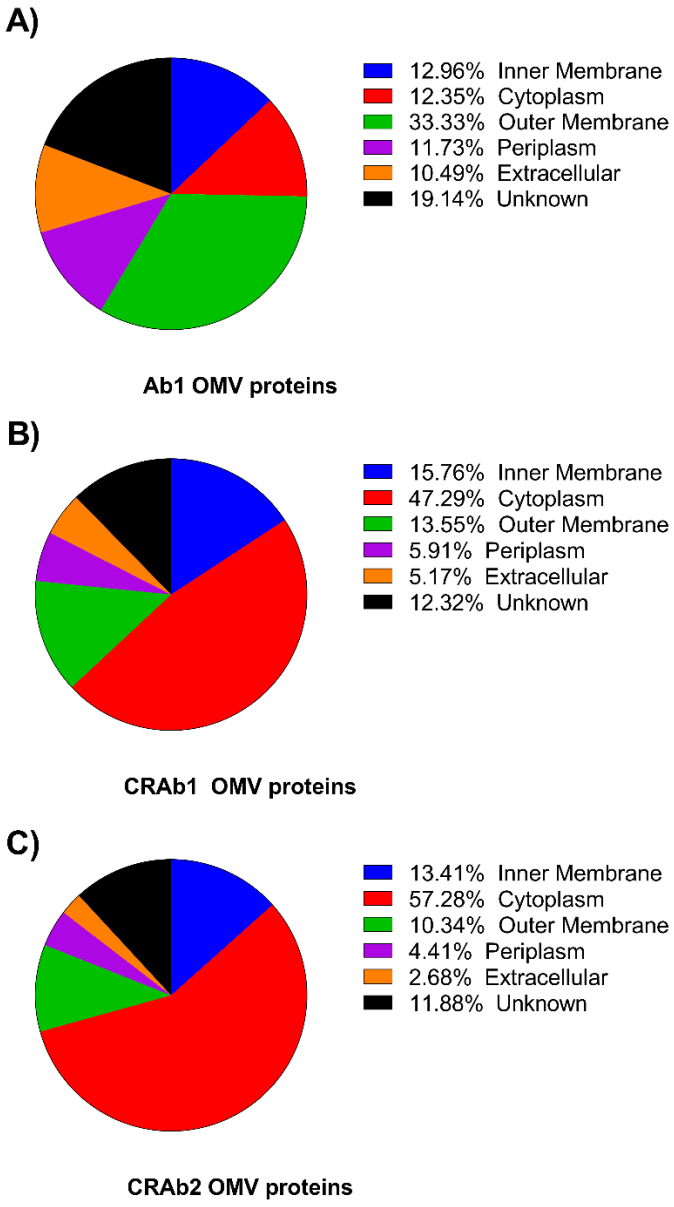


Figure S5.1. Predicted subcellular localization of identified OMV-associated proteins from the Ab1, CRAb1, CRAb2 isolates. Percentages are related to the number of proteins in each localization.

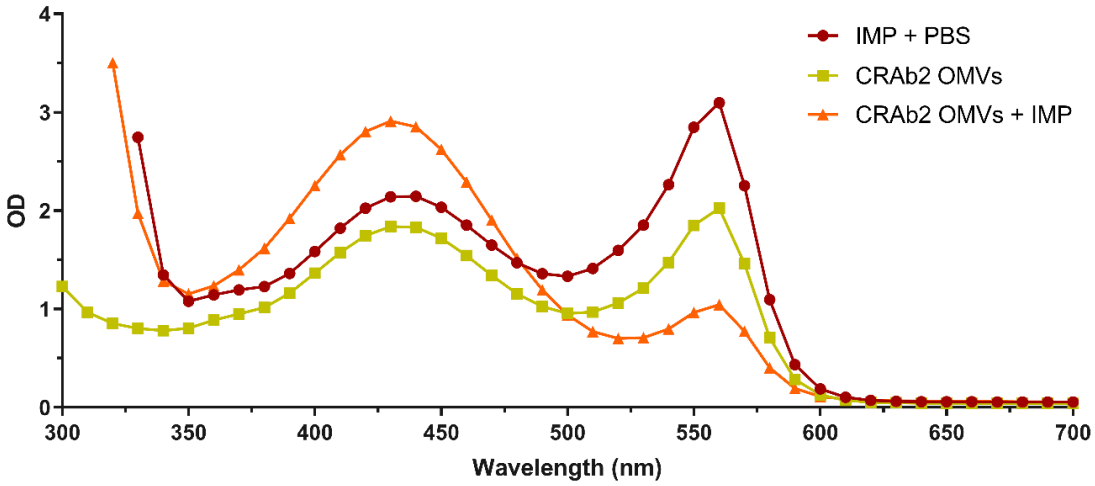


Figure S5.2. Spectral scanning upon CarbNP tests with OMVs from the CRAb2 isolate. OMVs were mixed with IMP or PBS. Spectral scans ranging from 300 nm to 700 nm were recorded using a Biotek microplate reader. Incubation of imipenem with the OMVs results in a shift from the red color peak (560 nm) to the yellow color peak (430 nm), which is indicative of imipenem hydrolysis and acidification of the solution. IMP, imipenem.

Chapter 6

Genomic and proteomic analyses of mobile genetic elements from recent outbreak-associated carbapenem- and tetracycline-resistant *A. baumannii* clinical isolates

- **R. Monteiro**, S. Piersma, S. Maaß, D. Becher, J. Azeredo, and J.M. van Dijl

Abstract

Acinetobacter baumannii, a pathogen that causes difficult-to-eradicate outbreaks in hospitals, was recently considered a top priority bacterium for the development of new therapies due to the emergence of multidrug-resistant variants, like the Carbapenem-Resistant *A. baumannii* (CRAb). In a recent study, three new clinical *A. baumannii* isolates from a hospital outbreak in the Netherlands, denoted Ab1, CRAb1, and CRAb2, were characterized. Two of the three isolates, CRAb1 and CRAb2, revealed high levels of antibiotic resistance, in particular against carbapenems and the last generation of tetracyclines. The emergence of antibiotic resistance, which is a highly worrisome phenomenon, is commonly associated with horizontal gene transfer (HGT) through mobile genetic elements such as plasmids and prophages, as well as outer membrane vesicles (OMVs). OMVs in particular, are vesicular structures released by Gram-negative bacteria that can facilitate host infection, attachment to surfaces, and protection against stresses and antibiotics. Importantly, they also carry virulence determinants into the bacterial environment and to other cells. To better understand the various roles of these elements, extensive genomic and proteomic analyses were performed. The three investigated isolates revealed a significant number of mobile genetic elements with potential for horizontal gene transfer, including several intact and defective prophages as well as plasmids. Prophages were shown to be inducible, as different phage structures could be observed by transmission electron microscopy. Annotation of both prophages and plasmids revealed genes that are potentially related to virulence and fitness. The proteome of OMVs isolated from two different media was also analyzed, revealing several virulence-related and antibiotic-resistant proteins. Inspection of the OMV proteomes of the bacteria cultured in the cell culture medium DMEM revealed no absolute differences between isolates. Conversely, the 'LB-OMVs' showed significantly different proteomic profiles, specifically in the abundance of particular proteins between the OMVs of the different isolates. Importantly, the CRAb2 isolate was shown to harbor the most mobile genetic elements and to present the 'most antibiotic-resistant' OMV proteome profile. On the other hand, CRAb1 OMVs presented the 'most virulent' proteome profile. Altogether, this study shows that the combined portfolio of prophages, plasmids and OMVs has greatly contributed to the emergence of highly virulent antibiotic-resistant *A. baumannii* variants.

Keywords: *A. baumannii*; MGE; OMVs; Prophages; Plasmids; Virulence

6.1. INTRODUCTION

Acinetobacter baumannii is considered a critical target pathogen for the development of new antimicrobial therapies, because of its high resistance against last-resort antibiotics including carbapenems. In addition, this Gram-negative bacterium is highly adaptable and thrives in clinical settings. Together, these features make *A. baumannii* a common cause of readily transmissible nosocomial infections, which may lead to outbreaks that are difficult to control.

A. baumannii employs different mechanisms to colonize and invade its human host. These include biofilm formation and effective secretion systems for virulence factors that facilitate bacterial adherence, host cell colonization, tissue invasion, serum resistance, and persistence. In addition, they increase the resistance to antimicrobial treatments (1). For instance, an outer membrane protein, such as OmpA, plays a critical role in the virulence of *A. baumannii* by mediating attachment to host cells and inducing host cell apoptosis (2).

A major feature of *A. baumannii* species is its resistance to antibiotic treatments. These resistance mechanisms are both intrinsic and acquired from the environment through horizontal gene transfer (HGT). Together, they have allowed the emergence of multidrug-resistant variants. The resistance to different antibiotic classes, including beta-lactams, fluoroquinolones, aminoglycosides, and colistin, is facilitated by efflux pumps, modification of antibiotic target sites, and the enzymatic degradation of antibiotics (3). The HGT of genes that code for these resistance mechanisms and virulence factors is mediated by different vectors, including prophages, plasmids, and outer membrane vesicles (OMVs) (4,5).

OMVs are vesicles produced by Gram-negative bacteria through extrusion from the outer membrane and subsequent release into the environment together with a cargo of DNA, RNA and proteins (6). These vesicles have attracted attention due to their roles in bacterial pathogenesis and their potential usage as effective vaccines for immunization against problematic pathogens (7). Furthermore, recent studies have pointed out that the cargo of OMVs may be absorbed by neighboring cells, thereby promoting the spread of antibiotic resistance and virulence within bacterial populations (8–10).

In the course of a recent hospital outbreak in the Netherlands, which started with a carbapenem-susceptible *A. baumannii* in the index patient (denoted Ab1), two distinct carbapenem- and tetracycline-resistant *A. baumannii* (CRAb) strains (denoted CRAb1 and CRAb2) were isolated. The resistance of these CRAb isolates to tetracyclines and beta-lactams was associated with the presence of a 260-kb plasmid (pCRAb1) carrying a broad set of resistance genes. The present study was aimed at

understanding the interplay between virulence factors, resistance mechanisms, and mobile genetic elements in the pathogenicity of these clinical *A. baumannii* isolates using genomic and proteomic approaches.

6.2. MATERIAL AND METHODS

6.2.1. Bacterial strains

The three *A. baumannii* isolates used for this study were denoted Ab1 (bla_{ADC-79}, $bla_{OXA-100}$), CRAb1 (bla_{ADC-79}, $bla_{OXA-100}$, bla_{NDM-1}, bla_{OXA-97}, *tet(x3)*, *sul2*, *ant(2")-Ia*, *aph(3")-Ib*, *aph(3')-Ia*, *aph(6)-Id*, *ant(3")-IIa*, *mph(E)*, *msr(E)*), and CRAb2 (bla_{ADC-79}, $bla_{OXA-100}$, bla_{NDM-1}, bla_{OXA-97}, *tet(x3)*, *sul2*, *abaF*, *ant(2")-Ia*, *aph(3")-Ib*, *aph(3')-Ia*, *aph(6)-Id*, *ant(3")-IIa*, *mph(E)*, *msr(E)*). The genome sequences of these isolates have been submitted to the NCBI GenBank database and are available under the BioProject number PRJNA1011532. The isolates were routinely grown on Lysogeny Broth (LB, BD Difco™) or Dulbecco's Modified Eagle Medium (DMEM High Glucose, GlutaMAX™ supplement, Gibco) at 37 °C. Liquid cultures were shaken at 120 rpm using a Multitron Triple Incubator Shaker (Infors HT). LB plates contained 1.2% agar (BD Difco™). For prophage induction experiments, 5 mL of overnight culture was diluted 1:100 into 25 mL of fresh LB medium and incubation was continued with shaking until cells reached an optical density at 600 nm (OD_{600}) of 0.3-0.4. At this time, cultures were divided into two flasks with 10 mL of cells, and mitomycin C (MMC, ThermoFisher) was added at 3 µg/mL to one of the flasks, followed by continued incubation for 5 h. The cultures were then centrifuged to remove bacterial cells, filtered using a 0.22 µm polyethersulfone (PES) filter, and stored at 4 °C.

6.2.2. OMV purification

For each *A. baumannii* isolate, OMVs were produced by incubating the inoculum, made from a 1:100 dilution of an overnight pre-inoculum, in 250 mL of LB for 24 h at 37 °C and 120 rpm. Next, the cells were removed by centrifugation (Avanti J-26S XP, Beckman Coulter Inc., Brea, California, USA) at 8,000 × g for 20 min, at 4 °C, and the supernatant containing OMVs was filtered through a 0.22 µm PES filter and stored at 4 °C. The OMV fraction was isolated by ultracentrifugation using an OptimaTM XL-80K ultracentrifuge (Beckman Coulter Inc., Brea, California, USA) at 30,000 rpm (150,000 × g) for 4 h, at 4 °C. The supernatant was discarded, and the pelleted bacteria were washed three times by resuspension in phosphate-buffered saline (PBS) and ultracentrifugation at 100,000 × g for 3 h at 4 °C. OMVs were resuspended in 300-500 µL of PBS for further analyses. Quantification of

the OMVs was performed using the Pierce™ BCA Protein Assay Kit (ThermoFisher) after OMVs solubilization with 2% SDS (11).

6.2.3. Transmission electron microscopy (TEM)

For visualization of induced phages and OMVs by TEM, negative staining was performed using a solution of 5% uranyl acetate, as previously described (12). Induced phages were collected by centrifugation (18,500 × *g*, 4°C, 60 min). The sedimented particles were washed twice with ddH_2O and centrifuged again. A drop of OMVs or washed phages was deposited onto a copper grid with carbon-coated Formvar films. After 15 min of incubation, the grids were rinsed with ultrapure water, stained with uranyl acetate, and washed again before visualization using a Talos F200i electron microscope at 80 kV.

6.2.4. Dynamic light scattering (DLS)

For dynamic light scattering (DLS) analysis, a Zetasizer Nano ZS (Malvern Panalytical Ltd, UK) was used. Forty microliters of PBS-diluted OMVs containing 100-200 µg/mL was subjected to DLS in micro cuvettes (part no. ZEN0040, Malvern Panalytical). The refractory index (RI) of the material was set to 1.45 with an absorption of 0.001 and the dispersant RI was set to 1.335 with a viscosity of 0.8882. The temperature was set to 25 °C. Measurements were performed in triplicate, with an equilibration time of 90 s.

6.2.5. LDS-PAGE

OMV samples (20 µg) were precipitated with TCA (trichloroacetic acid) at a final concentration of 10% by incubation for 18 h at 4 °C. Subsequently, the precipitated proteins were pelleted at 18,500 × *g*, at 4 °C for 20 min, washed with 1 mL of ice-cold acetone, centrifuged for 10 min, and dried by incubating the pellets at 60 °C for 10 min. The OMV proteins were then resuspended in a gel loading buffer containing NuPAGE 10× sample reducing agent and 4× lithium dodecyl sulfate (LDS) sample buffer (Invitrogen, USA), boiled at 98 °C for 10 min, and separated on 10% NuPAGE gels (Invitrogen, USA) by LDS polyacrylamide gel electrophoresis (PAGE). After electrophoresis proteins were stained with SimplyBlue SafeStain (Life Technologies, CA) and analyzed.

6.2.6. LC-MS/MS sample preparation

OMV preparation for mass spectrometry (MS) was performed by TCA precipitation of 20 µg of each sample. Subsequently, precipitated samples were separated for 1 cm by LDS-PAGE and stained using SimplyBlue SafeStain (Life Technologies, CA). Gel lanes were excised in one piece and subjected

to trypsin digestion as described previously (13). For the subsequent liquid chromatography (LC) MS/MS measurements, the digests were separated by reversed phase column chromatography using an EASY nLC 1000 (Thermo Fisher Scientific) with self-packed columns (OD 360 µm, ID 100 µm, length 20 cm) filled with 3 µm diameter C18 particles (Dr. Maisch, Ammerbuch-Entringen, Germany). Following loading/desalting in 0.1 % acetic acid in water, the peptides were separated by applying a binary non-linear gradient from 1-99 % acetonitrile in 0.1 % acetic acid over 162 min. The LC was coupled online to a LTQ Orbitrap Velos mass spectrometer (Thermo Fisher, Bremen, Germany) with a spray voltage of 2.6 kV. After a survey scan in the Orbitrap (r = 30,000), MS/MS data were recorded for the twenty most intensive precursor ions in the linear ion trap. Singly charged ions were not considered for MS/MS analysis. The lock mass option was enabled throughout all analysis. After mass spectrometric measurement, database searches were performed using MaxQuant (version 2.0.3.0). To this end, we used separate databases of the *A. baumannii* Ab1, CRAb1, and CRAb2 isolates (3752, 3922, and 4119 entries, respectively) and a combined single database (12,061 entries). The databases were obtained from a Prokka v1.14.6 annotation (14). For strain CRAb1 also protein sequences encoded by the plasmid (268 entries) were used for spectrum identification. Common laboratory contaminants and reversed sequences were included by MaxQuant. Search parameters were set as follows: Trypsin/P specific digestion with up to two missed cleavages, methionine oxidation, and N-terminal acetylation as variable modification, match between runs with default parameters enabled. The FDRs (false discovery rates) of protein and PSM (peptide spectrum match) levels were set to 0.01. Two identified unique peptides were required for protein identification. MaxLFQ (15) and iBAQ (16) values were calculated in MaxQuant with default settings as a proxy for protein abundance.

6.2.7. Proteome data analysis

Functions of detected proteins were assessed using BLASTp and manually curated using UniProt webserver (17). The COG categories were attributed using eggNOG (ver.6.0.0) (18) and reCOGnizer (ver.1.10.0) (19). The localization of each outer membrane vesicle protein was predicted using PSORTb (ver.3.0) (20) and the literature. For protein comparison across the isolates, VENN diagrams were drawn using InteractiVENN (21). Antibiotic resistance proteins were predicted using CARD (22). Virulence genes were determined by complementing the afore-mentioned tools with the VirulentPred algorithm (ver.1.0) (23), which predicts bacterial virulence factors based on their amino acid composition, the bilayer cascade Support Vector Machine module (SVM), and the Predict Pathogenic Proteins in Metagenomic data sets (MP3) website (24). Heatmap plots were generated using ClustVis (25). Prophage regions were detected using the PHASTER web tool (26).

6.2.8. Statistical analysis

Statistical calculations were performed using GraphPad software, version 7.0. All data are expressed as means ± standard error of the mean (SEM) and statistical differences were calculated by two-way ANOVA and Tukey's multiple comparison tests.

6.2.9. Data Availability

The MS proteomics data discussed in this publication have been deposited to the ProteomeXchange Consortium via the PRIDE partner repository (27) with the dataset identifier PXD051698 (Reviewer account details: Username, reviewer_pxd051698@ebi.ac.uk; Password, AYb7LRlF). Supplemental Material Tables can be accessed at (LINK).

6.3. RESULTS AND DISCUSSION

Three recently collected *A. baumannii* isolates denoted Ab1, CRAb1, and CRAb2 were used in this study (28). Since these isolates presented various interesting features, including a large transmissible plasmid and prophages, we decided to analyze these different elements, as well as their OMVs to understand what roles each of them may have in virulence and antibiotic resistance. Table 6.1 presents an overview of the mobile genetic elements in the three isolates.

Table 6.1. Mobile genetic elements carried by the *A. baumannii* isolates Ab1, CRAb1, and CRAb2, and their respective sizes. Prophage regions were detected using the PHASTER tool (26)

Isolate	Mobile genetic element	Size (bp)
Ab1	Prophage intact 1	32,612
	Prophage incomplete 1	27,108
	Prophage incomplete 2	13,048
	Prophage intact 2	51,373
	Prophage intact 3	50,319
	Prophage intact 4	52,024
	Plasmid pAb1	90,078
	Prophage intact 5	19,265
	Prophage incomplete 3	8,794
	Plasmid pAb1_2	7,818
CRAb1	Prophage intact 1	32,612
	Prophage incomplete 1	27,108
	Prophage incomplete 2	13,048
	Prophage intact 2	50,319
	Prophage intact 3	52,029
	Plasmid pCRAb1	261,943

	Prophage incomplete 3	8,417
	Prophage incomplete 4	55,46
	Plasmid pCRAb1_2	90,078
	Prophage incomplete 5	33,119
	Prophage intact 4	25,504
	Plasmid pCRAb1_3	7,818
	Plasmid pCRAb1_4	5,281
CRAb2	Prophage intact 1	44,630
	Prophage intact 2	51,278
	Prophage intact 3	26,180
	Prophage incomplete 1	21,369
	Prophage incomplete 2	30,170
	Prophage intact 4	31,048
	Prophage intact 5	49,291
	Plasmid pCRAb2	265,260
	Prophage incomplete 3	5,561
	Prophage incomplete 4	23,222
	Plasmid pCRAb2_2	101,308
	Prophage incomplete 5	8,794
	Prophage intact 6	25,504
	Plasmid pCRAb2_3	10,891
	Plasmid pCRAb2_4	6,508
	Plasmid pCRAb2_5	2,968

6.3.1. Mobile genetic element characterization

According to PHASTER the Ab1, CRAb1, and CRAb2 isolates carried 5, 4, and 6 intact prophages, respectively. This is in accordance with previous studies, where prophages were proven to be highly prevalent among this species, with the average number per strain reaching up to six prophages (29,30). To verify that these intact prophages were active, the isolates were grown in the presence of MMC for 5 h, and the lysates were subsequently filtered for plaque formation tests and visualization of the prophages by TEM. All isolates contained inducible prophages, as shown in the induction graph (Figure 6.1). The induced prophages were then visualized by TEM (Figure 6.2). As shown in these images, phages with different morphologies were detectable in the three lysates. Interestingly, the CRAb2 induction curve showed a drastic decrease in optical density within less than two hours after the addition of MMC. On the other hand, the optical densities of both the Ab1 and CRAb1 isolates decreased only after three hours of incubation. Since the observed turbidity decrease is related to cell death, mostly caused by prophage induction, the difference observed could be related to the presence of more prophages in the CRAb2 isolate and consequently a more unstable state of lysogeny. It should also be mentioned that the Ab1 and CRAb1 isolates are isogenic, with the main differences being the

absence of the Ab1 prophage intact 2 from the CRAb1 isolate and the presence of the pCRAb1 and pCRAb1_4 plasmids in the CRAb1 isolate (Table 6.1).

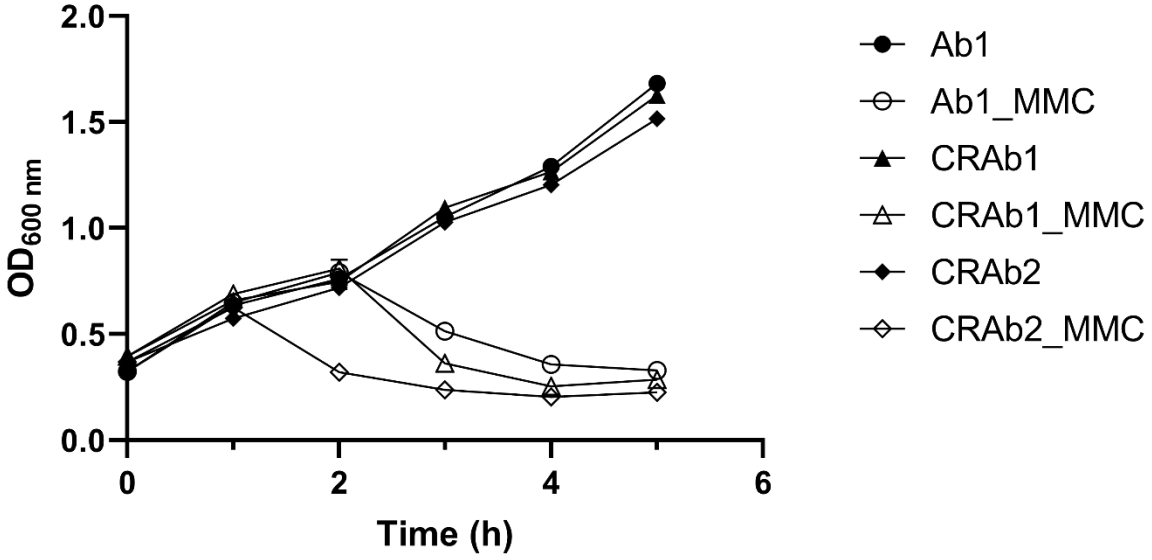


Figure 6.1. Induction curve of Ab1, CRAb1, and CRAb2 *A. baumannii* isolates using MMC at 3 µg/mL added at T0.

A careful inspection of the prophages from the Ab1, CRAb1, and CRAb2 isolates shows different virulence/fitness-related and non-phage genes of interest, albeit that no antibiotic-resistance genes (ARGs) could be detected. Table 6.2 shows the different types of genes found, some of which have potential roles in virulence or fitness as judged from the results of studies on other bacterial species. Interestingly, almost all prophages were shown to encode toxin-antitoxin (TA) systems, mostly belonging to the type II HicAB, which provide more stability to prophages and can facilitate bacterial persistence and antibiotic resistance (31). One prophage from the Ab1 isolates was shown to also encode a type IV TA system, AbiH, and another one encodes a type I restriction enzyme M protein that also protects the host against incoming foreign DNA (32,33). All prophages harbored transposase genes. Intriguingly, the plasmids pAb1, pCRAb1_2, and pCRAb2_2 carried prophages that presented a relatively higher prevalence of transposase genes, which are responsible for the mobility of specific DNA fragments across the genome, leading to mutations that may result in antibiotic resistance (34). Furthermore, the glutamate 5-kinase gene was also prevalent among the majority of the intact prophages, which is relevant as this gene may be related to colistin resistance as was previously reported (35). Other genes that may play a role in antibiotic resistance include class I SAM-dependent methyltransferase (36), an Ish1 domain-containing protein (35), and a phosphoethanolamine lipid A transferase (37). Genes involved in DNA repair encoded by some prophages, such as DNA polymerase V and SOS-response-

associated peptidase (SRAP), might lead to antibiotic resistance as well (38,39). Two prophages, intact 3 and intact 2 from the Ab1 and CRAb1 isolates, respectively, encode sigma-fimbrial proteins, which increase bacterial adhesion to surfaces (40). Besides, genes for other survival-related proteins, such as glutathione S-transferase or the N-ethylmaleimide reductase that are related to detoxification, were encoded within prophage genomes (41,42). Genes for the virulence regulators TraR/DksA and YebC/PmpR (43,44), as well as several fitness-related genes, were also detected, which is consistent with the results from previous studies on the influence of prophages on host virulence and pathogenicity (29,30).

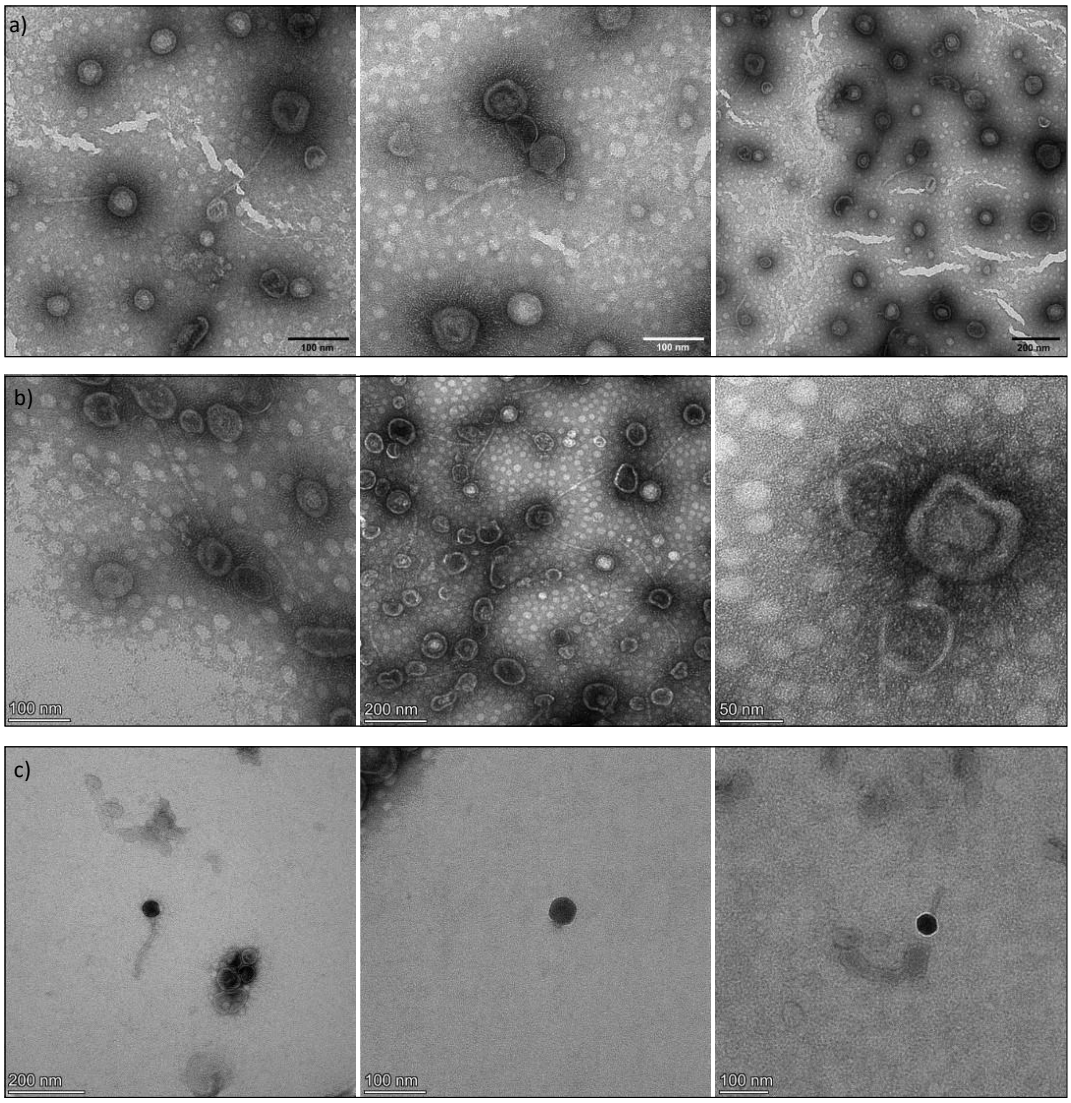


Figure 6.2. TEM images of phages produced by the MMC-induced a) Ab1, b) CRAb1, and c) CRAb2 isolates.

Table 6.2. Proteins of interest encoded by the intact prophages of the clinical *A. baumannii* isolates Ab1, CRAb1, and CRAb2, and their functions

Proteins	Function
Sigma-fimbriae tip adhesin Sigma-fimbriae usher protein Sigma-fimbriae chaperone protein Sigma-fimbriae tip adhesin Lipoprotein	Adhesion
Glutamate 5-kinase Ish1 domain-containing protein; stress-responsive nuclear envelope protein Class I SAM-dependent methyltransferase Phosphoethanolamine–lipid A transferase	Antibiotic-resistance
Y-family DNA polymerase Translesion error-prone DNA polymerase V autoproteolytic subunit SOS response-associated peptidase family protein Glutathione S-transferase N-ethylmaleimide reductase KefB	Survival
Zinc-type alcohol dehydrogenase-like protein YbdR Oxidoreductase YqhD S-formylglutathione hydrolase Negative transcriptional regulator of formaldehyde detoxification operon Metallophosphoesterase 1-acyl-sn-glycerol-3-phosphate acyltransferase GNAT family N-acetyltransferase NADP-dependent oxidoreductase S-formylglutathione hydrolase	Fitness
IS1 transposase ISPsy4, transposase IS30-like element ISAba125 family transposase Transposase IS66 family protein IS21 family transposase IS256 family transposase Transposase OrfAB subunit B IS5 family transposase	Mobile genetic element
TraR/DksA C4-type zinc finger protein YebC/PmpR family DNA-binding transcriptional regulator	Virulence regulator
Type I restriction enzyme M protein Type II toxin-antitoxin system HicA family toxin Type II toxin-antitoxin system HicB family antitoxin Type II toxin-antitoxin system VapC family toxin (57% id) Bacteriophage abortive infection AbiH family protein	Defense
Recombinase RecT	Other

Regarding the presence of plasmids, the Ab1, CRAb1 and CRAb2 isolates harbored two, four, and five plasmids, respectively, which together with the active prophages may increase the chances of HGT

events through transduction, conjugation, and/or transformation (45). As the Ab1 and CRAb1 isolates are isogenic, the fact that pCRAb1 is missing from the Ab1 isolate shows that plasmid transfer by HGT had occurred, but how it occurred exactly remains unknown, because the respective donor strain could not be identified during the outbreak. A detailed analysis of this plasmid of about 261 kb showed that it carries several antibiotic resistance genes such as bla_{NDM-1}, bla_{OXA-97}, *tet(x3)*, *sul2*, *ant(2")-Ia*, *aph(3")-Ib*, *aph(3')-Ia*, *aph(6)-Id*, *ant(3")-IIa*, *mph(E)*, and *msr(E)*. In addition, it carries virulence genes for major facilitator superfamily (MFS) transporters, iron uptake proteins, lipoproteins, and secretion systems (46–49). It also carries typical conjugation genes, such as *traX*, *dotL*, *dotM*, *dotO*, and a gene encoding a TrbI-like protein that is responsible for mobility (50–52). Furthermore, plasmid pCRAb1 also encodes a toxin-antitoxin HigAB system (53). The CRAb2 isolate also possesses a large plasmid named pCRAb2 (>260 kb), which shares 99.98% nucleotide similarity with pCRAb1, reinforcing the view that this plasmid can be mobilized quite readily. Plasmids pAb1 and pAb2 are identical to pCRAb1_2 and pCRAb1_3. respectively. pAb1/pCRAb1_2 harbor intact prophage regions, and all four plasmids carry several fitness and virulence-related genes, such as a guanylate kinase (54), a quinone oxidoreductase (55), the alcohol dehydrogenase YqhD (56), and the cold shock-like protein CspE (57). The HigAB toxin-antitoxin system was also encoded by the pAb1_2/pCRAb1_3 plasmids. The smallest plasmid from the CRAb1 isolate (pCRAb1_4) also carries two virulence genes, namely *emrE* and *acrR* (58,59). Regarding the other plasmids from the CRAb2 isolate, pCRAb2_2 was 100% identical to pCRAb1_2 and pAB1 with 88% sequence coverage. This plasmid encoded a higher number of transposases, which are responsible for the differences between the plasmids. Moreover, plasmids pCRAb2_3, pCRAb2_4, and pCRAb2_5 differed from the other plasmids, and encoded mostly hypothetical proteins, except for pCRAb2_3, which also carried genes for the HigAB toxin-antitoxin system and the cold shock-like protein CspE. A complete genomic annotation of the different plasmids and prophages is provided in Supplemental Table S6.1.

6.3.2. Outer membrane vesicle characterization

OMVs released from Gram-negative bacteria can perform different functions during bacterial growth and infection. Increasing biofilm formation (60), HGT (10,61), antimicrobial protection (62,63), and colonization (2) are some of the roles that OMVs can play to help particular bacteria thrive. OMVs were produced by the Ab1, CRAb1, and CRAb2 isolates when cultured in LB or DMEM media for 24 h. These OMVs were subsequently isolated and their physical characterization was performed using DLS. The results are summarized in Table 6.3. The vesicle size ranged between 30 nm and 500 nm and could be divided into two differently sized populations, denoted Peak 1 and Peak 2, irrespective of the

isolate or growth medium used. Judged from the inspection of the OMVs by TEM, the smaller peak (Peak 2) probably corresponds to the actual size of the vesicles as shown in Figure 6.2, where induced phages are attached to vesicles that, on average, are smaller than 100 nm in diameter. The observed interactions between phages and vesicles may explain the presence of Peak 1 in OMVs isolated from both media. It thus seems that the OMVs represent a way for the host to defend itself against phages, which are its natural predators (62). Interestingly, OMVs isolated from bacteria cultured in DMEM have, on average, a larger diameter than those isolated from bacteria cultured in LB, the only exception being the OMVs of the CRAb2 isolate. This difference can be explained by the higher prophage prevalence in this isolate and, accordingly, spontaneous induction that leads to increased OMV-phage interactions. Since DMEM is more nutrient-limited compared to LB, the larger vesicles could help to collect more nutrients, including iron or carbohydrates (64). Another possible explanation could be the lowered prophage stability in DMEM, which readily leads to phage bursts that, in turn, could lead to the production of larger OMVs.

Table 6.3. DLS measurement of OMVs from the AB1, CRAb1, and CRAb2 isolates grown in LB or DMEM

***A. baumannii* isolates**	**LB**		**DMEM**	
	Peak 1 Average size (nm)	Peak 2 Average size (nm)	Peak 1 Average size (nm)	Peak 2 Average size (nm)
Ab1	194.9 ± 81.91	36.15 ± 9.61	465.10 ± 198.60	56.67 ± 12.15
CRAb1	275.5 ± 133.2	48.59 ± 14.89	543.70 ± 203.9	71.30 ± 18.33
CRAb2	266.1 ± 137.5	45.86 ± 13.04	290.00 ± 146.4	31.60± 12.59

6.3.3. Proteomic analysis of OMVs produced by clinical isolates

The proteomes of OMVs produced by the AB1, CRAb1 and CRAb2 isolates grown in LB or DMEM were analyzed by LC-MS/MS. Databases containing the annotated proteins for each isolate were obtained with Prokka and used for protein identification. Two distinct analyses were performed, namely one using a single-strain database from each isolate to inspect proteins in the corresponding isolate's OMV sample, and another analysis using a single database including all proteins to allow a comparison of the numbers of identified proteins in the different isolate samples. For the assembly of this single database, proteins were first compared by BLASTp, and those with 100% coverage and > 95% amino acid identity were considered to be the same.

As shown in Figure 6.3, OMVs of the Ab1 isolate contained the lowest numbers of proteins irrespective of whether they were obtained from bacteria grown in LB or DMEM (162 and 156 proteins, respectively). OMVs from the CRAb2 isolate presented the highest number of identified proteins, with

522 proteins identified for the OMVs from bacteria grown in LB, and 512 proteins from OMVs produced by bacteria grown in DMEM. Also, OMVs from the CRAb1 isolate presented significantly more proteins when the bacteria were grown in LB (496 proteins), than when the bacteria were grown in DMEM (339 proteins). Furthermore, there was a clear difference between OMVs from the susceptible isolate Ab1 and both CRAb isolates regarding the numbers of identified proteins, which could be related to the presence of pCRAb1/pCRAb2 plasmids. A previous proteomic study of two clinical isolates, one multi-drug resistant (MDR) and the other one non-MDR, showed the opposite trend with small differences between the OMVs (65). To predict the subcellular localization of the identified OMV proteins, PSORTb was used, and the results were manually checked through literature surveys and the UniProt database (17,20). According to the results, there was no significant difference in the protein distribution proportions for OMVs from the Ab1 isolate grown in LB or DMEM (Table 6.4). The only relevant differences were observed for OMV-borne inner membrane proteins (16% in LB-OMV proteins, 32% in DMEM-OMV proteins), and for OMV-borne cytoplasmic proteins, where LB-OMVs accounted for 47% of the identified cytoplasmic proteins, while DMEM-OMVs accounted for 27%. A high proportion of cytoplasmic proteins was identified in OMVs from both the CRAb1 and CRAb2 isolates. This may be caused by the toxin-antitoxin system in the pCRAb1/pCRAb2 plasmids. Despite the prophage prevalence being similar in the Ab1 and CRAb1 isolates, this type of mobile genetic element can also be more unstable and increase the release of proteins from the cytoplasm. No additional purification procedure was performed with the OMVs prior to the proteomic analysis and, therefore, a higher number of cytoplasmic proteins could be expected for strains with a higher propensity to lyse. Except for the OMV-borne cytoplasmic proteins, the distribution among the other predicted localizations of OMV-associated proteins was comparable to what was already reported for OMVs *of A. baumannii* clinical isolates (8,66).

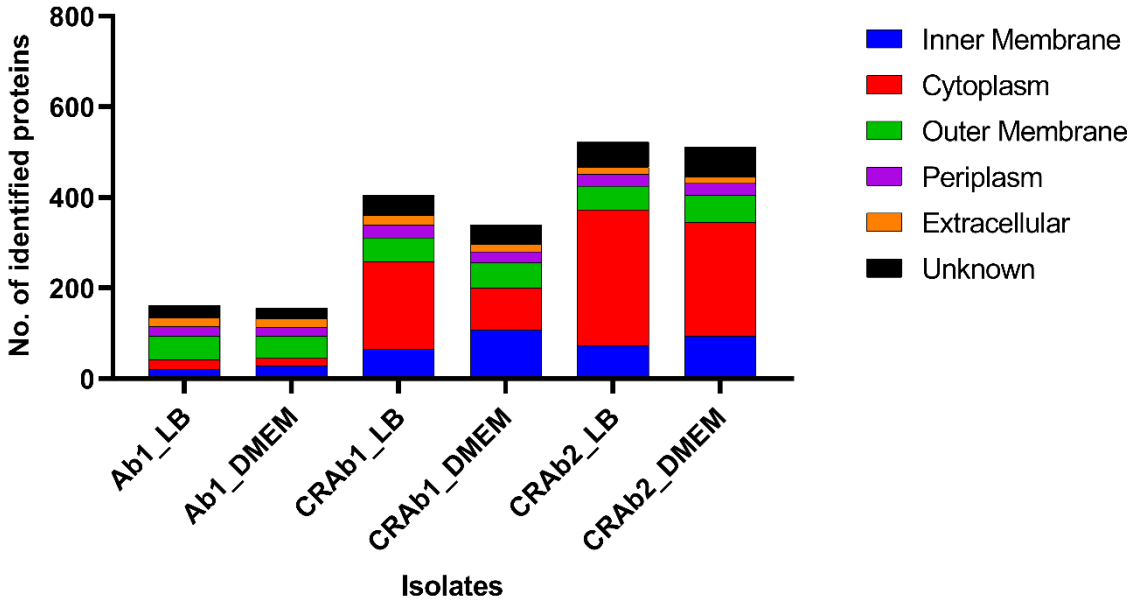


Figure 6.3. Numbers of identified OMV-associated proteins from the Ab1, CRAb1, and CRAb2 isolates and their predicted subcellular or extracellular localization. OMVs were collected from bacteria grown in LB or DMEM.

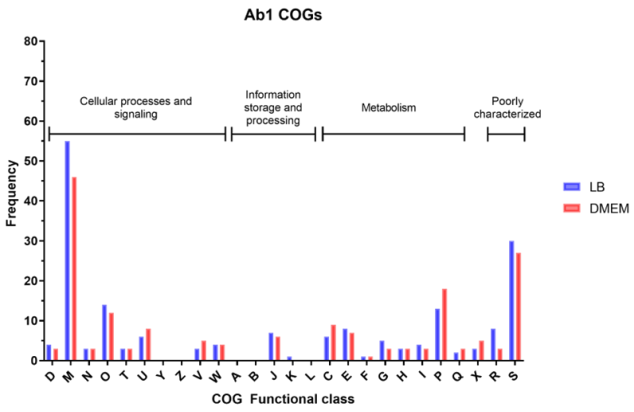
Table 6.4. Comparison of the proportions of OMV-associated proteins with a particular predicted subcellular localization for OMVs collected from the Ab1, CRAb1, and CRAb2 isolates grown in LB or DMEM

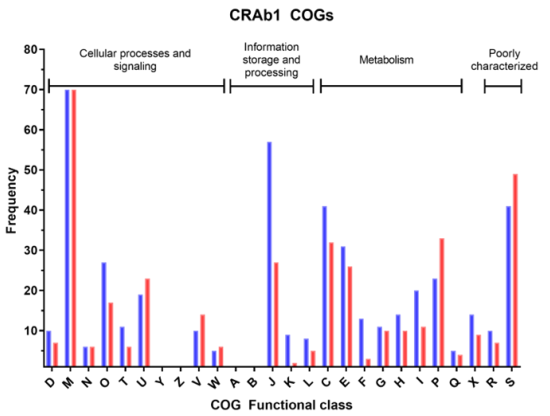
	LB vs DMEM (%)		
Localization/Isolates	Ab1	CRAb1	CRAb2
Inner Membrane	12.96 vs 18.59	16.01 vs 31.86	13.98 vs 18.55
Cytoplasm	12.96 vs 10.26	47.54 vs 27.14	47.47 vs 49.02
Outer membrane	32.10 vs 32.05	13.05 vs 16.52	9.96 vs 11.52
Periplasm	13.58 vs 11.54	6.9 vs 7.08	5.17 vs 5.08
Extracellular	11.11 vs 12.84	5.42 vs 5.01	2.87 vs 2.93
Unknown	17.28 vs 14.74	11.08 vs 12.39	10.54 vs 12.89

6.3.4. Functional analysis of OMV proteins

Proteins were annotated based on their functional role using the cluster of orthologous groups (COG) predicted by the reCOGnizer algorithm (19). Figure 6.4 shows a comparison of the different COGs identified for OMV proteins of each isolate upon growth in LB or DMEM. OMV proteins from the Ab1 isolate were predominantly related to cellular processes and signaling, specifically cell wall biogenesis and chaperones, metabolism through energy production, amino acid metabolism and, most prevalent, inorganic transport. Among OMV-associated proteins of the CRAb1 isolate, the identified COGs were well distributed over the three main categories, cellular processes and signaling, information storage and processing, and metabolism. Proteins were significantly associated with cell

wall assembly, protein translation, energy production, and metabolism. In addition, OMV-associated proteins related to defense mechanisms were identified. When comparing the effects of the two growth media, LB-OMVs contained more proteins belonging to information storage and processing than DMEM-OMVs. For example, proteins associated with translation and ribosomal structure biogenesis were almost doubled in LB-OMV. Interestingly, proteins related to inorganic ions transport and metabolism were more prevalent in DMEM-OMVs than in LB-OMVs. This should be related, for example, to the limited amount of iron present. The same was observed in OMVs from the CRAb2 isolate. Here the functional profile was similar to that of OMVs from the CRAb1 isolate, with more proteins related to metabolism and information storage and processing. Here it is noteworthy that the CRAb1 isolate's OMV-protein functions do not change significantly upon growth in either of the two media. These results are in accordance with what was previously reported, where differences in OMVs produced by an MDR and a non-MDR strain and both grown in LB, were mainly the presence of genes related to survival/defense mechanisms (8). The complete set of detected and annotated proteins with corresponding COG categories can be consulted in the Supplemental Table S6.2.





COG functions		
Cellular processes and signaling	D	cell cycle control, cell division, chromosome partitioning;
	M	cell wall/membrane/envelope biogenesis;
	N	cell motility;
	O	posttranslational modification, protein turnover, chaperones;
	T	signal transduction mechanisms;
	U	intracellular trafficking, secretion and vesicular transport;
	Y	nuclear structure;
	Z	cytoskeleton;
	V	defense mechanisms;
	W	extracellular structures;
Information storage and processing	A	RNA processing and modification;
	B	chromatin structure and dynamics;
	J	translation, ribosomal structure and biogenesis;
	K	transcription;
	L	replication, recombination and repair;
Metabolism	C	energy production and conversion;
	E	amino acid transport and metabolism;
	F	nucleotide transport and metabolism;
	G	carbohydrate transport and metabolism;
	H	coenzyme transport and metabolism;
	I	lipid transport and metabolism;
	P	inorganic ion transport and metabolism;
	Q	secondary metabolites biosynthesis, transport and catabolism;
Poorly characterized	R	general function prediction only;
	S	function unknown;
	X	mobilone: prophages, transposon

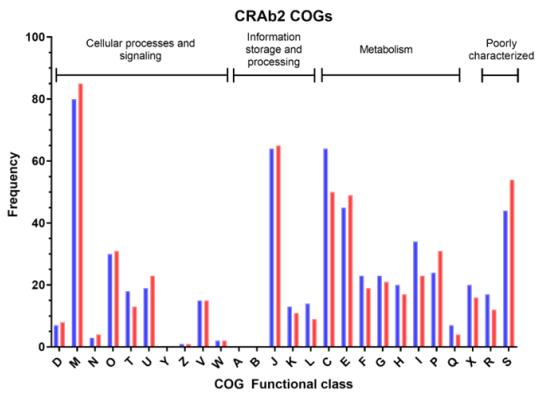


Figure 6.4. Functional annotation of OMV-borne proteins from isolates Ab1, CRAb1, and CRAb2, grown in LB or DMEM by the cluster of orthologous groups (COG). Each plot shows a comparison of the numbers of proteins assigned to each COG attributed between LB and DMEM.

6.3.5. Virulence- and fitness-related OMV-derived proteins

Comparing OMV-proteins between the different isolates cultured in LB shows that 6 proteins were uniquely present in OMVs from the Ab1 isolate, 43 proteins in CRAb1 OMVs, and 176 proteins in CRAb2 OMVs (Figure 6.5). On the other hand, only 3 DMEM-OMV proteins were unique in the Ab1 isolate, and the same was true for 51 proteins of the CRAb1 isolate, and 227 proteins of the CRAb2 isolate (Figure 6.5). As the Venn diagrams below show, there were 129 proteins commonly identified in OMVs of all isolates upon culturing in LB, and 122 common OMV proteins were identified upon culturing of the bacteria in DMEM for OMV production. Between these two groups, there are 100 proteins always present in all OMV preparations. Furthermore, 27 proteins were identified only in LB-OMVs and 22 proteins in DMEM-OMVs. Curiously, although genotypically similar, OMVs produced by the Ab1- and CRAb1 isolates displayed more differences at the proteome level. These differences were expected to be related to the Ab1 prophage, which is absent from the CRAb1 isolate, and/or the pCRAb1 presence in the latter and absence from the Ab1 isolate. In OMVs produced upon growth in LB, there were 11 OMV-associated proteins of the Ab1 isolate absent from OMVs of the CRAb1 isolate, and there were 255 identified proteins present in OMVs of the CRAb1 isolate, but not in OMVs from the Ab1 isolate. Within OMV-associated proteins from the Ab1 isolate, only a major capsid protein that belonged to the absent prophage was present, meaning that the other proteins might be influenced by this prophage. Following this, we looked into the 250 OMV-borne proteins of the CRAb1 isolate, and only four proteins were encoded in the pCRAb1 plasmid, namely the strawberry notch C-terminal domain-containing protein (OBIAGLBL_03749), a hypothetical protein (OBIAGLBL_03839), the beta-lactamase OXA-97 (OBIAGLBL_03698), and the metallo-β-lactamase type-2 NDM-1 (OBIAGLBL_03845). This was also observed for the proteome of OMVs from bacteria grown in DMEM, showing that probably both the prophage and the plasmid pCRAb1 are influencing the production and release of other proteins through the OMVs, which is a process that should be looked into further. Interestingly, the two carbapenemases OXA-97 and NDM-1 were also detected in OMVs from the CRAb2 isolate, but the latter one was not found in any OMVs of bacteria grown in DMEM. This phenomenon was already described in the literature, as these proteins accumulate in the periplasm, where they are anchored to the outer membrane. During the process of OMV formation, the carbapenemases are selectively incorporated within the OMVs periplasm (67). This mechanism allows

for efficient OMV-mediated protection through beta-lactam inactivation as shown in other studies (63,68,69), increasing not only the host tolerance against the antibiotic but also protecting susceptible neighbor cells. Unexpectedly, despite the strong presence of ARGs and other virulence genes within the pCRAb1/pCRAb2 plasmids, there was no other plasmid-derived protein within OMVs detectable.

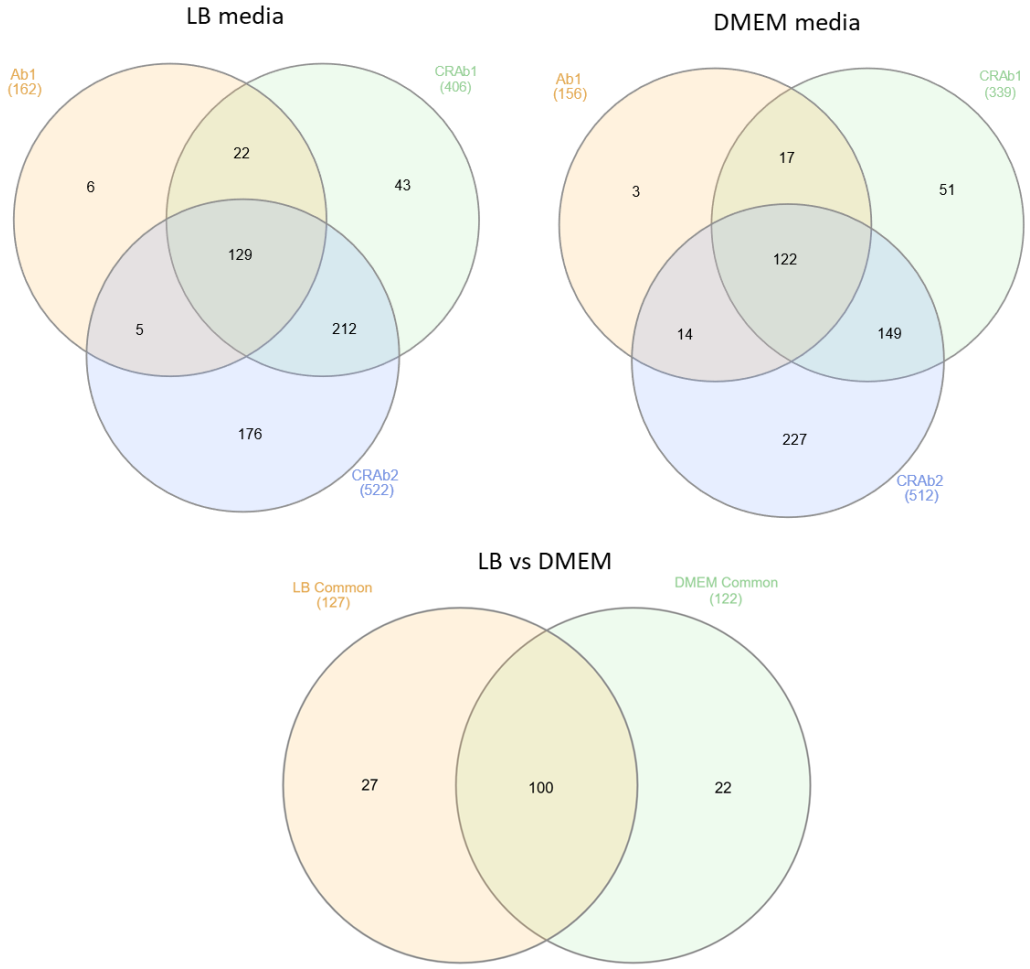


Figure 6.5. Venn diagrams with numbers of OMV-associated proteins produced by the Ab1, CRAb1 and CRAb2 isolates grown in LB or DMEM. The bottom diagram was plotted using the common proteins from LB and from DMEM.

Virulence- and fitness-related proteins of *A. baumannii* that were identified in OMV proteomes were collected and summarized in Table 6.5, following what is reported in the literature. These proteins were divided according to their roles in *A. baumannii* virulence and fitness, such as antibiotic resistance, biofilm formation/adhesion, host colonization/invasion, survival, and others that were proven to be virulence-related, but out of these main functions. As Table 6.5 shows, there are several proteins related to antibiotic resistance, some already mentioned before, like the OXA-97 and NDM-1 β-lactamases. A few identified efflux pumps, such as AdeT (70), AdeJ (71), AcrA (72), and MacA (73)

confer resistance to a wide range of antibiotic classes such as aminoglycosides, tetracyclines, tigecyclines, colistin, fluoroquinolones, and macrolides. Several studies showed the presence of antibiotic resistance proteins within OMVs, including not only antibiotic-inactivating proteins but also membrane proteins capable of absorbing the antibiotics from the environment (8,61). Furthermore, we identified proteins like the fluoroquinolone-resistant PaC (74), the lipid A hydroxylase LpxO (75), the quorum quenching lactonase YtnP (76), and other outer membrane proteins like the lipoprotein YiaD (77), CarO (78), OprM (71), which together also cover a wide range of resistance against different classes of antibiotics. Most of these proteins are present in the bacterial outer membrane and, therefore, it is expected that they would also be found within OMVs. Some proteins increase the ability of *A. baumannii* to adhere and form biofilms. These are mostly lipoproteins like the peptidoglycan-associated lipoproteins Pal (79), Blp2 (80), NlpE (81), and LolB (82), but also the CsuA/B pili (83), the CsuC chaperone, the elongation factor P (84), the polyphosphatase kinase (85), and the zinc-type dehydrogenase (86). Other identified OMV proteins are involved in host colonization, such as the porins Omp38 (87) and Omp33-36, with the latter being also associated with antibiotic resistance (88). Moreover, there were OMV-associated proteins like the metalloendopeptidase CpaA (89), the elongation factor Tuf (90), the ClpB and ClpA (91), and the VacJ lipoprotein (92). Due to the ability of *A. baumannii* to persist and survive in harsh conditions, it was not surprising to identify proteins related to iron-uptake, such as the vitamin B12 transporter BtuB (93), the ferric receptors/transporters like TonB-dependent BfrD (93), the FeoB protein, and a hemin receptor (94). In fact, the presence of the iron receptors/transporters in OMVs was previously shown (8,9), and according to Dhurve *et al*, these proteins can be selectively enriched within OMVs, in order to increase the capture of iron and other scarce nutrients from the environment (64). In addition, there were OMV-associated proteins, like superoxide dismutase, that detoxifies reactive oxygen species (ROS) (95), CzcA that is involved in resistance to heavy metals, such as cadmium (96), GroEL which may have a role during stress responses (97), and RecA, a core SOS protein responsible for the activation of different proteins involved in DNA repair to increase survival under mutagenic conditions (95). Proteins related to the capsule transport/biogenesis were also found, such as Wzi (98), TolA/TolQ (99), MlaC/MlaD (100), Ptk (101), and LptA (102), as well as transcriptional regulators/sensors that regulate virulence expression like BaeR (103) and BfmSR (104). Finally, proteins such as DnaK (105), CopA (106), and SurA (107), which were found to influence virulence in different ways, were also present in the OMV proteome.

To understand the distribution and prevalence of genes encoding these virulence-related proteins, a heatmap was generated (Figure 6.6) using the LFQ log_2-transformed values from the general database analysis. As mentioned above, we used a single combined database with proteins from the three isolates to allow comparisons. There are two distinct profiles between OMVs from *A. baumannii* grown in LB or DMEM. While each isolate shows a similar OMV-specific proteomic profile upon culturing in the DMEM medium, profiles change drastically upon culturing in LB, even for the two isogenic isolates Ab1 and CRAb1. OMVs from bacteria grown in DMEM showed overexpression of several ferric transporters, like BtuB, as well as outer membrane proteins such as Omp38, BfrD, and lipoproteins that are involved in host colonization, survival, and biofilm formation, respectively. Notably, CRAb2 OMVs presented the highest expression level of the hemolysin transporter protein ShlB, which is involved in host colonization (108). Despite the absence of carbapenemases from OMVs of the CRAb1 and CRAb2 isolates, there were other antibiotic-resistance proteins detected, such as the RND efflux pumps AdeJ, AdeT, and AcrA. Biofilm-related proteins, such as the lipoproteins Pal, or biofilm synthesis proteins, presented a low-level expression in OMVs cultured in DMEM.

Regarding OMVs produced by bacteria grown in LB, these presented a different virulence profile, with a higher diversity of proteins being overexpressed. The same proteins that were moderately expressed in DMEM-OMVs, were significantly overexpressed among LB-OMVs from the three isolates. Ab1 OMVs presented 10 proteins that were more abundantly expressed than in both CRAb1 and CRAb2 LB-OMVs. Among these are biofilm-related proteins such as Pal, lipoproteins, a biofilm synthesis protein, and CsuA/B, and other proteins like OmpA, TolB, CopB, and a Zn-dependent protease, which was the most abundantly expressed protein. Specifically, one of the most abundant outer membrane proteins, OmpA, was shown to be critical for *A. baumannii* survival during murine infection (2). CRAb1 on the other hand produced different OMV-associated lipoproteins, capsule- and biofilm-related proteins, showing a more aggressive virulence profile. Curiously, the two most expressed proteins are the vitamin B12 transporter BtuB, which is interesting due to the lower expression of other ferric transporters when compared with DMEM-OMVs, and the Omp33-36 porin which is important for host invasion and colonization (88). Similarly, CRAb2 OMVs also presented a lower level of ferric transporter expression when compared with the DMEM-OMVs, and had the different lipoproteins overexpressed, as was the case for CRAb1 OMVs. On the other hand, the most abundantly expressed proteins were related to antibiotic resistance, as exemplified by efflux pumps and carbapenemases. Moreover, the porin B was also highly expressed, as well as the metalloendopeptidase CpaA that was the most

expressed protein, both relating to host colonization. Interestingly, biofilm-related proteins were either absent or present with a low expression profile.

In general, the most prevalent proteins from OMVs isolated from the Ab1 isolate cultured in LB are mostly related to biofilm formation. CRAb1 OMVs on the other hand, besides the high expression of proteins related to biofilm formation, presented prevalent proteins related to cell invasion and cytotoxicity, antibiotic resistance, and iron uptake. Similarly, CRAb2 OMVs displayed the highest prevalence of antibiotic-resistance proteins and proteins related to colonization and invasion. As opposed to CRAb1 OMVs, CRAb2 OMVs presented a lower prevalence of iron uptake proteins.

Table 6.5. Virulence-related proteins identified in OMVs from the *A. baumannii* isolates Ab1, CRAb1 and CRAb2, and their clustered orthologous groups (COGs)

Proteins	COG	Role in *A. baumannii* virulence	Refs
AdeT, RND type efflux pump	G	Antibiotic Resistance	(70–78,103,106, 109–111)
Outer membrane protein OprM	M		
Ornithine uptake porin CarO type 1	V		
Lipoprotein YiaD	M		
Copper resistance protein B	P		
Macrolide export protein MacA	MV		
Multidrug efflux RND transporter permease subunit AdeJ	V		
Multidrug efflux pump subunit AcrA	MV		
β-lactamase OXA-100	V		
β-lactamase OXA-97	V		
Metallo-β-lactamase type 2 NDM-1	V		
Fluoroquinolone resistant parC	L		
Lipid A hydroxylase LpxO	O		
Quorum-quenching lactonase YtnP	R		
DcaP family trimeric outer membrane transporter	MU	Biofilm formation/adhesion	(79–86,112,113)
Peptidoglycan-associated lipoprotein	M		
Ig-like repeat protein Blp2	S		
Lipoprotein	S		
Lipoprotein NlpE	MP		
Outer-membrane lipoprotein LolB	M		
Csu fimbrial major subunit CsuA/B	S		
Biofilm synthesis protein	W		
Lon protease	O		
Biofilm associated Ig-like domain-containing protein	NU		
Csu fimbrial biogenesis chaperone CsuC	NU		
Elongation factor P	J		
Polyphosphate kinase	H		
Zinc-type alcohol dehydrogenase-like protein	C		
Putative porin	M	Host Colonization/Invasion	(87,89–92,108,114–118)
Porin Omp33-36	M		
OmpA-like protein	M		

Porin B	M		
Outer membrane protein Omp38	M		
Outer membrane protein transport protein	I		
Metalloendopeptidase CpaA	TO		
Capsule assembly Wzi family protein	P		
Elongation factor Tuf	J		
Chaperone protein ClpB	O		
Osmolarity sensor protein EnvZ	T		
ATP-dependent Clp protease ATP-binding subunit ClpA	O		
VacJ family lipoprotein	M		
Capsular polysaccharide synthesis protein	M		
Hemolysin transporter protein ShlB	U		
Outer membrane beta-barrel protein	M	Other	(98–105,107,119–126)
Outer membrane beta-barrel protein	M		
Phospholipid transport system binding protein MlaC	M		
Metalloprotease	R		
Protein TolB	U		
Zn-dependent protease	MO		
Cell envelope integrity protein TolA	M		
Outer membrane protein TolC	MU		
Polysaccharide biosynthesis/export family protein Wza	M		
Tyrosine-protein kinase ptk	DM		
Copper resistance protein A	DPM		
Phospholipid ABC transporter-binding protein MlaD	M		
GTPase Obg CgtA	DL		
Lipopolysaccharide export system protein LptA	M		
Chaperone SurA	O		
Protein TolQ	U		
Transcriptional regulatory protein BaeR	K		
Bifunctional purine biosynthesis protein PurH	F		
OprD family outer membrane porin	S		
Lipase 1	I		
HlyD family secretion protein	V		
Sensor histidine kinase BfmS	T		
Response regulator transcription factor BfmR	K		
AraC family transcriptional regulator	K		
Type II secretion system major pseudopilin GspG	U		
Chaperone protein DnaK	O		
TolC family protein	MU		
Type II secretion system protein D	NU		
Cobalt-zinc-cadmium resistance protein CzcA	V	Survival	(65,93–97,127,128)
Superoxide dismutase [Cu-Zn]	P		
Vitamin B12 transporter BtuB	H		
Chaperonin GroEL	O		
Ferric aerobactin receptor	P		
Ferrichrome outer membrane transporter	P		
putative TonB-dependent receptor BfrD	P		
Outer membrane protein W	M		

Protein RecA	L
Bacterioferritin	P
Ferric enterobactin receptor	P
Fe(2+) transporter FeoB	P
Hemin receptor	P

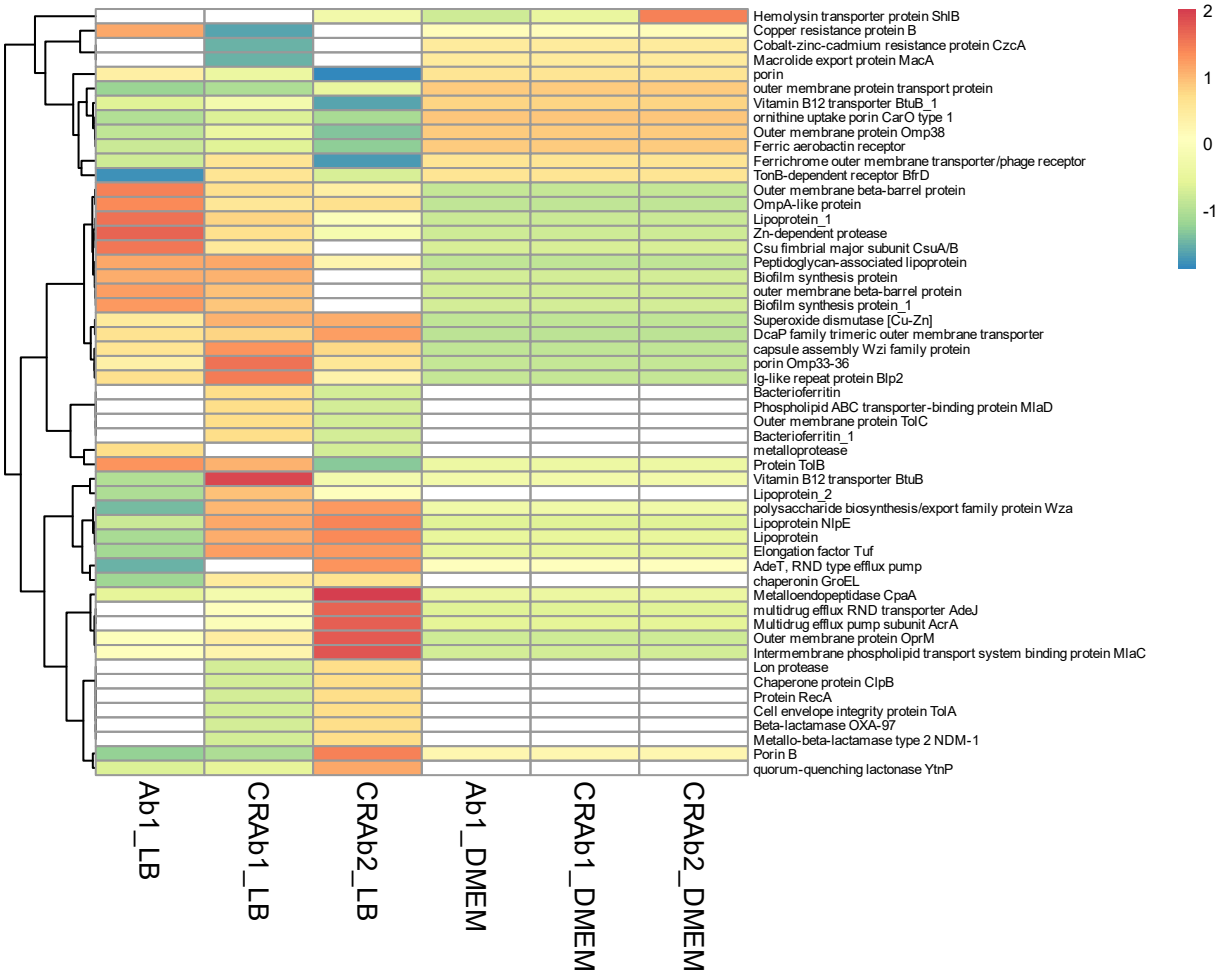


Figure 6.6. Heatmap with virulence genes identified within OMVs of the Ab1, CRAb1, and CRAb2 isolates upon growth in LB or DMEM. White squares mean the absence of a protein.

These results reinforce the idea that the investigated *A. baumannii* clinical isolates are highly virulent, harboring different mobile genetic elements that carry virulence-related genes. In a previous study, we described the outbreak caused by these three isolates, and different mobile genetic elements, such as plasmids and prophages that were found. These elements, combined with outer membrane vesicles, can lead to high genetic mobility and could be a cause of the outbreak previously described. In our present study, several prophages were found within the different isolates, with CRAb2 carrying the highest number of intact prophages. None of these prophages encoded antibiotic

resistance genes, but some of them encoded other virulence- and fitness-related genes, which confirms what was previously shown in the literature (30). Curiously, a prophage was detected within a plasmid with the potential for different ways of HGT. Between both the isogenic isolates Ab1 and CRAb1, a prophage was missing, which could be the reason for some differences. The presence or absence of certain plasmids can have a crucial influence on bacterial behavior, directly and indirectly. For instance, despite the presence of a plasmid encoding for several antibiotic-resistance genes, most of the corresponding proteins were not found within the OMVs, while only the encoded carbapenemases could be found. This shows that the plasmid was not directly responsible for protein differences found among the investigated OMVs. In the conditions tested, there was no antimicrobial stress, therefore no stimuli for the cell to produce these ARGs were generated. We would expect an increase of antibiotic-resistance proteins within OMVs if an antibiotic was incubated, as shown in the literature (66). Despite the fact that no differences were observed between the OMV proteomes of the different isolates grown in DMEM, when analyzing the OMVs from the bacteria grown on LB the more virulent profile of both CRAb isolates became clearly evident. Furthermore, most OMV cargo proteins from both CRAb isolates were predicted to be cytoplasmic, while the Ab1 isolate carried only a small proportion of cytoplasmic proteins. These differences could be related to the presence of the TA system of the pCRAb1/pCRAb2 plasmid that may increase cell lysis and consequently the number of cytoplasmic proteins within OMVs. Furthermore, COG classification showed that cell wall biogenesis proteins were highly prevalent among all OMVs and metabolism-related proteins were significantly more prevalent in both the CRAb1 and CRAb2 isolates. Defense mechanisms were more prevalent within CRAb isolates as well when compared with non-carbapenem-resistant isolate Ab1.

6.4. CONCLUDING REMARKS

Taken together, this study showed that mobile elements are crucial for the pathogenicity of *A. baumannii*, not only by providing fitness advantages to survive but also by providing channels to communicate and spread these fitness/virulence features to other cells in the environment, making this species highly prevalent within clinical settings. Different studies have shown how OMVs have different roles from delivering virulence factors to providing protection against antimicrobials, and only a few focused on recently isolated clinical strains. Analyzing recent clinical isolates makes the results more closely relevant to what is found within the clinic. Here we assessed the pathogenicity of these isolates on a more realistic medium like DMEM instead of only using LB, which is a nutrient-rich and a completely different medium. This type of studies is of great importance to understand how bacterial

pathogenicity increases, and what role the different MGEs have, in order to find new ways of blocking both transmission and/or virulence increase among these critical species.

6.5. REFERENCES

1. Antunes LCS, Imperi F, Carattoli A, Visca P. Deciphering the Multifactorial Nature of *Acinetobacter baumannii* Pathogenicity. PLoS One. 2011 Aug 1;6(8):e22674.
2. Tiku V, Kofoed EM, Yan D, Kang J, Xu M, Reichelt M, *et. al* Outer membrane vesicles containing OmpA induce mitochondrial fragmentation to promote pathogenesis of *Acinetobacter baumannii*. Sci Rep. 2021 Dec 1;11(1).
3. Shadan A, Pathak A, Ma Y, Pathania R, Singh RP. Deciphering the virulence factors, regulation, and immune response to *Acinetobacter baumannii* infection. Front Cell Infect Microbiol. 2023 Feb 23;13:1053968.
4. Arnold BJ, Huang IT, Hanage WP. Horizontal gene transfer and adaptive evolution in bacteria. Vol. 20, Nature Reviews Microbiology. Nature Research; 2022. p. 206–18.
5. Gyles C, Boerlin P. Horizontally Transferred Genetic Elements and Their Role in Pathogenesis of Bacterial Disease. Vet Pathol. 2014;51(2):328–40.
6. Domingues S, Nielsen KM. Membrane vesicles and horizontal gene transfer in prokaryotes. Curr Opin Microbiol. 2017;38:16–21.
7. Robbins PD, Morelli AE. Regulation of immune responses by extracellular vesicles. Nature Reviews Immunology 2014 14:3. 2014 Feb 25;14(3):195–208.
8. Li ZT, Zhang RL, Bi XG, Xu L, Fan M, Xie D, *et. al* Outer membrane vesicles isolated from two clinical *Acinetobacter baumannii* strains exhibit different toxicity and proteome characteristics. Microb Pathog. 2015 Apr 1;81:46–52.
9. Kwon SO, Gho YS, Lee JC, Kim S il. Proteome analysis of outer membrane vesicles from a clinical *Acinetobacter baumannii* isolate. FEMS Microbiol Lett. 2009 Aug;297(2):150–6.
10. Rumbo C, Fernández-Moreira E, Merino M, Poza M, Mendez JA, Soares NC, *et. al* Horizontal transfer of the OXA-24 carbapenemase gene via outer membrane vesicles: A new mechanism of dissemination of carbapenem resistance genes in *Acinetobacter baumannii*. Antimicrob Agents Chemother. 2011 Jul;55(7):3084–90.
11. Morton RE, Evans TA. Modification of the bicinchoninic acid protein assay to eliminate lipid interference in determining lipoprotein protein content. Anal Biochem. 1992 Aug 1;204(2):332–4.
12. Melo LDR, Sillankorva S, Ackermann HW, Kropinski AM, Azeredo J, Cerca N. Isolation and characterization of a new *Staphylococcus epidermidis* broad-spectrum bacteriophage. Journal of General Virology. 2014 Feb;95(PART 2):506–15.
13. Bonn F, Bartel J, Büttner K, Hecker M, Otto A, Becher D. Picking Vanished Proteins from the Void: How to Collect and Ship/Share Extremely Dilute Proteins in a Reproducible and Highly Efficient Manner. Anal Chem. 2014 Aug 5;86(15):7421–7.
14. Cox J, Mann M. MaxQuant enables high peptide identification rates, individualized p.p.b.-range mass accuracies and proteome-wide protein quantification. Nat Biotechnol. 2008;26(12):1367–72.
15. Rgen Cox J, Hein MY, Luber CA, Paron I, Nagaraj N, Mann M. Accurate Proteome-wide Label-free Quantification by Delayed Normalization and Maximal Peptide Ratio Extraction, Termed MaxLFQ*. S Technological Innovation and Resources. Molecular & Cellular Proteomics. 2014;13:2513–26.
16. Schwanhäusser B, Busse D, Li N, Dittmar G, Schuchhardt J, Wolf J, *et. al* Global quantification of mammalian gene expression control. Nature. 2011;473(7347):337–42.
17. Consortium TU, Bateman A, Martin MJ, Orchard S, Magrane M, Ahmad S, *et. al* UniProt: the Universal Protein Knowledgebase in 2023. Nucleic Acids Res. 2023 Jan 6;51(D1):D523–31.

18. Huerta-Cepas J, Szklarczyk D, Heller D, Hernández-Plaza A, Forslund SK, Cook H, *et. al* EggNOG 5.0: A hierarchical, functionally and phylogenetically annotated orthology resource based on 5090 organisms and 2502 viruses. Nucleic Acids Res. 2019 Jan 8;47(D1):D309–14.
19. Sequeira JC, Rocha M, Alves MM, Salvador AF. UPIMAPI, reCOGnizer and KEGGCharter: Bioinformatics tools for functional annotation and visualization of (meta)-omics datasets. Comput Struct Biotechnol J. 2022 Jan 1;20:1798–810.
20. Yu NY, Wagner JR, Laird MR, Melli G, Rey S, Lo R, *et. al* PSORTb 3.0: improved protein subcellular localization prediction with refined localization subcategories and predictive capabilities for all prokaryotes. Bioinformatics. 2010 Jul 1;26(13):1608–15.
21. Heberle H, Meirelles VG, da Silva FR, Telles GP, Minghim R. InteractiVenn: A web-based tool for the analysis of sets through Venn diagrams. BMC Bioinformatics. 2015 May 22;16(1):1–7.
22. Jia B, Raphenya AR, Alcock B, Waglechner N, Guo P, Tsang KK, *et. al* CARD 2017: expansion and model-centric curation of the comprehensive antibiotic resistance database. Nucleic Acids Res. 2017 Jan 1;45(D1):D566–73.
23. Garg A, Gupta D. VirulentPred: A SVM based prediction method for virulent proteins in bacterial pathogens. BMC Bioinformatics. 2008 Jan 28;9(1):1–12.
24. Gupta A, Kapil R, Dhakan DB, Sharma VK. MP3: A Software Tool for the Prediction of Pathogenic Proteins in Genomic and Metagenomic Data. PLoS One. 2014 Apr 15;9(4):e93907.
25. Metsalu T, Vilo J. ClustVis: A web tool for visualizing clustering of multivariate data using Principal Component Analysis and heatmap. Nucleic Acids Res. 2015;43(W1):W566–70.
26. Arndt D, Grant JR, Marcu A, Sajed T, Pon A, Liang Y, *et. al* PHASTER: a better, faster version of the PHAST phage search tool. Nucleic Acids Res. 2016 Jul;44(W1):W16-21.
27. Vizcaíno JA, Côté RG, Csordas A, Dianes JA, Fabregat A, Foster JM, *et. al* The Proteomics Identifications (PRIDE) database and associated tools: status in 2013. Nucleic Acids Res. 2013 Jan 1;41(D1):D1063–9.
28. Talsma DT, Monteiro R, Flores-Vallejo R del C, Heuvelmans M, Le TN, Hendrickx APA, *et. al* Nosocomial transmission of tet(x3), blaNDM-1, and blaOXA-97-carrying *Acinetobacter baumannii* conferring resistance to eravacycline and omadacycline, the Netherlands, March-August 2021. Eurosurveillance. 2024 Apr;
29. Loh B, Chen J, Manohar P, Yu Y, Hua X, Leptihn S. A Biological Inventory of Prophages in *A. baumannii* Genomes Reveal Distinct Distributions in Classes, Length, and Genomic Positions. Front Microbiol. 2020;11(December):1–13.
30. Costa AR, Monteiro R, Azeredo J. Genomic analysis of *Acinetobacter baumannii* prophages reveals remarkable diversity and suggests profound impact on bacterial virulence and fitness. Sci Rep. 2018;8(1):15346.
31. Fraikin N, Goormaghtigh F, Van Melderen L. Type II Toxin-Antitoxin Systems: Evolution and Revolutions. J Bacteriol. 2020 Mar 11;202(7).
32. Dy RL, Przybilski R, Semeijn K, Salmond GPC, Fineran PC. A widespread bacteriophage abortive infection system functions through a Type IV toxin–antitoxin mechanism. Nucleic Acids Res. 2014;42(7):4590.
33. Loenen WAM, Dryden DTF, Raleigh EA, Wilson GG. Type I restriction enzymes and their relatives. Nucleic Acids Res. 2014 Jan 1;42(1):20–44.
34. Lipszyc A, Szuplewska M, Bartosik D. How Do Transposable Elements Activate Expression of Transcriptionally Silent Antibiotic Resistance Genes? International Journal of Molecular Sciences 2022, Vol 23, Page 8063. 2022 Jul 22;23(15):8063.
35. Cafiso V, Stracquadanio S, Lo Verde F, Gabriele G, Mezzatesta ML, Caio C, *et. al* Colistin resistant *A. baumannii*: Genomic and transcriptomic traits acquired under colistin therapy. Front Microbiol. 2019 Jan 7;9:1–20.

36. Chen Q, Li X, Zhou H, Jiang Y, Chen Y, Hua X, *et. al* Decreased susceptibility to tigecycline in *Acinetobacter baumannii* mediated by a mutation in trm encoding SAM-dependent methyltransferase. Journal of Antimicrobial Chemotherapy. 2014 Jan 1;69(1):72–6.
37. Arroyo LA, Herrera CM, Fernandez L, Hankins J V., Trent MS, Hancock REW. The pmrCAB operon mediates polymyxin resistance in *Acinetobacter baumannii* ATCC 17978 and clinical isolates through phosphoethanolamine modification of lipid A. Antimicrob Agents Chemother. 2011 Aug;55(8):3743–51.
38. Aranda J, López M, Leiva E, Magán A, Adler B, Bou G, *et. al* Role of *Acinetobacter baumannii* UmuD homologs in antibiotic resistance acquired through DNA damage-induced mutagenesis. Antimicrob Agents Chemother. 2014 Mar;58(3):1771–3.
39. Hare JM, Ferrell JC, Witkowski TA, Grice AN. Prophage induction and differential RecA and UmuDAb transcriptome regulation in the DNA damage responses of *Acinetobacter baumannii* and *Acinetobacter baylyi*. PLoS One. 2014 Apr 7;9(4).
40. Busch A, Waksman G. Chaperone–usher pathways: diversity and pilus assembly mechanism. Philosophical Transactions of the Royal Society B: Biological Sciences. 2012;367(1592):1112–22.
41. Longkumer T, Parthasarathy S, Vemuri SG, Siddavattam D. OxyR-dependent expression of a novel glutathione S-transferase (Abgst01) gene in *Acinetobacter baumannii* DS002 and its role in biotransformation of organophosphate insecticides. Microbiology (United Kingdom). 2014 Jan 1;160(PART 1):102–12.
42. Subhadra B, Surendran S, Kim DH, Woo K, Oh MH, Choi CH. The transcription factor NemR is an electrophile-sensing regulator important for the detoxification of reactive electrophiles in *Acinetobacter nosocomialis*. Res Microbiol. 2019 Apr 1;170(3):123–30.
43. Jude F, Köhler T, Branny P, Perron K, Mayer MP, Comte R, *et. al* Posttranscriptional control of quorum-sensing-dependent virulence genes by DksA in *Pseudomonas aeruginosa*. J Bacteriol. 2003;185(12):3558–66.
44. Wei L, Wu Y, Qiao H, Xu W, Zhang Y, Liu X, *et. al* YebC controls virulence by activating T3SS gene expression in the pathogen Edwardsiella piscicida. FEMS Microbiol Lett. 2018 Jul 1;365(14).
45. Thomas CM, Nielsen KM. Mechanisms of, and barriers to, horizontal gene transfer between bacteria. Nat Rev Microbiol. 2005;3(9):711–21.
46. Kovacs-Simon A, Titball RW, Michell SL. Lipoproteins of Bacterial Pathogens. Infect Immun. 2011 Jan 21;79(2):548–61.
47. R GE, Joan M. Bacterial Secretion Systems: An Overview. Microbiol Spectr. 2016 Feb 26;4(1):10.1128/microbiolspec.vmbf-0012–2015.
48. C CJ, V WR, M RK, J FM. Quorum Sensing Regulation of a Major Facilitator Superfamily Transporter Affects Multiple Streptococcal Virulence Factors. J Bacteriol. 2022 Aug 8;204(9):e00176-22.
49. Akhtar AA, Turner DPJ. The role of bacterial ATP-binding cassette (ABC) transporters in pathogenesis and virulence: Therapeutic and vaccine potential. Microb Pathog. 2022;171:105734.
50. Maneewannakul K, Maneewannakul S, Ippen-Ihler K. Characterization of traX, the F plasmid locus required for acetylation of F-pilin subunits. J Bacteriol. 1995 Jun 1;177(11):2957–64.
51. Grace LY, Bo H, J CP. Biological and Structural Diversity of Type IV Secretion Systems. Microbiol Spectr. 2019 Apr 5;7(2):10.1128/microbiolspec.psib-0012–2018.
52. Alt-Mo¨rbe J, Mo¨rbe M, Stryker JL, Fuqua ‡ Clay, Li § Pei-Li, Farrand SK, *et. al* The Conjugal Transfer System of *Agrobacterium tumefaciens* Octopine-Type Ti Plasmids Is Closely Related to

the Transfer System of an IncP Plasmid and Distantly Related to Ti Plasmid vir Genes. Vol. 178, Journal of Bacteriology. 1996.

53. Singh G, Yadav M, Ghosh C, Rathore JS. Bacterial toxin-antitoxin modules: classification, functions, and association with persistence. Curr Res Microb Sci. 2021;2:100047.
54. Liu K, Myers AR, Pisithkul T, Claas KR, Satyshur KA, Amador-Noguez D, *et. al* Molecular Mechanism and Evolution of Guanylate Kinase Regulation by (p)ppGpp. Mol Cell. 2015 Feb 19;57(4):735–49.
55. Ryan A, Kaplan E, Nebel JC, Polycarpou E, Crescente V, Lowe E, *et. al* Identification of NAD(P)H Quinone Oxidoreductase Activity in Azoreductases from *P. aeruginosa*: Azoreductases and NAD(P)H Quinone Oxidoreductases Belong to the Same FMN-Dependent Superfamily of Enzymes. PLoS One. 2014 Jun 10;9(6):e98551-.
56. Lee C, Kim I, Park C. Glyoxal detoxification in *Escherichia coli* K-12 by NADPH dependent aldo-keto reductases. Journal of Microbiology. 2013;51(4):527–30.
57. Michaux C, Holmqvist E, Vasicek E, Sharan M, Barquist L, Westermann AJ, *et. al* RNA target profiles direct the discovery of virulence functions for the cold-shock proteins CspC and CspE. Proceedings of the National Academy of Sciences. 2017 Jun 27;114(26):6824–9.
58. L RJ, Manuel MB, J MHA, Wilson T, Kazuya W, Xiaodong Z, *et. al* The TetR Family of Transcriptional Repressors. Microbiology and Molecular Biology Reviews. 2005 Jun 1;69(2):326–56.
59. Schuldiner S. EmrE, a model for studying evolution and mechanism of ion-coupled transporters. Biochimica et Biophysica Acta (BBA) - Proteins and Proteomics. 2009;1794(5):748–62.
60. Thomas B, Stefanie S, Jana S, Martin von B, Frank S, Y WL, *et. al* Membrane Vesicle Formation as a Multiple-Stress Response Mechanism Enhances *Pseudomonas putida* DOT-T1E Cell Surface Hydrophobicity and Biofilm Formation. Appl Environ Microbiol. 2012 Sep 1;78(17):6217–24.
61. Chatterjee S, Mondal A, Mitra S, Basu S. *Acinetobacter baumannii* transfers the blaNDM-1 gene via outer membrane vesicles. Journal of Antimicrobial Chemotherapy. 2017 Aug 1;72(8):2201–7.
62. Manning AJ, Kuehn MJ. Contribution of bacterial outer membrane vesicles to innate bacterial defense. BMC Microbiol. 2011;11.
63. Kim SW, Park S Bin, Im SP, Lee JS, Jung JW, Gong TW, *et. al* Outer membrane vesicles from β-lactam-resistant *Escherichia coli* enable the survival of β-lactam-susceptible *E. coli* in the presence of β-lactam antibiotics. Sci Rep. 2018 Dec 1;8(1).
64. Dhurve G, Madikonda AK, Jagannadham MV, Siddavattam D. Outer Membrane Vesicles of *Acinetobacter baumannii* DS002 Are Selectively Enriched with TonB-Dependent Transporters and Play a Key Role in Iron Acquisition . Microbiol Spectr. 2022 Apr 27;10(2).
65. Jin JS, Kwon SO, Moon DC, Gurung M, Lee JH, Kim S Il, *et. al Acinetobacter baumannii* secretes cytotoxic outer membrane protein a via outer membrane vesicles. PLoS One. 2011;6(2).
66. Kesavan D, Vasudevan A, Wu L, Chen J, Su Z, Wang S, *et. al* Integrative analysis of outer membrane vesicles proteomics and whole-cell transcriptome analysis of eravacycline induced *Acinetobacter baumannii* strains. BMC Microbiol. 2020 Feb 11;20(1).
67. López C, Prunotto A, Bahr G, Bonomo RA, González LJ, Peraro MD, *et. al* Specific Protein-Membrane Interactions Promote Packaging of Metallo-β-Lactamases into Outer Membrane Vesicles. Antimicrob Agents Chemother. 2021 Oct 1;65(10).
68. González LJ, Bahr G, Nakashige TG, Nolan EM, Bonomo RA, Vila AJ. Membrane anchoring stabilizes and favors secretion of New Delhi metallo-β-lactamase. Nat Chem Biol. 2016 Jul 1;12(7):516–22.

69. Ciofu O, Beveridge TJ, Kadurugamuwa J, Walther-Rasmussen J, Høiby N. Chromosomal beta-lactamase is packaged into membrane vesicles and secreted from *Pseudomonas aeruginosa*. J Antimicrob Chemother. 2000;45(1):9–13.
70. Bharathi Srinivasan V, Rajamohan G, Pancholi P, Marcon M, Gebreyes WA. Molecular cloning and functional characterization of two novel membrane fusion proteins in conferring antimicrobial resistance in *Acinetobacter baumannii*. Journal of Antimicrobial Chemotherapy. 2011 Mar 1;66(3):499–504.
71. Kyriakidis I, Vasileiou E, Pana ZD, Tragiannidis A. *Acinetobacter baumannii* Antibiotic Resistance Mechanisms. Pathogens. 2021 Mar 19;10(3):373.
72. Vanessa K, Ayush K. Update on Multidrug Resistance Efflux Pumps in *Acinetobacter* spp. Antimicrob Agents Chemother. 2021 Jun 17;65(7):10.1128/aac.00514-21.
73. Robin B, Nicol M, Le H, Tahrioui A, Schaumann A, Vuillemenot JB, *et. al* MacAB-TolC Contributes to the Development of *Acinetobacter baumannii* Biofilm at the Solid–Liquid Interface. Front Microbiol. 2022;12.
74. Liu YH, Kuo SC, Lee YT, Chang ICY, Yang SP, Chen TL, *et. al* Amino acid substitutions of quinolone resistance determining regions in GyrA and ParC associated with quinolone resistance in *Acinetobacter baumannii* and *Acinetobacter* genomic species 13TU. Journal of Microbiology, Immunology and Infection. 2012;45(2):108–12.
75. L BT, J KT, Joana SP, Raquel CÁ, A BJ. 2-Hydroxylation of *Acinetobacter baumannii* Lipid A Contributes to Virulence. Infect Immun. 2019 Mar 25;87(4):10.1128/iai.00066-19.
76. Scribano D, Marzano V, Mortera SL, Sarshar M, Vernocchi P, Zagaglia C, *et. al* Insights into the Periplasmic Proteins of *Acinetobacter baumannii* AB5075 and the Impact of Imipenem Exposure: A Proteomic Approach. Int J Mol Sci. 2019 Jul 13;20(14):3451.
77. Lei H, Yiyuan G, Yuqing L, Siyu Y, Shuyan Z, Sirui Z, *et. al* An Outer Membrane Protein YiaD Contributes to Adaptive Resistance of Meropenem in *Acinetobacter baumannii*. Microbiol Spectr. 2022 Apr 4;10(2):e00173-22.
78. Zhu LJ, Chen XY, Hou PF. Mutation of CarO participates in drug resistance in imipenem-resistant *Acinetobacter baumannii*. J Clin Lab Anal. 2019 Oct 1;33(8):e22976. Available from: https://doi.org/10.1002/jcla.22976
79. Vandana S, Monalisa T, Vishvanath T. Investigation of Peptidoglycan-Associated Lipoprotein of *Acinetobacter baumannii* and Its Interaction with Fibronectin To Find Its Therapeutic Potential. Infect Immun. 2023 Apr 5;91(5):e00023-23.
80. De Gregorio E, Del Franco M, Martinucci M, Roscetto E, Zarrilli R, Di Nocera PP. Biofilm-associated proteins: news from *Acinetobacter*. BMC Genomics. 2015;16(1):933.
81. Siroy A, Cosette P, Seyer D, Lemaître-Guillier C, Vallenet D, Van Dorsselaer A, *et. al* Global Comparison of the Membrane Subproteomes between a Multidrug-Resistant *Acinetobacter baumannii* Strain and a Reference Strain. J Proteome Res. 2006 Dec 1;5(12):3385–98.
82. Rebekah H, Nuwan V, Paul H, Torsten S, Scott C, H MJ, *et. al* Colistin-Resistant, Lipopolysaccharide-Deficient *Acinetobacter baumannii* Responds to Lipopolysaccharide Loss through Increased Expression of Genes Involved in the Synthesis and Transport of Lipoproteins, Phospholipids, and Poly-β-1,6-N-Acetylglucosamine. Antimicrob Agents Chemother. 2012 Dec 26;56(1):59–69.
83. Pakharukova N, Tuittila M, Paavilainen S, Malmi H, Parilova O, Teneberg S, *et. al* Structural basis for *Acinetobacter baumannii* biofilm formation. Proceedings of the National Academy of Sciences. 2018 May 22;115(21):5558–63.
84. Guo Q, Cui B, Wang M, Li X, Tan H, Song S, *et. al* Elongation factor P modulates *Acinetobacter baumannii* physiology and virulence as a cyclic dimeric guanosine monophosphate effector. Proceedings of the National Academy of Sciences. 2022 Oct 11;119(41):e2209838119.

85. Hongfa L, Yonglin Z, Baichen L, Jian G, Peng Z, Xuming D, *et. al* Polyphosphate Kinase Is Required for the Processes of Virulence and Persistence in *Acinetobacter baumannii*. Microbiol Spectr. 2022 Jul 5;10(4):e01230-22.
86. Zhang K, Yang X, Yang J, Qiao X, Li F, Liu X, *et. al* Alcohol dehydrogenase modulates quorum sensing in biofilm formations of *Acinetobacter baumannii*. Microb Pathog. 2020;148:104451.
87. Choi CH, Lee EY, Lee YC, Park TI, Kim HJ, Hyun SH, *et. al* Outer membrane protein 38 of *Acinetobacter baumannii* localizes to the mitochondria and induces apoptosis of epithelial cells. Cell Microbiol. 2005 Aug 1;7(8):1127–38.
88. Carlos R, María T, Esteban FM, Cruz SN, Micaela C, Elena S, *et. al* The *Acinetobacter baumannii* Omp33-36 Porin Is a Virulence Factor That Induces Apoptosis and Modulates Autophagy in Human Cells. Infect Immun. 2014 Oct 7;82(11):4666–80.
89. Urusova D V, Kinsella RL, Salinas ND, Haurat MF, Feldman MF, Tolia NH. The structure of *Acinetobacter* secreted protease CpaA complexed with its chaperone CpaB reveals a novel mode of a T2SS chaperone-substrate interaction. Journal of Biological Chemistry. 2019 Sep 6;294(36):13344–54.
90. Koenigs A, Zipfel PF, Kraiczy P. Translation Elongation Factor Tuf of *Acinetobacter baumannii* Is a Plasminogen-Binding Protein. PLoS One. 2015 Jul 31;10(7):e0134418-.
91. Belisario JC, Lee HH, Luknauth H, Rigel NW, Martinez LR. *Acinetobacter baumannii* Strains Deficient in the Clp Chaperone-Protease Genes Have Reduced Virulence in a Murine Model of Pneumonia. Pathogens. 2021 Feb 13;10(2):204.
92. Nengding W, A OE, J MM, R HA. Genome-Wide Identification of *Acinetobacter baumannii* Genes Necessary for Persistence in the Lung. mBio. 2014 Jun 3;5(3):10.1128/mbio.01163-14.
93. Nwugo CC, Gaddy JA, Zimbler DL, Actis LA. Deciphering the iron response in *Acinetobacter baumannii*: A proteomics approach. J Proteomics. 2011;74(1):44–58.
94. Federica R, Valentina G, Emanuela F, Giordano R, Livia L, Massimiliano L, *et. al* Contribution of Active Iron Uptake to *Acinetobacter baumannii* Pathogenicity. Infect Immun. 2019 Mar 25;87(4):10.1128/iai.00755-18.
95. Aranda J, Bardina C, Beceiro A, Rumbo S, Cabral MP, Barbé J, *et. al Acinetobacter baumannii* reca protein in repair of DNA damage, antimicrobial resistance, general stress response, and virulence. J Bacteriol. 2011 Aug;193(15):3740–7.
96. F AS, G AF, Ram M, N DN, Maoge Z, Katherine G, *et. al* The Molecular Basis of *Acinetobacter baumannii* Cadmium Toxicity and Resistance. Appl Environ Microbiol. 2021 Oct 28;87(22):e01718-21.
97. Cardoso K, Gandra RF, Wisniewski ES, Osaku CA, Kadowaki MK, Felipach-Neto V, *et. al* DnaK and GroEL are induced in response to antibiotic and heat shock in *Acinetobacter baumannii*. J Med Microbiol. 2010 Sep 1;59(9):1061–8.
98. Niu T, Guo L, Luo Q, Zhou K, Yu W, Chen Y, *et. al* Wza gene knockout decreases *Acinetobacter baumannii* virulence and affects Wzy-dependent capsular polysaccharide synthesis. Virulence. 2020 Dec 31;11(1):1–13.
99. Hubloher JJ, Van der Sande L, Schaudinn C, Müller V, Averhoff B. The Tol-Pal system of *Acinetobacter baumannii* is important for cell morphology, antibiotic resistance and virulence. International Microbiology. 2023;26(3):543–50.
100. Kamischke C, Fan J, Bergeron J, Kulasekara HD, Dalebroux ZD, Burrell A, *et. al* The *Acinetobacter baumannii* Mla system and glycerophospholipid transport to the outer membrane. Garrett WS, Mignot T, editors. Elife. 2019;8:e40171.
101. Hua X, Zhou Z, Yang Q, Shi Q, Xu Q, Wang J, *et. al* Evolution of *Acinetobacter baumannii* In Vivo: International Clone II, More Resistance to Ceftazidime, Mutation in ptk. Front Microbiol. 2017;8.

102. Oi KK, Moehle K, Schuster M, Zerbe O. Early Molecular Insights into Thanatin Analogues Binding to *A. baumannii* LptA. Molecules. 2023 May 25;28(11):4335.
103. Lin MF, Lin YY, Lan CY. The Role of the Two-Component System BaeSR in Disposing Chemicals through Regulating Transporter Systems in *Acinetobacter baumannii*. PLoS One. 2015 Jul 10;10(7):e0132843-.
104. Geisinger E, Mortman NJ, Vargas-Cuebas G, Tai AK, Isberg RR. A global regulatory system links virulence and antibiotic resistance to envelope homeostasis in *Acinetobacter baumannii*. PLoS Pathog. 2018 May 24;14(5):e1007030-.
105. Chiappori F, Fumian M, Milanesi L, Merelli I. DnaK as Antibiotic Target: Hot Spot Residues Analysis for Differential Inhibition of the Bacterial Protein in Comparison with the Human HSP70. PLoS One. 2015 Apr 23;10(4):e0124563-.
106. Williams CL, Neu HM, Alamneh YA, Reddinger RM, Jacobs AC, Singh S, *et. al* Characterization of *Acinetobacter baumannii* Copper Resistance Reveals a Role in Virulence. Front Microbiol. 2020;11.
107. Karolin B, Fabian R, Angel A, Gottfried W, Mirita FW, Boris M, *et. al* An Unprecedented Tolerance to Deletion of the Periplasmic Chaperones SurA, Skp, and DegP in the Nosocomial Pathogen *Acinetobacter baumannii*. J Bacteriol. 2022 Sep 15;204(10):e00054-22.
108. Pérez A, Merino M, Rumbo-Feal S, Álvarez-Fraga L, Vallejo JA, Beceiro A, *et. al* The FhaB/FhaC two-partner secretion system is involved in adhesion of *Acinetobacter baumannii* AbH12O-A2 strain. Virulence. 2017 Aug 18;8(6):959–74.
109. Patrick M, Michael M, J CR, Erik S, Lindsay S, G BM, *et. al* Detection of New Delhi Metallo-β-Lactamase (Encoded by bla NDM-1) in *Acinetobacter* schindleri during Routine Surveillance. J Clin Microbiol. 2020 Dec 21;51(6):1942–4.
110. Laurent P, Wejdene M, Olfa B, Patrice N. Carbapenem-Resistant *Acinetobacter baumannii* Isolates from Tunisia Producing the OXA-58-Like Carbapenem-Hydrolyzing Oxacillinase OXA-97. Antimicrob Agents Chemother. 2008 May 1;52(5):1613–7.
111. Samy F, Laurent P, Anna P, Vassiliki K, Patrice N. Overexpression of the Naturally Occurring blaOXA-51 Gene in *Acinetobacter baumannii* Mediated by Novel Insertion Sequence ISAba9. Antimicrob Agents Chemother. 2009 Sep 1;53(9):4045–7.
112. Carly C, Brendan Y, Chineme O, David L, Andrew C, G GV. Lon Protease Has Multifaceted Biological Functions in *Acinetobacter baumannii*. J Bacteriol. 2018 Dec 20;201(2):10.1128/jb.00536-18.
113. Cabral MP, Soares NC, Aranda J, Parreira JR, Rumbo C, Poza M, *et. al* Proteomic and Functional Analyses Reveal a Unique Lifestyle for *Acinetobacter baumannii* Biofilms and a Key Role for Histidine Metabolism. J Proteome Res. 2011 Aug 5;10(8):3399–417.
114. Singh JK, Adams FG, Brown MH. Diversity and Function of Capsular Polysaccharide in *Acinetobacter baumannii*. Front Microbiol. 2019;9.
115. A TK, N RP. An ompR-envZ Two-Component System Ortholog Regulates Phase Variation, Osmotic Tolerance, Motility, and Virulence in *Acinetobacter baumannii* Strain AB5075. J Bacteriol. 2017 Jan 12;199(3):10.1128/jb.00705-16.
116. Tickner J, Hawas S, Totsika M, Kenyon JJ. The Wzi outer membrane protein mediates assembly of a tight capsular polysaccharide layer on the *Acinetobacter baumannii* cell surface. Sci Rep. 2021;11(1):21741.
117. Zhang W, Zhou H, Jiang Y, He J, Yao Y, Wang J, *et. al Acinetobacter baumannii* Outer Membrane Protein A Induces Pulmonary Epithelial Barrier Dysfunction and Bacterial Translocation Through The TLR2/IQGAP1 Axis. Front Immunol. 2022;13.

118. Huang W, Yao Y, Wang S, Xia Y, Yang X, Long Q, *et. al* Immunization with a 22-kDa outer membrane protein elicits protective immunity to multidrug-resistant *Acinetobacter baumannii*. Sci Rep. 2016;6(1):20724.
119. Wood CR, Mack LE, Actis LA. An Update on the *Acinetobacter baumannii* Regulatory Circuitry. Trends Microbiol. 2018 Jul 1;26(7):560–2.
120. Elhosseiny NM, Attia AS. *Acinetobacter*: an emerging pathogen with a versatile secretome. Emerg Microbes Infect. 2018 Dec 1;7(1):1–15.
121. Hua M, Liu J, Du P, Liu X, Li M, Wang H, *et. al* The novel outer membrane protein from OprD/Occ family is associated with hypervirulence of carbapenem-resistant *Acinetobacter baumannii* ST2/KL22. Virulence. 2021 Dec 31;12(1):1–11.
122. Bharathi SV, Vasanth V, Govindan R. AbuO, a TolC-Like Outer Membrane Protein of *Acinetobacter baumannii*, Is Involved in Antimicrobial and Oxidative Stress Resistance. Antimicrob Agents Chemother. 2015 Jan 27;59(2):1236–45.
123. Blaschke U, Skiebe E, Wilharm G. Novel Genes Required for Surface-Associated Motility in *Acinetobacter baumannii*. Curr Microbiol. 2021;78(4):1509–28.
124. Harding CM, Pulido MR, Di Venanzio G, Kinsella RL, Webb AI, Scott NE, *et. al* Pathogenic *Acinetobacter* species have a functional type I secretion system and contact-dependent inhibition systems. Journal of Biological Chemistry. 2017.
125. Hussein Almola A, Al-Omari AW, Younis Mahdy Al-Hamadany A. Molecular Study of *Acinetobacter baumannii* that Lacking Some Essentials Genes Responsible of Toxin-Antitoxin System. Arch Razi Inst. 2022;77(1):483–90.
126. R NH, Sowmya K, Xiaomei R, D WJ, M TJ, D PL. Genetic synergy between *Acinetobacter baumannii* undecaprenyl phosphate biosynthesis and the Mla system impacts cell envelope and antimicrobial resistance. mBio. 2024 Feb 16;15(3):e02804-23.
127. Catel-Ferreira M, Marti S, Guillon L, Jara L, Coadou G, Molle V, *et. al* The outer membrane porin OmpW of *Acinetobacter baumannii* is involved in iron uptake and colistin binding. FEBS Lett. 2016 Jan 1;590(2):224–31.
128. R GE, J JL, P SE. The Manganese-Responsive Transcriptional Regulator MumR Protects *Acinetobacter baumannii* from Oxidative Stress. Infect Immun. 2020 Feb 20;88(3):10.1128/iai.00762-19.

Chapter 7

General conclusions and future perspectives

7.1. GENERAL CONCLUSIONS

Bacterial pathogens have been evolving to better resist antimicrobial therapies, presenting a significant challenge in healthcare. Among these pathogens, some are particularly dangerous due to their multidrug resistance (MDR), which includes carbapenems, a class of antibiotics often considered as a last resort. The Gram-negative bacterium *Acinetobacter baumannii* emerged as a critical pathogen in hospital settings due to its ability to colonize, resist desiccation, and form biofilms making it challenging to eradicate. These features are facilitated by numerous virulence factors, like the capsule and lipopolysaccharides (LPS), protein secretion, iron acquisition, pili, outer membrane vesicles, and others inherent to *A. baumannii*. Moreover, this bacterium exhibits a unique SOS response, which has been reported to enhance its adaptability by interacting with proteins involved in DNA repair, thereby introducing mutations, and promoting genomic variability. One of the most alarming developments is the emergence of MDR-resistant variants within *A. baumannii* isolates, particularly the Carbapenem-Resistant *A. baumannii* (CRAb) variants.

While this species did not inherently possess antibiotic-resistance genes, studies have demonstrated that these genes were acquired externally through horizontal gene transfer (HGT) mediated by mobile elements, such as plasmids, prophages and OMVs. One of the regulators of this HGT is the SOS system encoded by *A. baumannii*, which can induce the mobilization of mobile genetic elements, such as prophages. The main goal of the research described in this thesis was to comprehend the role of HGT vehicles in the evolution of the drug resistance and pathogenicity of *A. baumannii*.

To better understand the relevance of prophages within *A. baumannii*, an extensive analysis of all complete genomes submitted to NCBI was conducted. To accomplish this, a bioinformatic tool, ProphAnTool, was developed, integrating several available genomic analysis tools, to search and characterize prophages from large batches of whole genome sequences. This analysis verified previous observations regarding the widespread presence of prophages in *A. baumannii* isolates. Furthermore, these prophages were detected both in the bacterial genomes and plasmids, likely indicating the existence of phage-plasmids, and highlighting their potential for horizontal gene transfer. Among these prophages, a small group harbored a diverse set of antibiotic-resistance genes, conferring resistance to multiple antibiotics. Additionally, other virulence and fitness-related genes were highly prevalent, indicating their potential contribution to bacterial adaptation. While several defense systems were identified within these prophages, the majority of them have so far remained poorly characterized.

As the SOS response employs a unique mechanism in *A. baumannii*, the way this system influences prophage gene expression was investigated by looking at induction and virulence/fitness-related gene

expressions through transcriptomics. This survival mechanism is known to be a major prophage inducer in most bacteria, including *A. baumannii*. Since this system relies upon a different set of genes, it became important to understand how it interacts with integrated prophages. Besides, since this species' SOS response is still poorly understood, the role of one of its regulators, DdrR, was also explored. This small co-regulatory protein was shown to be crucial to keep critical SOS genes, such as error-prone polymerases repressed, and to greatly influence the expression of non-DNA damage-related genes, including genes related to prophage induction, such as the phage repressor CI, Cro, and protein Q, which is the main regulator of late gene expression in prophages. The Protein Q gene, together with most structural phage genes, was found to be overexpressed in the absence of stress. Moreover, under stress conditions, the protein Q gene was induced in all three prophages of the investigated strain, but only in the absence of the *ddrR* gene, suggesting a potential direct interaction with protein Q expression and its repressor CII. Regrettably, experimental validation of this hypothesis was not possible, due to an inaccurate phage counting method, as phage plaques were too small and, in some situations, almost impossible to count. The use of a different propagation host could improve phage counting, but unfortunately, after several attempts, no compatible host was found due to the narrow host range of these phages.

Another study detailed in this thesis involved the characterization of three new *A. baumannii* clinical isolates that were collected during an outbreak at a hospital in The Netherlands. These three isolates included a non-CRAb isolate from the index patient and two CRAb strains that emerged at a later stage during the outbreak. All three isolates were sequenced by Illumina and Nanopore technologies, resulting in closed genomes. The subsequent analyses revealed the presence of a novel MDR plasmid in two out of the three isolates. This newly identified plasmid was found to be a conjugative plasmid, and it conferred resistance to a wide variety of antibiotics, including carbapenems and the last generation of tetracyclines. Subsequently, the outer membrane vesicles of these three new isolates were characterized based on their proteomes. This analysis revealed that the OMV proteomic content was different, mainly between the non-CRAb and the two CRAb isolates. Of significance, carbapenemases encoded by the MDR-plasmid was identified in the OMV fraction of the two CRAb isolates. Therefore, the carbapenemase activity of these OMVs was characterized, demonstrating their ability to degrade carbapenems, potentially protecting the host against this class of antibiotics. Furthermore, the protective effect was demonstrated to be extensible to other species through OMV-protection experiments, wherein other susceptible species were shielded from carbapenems by the OMVs.

Lastly, a comprehensive analysis of the mobile genetic elements of the three outbreak-associated isolates was performed, as well as an extensive study of their OMV proteomes. This involved OMV isolation

from the bacteria cultured in two different media, the regular and nutrient-rich Lysogeny Broth (LB) and a typical cell culture medium known as DMEM. Several mobile genetic elements (MGEs) were detected among the three isolates. These MGEs included several intact prophages, as well as different plasmids, besides the afore-mentioned MDR plasmid. However, a careful characterization revealed a low prevalence of virulence genes among these MGEs. Nevertheless, prophages were inducible as observed through TEM, confirming their mobility potential. Conversely, OMV proteomes, showed a high prevalence of virulence effectors and antibiotic-resistance proteins, that were implicated in increased host colonization and invasion, attachment and biofilm formation, survival, and other capabilities. In addition, there were no absolute differences between the different isolates 'DMEM-OMV' proteomes. Conversely, 'LB-OMV' proteomes significantly differed between the different isolates. Additionally, virulence-associated proteins were detected in higher amounts in OMVs from bacteria cultured in LB than in OMVs from bacteria cultured in DMEM. It was also concluded that the MDR plasmid was not directly responsible for proteome differences between the CRAb and non-CRAb isolates. Instead, it is hypothesized that either the plasmid or the afore-mentioned prophages are regulating the expression of specific genes that lead to these differences.

In conclusion, the analysis of mobile elements in *A. baumannii* verified their important role in the emergence of highly virulent and multidrug-resistant variants, particularly those resistant to carbapenems. Furthermore, the investigations into the interactions between the SOS response and prophages in this pathogen are beginning to shed light on previously unexplored gene regulatory mechanisms.

7.2. FUTURE PERSPECTIVES

The work described in this thesis represents a significant step to a broader objective aiming at understanding all interactions between the mobile elements and *A. baumannii*. Despite the progress made, several mechanisms remain unknown. For example, how do prophages, plasmids, and OMVs interact all together? It is known that OMVs can carry plasmids to another host, but can they also carry prophages? In theory, it would be possible, since prophages are DNA fragments, therefore they could be incorporated into the OMVs. Moreover, can prophages influence OMV production to promote plasmid mobilization, or how are OMVs formed and how do they select their cargo? These are some of the questions that are still awaiting answers.

To tackle these questions, various approaches can be employed. For example, to search for prophage DNA within the OMVs, DNA could be extracted from OMVs and sequenced to map all DNA content. With this, it could be possible to detect, not only prophage DNA, but also other mobile genetic elements or

genes, which could be critical to understanding how the outbreak described in this thesis started, and if OMVs drove this event by mobilizing the plasmid (1). It would also be interesting to show that prophage DNA mobilized through OMVs could integrate into a new host, with a prophage-cured variant, and by inserting in the prophage a selective marker, it could be possible to prove this phenomenon, which has not been described yet.

Prophages are still the mobile genetic element that have been subject to relatively few studies in *A. baumannii*, although they have been proven to have the potential to influence their host's behavior. Therefore, to identify the mechanisms that could be influencing OMV production, first different knockouts would be necessary to verify the genes that are responsible for OMV production. Then, using a prophage-cured variant, in comparison to the wild-type, for transcriptomics would provide a gene expression profile showing the genes that are potentially influencing it.

Lastly, it would be very interesting to verify whether DdrR is indeed influencing prophage induction by screening protein-protein interactions between DdrR and other phage proteins. For example, as performed with DdrR and LexA/UmuDAb proteins (2), using surface plasmon resonance it could be investigated whether DdrR interacts with the CII repressor or protein Q, which were seen to be influenced by DdrR, according to the results described in this thesis. Besides, improving phage detection would also benefit this study, so a different phage detection method could be used, for example, flow cytometry to count phage particles as shown in some studies (3,4). Understanding all these interactions would unveil the main mechanisms of prophage induction in *A. baumannii*, thereby providing important knowledge for dealing with this increasingly dangerous pathogen.

7.3. REFERENCES

1. Bitto NJ, Chapman R, Pidot S, Costin A, Lo C, Choi J, et al. Bacterial membrane vesicles transport their DNA cargo into host cells. Sci Rep. 2017 Dec 1;7(1).
2. Pavlin A, Bajc G, Fornelos N, Browning DF, Butala M. The Small DdrR Protein Directly Interacts with the UmuDAb Regulator of the Mutagenic DNA Damage Response in *Acinetobacter baumannii*. J Bacteriol. 2022 Mar 1;204(3).
3. Dlusskaya EA, Dey R. Flow Virometry: A Fluorescence-Based Approach to Enumerate Bacteriophages in Liquid Samples. Methods in Molecular Biology. 2024;2738:175–84.
4. Oliveira J, Mahony J, Hanemaaijer L, Kouwen TRHM, Neve H, MacSharry J, et al. Detecting *Lactococcus lactis* prophages by mitomycin C-mediated induction coupled to flow cytometry analysis. Front Microbiol. 2017 Jul 19;8(JUL).